

**RIGID AND NON-RIGID PLATE RECONSTRUCTION OF THE EAST AFRICA AND
ANTARCTICA CONTINENTAL MARGINS**

A Thesis Presented to
the Faculty of the Department of Earth and Atmospheric Sciences
University of Houston

In Partial Fulfillment
of the Requirements for the Degree
Master of Science

By
Luan Chan Nguyen

August 2015

**RIGID AND NON-RIGID PLATE RECONSTRUCTION OF THE EAST AFRICA AND
ANTARCTICA CONTINENTAL MARGINS**

Luan Chan Nguyen

APPROVED:

Dr. Stuart A. Hall

Dr. Dale E. Bird

Dr. Philip J. Ball

Dr. William W. Sager

Dean, College of Natural Sciences and Mathematics

ACKNOWLEDGEMENTS

Finishing this thesis work is a milestone in my academic career. I would not have accomplished this without the help and support from my research committee. I would like to thank my research advisor, Dr. Stuart Hall, who has trusted me from the beginning and has always been patient and encouraging. Dr. Hall has taught me how to properly approach and resolve scientific problems. I also would like to express my gratitude to Dr. Dale Bird, without whose support and guidance I would not have had a chance at pursuing a graduate degree. Dr. Bird also provided me access to the specialized software required for this study along with his tremendous tutoring. I am grateful for the guidance from Dr. Philip Ball with Conoco Phillips Company whose passion for geoscience has been truly inspirational. I thank Dr. William Sager for his insightful critiques that helped me improve my work.

I appreciate Conoco Phillips Company for supporting this project financially. I am also thankful for their permission that allowed me to look at the seismic reflection data.

I am grateful to my parents and my family. Financially and emotionally, they have always supported me throughout this whole journey. Above all, I thank God for everything. I have been blessed with the opportunity to be part of this project working with and learning from great people.

**RIGID AND NON-RIGID PLATE RECONSTRUCTION OF THE EAST AFRICA AND
ANTARCTICA CONTINENTAL MARGINS**

An Abstract of a Thesis

Presented to

the Faculty of the Department of Earth and Atmospheric Sciences

University of Houston

In Partial Fulfillment

of the Requirements for the Degree

Master of Science

By

Luan Chan Nguyen

August 2015

ABSTRACT

The Early Jurassic separation of Antarctica from Africa plays an important role in our understanding of the dispersal of the Gondwana supercontinent. Previously proposed reconstruction models often contain overlaps and gaps in the restored margins that reflect difficulties in accurately delineating the continent-ocean boundary (COB) and determining the amount and distribution of extended continental crust. This study focuses on the evolution of the African margin adjacent to the Mozambique Basin and the conjugate margin of Antarctica near the Riiser Larsen Sea. A complete break-up history involving both seafloor spreading and continental rifting has been investigated.

New satellite-derived gravity data have been used to trace the orientations and landward limits of fracture zones in the study area. A 3-D gravity inversion has produced a crustal thickness model that reliably quantifies the extent and amount of stretched crust. Information on crustal thickness along with the identification of magnetic isochrons reveal COBs that are located significantly closer to the coasts of Africa and Antarctica than previously recognized. Correlation of both fracture zone azimuths and magnetic isochrons in addition to the identified COBs over the conjugate margins suggest Antarctica began drifting away from Africa at approximately 171 Ma in a roughly SSE direction. Of several scenarios examined to determine the crustal character of the Beira High, the preferred model assigns it an oceanic origin and suggests that it may be a conjugate feature of the southern Astrid Ridge in Antarctica.

An areal-balancing method that involves restoring the crust to a uniform pre-rift thickness has been used to perform the non-rigid reconstruction. This restoration has been carried out for both a non-volcanic and volcanic margin with magmatic underplating. Based upon the results, Africa underwent extension of 65-105 km while Antarctic crust was stretched by 90-190 km. Both margins reveal a trend of increasing extension from east to west. Various models tested to determine the direction of extension during rifting suggest that Antarctica underwent a counter-clockwise rotation with respect to Africa during the period between 186-171 Ma.

TABLE OF CONTENTS

List of Figures	x
List of Tables	xiv
Chapter	Page
1. Introduction	
1.1 Dispersal of Gondwana	1
1.2 Africa and Antarctica conjugate margins.....	3
1.3 Geophysical surveys in the Mozambique Basin and the Riiser Larsen Sea	12
1.4 Reconstruction models	18
1.5 Remaining issues.....	20
2. Data.....	23
2.1 Gravity.....	23
2.2 Magnetic	26
2.3 Topography and bathymetry	26
2.4 Sediment thickness	31
2.5 Age of the oceanic crust.....	31
2.6 Seismic data	37
2.7 Wells data.....	38
3. Methods	43
3.1 Rigid plate reconstruction	43
3.1.1 <i>Satellite-derived gravity enhancement</i>	45
3.1.2 <i>Magnetic isochron identification</i>	47
3.1.3 <i>Reconstruction poles</i>	49
3.2 Three-dimensional gravity inversion on the base of the crust	51
3.2.1 <i>Building topography, sediment thickness, sediment density and basement grids</i>	51

TABLE OF CONTENTS (Continued)

Chapter	Page
3.2.2 <i>Calculating isostatic Moho</i>	58
3.2.3 <i>Three-dimensional gravity inversion</i>	59
3.3 Non-rigid reconstruction	65
4. Results	
4.1 Fracture zones tracing	74
4.2 Magnetic isochron identification	82
4.3 Three-dimensional gravity inversion.....	92
4.4 Locations of the continent-ocean boundaries (COBs)	103
4.5 Rigid reconstruction	110
4.6 Non-rigid reconstruction	115
5. Discussion	134
5.1 Magnetic isochron identification	134
5.2 Rigid reconstruction	136
5.3 Alternatives models	147
5.4. Model assumptions and limitations.....	155
6. Conclusion	162
Bibliography	165
Appendix 1. Picked magnetic isochrons	177
Appendix 2. FORTRAN programs	182

LIST OF FIGURES

Figure	Page
1.1: Supercontinent Gondwana reconstructed by de Wit et al. (1988)	2
1.2: Gondwana plate reconstruction circuit	4
1.3: The Africa-Antarctica Corridor	7
1.4: Free-air gravity anomaly map showing geology of Mozambique Basin	8
1.5: Free-air gravity anomaly map showing geology of the Riiser Larsen Sea	10
1.6: Age correlation of crustal blocks of Africa and Antarctica	14
1.7: Geophysical surveys over the Mozambique Basin	15
1.8: Geophysical surveys over the Riiser Larsen Sea	27
1.9: Previous reconstruction models	22
2.1: Free-air gravity anomaly grid from Sandwell et al. (2014)	24
2.2: Locations of ship tracks from NGDC that collected gravity data in study areas..	25
2.3: Magnetic anomaly profile data over the Mozambique Basin	27
2.4: Magnetic anomaly profile data over the Riiser Larsen Sea	28
2.5: World Digital Magnetic Anomaly Map (Maus et al., 2007)	29
2.6: 5-arc minute grid of the Global Terrain Base from NGDC	30
2.7: 30-arc second grid of the Gtopo30 topography from USGS	32
2.8: 1-degree grid of global sediment thickness	33
2.9: 5-arc minute grid of global marine sediment thickness	34
2.10: Published depth-to-basement map over the Riiser Larsen Sea	35
2.11: Published depth-to-basement map over the Mozambique Basin	36
2.12: 2-arc minute grid of the age of the ocean crust	39
2.13: Available seismic and well data in the study areas	40
2.14: Zoom in view of the wells locations over the Mozambique Basin	41
3.1: Cross sectional diagrams showing the concepts of rigid and non-rigid reconstructions	44

3.2: Merged topography/bathymetry grid	53
3.3: Merged sediment thickness grid	54
3.4: Calculated sediment density grid	56
3.5: Depth-to-basement grid derived from global sediment thickness	57
3.6: Local depth-to-basement grid derived from seismic controls in the Mozambique Basin	60
3.7: Calibrated depth to basement grid	61
3.8: Calibrated sediment density grid	62
3.9: Difference between calibrated and un-calibrated depth to basement grids	63
3.10: Diagram illustrating the concept of isostasy	64
3.11: Isostatic Moho	66
3.12: Isostatic Moho constrained by seismic refraction data	67
3.13: Crustal thickness model derived from constrained isostatic Moho	68
3.14: Illustration of areal-balancing method used in non-rigid reconstruction	73
4.1: Tilt derivative of 5 km residual gravity anomaly over the Mozambique Basin	76
4.2: Tilt derivative of 30 km residual gravity anomaly over the Mozambique Basin	77
4.3: Tilt derivative of 90 km residual gravity anomaly over the Mozambique Basin	78
4.4: Tilt derivative of 5 km residual gravity anomaly over the Riiser Larsen Sea	79
4.5: Tilt derivative of 30 km residual gravity anomaly over the Riiser Larsen Sea	80
4.6: Tilt derivative of 90 km residual gravity anomaly over the Riiser Larsen Sea	81
4.7: Identified magnetic isochrons over the Mozambique Basin	83

4.8: Identified magnetic isochrons over the Riiser Larsen Sea	84
4.9: Correlation of magnetic anomaly profiles over the Mozambique Basin	86
4.10: Correlation of magnetic anomaly profiles over the Mozambique Basin (continued)	87
4.11: Correlation of magnetic anomaly profiles over the Mozambique Basin (continued)	88
4.12: Correlation of magnetic anomaly profiles over the Mozambique Basin (continued)	89
4.13: Correlation of magnetic anomaly profiles over the Riiser Larsen Sea	90
4.14: Correlation of magnetic anomaly profiles over the Riiser Larsen Sea (continued)	91
4.15: Free-air gravity anomaly calculated from inversion model	93
4.16: Observed Free-air gravity anomaly	94
4.17: Error Free-air gravity anomaly	95
4.18: Depth to Moho map generated by gravity inversion	98
4.19: Difference between inverted Moho and isostatic Moho	99
4.20: Crustal thickness model calculated from gravity inversion	100
4.21: Comparison of crustal thickness derived from gravity inversion and P-wave modeling over the Mozambique Basin	101
4.22: Comparison of crustal thickness derived from gravity inversion and 2-D gravity modeling over the Riiser Larsen Sea	102
4.23: Antarctic COB overlay on magnetic and crustal thickness maps	107
4.24: African COB overlay on magnetic map	108
4.25: Africa COB overlay on crustal thickness map	109
4.26: Plate reconstruction to M0r (124.8 Ma)	111
4.27: Plate reconstruction to M10n (133.7 Ma)	112
4.28: Plate reconstruction to M22n1n (149.5 Ma)	113

4.29: Reconstruction of the conjugate COBs (171Ma)	114
4.30: Construction of N-S 2-D profiles over the African margin	116
4.31: Construction of N-S 2-D profiles over the Antarctic margin	117
4.32: Non-rigid reconstruction in a N-S direction	119
4.33: Construction of NW-SE 2-D profiles over the African margin	121
4.34: Construction of NW-SE 2-D profiles over the African margin	122
4.35: Non-rigid reconstruction in a uniform NW-SE direction	123
4.36: Construction of 2-D profiles in non-uniform NW-SE direction over the African margin	126
4.37: Construction of 2-D profiles in non-uniform NW-SE direction over the Antarctic margin	127
4.38: Non-rigid reconstruction with a clockwise rotation of Antarctica	128
4.39: Correlation of magnetic anomalies over the Africa and Antarctica continents at 186 Ma	129
5.1: Comparison of magnetic isochrons from this study with previous works	135
5.2: Relative positions of the Beira High and the southern Astrid Ridge at 158 and 162 Ma	138
5.3: Alternative COBs overlay on the magnetic anomaly maps over the Mozambique Basin and the Riiser Larsen Sea	141
5.4: Alternative COBs overlay on the crustal thickness maps over the Mozambique Basin and the Riiser Larsen Sea	143
5.5: Non-rigid fit results from using the alternative COBs	144
5.6: Free-air gravity anomaly over the Mozambique Coastal Plain	146
5.7: Plate reconstruction at 162 and 166 Ma assuming a continental Beira High ..	148
5.8: Rigid-reconstructions to accommodate a continental Beira High	149
5.9: Correlation of the modified African COB to magnetic anomalies and crustal thickness	152

5.10: Correlation of the modified Antarctic COB to magnetic anomalies and crustal thickness	154
5.11: Non-rigid reconstruction assuming non-volcanic margins	158
5.12: Contours of 40, 42, 44, and 46 km crustal thickness over the Africa continent	160
6.1: Recap of plate reconstruction sequence from 124.8 Ma to 186 Ma	164

LIST OF TABLES

Table	Page
2.1: Published wells information over the Mozambique Basin	42
3.1: Parameters used to generate synthetic seafloor spreading model	50
3.2: Layer densities used in gravity inversion model	50
3.3: Sclater's factor used to scale the isostatic calculation based on crustal age	69
3.4: Relationship between amount of SDR and underplating from volcanic margins	72
4.1: N-S profiles information	130
4.2: Uniform NW-SE profiles information	131
4.3: Non-uniform NW-SE profiles information	132
4.4: Total reconstruction poles for Antarctica with respect to Africa	133
5.1: Impact of using different values for the initial crustal thickness on locations, of the pre-rift boundaries over the conjugate margins of Africa and Antarctica	161

CHAPTER 1

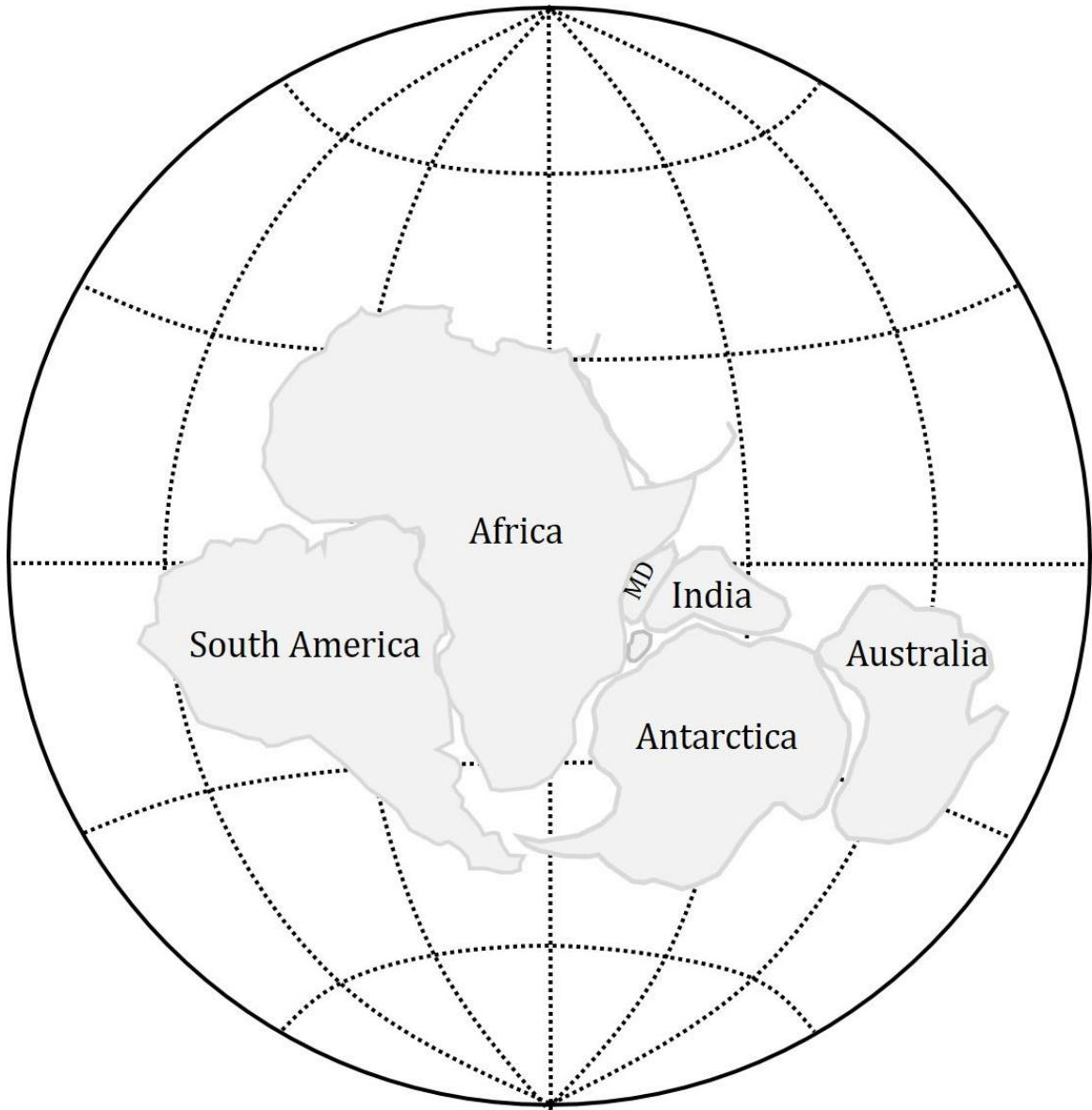
INTRODUCTION

1.1 Dispersal of Gondwana

Pangea, the most recent supercontinent, formed around 300 Ma and reached its stable configuration during the Late Triassic (Stampfli et al., 2013). Gondwana was a major part of Pangea consisting of the continents and continental blocks of South America, Africa, Madagascar, India, Sri Lanka, Antarctica and Australia (Figure 1.1). The Mesozoic break up of Gondwana that subsequently formed the Indian Ocean was initiated by continental rifting between Africa and Antarctica during the late Early Jurassic (Cox, 1992; Reeves and Wit, 2000; Eagles and Konig, 2008). Several geophysical datasets have enabled various scholars to study the kinematic movement of the sub-continents within Gondwana since its breakup (Bergh, 1977; Norton and Sclater, 1979; Martin and Hartnady, 1986; Roeser et al., 1996; Jokat et al., 2003; Eagles and Konig, 2008; Leinweber and Jokat, 2012). General timing for the breakup of Gondwana can be summarized as follows:

- Africa-Antarctica: ~166 Ma (Leinweber and Jokat, 2012)
- Madagascar-Africa: ~166 Ma (Eagles and Konig, 2008; Rabinowitz et al., 1983)
- South America-Africa: ~130 Ma (Reeves and de Wit, 2000)
- India-Antarctica: ~130 Ma (Gaina et al., 2007)
- Australia-Antarctica: ~84 Ma (Ball et al., 2013; Totterdell et al., 2000)

Figure 1.1: Supercontinent Gondwana reconstructed by de Wit et al. (1988). Gondwana was part of the supercontinent Pangea until its dispersal in the Late Jurassic when breakup between Africa and Antarctica began. MD: Madagascar. Sri Lanka is not labelled and is located south of Madagascar.

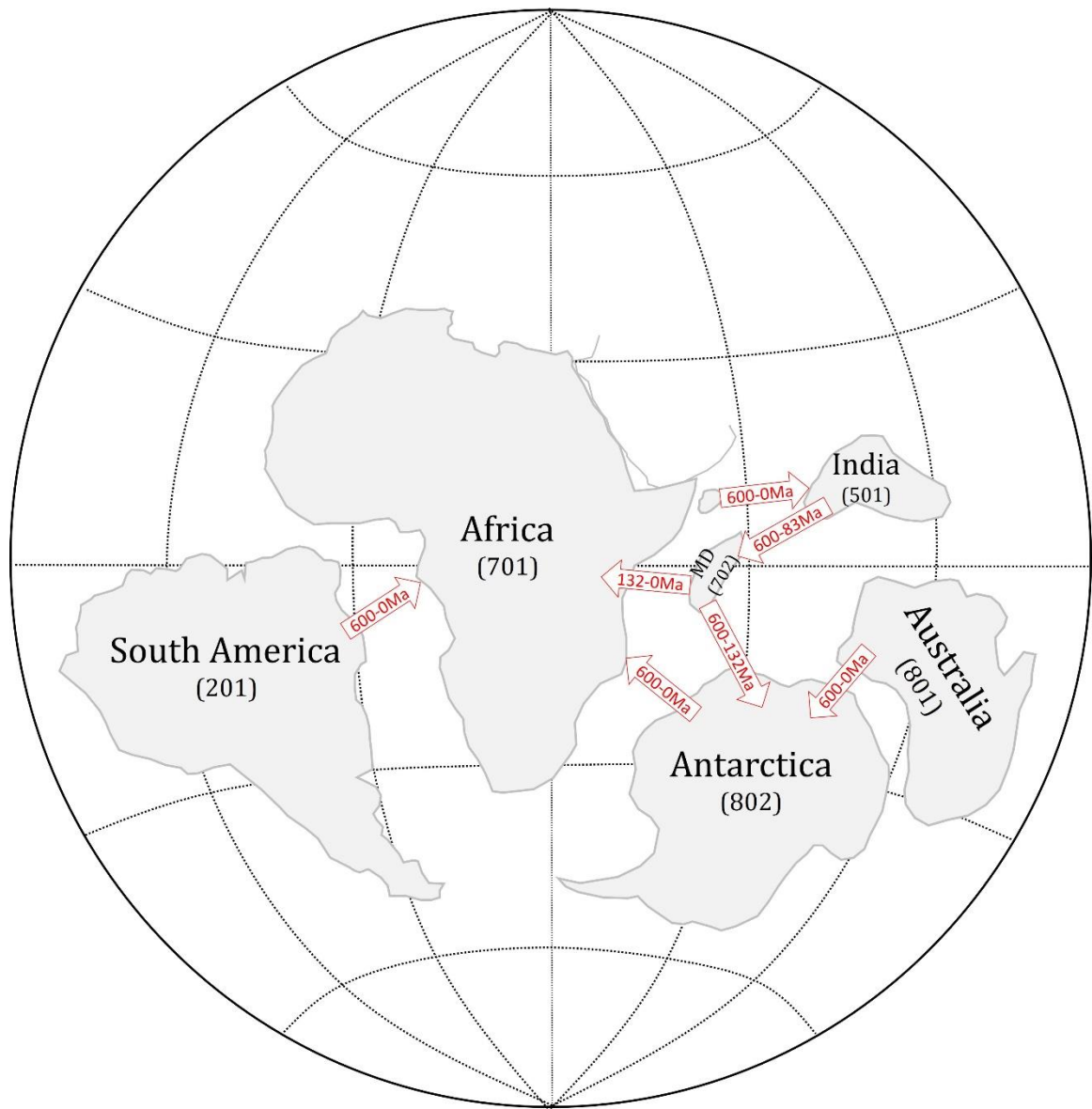


The Mesozoic breakup of Gondwana was associated with the Karoo and Ferrar volcanic events. These events are interpreted to have originated from a large scale mantle plume which was active during the period between 184 and 174 Ma (Cox, 1992; Duncan et al., 1997; Jordan, 2007). Remnants of Karoo volcanism are mostly located onshore Africa while the Ferrar igneous province is situated in east Antarctica. Due to the temporal proximity between these volcanic events and timing of continental break up, it has been postulated that they are the driving force behind continental rifting and subsequent drifting of Gondwana's sub-continents (Encarnacion, 1996; Duncan, 1997).

1.2 Africa and Antarctica conjugate margins

Although there is a consensus on the general timing and geometry of Gondwana breakup, various issues remain regarding the details of their kinematic plate movements. Central to these issues is the pre-rifting fit between Africa and Antarctica as well as their respective positions at the onset of sea-floor spreading (Jokat et al, 2003; Leinweber and Jokat, 2012). In most of reconstruction models, Africa and Antarctica are considered as anchor plates to either of which other continents within Gondwana are tied to (Seton et al., 2012) (Figure 1.2). Thus, the separation between Africa and Antarctica plays an important role in understanding the dispersal of Gondwana as a whole. Nevertheless, a complete reconstruction of Africa and Antarctica conjugate margins remains challenging due to two main difficulties. First, there is a lack of high-quality geophysical data necessary to determine the location and age of the oldest oceanic crust. Second, it is difficult to estimate the amount and

Figure 1.2: Illustration showing the reconstruction circuit among continents of Gondwana from Seton et al. (2012). Red arrows point to the anchor plates with red numbers indicate the time interval during which a particular plate is reconstructed with respect to its anchor plate. Numbers in parentheses are plate identification numbers assigned in Gplates. Note that every continent of Gondwana is tied to either Africa or Antarctica which in turn are linked together in the reconstruction model



distribution of extended continental crust. Evidence for the separation between Africa and Antarctica is found in the Africa-Antarctica Corridor (AAC). Figure 1.3 shows the north-south extent of the AAC which runs from the Mozambique Basin offshore of Mozambique to the Riiser Larsen Sea off the coast of Antarctica. The Mozambique ocean basin is located along the southeast African margin off the coast of Mozambique. It is bounded by the Madagascar Ridge to the east and the sub-aerial Mozambique Ridge to the west. The West Somali Basin is situated north of the Mozambique Basin and connected by the Mozambique Channel. The Mozambique Basin extends over an area of approximately $1 \times 10^6 \text{ km}^2$ beneath water depths ranging from a few meters to more than 5500 m. This basin formed as a result of the separation of Antarctica from Africa starting in the Middle Jurassic (Konig and Jokat, 2010). The southern coast of the Riiser Larsen Sea, off Antarctica, is considered to be the conjugate margin of the Mozambique Basin's northern coast. It covers an area of approximately $8 \times 10^5 \text{ km}^2$ from shoreline to deep water region ($\sim 6000 \text{ m}$). The Riiser Larsen Sea is bounded by the Astrid Ridge in the west and the Gunnerus Ridge in the east.

The linkage between the Mozambique Basin and the Riiser Larsen Sea is revealed by traces of fracture zones within the AAC. Figure 1.4 displays important geological features surrounding the Mozambique Basin. One feature that stands out in most reconstructions is the subaerial Mozambique Ridge. The structure and origin of this ridge is still a matter of speculation. Whether it is an oceanic plateau or a continental

fragment affects the reliability of various models as a continental ridge often yields an overlap on the Antarctic continent. Several studies have presented conflicting support for either continental or oceanic origin for the Mozambique Ridge (Leinweber and Jokat, 2011; König and Jokat 2010; Tucholke et al, 1981; Simpson et al., 1974; Hales and Nation, 1973, Chetty and Green, 1997). In general, interpretation of potential field and seismic data suggests an oceanic origin of the ridge (Leinweber and Jokat, 2011; König and Jokat, 2010, Hales and Nation, 1973). Strongest support for a continental Mozambique Ridge are the dredged samples along the edge of the ridge which show characteristics of Africa Precambrian rocks (Mougenot et al., 1991; Hartnady et al., 1992; Ben-Avraham, 1995) even though there is no radiometric dating available for these samples. An oceanic core surrounded by continental fragments has also been proposed to explain the structure of the ridge (König and Jokat, 2010). Besides the Mozambique Ridge, the Beira High is another significant structure, whose origin is also debated. Detailed gravity modelling from Watts (2001) points to a thickened oceanic crust flooring the Beira High whereas seismic reflection study of Mahanjane (2012) suggests this is a continental structure. The composition of the Beira High is crucial in restoring the conjugate margins of Africa and Antarctica since it controls the determination of the location of continent-ocean boundary in the Mozambique Basin. To the eastern end of the basin is the Madagascar microplate along with the Davie Fracture Zone which is considered as a fossil transform fault that has accommodated the southward drifting of Madagascar from Africa in the Late Jurassic (Rabinowitz et al., 1983).

Figure 1.3: Location map, overlay of topography (NGDC and USGS), showing the Africa-Antarctica Corridor (AAC) extending from the Mozambique Basin to the Riiser Larsen Sea. This zone contains oceanic crust formed during the drifting of Antarctica from Africa. Dashed white boxes indicate locations of the Mozambique Basin in the north and the Riiser Larsen Sea in the south with their adjacent onshore areas. MZR: Mozambique Ridge, MP: Madagascar Plateau, AR: Astrid Ridge, GR: Gunnerus Ridge

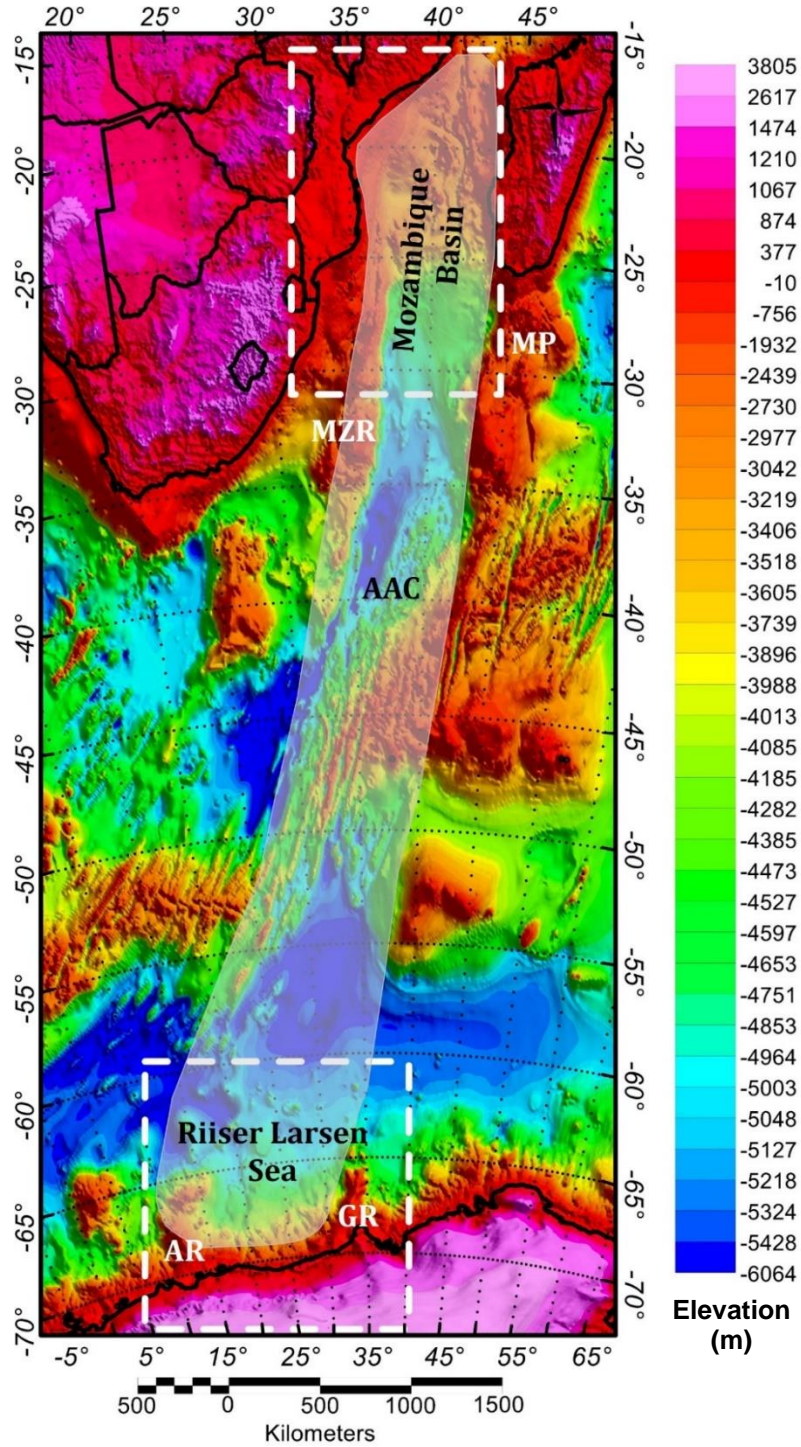
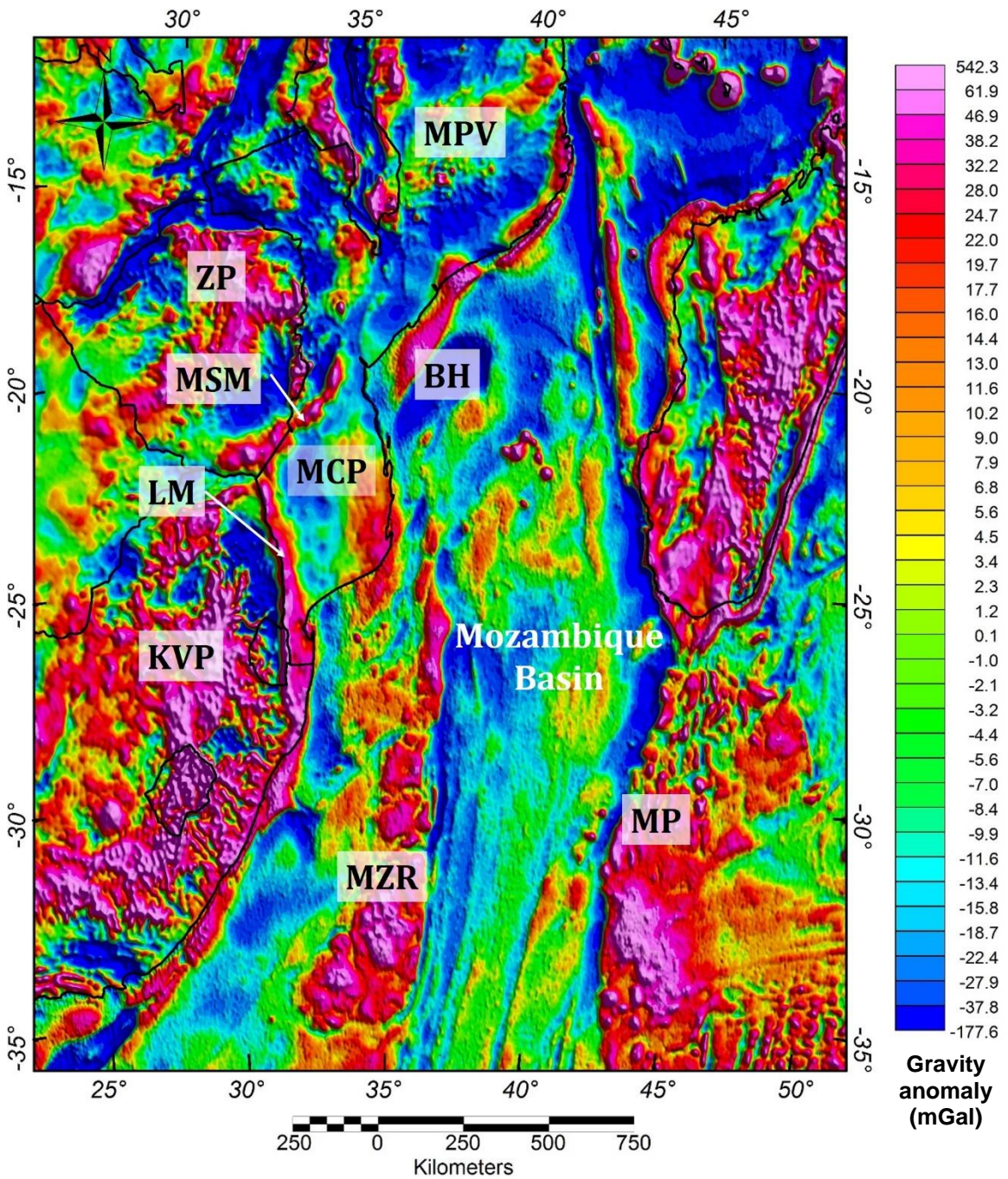


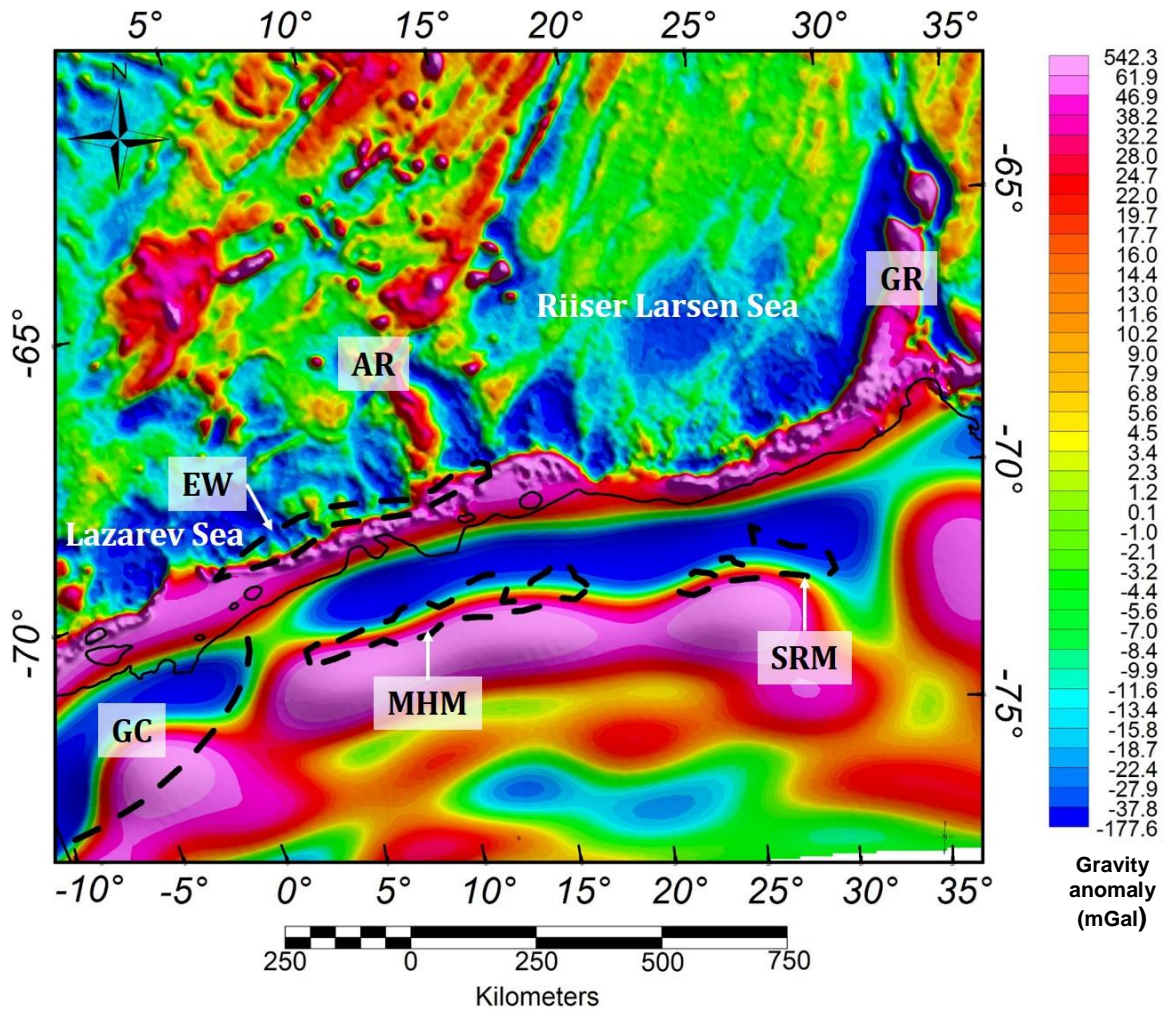
Figure 1.4: Free-air gravity anomaly map (Sandwell et al., 2014) of the Mozambique Basin and its adjacent structures. BH: Beira High, LM: Lebombo Monocline, KVP: Kaapvaal Province, MCP: Mozambique Coastal Plain, MP: Madagascar Plateau, MPV: Mozambique Province, MSM: Mateke-Sabi Monocline, MZR: Mozambique Ridge, ZP Zimbabwe Province.



Onshore Africa geology adjacent to the Mozambique Basin includes the Mozambique Province and the Mozambique Coastal Plain. The Mozambique Province is described as a cratonic terrain consisting of igneous and metamorphic basement, meta-sedimentary and meta-volcanic sequence that date back to as far as 1000 Ma (Groenewald et al., 1991). This was initially an area of intense folding and thrusting from 1000 to 500 Ma at which time folding became gentle. On the other hand, the Mozambique Coastal Plain (MCP) is covered by sedimentary layers that postdate the Karoo volcanism (184-174Ma). The underlying crust of the MCP has been interpreted as thickened oceanic crust (Watts, 2001; Leinweber and Jokat, 2011; Eagles and Konig, 2008) and thinned continental crust (Konig and Jokat, 2010; Cox, 1992) or a mixture of both. Wells drilled at this area terminated against basalt layers that that speculated to be in the age range of 160-140 Ma (Flores, 1973; Kamen-Kaye, 1983). The MCP is bounded to the west and northwest by the Lebombo and the Mateke-Sabi Monoclines respectively. These are volcanic remnants of the Karoo eruptions. landward of these monoclines are the Zimbabwe and Kaapvaal provinces which have Archaean to mid-Proterozoic basement (Groenewald et al., 1991).

On the conjugate margin of Antarctica within the Riiser Larsen Sea, pronounced geologic features include the Astrid and Gunnerus Ridges (Figure 1.5). From seismic and potential field studies, the Astrid Ridge has been interpreted as an oceanic structure which is separated into a northern and southern parts by the Astrid Fracture Zone (Bergh, 1987; Roeser et al., 1996; Hinz et al., 2004., Jokat et al., 2004; Leinweber and Jokat, 2012). Leinweber and Jokat (2012) revealed that the two parts

Figure 1.5: Free-air gravity anomaly map (Sandwell et al., 2014) of the Riiser Larsen Sea area. AR: Astrid Ridge, EW: Explora Wedge SDR, GC: Grunehogna Craton, GR: Gunnerus Ridge, MHM: Muhlig-Hofmannfjella Mountain, SRM: Sor Rodane Mountain.



of the Astrid Ridge expressed significantly different magnetic signature and thus might have formed at different times or by different mechanisms. The Gunnerus Ridge marks the eastern boundary of the Riiser Larsen Sea and has been the subject of seismic and potential field studies (Saki et al., 1987; Hinz et al., 2004; Leitchenkov et al., 2008) as well as dredged samples (Saki et al., 1987). Continental crust is ascribed to the Gunnerus Ridge based on its top basement seismic velocity of 5.10-6.1 km/s and autochthonous metamorphic debris sample at the ridge (Leitchenkov et al., 2008; Saki et al., 1987). Different ages of volcanic extrusion in the form of seaward-dipping reflectors (SDRs) have also been identified in the adjacent Lazarev and Weddell Seas (Hinz et al., 2004; Jokat et al., 2004). The inner part of the SDR wedges in the Lazarev Sea were emplaced synchronously with the Karoo volcanism whereas its outer part and the SDRs in the Weddell Sea are younger (150-138 Ma) and formed long after seafloor spreading (Konig and Jokat, 2010). SDRs found in the Antarctic margins have been considered as conjugate features of the Lebombo and Mateke-Sabi Monoclines in different reconstruction models (Cox, 1992; Martin and Hartnady, 1986; Konig and Jokat, 2010), Leinweber and Jokat, 2012).

Figure 1.5 also lays out the general onshore geology of Antarctica in the area close to the Riiser Larsen Sea. Three different age groups were recorded (Granham et al., 2008; Marschall et al., 2010) for various crustal blocks in this region. The Grunehogna Craton at the eastern end of the Lazarev Sea consists of basement rocks older than 3000 Ma. Age and lithology of this terrain are similar to those found in the Kaapvaal Province in southeast Africa. The Dronning Maud Land in the area landward from the

Riiser Larsen Sea comprises several mountain terrains including the Muhlig-Hofmannfjella and Sor Rodane mountains. These are basement structures that display rocks with two distinctive age ranges. Areas closer to shore and extending eastward shows age range of 500-650 Ma while further landward and westward structures are much older (1000-1200 Ma). Figure 1.6 illustrates a schematic correlation of the crustal blocks in both southeast Africa and east Antarctica.

1.3 Geophysical surveys in the Mozambique Basin and the Riiser Larsen Sea

In 1970s, one of the first geophysical studies in the Mozambique Basin was carried out by French expeditions that acquired seismic and marine magnetic data (Segoufin, 1978). This effort was followed by various expeditions from the United States and the Republic of South Africa that introduced additional magnetic anomaly data for the central Mozambique Basin (Simpson et al., 1979). Throughout the following years, different ships transiting through the basin had collected considerable amount of magnetic data which are now available through the National Geophysical Data Center. Note that these data were difficult to interpret since they were surveyed by different ships that transited across the basin in rather random paths. A systematic 16000-km magnetic and gravity survey was conducted by the Alfred Wegener Institute (AWI) in 2005 that extended data cover to the northern and eastern part of the basin (Konig and Jokat, 2010). In 2007, a French research project also conducted magnetic and refraction surveys in a systematic manner in the northern Mozambique continental margin closer to the coast line (Leinweber et al., 2013). Chetty and Green (1977) provided an overview and interpretation of vintage seismic refraction data on the

Mozambique Ridge and adjacent areas. Figure 1.7 summarizes the magnetic and refraction data collected in the Mozambique Basin

Bergh (1977, 1987) presented interpretation of the first seismic and magnetic data in the Riiser Larsen Sea acquired by the South African National Antarctic Expedition. This was then followed by numerous research expeditions from various countries and institutions. 450 km of high resolution seismic reflection data across the southern Astrid Ridge were collected by the Indian Antarctic Expedition in 1981 (Leitchenkov et al., 2008). In 1978, the Federal Institute for Geosciences and Natural Resources of Germany (BGR) carried out survey across the Lazarev Sea and the western RSL that resulted in 1500 km of multichannel seismic data (Hinz and Krause, 1982). Areas of the eastern RSL and the Gunnerus Ridge was surveyed during research by the Japan National Oil Corporation in 1985. From that expedition, a combined 2500 km of multichannel seismic, magnetic and gravity data were collected (Leitchenkov et al., 2008). Geophysical data were acquired in the central Riiser Larsen Sea and over Gunnerus Ridge during the joint expedition of the BGR and the AWI in 1990. Jokat et al. (2004) published the results for their interpretation of more than 10000 km of multichannel seismic, gravity and magnetic data in the Lazarev Sea and the Riiser Larsen Sea. In 1999, AWI conducted a dense, systematic aeromagnetic survey in the central Riiser Larsen Sea (Jokat et al., 2003). Leinweber and Jokat (2012) reported one a study of the new potential field data over the Astrid Ridge acquired by the AWI in 2010. Leitchenkov et al. (2008) synthesized all geophysical data in the area of the Riiser Larsen Sea (Figure 1.8).

Figure 1.6: Schematic correlation of crustal blocks between Africa and Antarctica. Closing the ocean basin along the ACC brings Antarctica to a location that allows an age correlation of the crustal provinces between the two continents. Red hatchures indicate marginal areas of the Mozambique Basin and the Riser Larsen Sea and the Riser Larsen Sea. Map modified from Grantham et al. (2008).

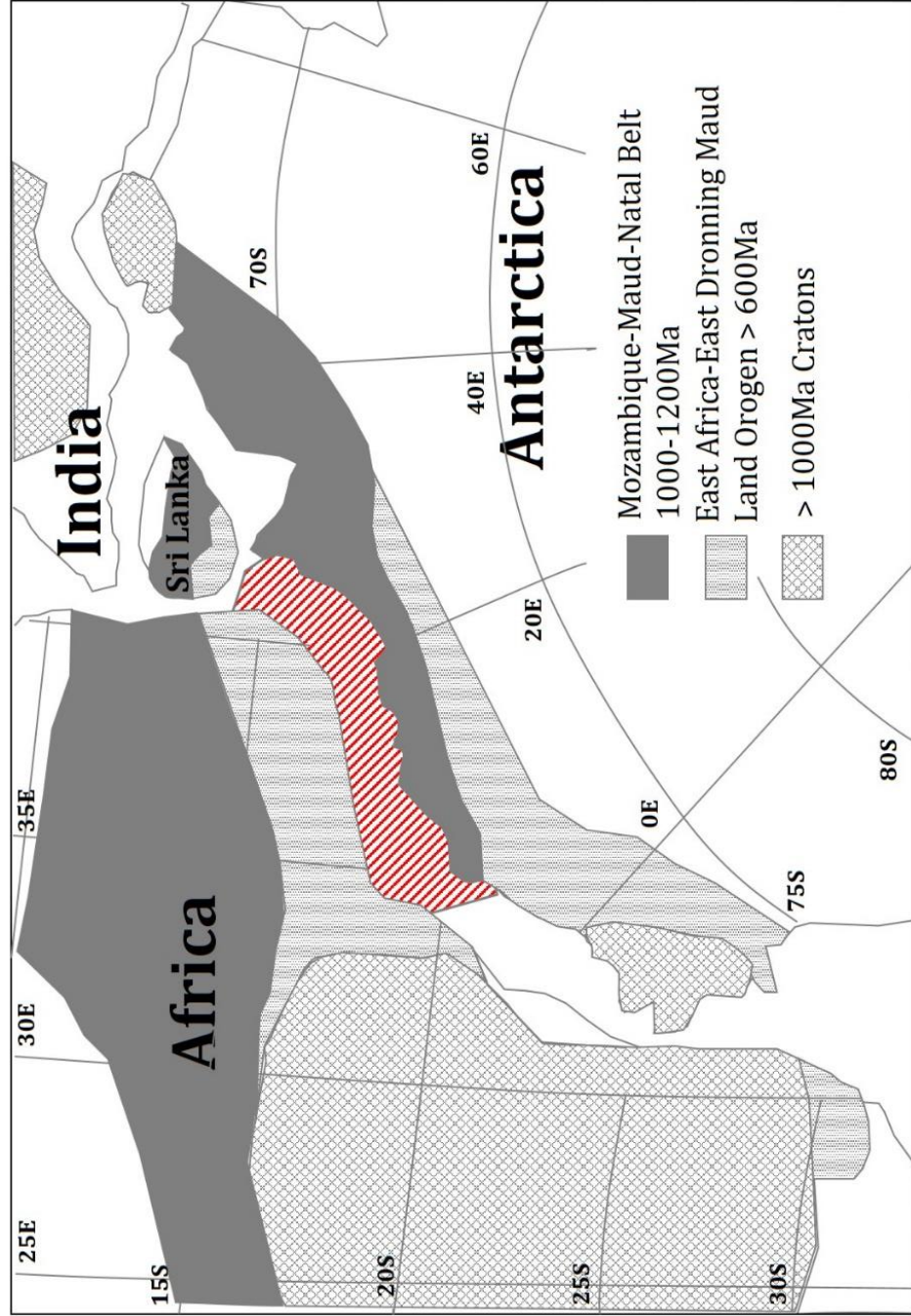


Figure 1.7: Geophysical data collected in the Mozambique Basin and adjacent areas include seismic reflection, seismic refraction, magnetic, gravity and topography. Black triangles are seismic refraction stations from published sources (Chapter 2). Blue lines are ship tracks from the NGDC that collected gravity, magnetic and topography data (see Chapter 2). Orange lines are seismic reflection profiles (Mahanjane, 2012). Magnetic anomaly profiles from Simpson et al. (1979) and Segoufin (1978) are shown in red. Green lines represent magnetic anomaly data from the AWI that were used in (Konig and Jokat, 2010; Leinweber and Jokat, 2012). Thin lines are bathymetric contours at 1000-m interval

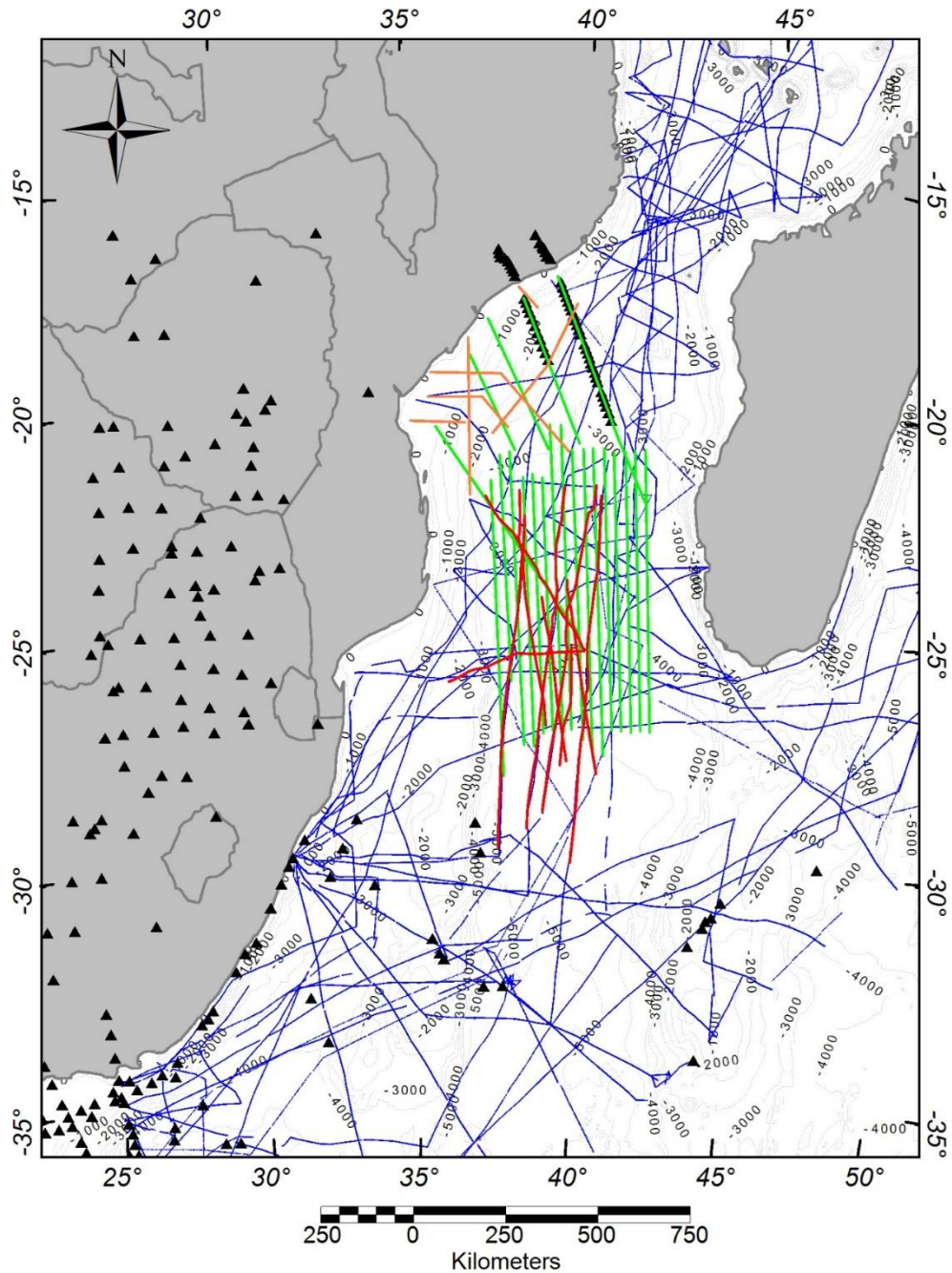
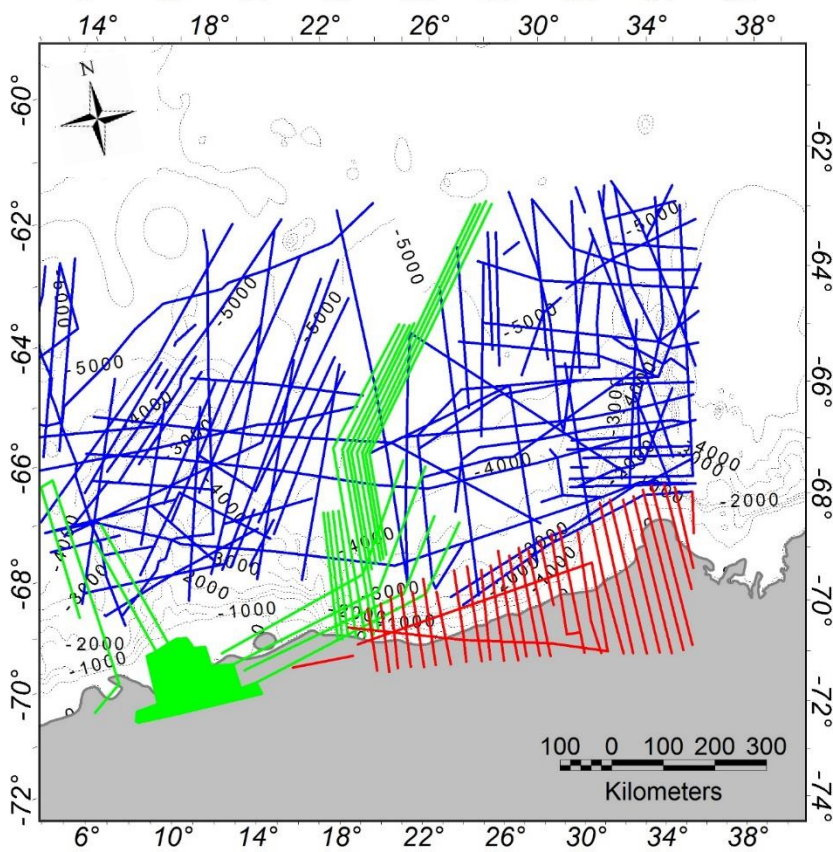
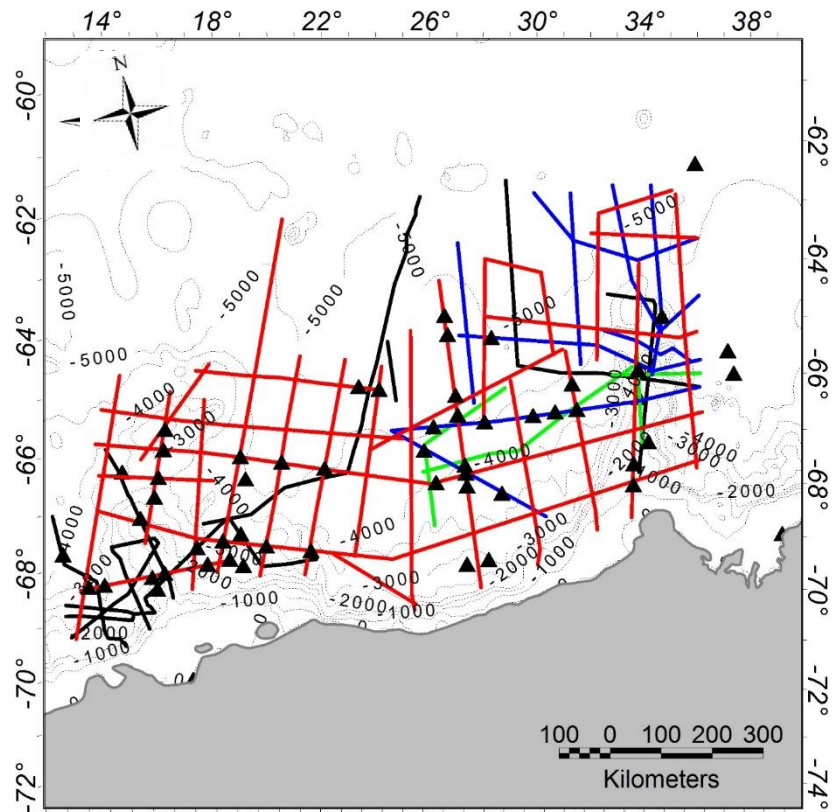


Figure 1.8: Compilation of geophysical data in the Riiser Larsen Sea area as synthesized by Leitchenkov et al. (2008). Upper map shows multichannel seismic reflection (lines) and refraction (triangles) data. Colors indicate countries that conducted surveys: red-Russia, green-Japan, black-Germany and blue is Norway-Russia). Airborne geophysical surveys are shown in the lower map: red-Russian, green-German. Blue lines are marine magnetic surveys from various sources. Thin lines are bathymetric contours at 1000-m intervals.



1.4 Reconstruction models

Considerable amount of effort has been devoted to reconstructing the conjugate margins of Africa and Antarctica. The following is a review of a few models that yield different results from interpretation of various geophysical data. One of the earliest reconstruction models was published by Martin and Hartnady (1986). Their model was based on the magnetic anomalies in the Riiser Larsen Sea and the Mozambique Basin as reported in Bergh (1977), Segoufin (1978) and Simpson et al. (1979). In this model, Africa and Antarctica were restored to magnetic anomaly M21 (145 Ma) essentially placing the continental margin of east Antarctica on to the Mozambique Coastal Plain and against the Lebombo Monocline. The early plate motion was described as a southward drift of Antarctica along a pair of transform faults: the Davie Fracture Zone in the east and a postulated parallel transform fault stretching from the Lebombo Monocline seaward into the Northern Natal Valley (NNV) in the west. The MZR was treated as an oceanic plateau and therefore produced no overlap in the final reconstruction. New magnetic data were interpreted in the study of Roeser (1996) where anomalies M24 were identified as the oldest isochrons in the Riser Larsen Sea. However, the model was reconstructed to 150 Ma using mainly anomalies M22 in the Somali Basin. From there, the age of continental break up was computed to be 165 Ma using a fixed spreading rate and the amount of opening of the margin between M25 and an assumed initial fit position. This model shows large overlap of Antarctica onto Africa and the MZR. Marks and Tikku (2001) adopted the finite rotation at 165 Ma from Livermore and Hunter (1996) to achieve a pre-breakup fit in which the MZR is

placed within the area of the present MCP. Here, they incorporated an extinct spreading center in the NNV which lasted from 133 to 125.3 Ma as was interpreted by Tikku et al. (2002). Moreover, the MZR was considered as a continental fragment and thus moved as an independent plate during the time between M11 to M2. The proposal of an extinct ridge in the NNV helped resolve the issue of overlapping MZR onto Antarctica in previous reconstructions. Reconstructing the conjugate margins using polar-wander path has also been attempted. Schettino and Scotese (2005) used paleomagnetic data to calculate the polar-wander path for multiple continents resulting in a fit of Africa and Antarctica at M25 (154.23 Ma) with significant amount of oceanic crust remains unaccounted for. New magnetic anomaly data enabled Jokat et al. (2003) to confirm the oldest oceanic crust in the RSL formed around 155 Ma which was consistent with previously identified anomaly M24 (Roeser, 1996). As a result, Africa and Antarctica were restored to 155 Ma leaving a significant gap between the margins. While most of the previously mentioned models produce good fits of the conjugate magnetic isochrons, their synthetic flowlines which are generated from rotation poles do not match well with the fracture zones over the margins (Eagles and Konig, 2008). By re-interpreting the previous magnetic data from Jokat et al. (2003), Eagles and Konig (2008) presented a model that simultaneously fits the conjugate magnetic anomalies and matches the flowlines with fracture zones. Antarctica was restored to Africa to a pre-rift position at time between 183-177 Ma based on gravity isochrons (Eagles and Konig, 2008). This model resulted in a full overlap of the MZR onto the MCP. The most recent studies regarding

the original fit of Gondwana include König and Jokat (2010) and Leinweber and Jokat (2012). The former study presented new magnetic data set in the Mozambique Basin where oldest anomalies were identified as M26 (155.3 Ma). Breakup between Africa and Antarctica was described as a direct southward drifting of Antarctica at around 160 Ma. The MZR was produced as excess volcanism during a series of ridge jumps. The SDR wedge in the Lazarev Sea was considered as conjugate feature of the Lebombo Monocline in Africa. Interpreting the same data set, Leinweber and Jokat (2012) identified magnetic anomalies M33 (159.08 Ma) and M41 (166 Ma) in the northern Mozambique Basin. In their reconstruction, initial breakup of Gondwana proceeded in two stages. During the first stage, from the original fit as postulated by Cox (1992) on the basis of geologic correlations, Antarctica rotated counter-clockwise with respect to Africa until M33. The second stage continued as Antarctica began its southward drifting. Figure 1.9 illustrates reconstruction models from several studies mentioned previously.

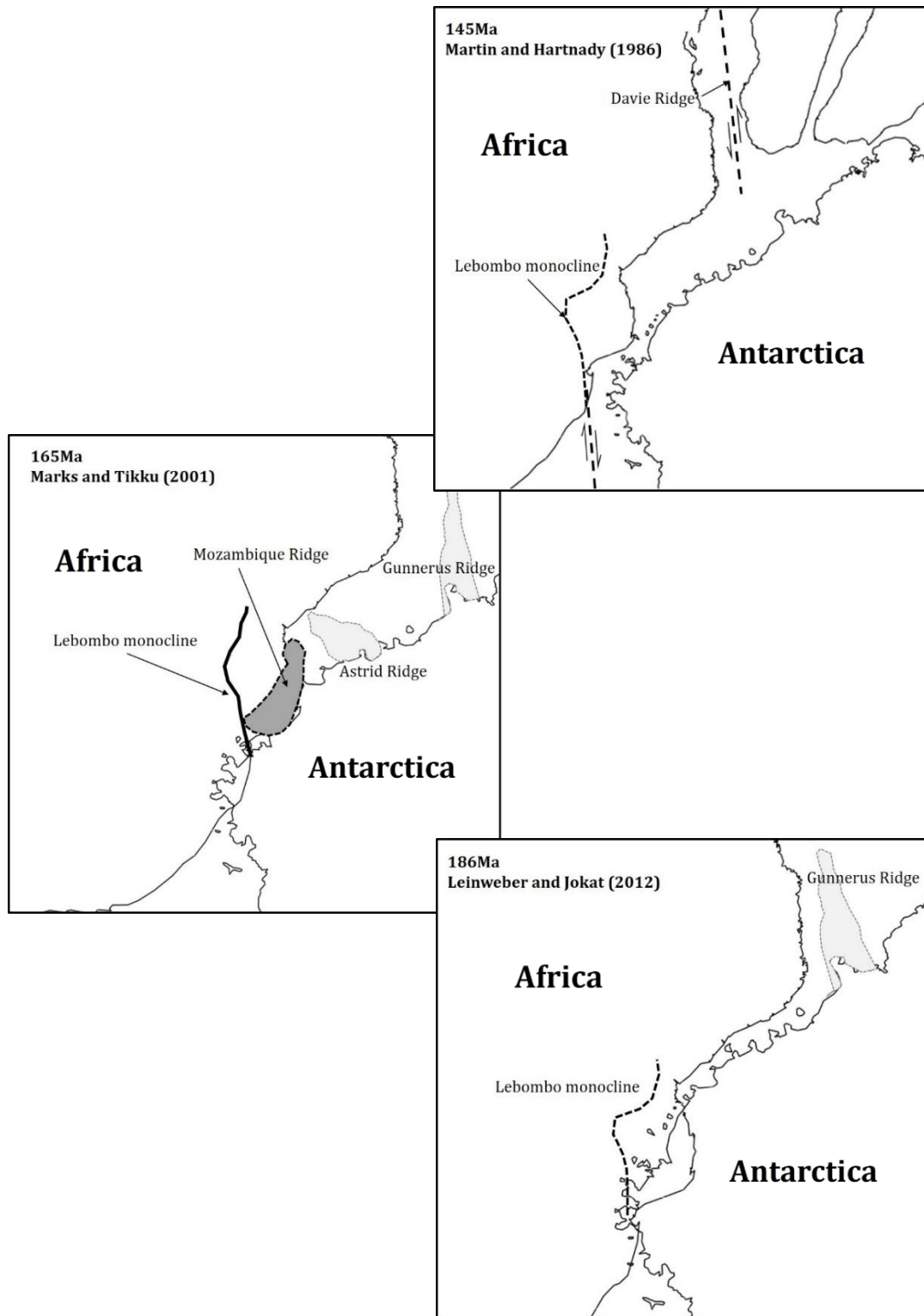
1.5 Remaining issues

Though tremendous efforts have been devoted into decoding the breakup history of Gondwana, there are still gaps in our knowledge regarding the timing and geometry of the breakup. This is especially true in restoring the African and Antarctic margins. Each of the previous studies contains some extent of uncertainties and contradictions. Each study proposes a different picture of how and when continental drift took place. The final fit of the conjugate margins has been based mainly on visual

kinematic fit or geological correlation. Up to this point, no quantitative study to account for the extension during rifting has been conducted.

This study re-examines the magnetic anomalies to determine the COB in the east African margins along the Mozambique Basin and the Riiser Larsen Sea in the conjugate margin of Antarctica. As a result, the margins are reconstructed to their orientation at the time immediately preceding seafloor spreading. Three-dimensional gravity inversion is used to construct a crustal thickness model for both conjugate margins. Consequently, the amount of continental stretching is quantified and the two continents are restored back to their original position prior to rifting. This study also considers the volcanic nature of the margin and accounts for the presence of extrusive and intrusive magma in calculations for the restoration.

Figure 1.9: Reconstruction models for the breakup between Africa and Antarctica. See text for discussion on each model.



CHAPTER 2

DATA

With the exception of Figures 2.10 and 2.11, all maps shown in this chapter are projected using Albert equal-area conic projection with the following parameters: Datum: WGS84. Units: meters. Latitude origin: 0°. Longitude origin: 37°E. First parallel: 5°S. Second parallel: 65°S. False easting: 0. False northing: 0.

2.1 Gravity

The main gravity data used in this study were published in Sandwell et al. (2014). The new data set includes global marine free-air gravity calculated from geoid elevation measured by the Cryosat-2, Envisat-1 and Jason-1 satellites. A significant improvement from its previous version, this new satellite-derived gravity data set provides accuracy of 1.7 mGal at latitude less than 72° and 2-3 mGal at higher latitudes with horizontal resolution of 7 km. Figure 2.1 shows the data gridded in 1 arc-minute cell size with the onshore free-air gravity calculated from the EGM2008 geoid model (Pavlis et al., 2007). Supplemental to this data set are the gravity anomaly data acquired by research vessels. These ship tracks are from the National Geophysical Data Center (NGDC) data base which contains data collected by different cruises in the past decades. Figure 2.2 shows locations of the NGDC ship tracks that collected and processed gravity data over the study areas.

Figure 2.1: Satellite-derived marine free-air gravity anomaly map from Sandwell et al. (2014) in 1 arc-minute grid with the onshore free-air gravity calculated from EGM2008 geoid model (Pavlis et al., 2008). Dashed white boxes indicate locations of the Mozambique Basin in the north and the Riiser Larsen Sea in the south with their adjacent onshore areas.

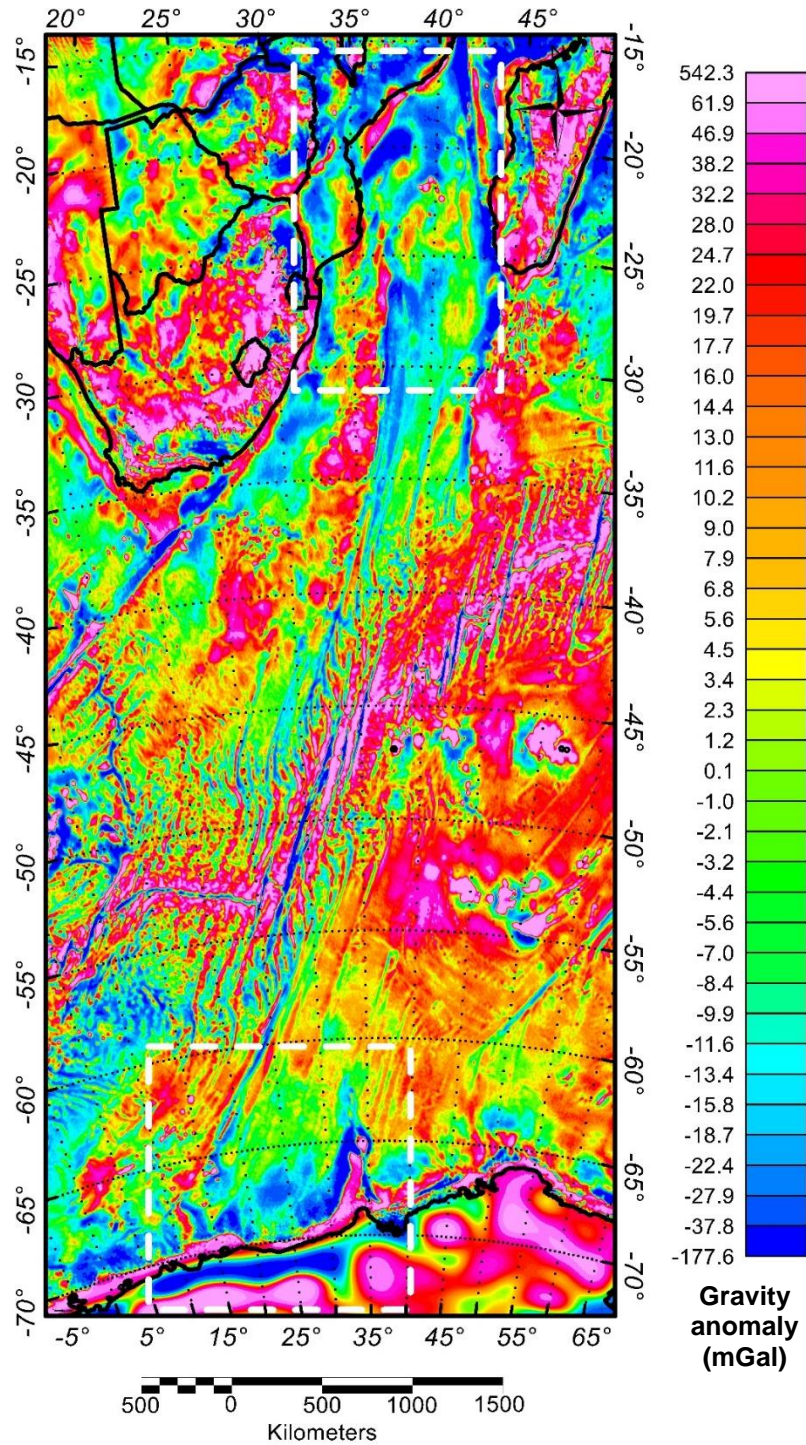
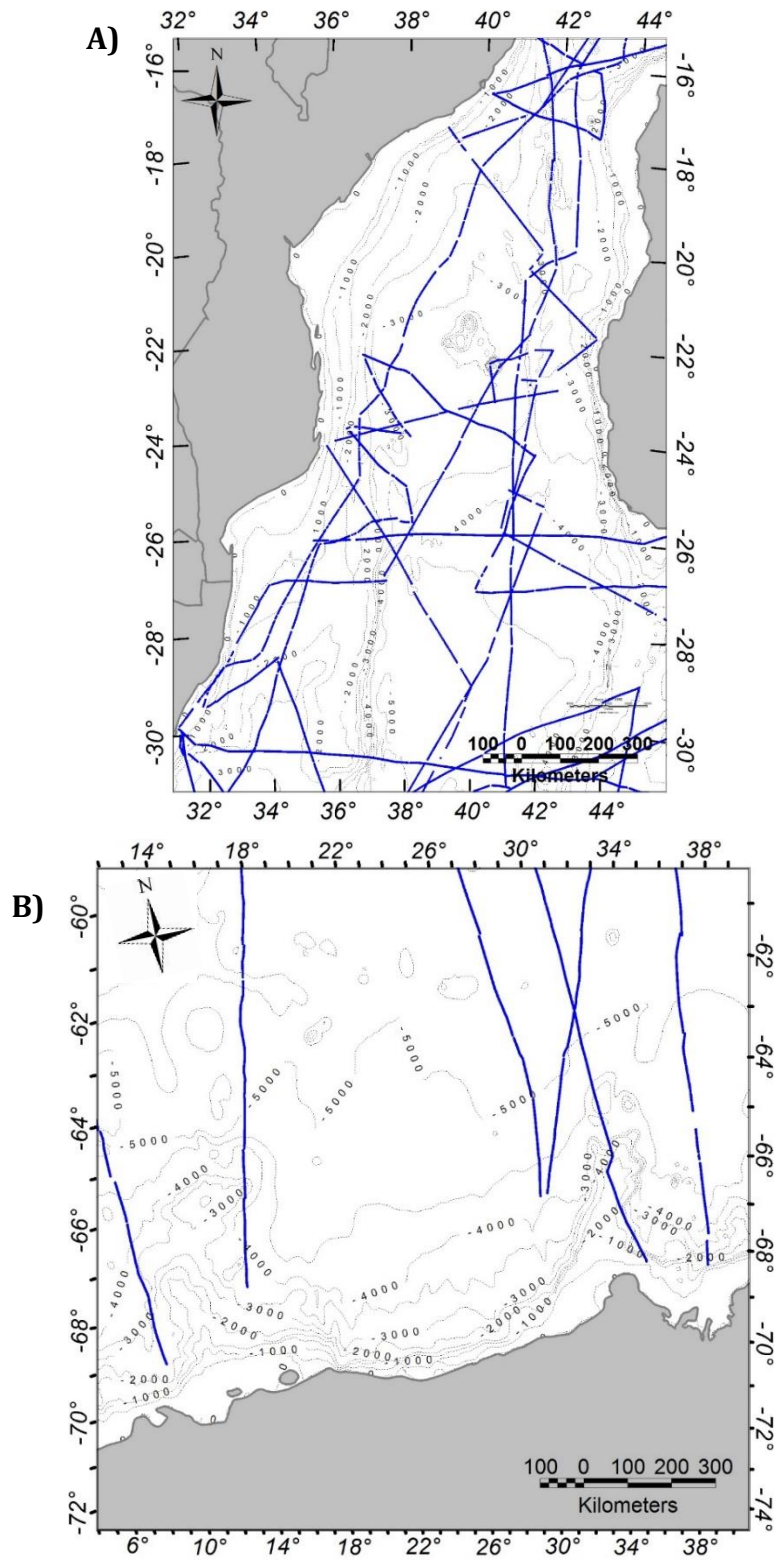


Figure 2.2: Locations of the NGDC ship tracks (blue lines) that collected gravity data in the Mozambique Basin (A) and the Riser Larsen Sea (B). Maps show bathymetry with contour interval of 1000 m



2.2 Magnetic

Several sources of magnetic data are available for this study. NGDC ship tracks that collected magnetic anomaly data are shown in Figures 2.3 and 2.4. Gridded magnetic data are also provided by the World Digital Magnetic Anomaly Map (WDMAM) which is a global compilation of satellite, airborne, marine and ground-based magnetic data sets. The NGDC provides access to the WDMAM in 3-arc-minute grid that represents Earth's magnetic anomaly at altitude of 5 km. This grid is a result of merging the long-wavelength satellite signal and short-wavelength near-surface measurement using Least-Squares Collocation (Maus et al., 2007). Included within the WDMAM is magnetic anomaly data collected by the Antarctic Digital Magnetic Anomaly Project (ADMAP) which compiled marine and airborne magnetic measurements in the Antarctic region in a 5-km-interval grid (Golynsky et al., 2002). The WDMAM is displayed in Figure 2.5. In addition to the mentioned data, magnetic anomaly profiles that have been published in the literature are also captured and utilized in this study (Figures 2.3 and 2.4). Also available to this study are the identifications of magnetic isochrons as well as poles of rotation from Leinweber and Jokat (2013) who studied the most updated magnetic anomaly profiles in the study areas.

2.3 Topography and bathymetry

Bathymetric constraint is taken from the Global Terrain Base grid available through the NGDC. This is a 5-arc-minute grid generated from multiple land surveys and marine depth soundings available up to 1988 (Figure 2.6). In conjunction,

Figure 2.3: Magnetic data available in the Mozambique Basin. Locations of the NGDC ship tracks (blue lines), published magnetic anomaly profiles from Leinweber and Jokat (2013) (orange lines), König and Jokat (2010) (green lines), Simpson et al. (1979) and Segoufin (1978) (red lines), Bergh (1977) (yellow lines). Black dots represent identified magnetic isochrons from Leinweber and Jokat (2012). Bathymetry is shown with contour interval of 1000 m.

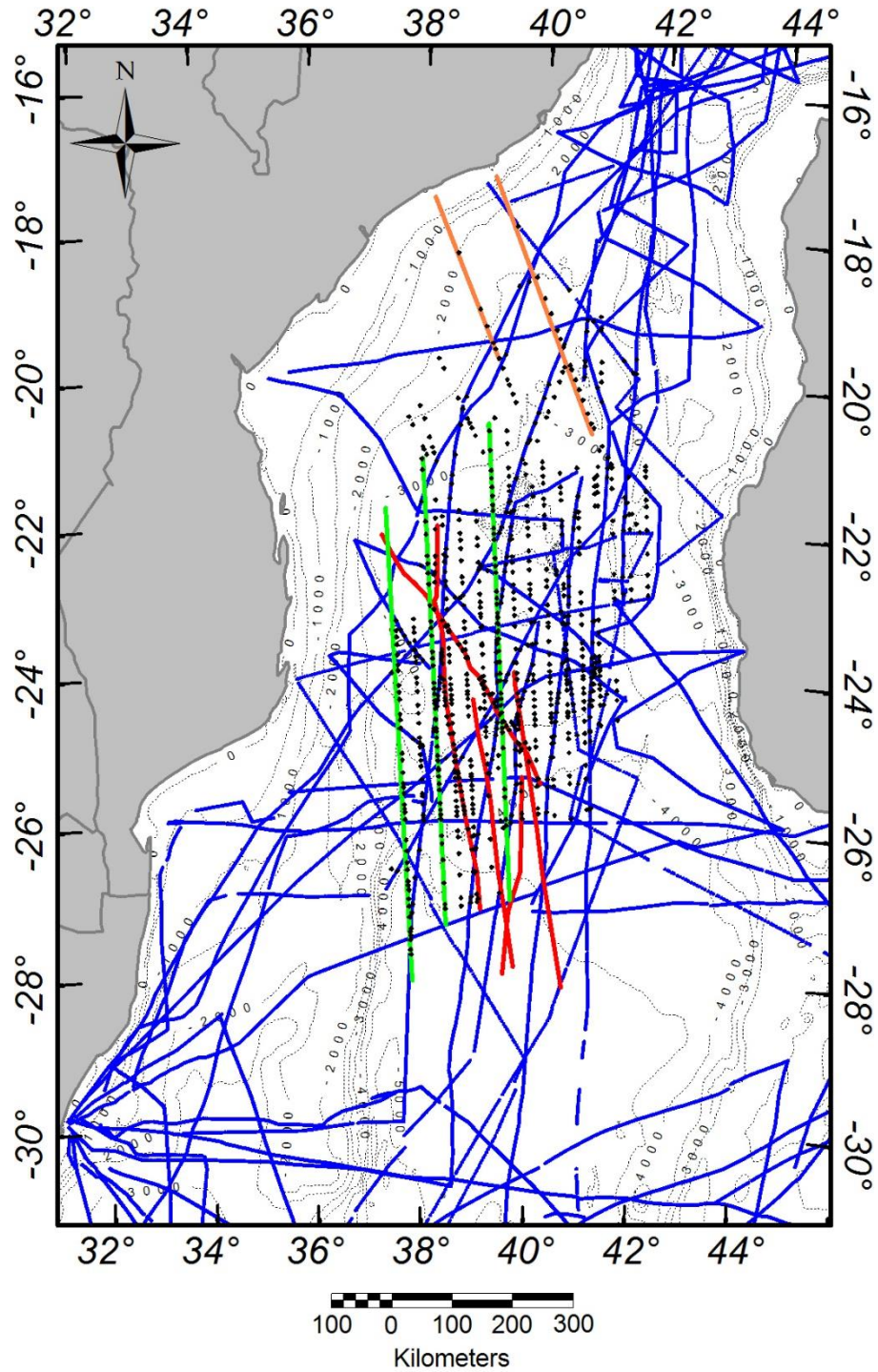


Figure 2.4: Magnetic data available in the Riiser Larsen Sea. Locations of the ship tracks from NGDC (blue lines), published magnetic anomaly profiles from König and Jokat (2010) (green lines), Bergh (1977) (yellow lines), Leitchenkov et al. (2008) (red lines). Black dots represent identified magnetic isochrons from Leinweber and Jokat (2012). Bathymetry is shown with contour interval of 1000 m.

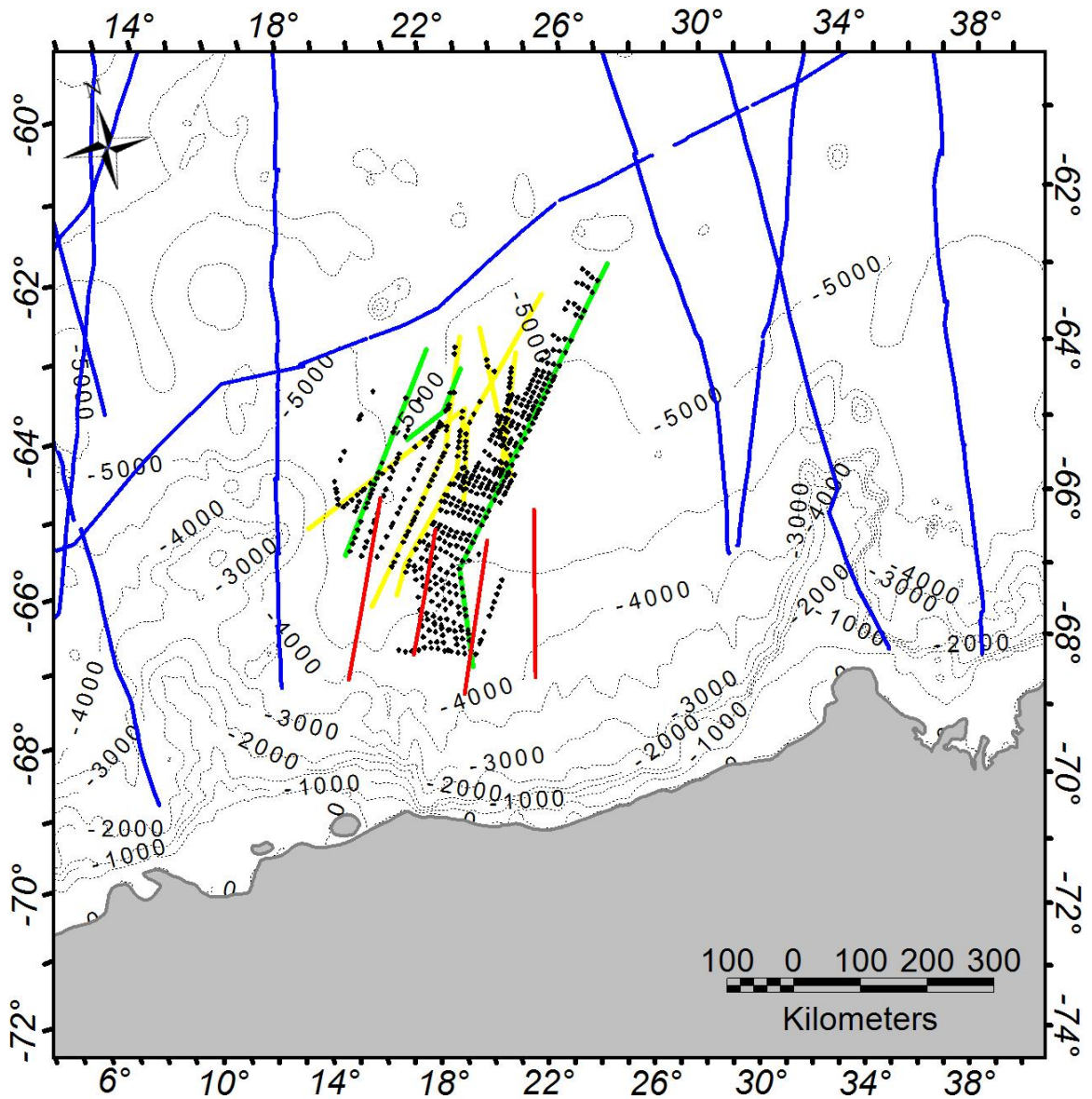


Figure 2.5: 3 arc-minute grid of the World Digital Magnetic Anomaly Map (Maus et al., 2007) which includes the Antarctic data from the Antarctic Digital Magnetic Anomaly Project (Golynsky et al., 2002). Dashed white boxes indicate location of the Mozambique Basin in the north and the Riser Larsen Sea in the south with their adjacent onshore areas.

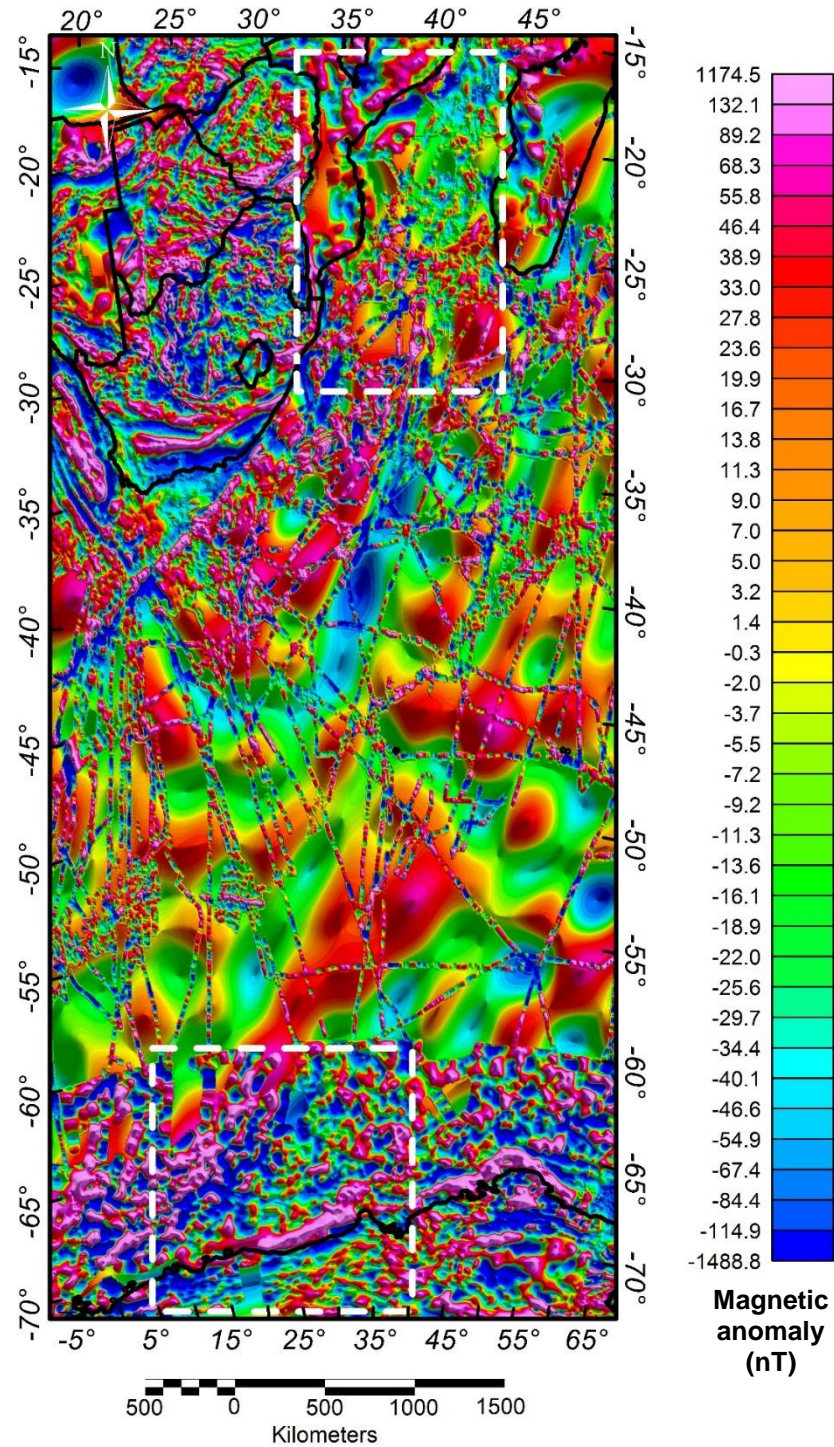
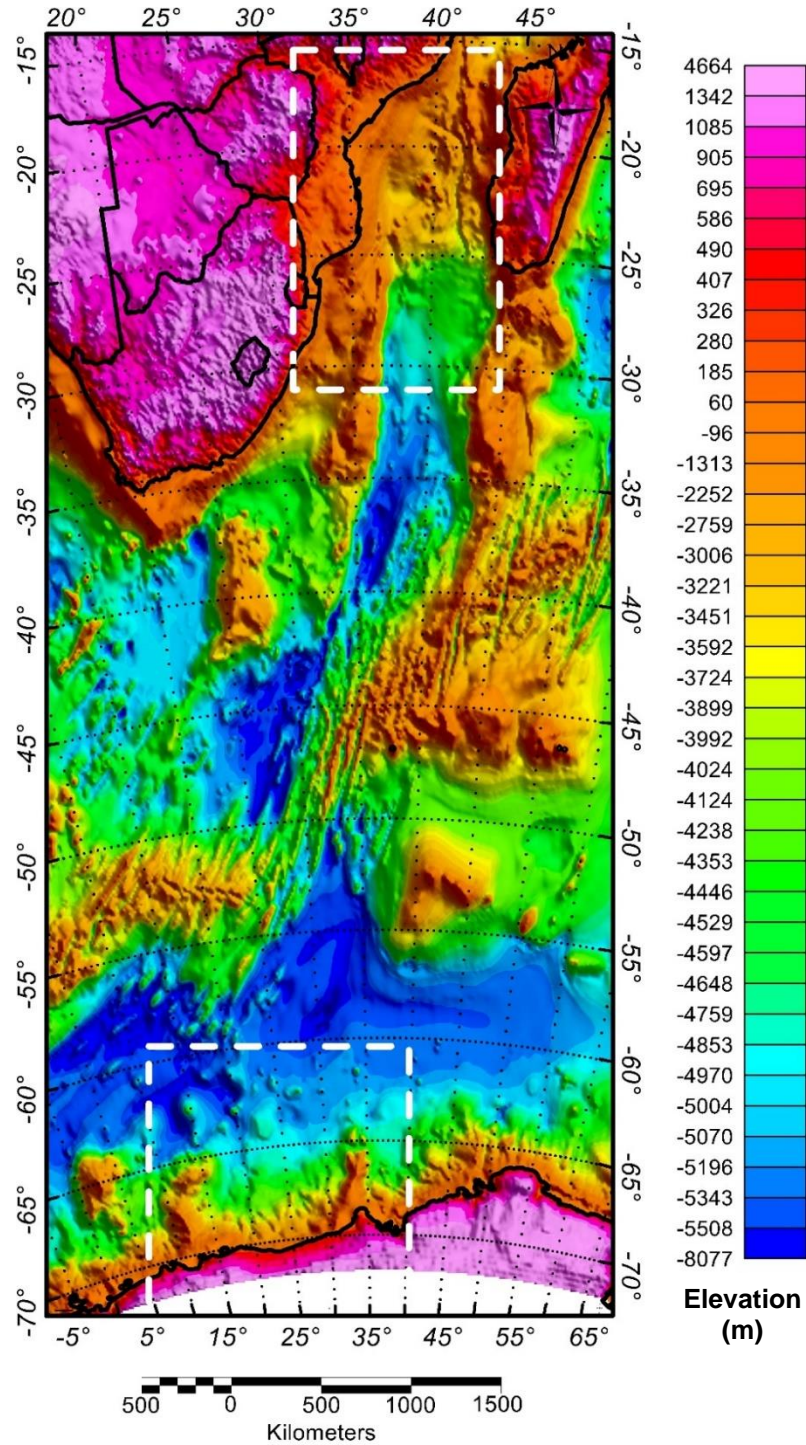


Figure 2.6: 5-arc-minute grid of the Global Terrain Base from the NGDC that compiled land and marine elevation measurements in 1988. Dashed white boxes indicate locations of the Mozambique Basin in the north and the Riser Larsen Sea in the south with their adjacent onshore areas.



onshore topography is extracted from the global 30-arc-second Gtopo30 grid (Figure 2.7) which was completed in 1996 based on various sources including land survey data, digital elevation models and regional topographic maps. Gtopo30 is publicly accessible from the United State Geological Survey (USGS). Many ship tracks from the NGDC also carried bathymetric measurements that are used in this study (Figure 2.7).

2.4 Sediment thickness

Two separate sets of data provide for the thickness of sedimentary layers in the study areas. Laske and Master (1997) published a 1-degree-cell-size grid of global sediment thickness which integrated data from a mix of high and low-resolution atlases and maps as well as industry compilation (Figure 2.8). The other data set is the 5-arc-minute Total Sediment Thickness of the World's Oceans and Marginal Seas (Whittaker et al., 2013) (Figure 2.9). Originally, this grid was constructed using isopach maps of various scales and findings from different ocean drilling programs. Details have been added to this data set with recent results from seismic reflection and refraction data. Besides the mentioned global grids, local sedimentary thickness maps that are specific to the areas of interest is also available through published sources (Leitchenkov et al., 2008; Buyl and Flores, 1996) (Figures 2.10 and 2.11).

2.5 Age of the oceanic crust

Crustal age is estimated using Muller's age grid (Muller et al., 2008). This is a 2-arc-minute grid that provides age of ocean crust based on identified magnetic anomalies

Figure 2.7: 30-arc-second grid of the Gtopo30 topography data set available from the USGS that provides onshore topographic constraints. Blue lines represent ship tracks from the NGDC that collected depth sounding data in the areas of the Mozambique Basin and the Riser Larsen Sea. Dashed black boxes indicate locations of the Mozambique Basin in the north and the Riser Larsen Sea in the south with their adjacent onshore areas.

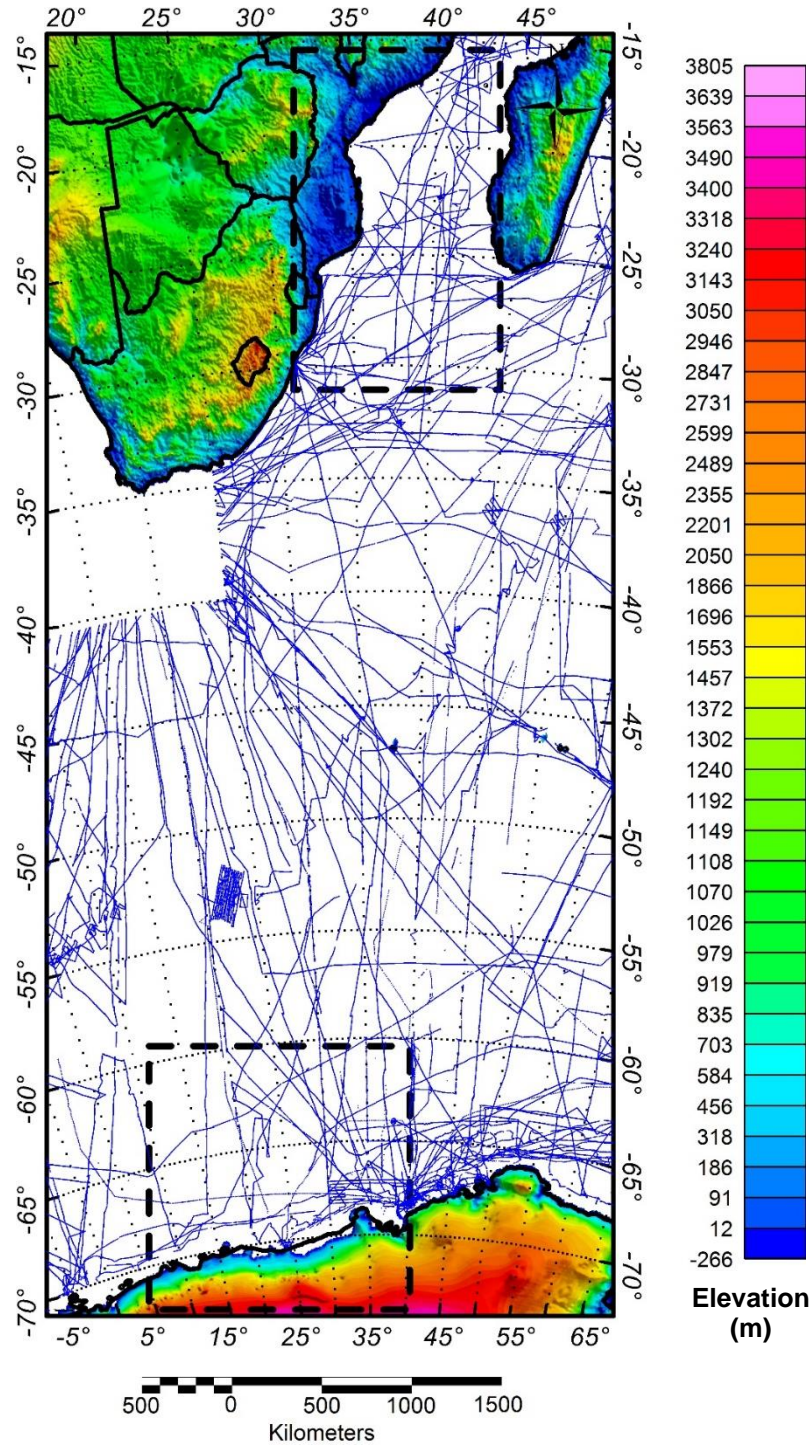


Figure 2.8: Sediment thickness map from Laske and Master (1997) shown in 1 degree cell size grid. Dashed white boxes indicate locations of the Mozambique Basin in the north and the Riser Larsen Sea in the south with their adjacent onshore areas. Dashed black boxes indicate locations of the Mozambique Basin in the north and the Riser Larsen Sea in the south with their adjacent onshore areas.

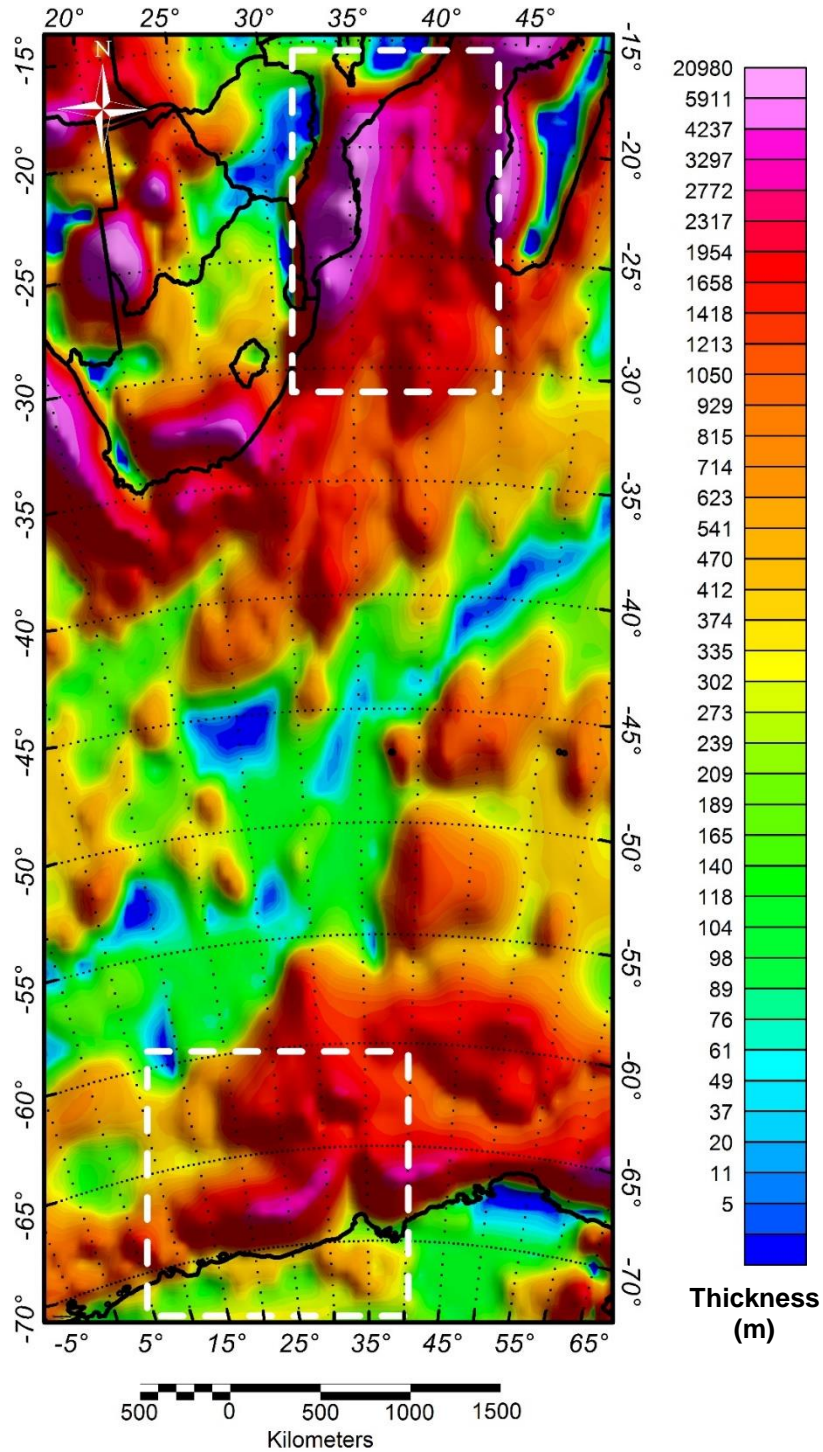


Figure 2.9: 5-arc-minute grid of the Total Sediment Thickness of the World's Oceans and Marginal Seas (Whittaker et al., 2013). Dashed black boxes indicate locations of the Mozambique Basin in the north and the Riser Larsen Sea in the south with their adjacent onshore areas.

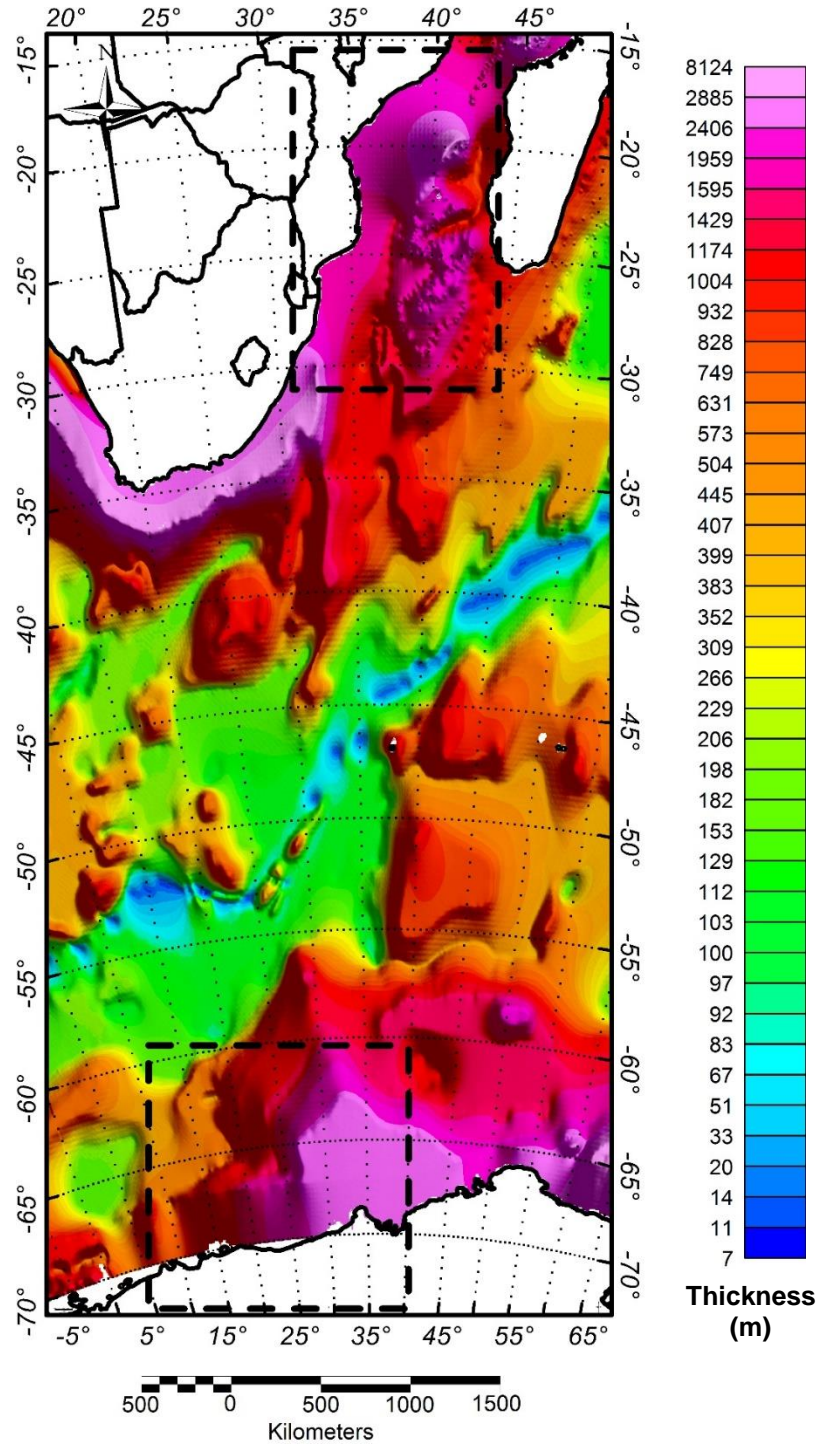


Figure 2.10: Map of basement depth over the Riiser-Larsen Sea based on seismic reflection and refraction data as extracted from Leitchenkov et al. (2008).

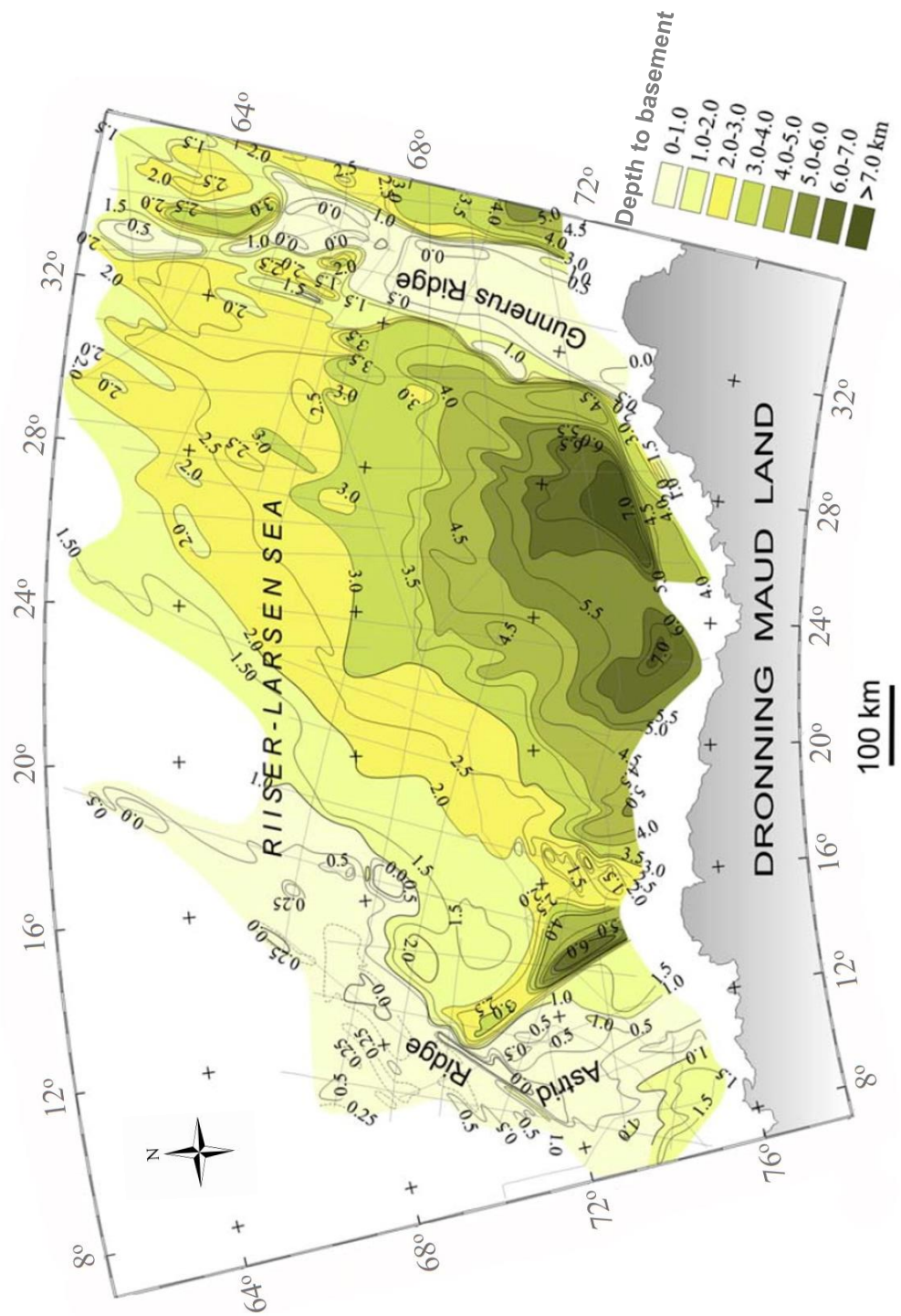
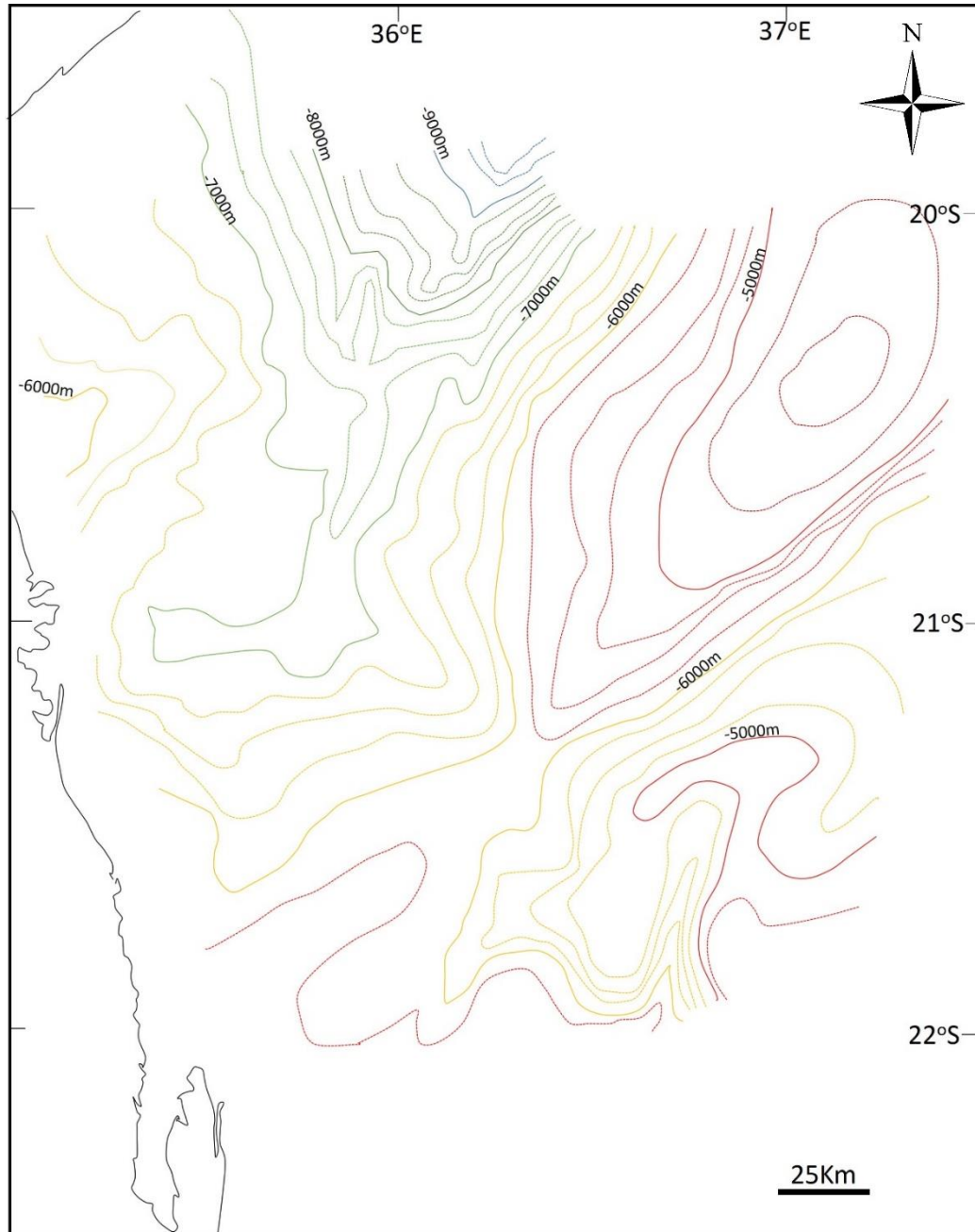


Figure 2.11: Depth to basement over the Mozambique Basin estimated from seismic reflection data (modified from Buyl and Flores, 1986). Map is contoured with interval of 250 m.



and linear interpolation in the direction of spreading. Muller's age grid for the study areas is displayed in Figure 2.12.

2.6 Seismic data

All seismic data used in this study are derived from published sources. Figure 2.13 shows locations and corresponding sources for the available reflection and refraction surveys. Acoustic basement is imaged in all of the refraction surveys, many of which also penetrate the Moho (Leinweber and Jokat, 2013; Parsiegla et al., 2009; Leitchenkov et al., 2008; Hinz et al., 2004; Gohl and Uenzelmann-Neben, 2001; Hirsh et al., 2009; Barrett, 1997; Chave, 1979; Qui et al., 1996; Nguuri et al., 2001; Webb et al., 2004; Nain et al., 2006; Zhao et al., 1999; Li et al., 2003; Gore et al., 2009; Fournon, 1987; Bertil and Regnault, 1998; Sinha et al., 1981; Kudryavtzev et al., 1991; Ikami et al., 1983; Ikami et al., 1984; Kurinin and Grikurov, 1982; Bauer et al., 2000; Neprochnov et al., 1988; Green and Hales, 1966; Hales and Nation, 1972; Hayes et al., 1991; Goslin et al., 1981; Tucholke et al., 1981; Steinhart and Meyer, 1961; Huebscher et al., 1996; Betley, 1991; Baier et al., 1983; Green and Durrheim, 1990; Stuart and Zengeni, 1987; Durrheim et al., 1992; Recq et al., 1998; Hales and Sacks, 1959; Bloch et al., 1959; Ludwig et al., 1968; Kogan, 1972). Single and multichannel seismic reflection data in the Mozambique Basin and the Riiser Larsen Sea are published in Mahanjane (2012), Leitchenkov (2008) and Hinz et al. (2004). Data are mostly shown as interpreted seismic sections in two way travel time that capture either volcanic or crystalline basement.

2.7 Well data

Well data from on and offshore of the Mozambique Basin available to this study are industry test wells published in Flores (1973), Kamen-Kaye (1983), and Deep Sea Drilling Program wells from Vallier (2007). Most of these wells stop within the sedimentary layer while some of them encounter volcanic basalts. Age of basalt layers are not well constrained as no radiometric dating is available. Wells data are summarized in Figure 2.14 and Table 2.1.

Figure 2.12: 2-arc-minute grid of the age of the ocean crust based on identified magnetic isochrons and linear interpolation (Muller et al., 2008). Dashed white boxes indicate locations of the Mozambique Basin in the north and the Riser Larsen Sea in the south with their adjacent onshore areas.

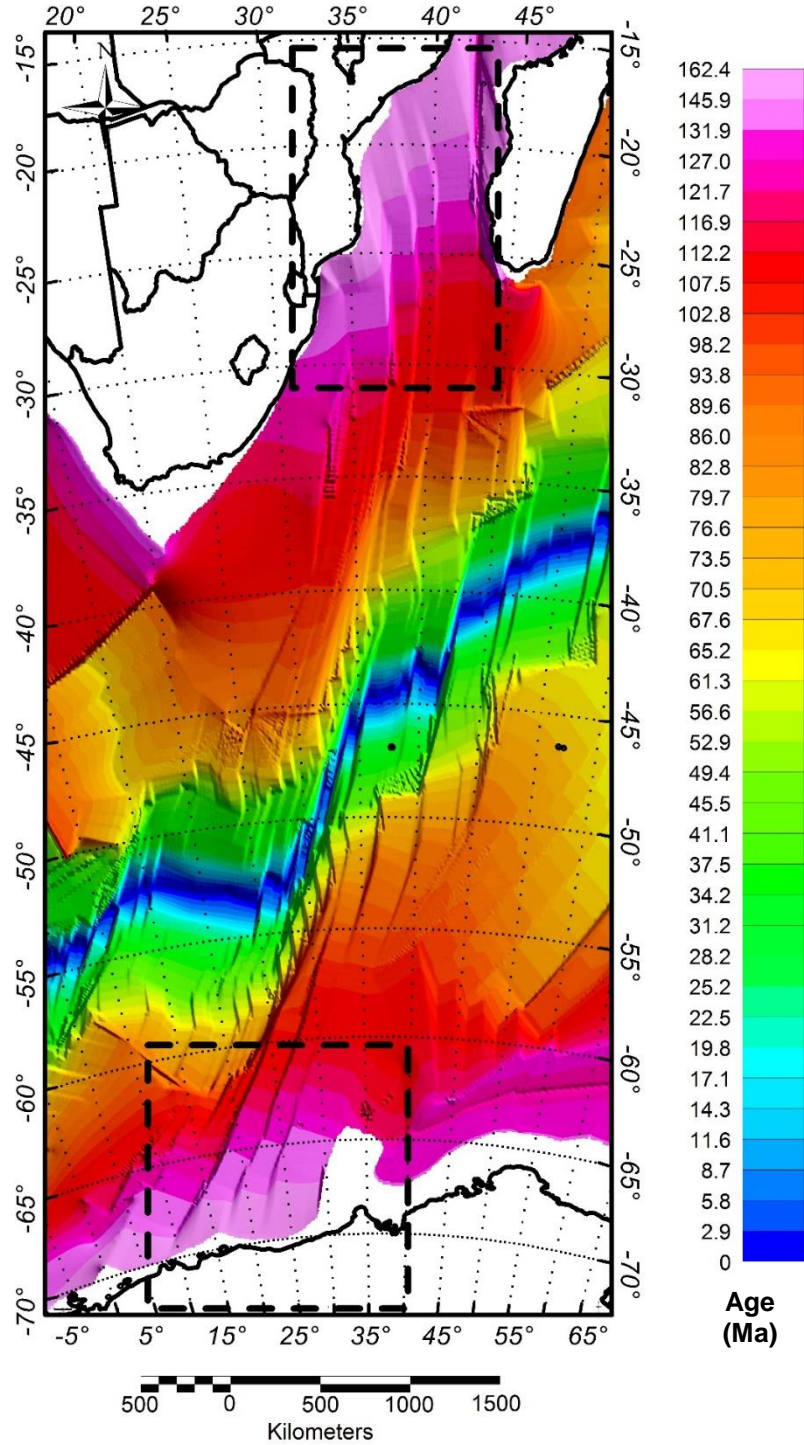


Figure 2.13: Available seismic and wells data from published sources: red triangles are seismic refraction stations from various sources (see text for references), orange lines are refraction profiles from Leinweber and Jokat (2013), blue lines are seismic cross sections in the Mozambique Basin (Mahanjane, 2010) and the Riser Larsen Sea (Leitchenkov, 2008 and Hinz et al., 2004). Orange diamonds represent wells published in Kame-Kaye (1983). Black diamonds are DSDP wells (Vallier, 2007). Wells are shown in more details in Figure 2.14 and Table 2.1. Dashed black boxes indicate locations of the Mozambique Basin in the north and the Riser Larsen Sea in the south with their adjacent onshore areas.

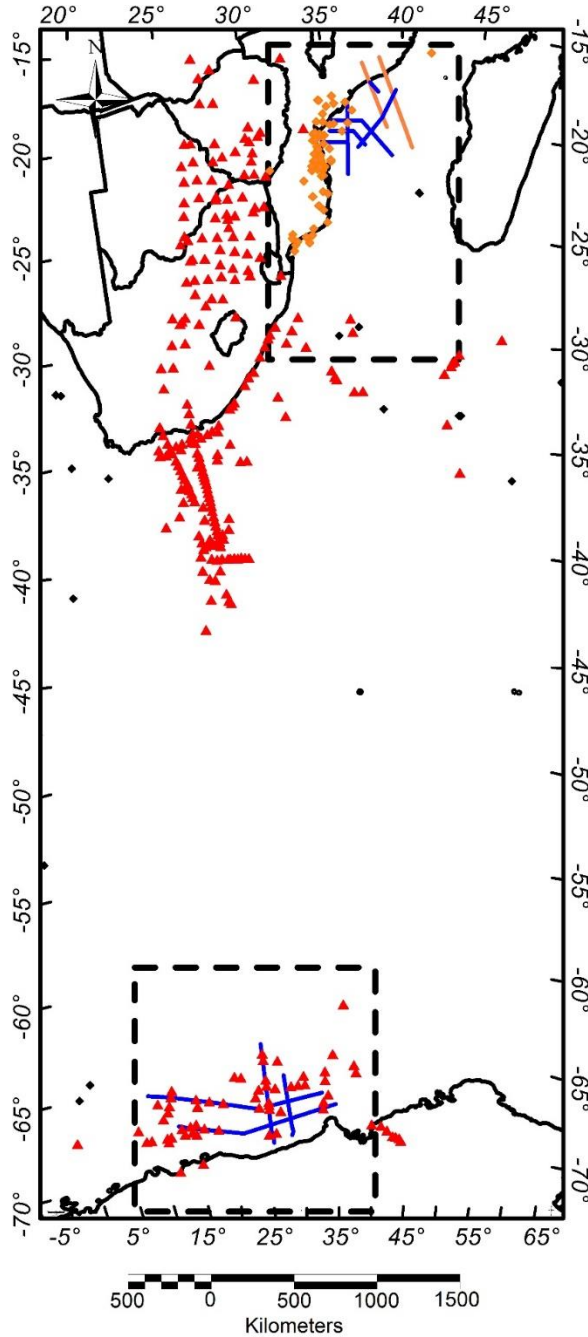


Figure 2.14: Zoom in view of locations of drilled wells over the Mozambique Basin. Orange dots are wells published in Kamen-Kaye (1983). Black dots are DSDP wells (Vallier, 2007). Well information is listed in Table 2.

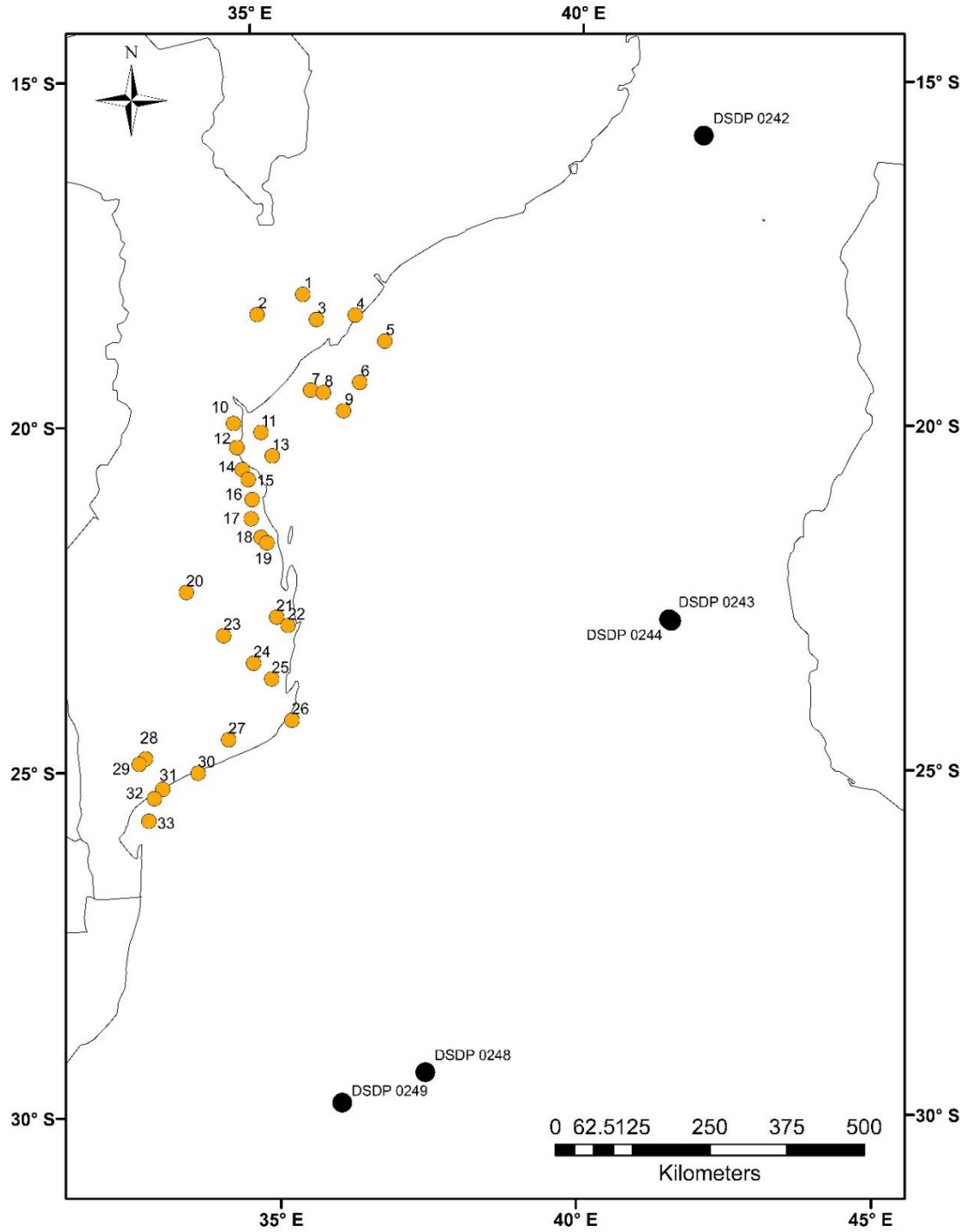


Table 2.1: Information for wells shown in Figure 2.14.

Map No.	Well Name	Total Depth (T.D) (m)	Formation at T.D
1	Nhamura-1	5498	Basement
2	Inyaminga-1	2463	Upper Cretaceous, Sena
3	Nhanguazi-1	3341	Lower Cretaceous, Sena
4	Micaune-1	4608	Cretaceous, Albian
5	Zambezi-1	4644	Cretaceous, Maastrichtian
6	Zambezi-2	N.D	N.D
7	Sim-1	3682	Cretaceous
8	Sam-1	4275	Cretaceous
9	Zambezi-3	4498	Cretaceous, Maastrichtian
10	Busi-1	3236	Lower Cretaceous
11	Sofala-1	3230	N.D
12	Janguene-1	3497	Upper Cretaceous, Domo
13	Nemo-1	4124	N.D
14	Divinhe-1	3837	Lower Cretaceous, Sena
15	Marrhupene-1	3110	Upper Cretaceous, Domo
16	Mambone-1	3610	Lower Cretaceous, Sena
17	Pande-1	3562	Lower Cretaceous, Sena
18	Temane-2	1746	Upper Cretaceous, Grudja
19	Temane-1	3505	Lower Cretaceous, Sena
20	Balone-1	3116	Basalt
21	Nhachenque-1	4029	Basalt
22	Pamene-1	2042	Upper Cretaceous, Grudja
23	Funhalouro-1	4226	Basalt
24	Mazenga-1	4291	Basalt
25	Domo-1	3480	Volcanic
26	Mozambique12-1	2454	Volcanic
27	Zandamela-1	2696	N.D
28	Mucia-1	2334	Volcanic
29	Pulmeira-1	4461	Volcanic
30	Mozambique 2-1A	1235	Basalt
31	Mozambique 7-1	3070	N.D
32	Mozambique 3-1	3576	N.D
33	Mozambique 1-1	3557	N.D
	DSDP2042	2961	Eocene Chalk
	DSDP2043	3921	Pleistocene
	DSDP2044	3805	Pleistocene
	DSDP2048	5438	Basalt
	DSDP2049	2520	Basalt

CHAPTER 3

METHODS

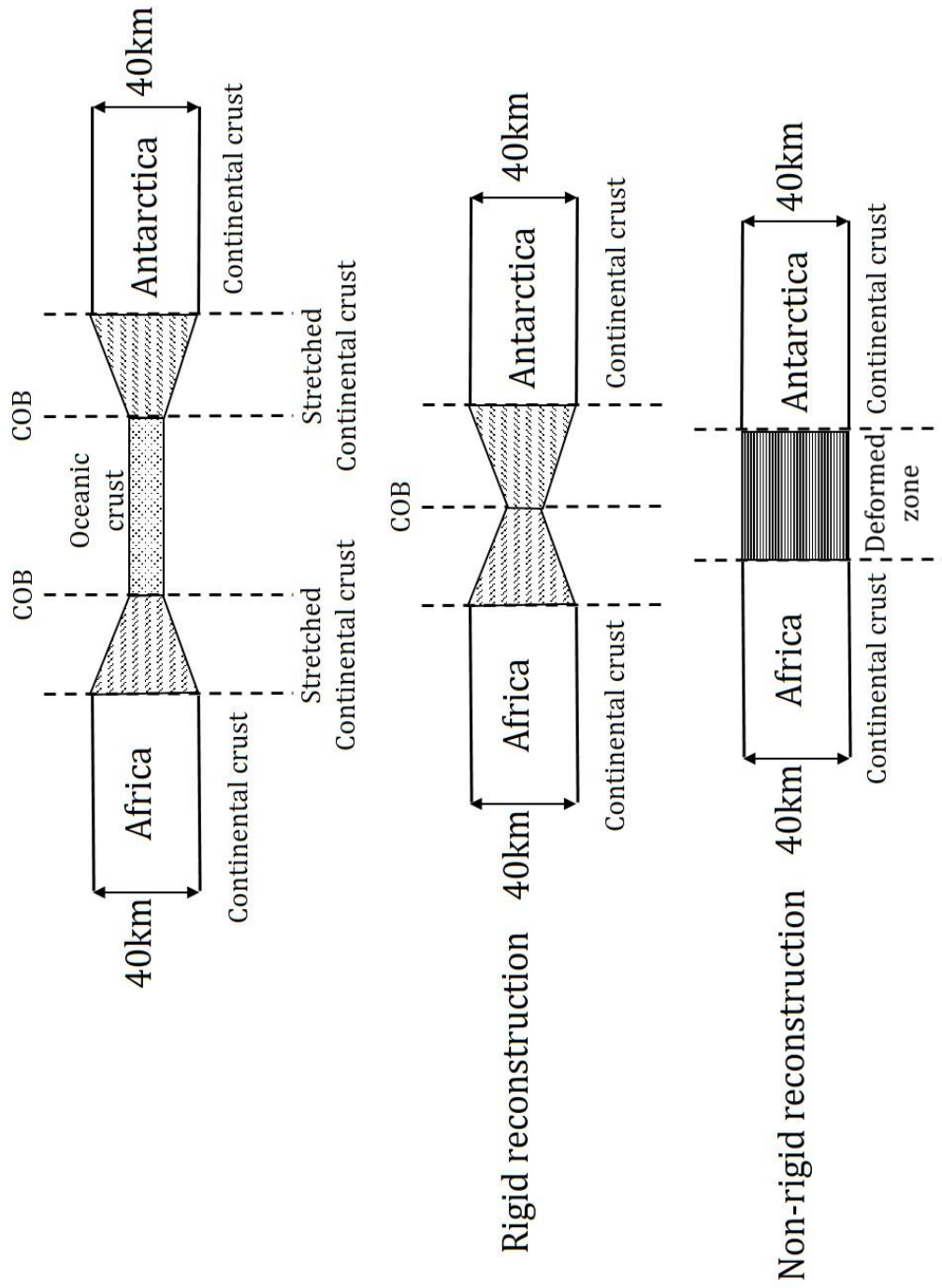
To develop a model for the pre-breakup reconstruction of the Africa and Antarctica plates the study is divided into three phases (Figure 3.1):

- 1) Rigid plate reconstruction,
- 2) 3D gravity inversion on the base of the crust,
- 3) Non-rigid reconstruction of the extended continental margins.

3.1 Rigid plate reconstruction:

Rigid reconstruction aims to reconstruct the relative positions of Africa and Antarctica at the time of initial seafloor spreading. This is done by closing the ocean basin and bringing the two continents back to their respective positions immediately before seafloor spreading took place. For this purpose, it is important to identify the age of oceanic crust in these margins as that will dictate the timing of plate motion during seafloor spreading. An effective method for determining the age of oceanic crust is magnetic isochron identification using marine magnetic anomaly profile data. Plate reconstructions using marine magnetic data have been carried out in other margins by other workers: Madagascar and Africa (Rabinowitz, 1983), India and Antarctica (Gaina et al., 2007), India and Australia (Gibbons et al., 2012). Marine magnetic anomalies are directly linked to the process of oceanic crust formation throughout geologic time (Vine & Matthews, 1963).

Figure 3.1: Diagram illustrating the main focus of this study. Rigid reconstruction closes the ocean basin and brings Africa and Antarctica back together at time prior to seafloor spreading. Non-rigid reconstruction attempts to reconstruct the two plates to their original positions prior to continental rifting.



Seafloor-spreading magnetic anomalies form linear patterns and consequently the first step is to distinguish between those observed anomalies that form such patterns and those that are due to isolated features (e.g., seamounts, etc.). This is done by correlating magnetic anomalies from profile to profile and identifying similar features that might represent oceanic crust of the same geologic age. Next, a synthetic magnetic anomaly profile is modeled based on a geomagnetic polarity timescale. This synthetic model represents a continuous record of magnetic polarity intervals in time. Lastly, observed magnetic profiles will be correlated with the synthetic models to identify magnetic isochrons which are tied to known, specific ages. In addition, fracture zones are structures that record the direction of plate motion and thus are important parameters in rigid reconstruction. Once all identifiable isochrons are located over both margins along with the conjugate fracture zones, plate motion can be traced back through time as the ocean basin is gradually closed as the same isochrons and fracture zones for each margin are brought back together. A continent-ocean boundary (COB) must also be determined in each margin. Consequently, the conjugate COBs are reconstructed to determine the fit of the continents at the onset of seafloor spreading. Plate motion tracing is done using Gplates1.4 (Seton et al., 2012), an interactive plate reconstruction software that can derive plates' motion based on specified Euler's poles of rotation and vice versa.

3.1.1 Satellite-derived gravity enhancement

The significance of fracture zones can be considered in two aspects. Depending on the location and orientation of a survey profile relative to a fracture zone, it can either

miss some magnetic isochrons or record duplication of isochrons. Therefore, the reliability of magnetic anomaly correlation greatly depends on the ability to detect fracture zones. Moreover, fracture zones are also crucial to rigid plate reconstruction as is discussed in the next chapter. Fracture zones are extensive linear zones of irregular topography of the oceanic basement (Muller and Roest, 1992) and are often associated with linear gravity anomaly highs and lows. Thus, satellite-derived gravity anomaly data are used to trace fracture zones. To enhance the visibility of the fracture zones, residual gravity maps are generated and enhanced with various filters including tilt derivative, vertical and horizontal gradient filters (Verduzco et al., 2004; Simpson et al., 1986). Enhancement is done in Geosoft Oasis Montaj (GOM) software package.

Residual gravity anomaly mapping is an attempt to remove the long-wavelength anomaly component produced by from the deep crust or mantle and therefore enhance the density distribution from within the upper crust (Jacobsen, 1987). To generate a residual map, first Bouguer gravity anomalies must be calculated from the free-air gravity anomalies. This is done by increasing the density of sea water such that it is the same density as the seafloor which is taken to be 2.0 g/cc. The long-wavelength anomaly can be generated by upward continuing the Bouguer anomalies. Upward continuation of gravity data is a mathematical process that simulates a gravity measurement at selected altitude above sea level (Pawlowski, 1995). This process is based on the differential attenuation between long and short wavelengths where short wavelength signal is attenuated much more rapidly with increasing

distance from the anomaly source. Different levels of upward continuation (2 to 90 km) were tested. Finally, the upward continued grid was subtracted from the Bouguer anomaly to yield a residual gravity grid. Each set of residual anomalies is further enhanced using derivative filters calculated by GOM. These filters are used for edge detection that highlights the gravity gradient in a specific direction (Simpson et al., 1986) (shown in the following chapter).

3.1.2 Magnetic isochron identification

The most detailed and systematic magnetic surveys in the Mozambique Basin and the Riiser Larsen Sea are those used in the study of Leinweber and Jokat (2012). Unfortunately, these data are not publicly available. Magnetic data used in this current study are shown in Figure 2.2. Though not as systematic as, and much sparser than those used in Leinweber and Jokat (2013), the available data are useful in calibrating the magnetic isochrons published by the previous workers in regions where the two data sets overlap. This is especially crucial in the northern area of the Mozambique Basin where data used in this study are very similar to those in Leinweber and Jokat (2013).

Before the magnetic anomaly profiles can be correlated to identify similar features, each profile must be projected to the direction subparallel to that of the fracture zones. This is to ensure magnetic anomalies are placed in their correct horizontal scales. The orientation of fracture zones can be visually detected using satellite-derived gravity data. Profile projection is done with FORTRAN programs provided by Bird Geophysical (Appendix 2) that calculates a midpoint of each profile and projects

the profile around this midpoint using the azimuth of the fracture zone. In addition, it is also important to determine which profiles cross fracture zones prior to correlation.

Synthetic magnetic anomaly profiles are generated using geomagnetic polarity time scales (GPTS) model. Recent GPTS models include those of Malinverno et al. (2012), Tominaga and Sager (2010) and Gradstein et al. (2004). To be consistent with recent studies in Gondwana reconstruction, the model of Gradstein et al. (2004) is chosen for this study. Parameters used to generate this synthetic profile include: present-day and paleo values of magnetic inclination and declination of the area, depth to the upper oceanic crust, thickness of the upper oceanic crust, orientation of the profile, the age range covered within the profile, and spreading rate at which new oceanic crust formed during a specific time frame. Table 3.1 summarizes the parameters used to construct the synthetic model. Thickness of the magnetic source is assumed to be the top 1 km of the upper crystalline crust (Jones, 1999). Remanent inclination and declinations are computed using polar-wander path models. Magnetization is assigned with a global average value. Values of spreading rates are determined through the process of trial and error. Different spreading rates for different time intervals are tested to see which models produce synthetic profiles that are most consistent and provide the best correlations with the observed profiles. Once the synthetic magnetic anomaly profile has been constructed, observed magnetic anomaly profiles are compared directly to the synthetic model to identify magnetic isochrons within each magnetic profile.

3.1.3 Reconstruction poles

According to Euler's Displacement Theorem, any motion on the surface of a sphere can be described as a rotation about an axis (Euler, 1776). Such rotation is defined by latitude and longitude of the pole, where the axis intersects the sphere, and an angle of rotation. A total reconstruction pole defines a finite rotation starting at the present and going backward in time (Cox and Hart, 1986). To model the full motion of a plate through time, a sequence of total reconstruction poles is required. In this study, total reconstruction poles are determined using isochrons and fracture zones traces. Once the isochrons are identified over both conjugate margins, the process starts with interactively adjusting the location and orientation of the Antarctica plate to yield the best visual fit between geometries of isochrons in the conjugate margins that represent the same geologic age. This manual fit of the isochrons is constrained by fracture-zone traces over both margins. Fracture zones document the direction in which conjugate plates move apart, thus when reconstructed to a specific time, the fracture zones over either side of the reconstructed isochrons should be coincident or at least parallel. Upon achievement of the best fit, a reconstruction pole for that specific time is computed automatically by Gplates1.4 software.

3.2 Three-dimensional gravity inversion on the base of the crust

To carry out the non-rigid reconstruction described in the next section, it is required that the spatial distribution and thickness of the extended continental crust to be known. A five-layer (air, water, sedimentary rocks, crystalline crust rocks, and upper

Table 3.1: Parameters used to construct the synthetic seafloor spreading model

	Africa	Antarctica
Depth Magnetic Source (km)	10	11
Depth to base of magnetic source (km)	11	12
Present inclination (°)	-60	-62
Present declination (°)	-20	-42
Remanent inclination (°)	-65	-58.2
Remanent declination (°)	-37	1.73
Strike of magnetic lineation (°)	276	286
Magnetization (Amp/m)	8	8
Gaussian Smoothing (Kms)	2	2
Number of spreading rate	8	8
Spreading rate from 124-128Ma (mm/yr)	20	20
Spreading rate from 128-130Ma (mm/yr)	22	22
Spreading rate from 130-133Ma (mm/yr)	24	24
Spreading rate from 133-134Ma (mm/yr)	27	27
Spreading rate from 134-138Ma (mm/yr)	23	23
Spreading rate from 138-148Ma (mm/yr)	22	22
Spreading rate from 148-160Ma (mm/yr)	19	19

Table 3.2: Layer densities used in gravity inversion model

Layer	Density (g/cc)
Air	0
Sea Water	1.03
Sediment	1.8-2.6
Crystalline Crust	2.85
Mantle	3.0-3.3

mantle) three-dimensional gravity model is constructed and the base of the crust is determined to achieve a crustal thickness model. Initial values of depth to the base of the crust would be estimated using the principle of isostasy. The model uses constant densities for water, and crystalline crust. The sedimentary rock layer density will vary laterally according to formulae developed by Sykes (1996). The upper mantle density will be estimated to vary as a function of oceanic crustal age (Muller et al., 2008) using heat flow (Slater et al., 1980) as proxy to scale the density variation. Layer densities are summarized in Table 3.2. The inversion is constrained by free-air gravity and seismic refraction data. Data employed to construct the 3-D model as well as to conduct the inversion are described in Chapter 2.

In preparation for constructing the model, several grids must be built including: merged sedimentary thickness grid, sedimentary density grid, crustal basement grid and isostatic Moho grid. Since each data set is gridded in different cell size from 900 to 9000 m (with the exception of 1-degree grid from Laske and Master, 1997), all data are re-gridded to 5000 m cell size to ensure consistency.

3.2.1 Building topography, sediment-thickness, sediment-density and basement grids

As described in Chapter 2, there are two gridded data sets available for onshore and offshore topography. Since Gtopo30 provides higher resolution for land elevation, this is merged with the Global Terrain Base (GTB) grid. To create a smooth transition between onshore and offshore data, points of 100 m and higher elevations are omitted from the GTB grid. This leaves a small overlap region (from 0 to 100m)

between the two grids. Merging process is done in Geosoft Oasis Montaj using a blending function that calculates a weighted average for the overlap region while keeping non-overlap data unchanged. Figure 3.2 shows the merged topography grid.

Similarly, there are two available sediment thickness grids. The first one covers both onshore and offshore areas (Laske and Master, 1997). The second dataset only provides thickness for marine sediment but with a higher resolution (Whittaker et al., 2013). To obtain both onshore and offshore sediment thickness with the highest possible resolution, it is necessary to merge the two data sets together. The merging process involves masking the grid from Laske and Master (1997) with the merged topography grid so that locations with elevation lower than -100 m are omitted from the onshore sediment thickness grid, again leaving a small overlap area to merge with the offshore sediment grid. Consequently, the two grids are knitted together using the same technique as with the topography grids. Figure 3.3 shows the resulting merged sediment thickness grid.

Density of the sedimentary rock layer varies laterally as a function of water depth and sediment thickness as proposed by Sykes (1996). The computed sediment density grid is illustrated in Figure 3.4

Once a final version of the sediment thickness grid is completed, depth to the crustal basement (Figure 3.5) is achieved by simply subtracting sediment thickness from topography. However, since global datasets are built by interpolating small number of control points, the sediment thickness grid might not provide accurate

Figure 3.2: Topography grid results from merging the onshore Gtopo30 (USGS) and offshore Global Terrain Base (NGDC). Dashed white boxes indicate locations of the Mozambique Basin in the north and the Riiser Larsen Sea in the south with their adjacent onshore areas.

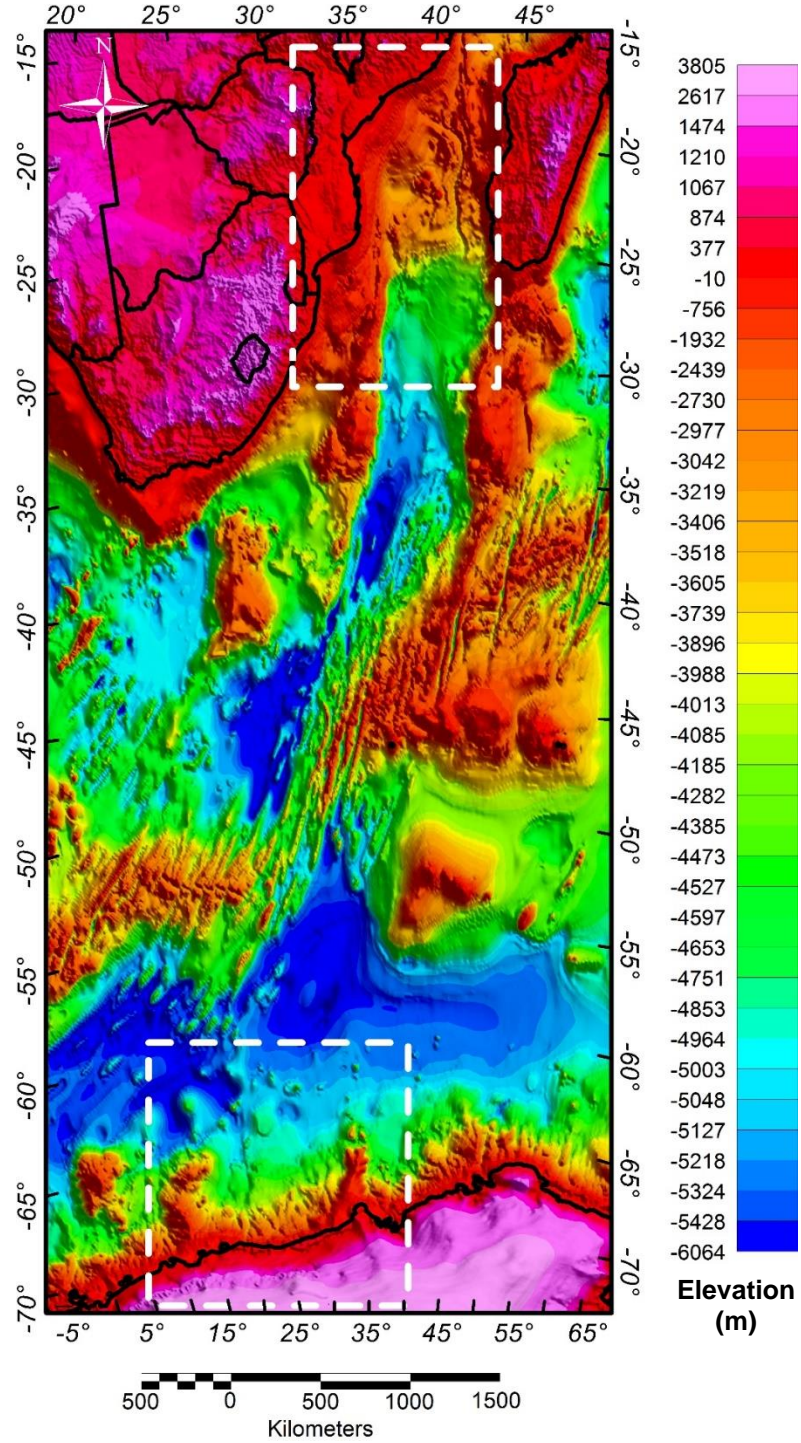
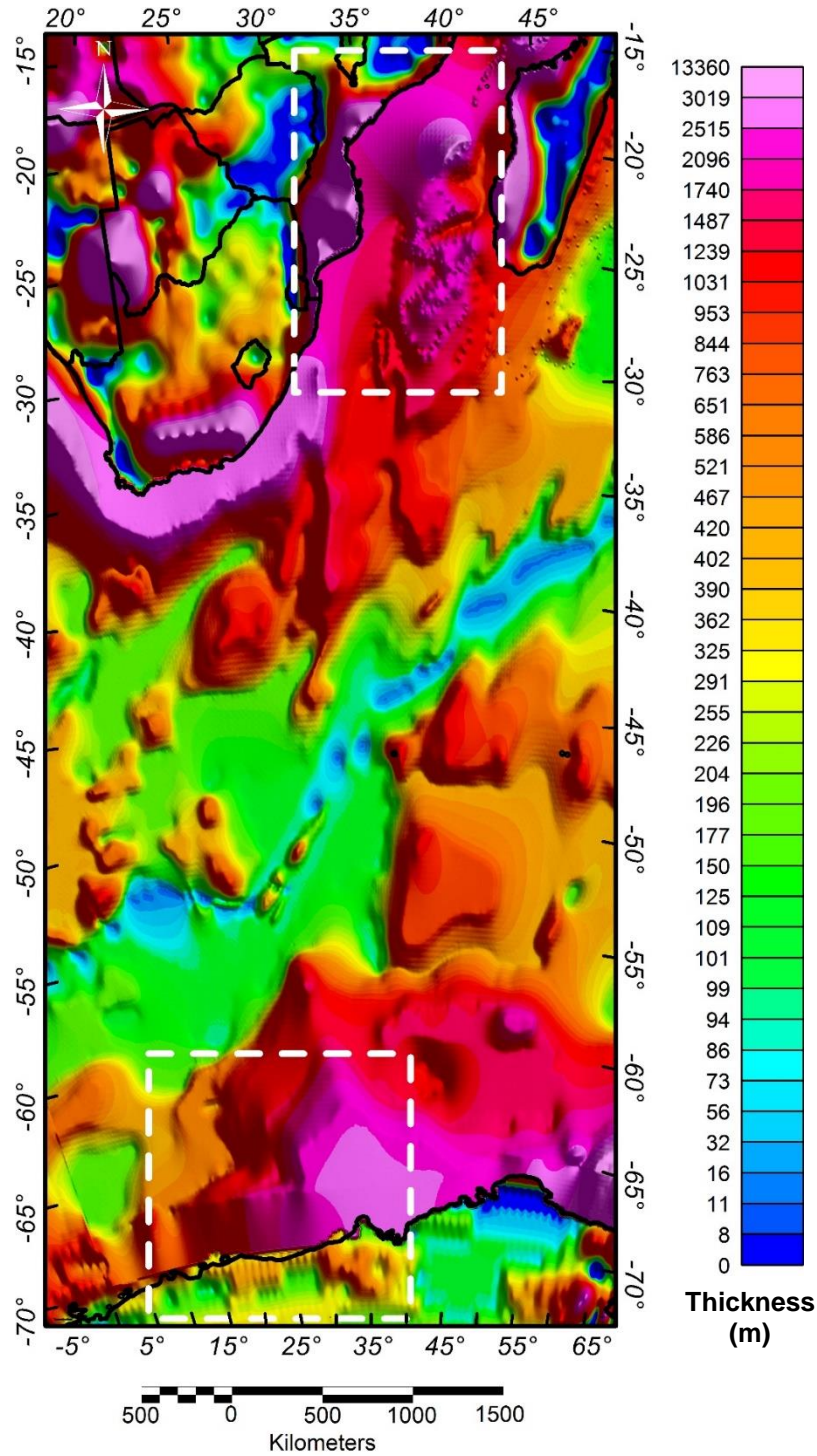


Figure 3.3: Grid of sediment thickness merged from the onshore grid from Laske and Master (1997) and offshore World Sediment Thickness of The Oceans and Marginal Seas from (Whittaker et al., 2013). Dashed white boxes indicate locations of the Mozambique Basin in the north and the Riiser Larsen Sea in the south with their adjacent onshore areas.



information for local areas of interest in the Mozambique Basin and the Riiser Larsen Sea. It is therefore necessary to calibrate the basement grid using local seismic reflection and refraction data as well as well data.

In the Mozambique Basin, seismic refraction profiles from Leinweber and Jokat (2013) provide direct measurements for basement depth. Seismic reflection sections from Mahanjane (2012) provide depth to basement in time which is converted to depth by estimating layers velocities using tie points with Leinweber and Jokat (2013) refraction lines. These measurements are combined with the depth-to-basement map in Buyl and Flores (1996) to generate a new basement grid for offshore Mozambique Basin (Figure 3.6). Well data onshore Mozambique show that basement depths in the area of the Coastal Plain are overestimated by about 1 to 2 km. Therefore basement in this area is adjusted with a bulk upward shift of 1.5 km. Leitchenkov et al. (2008) compiled a depth-to-basement map in the Riiser Larsen Sea based on seismic refraction and reflection data. This map is digitized to generate a new basement grid for this area.

Finally, new offshore basement grids in the Mozambique Basin and Riiser Larsen Sea are merged with the global grid that had been calculated from global sediment thickness, to achieve the final grid of basement depth. The merging method is similar to that used for topography and sediment-thickness data. The calibrated basement grid is shown in Figure 3.7. The sediment density grid is also re-computed accordingly (Figure 3.8). The difference between calibrated and un-calibrated basement grids are shown in Figure 3.9.

Figure 3.4: Sediment density grid calculated as a function of sediment thickness and water depth as formulated by Sykes (1996). Dashed white boxes indicate locations of the Mozambique Basin in the north and the Riiser Larsen Sea in the south with their adjacent onshore areas.

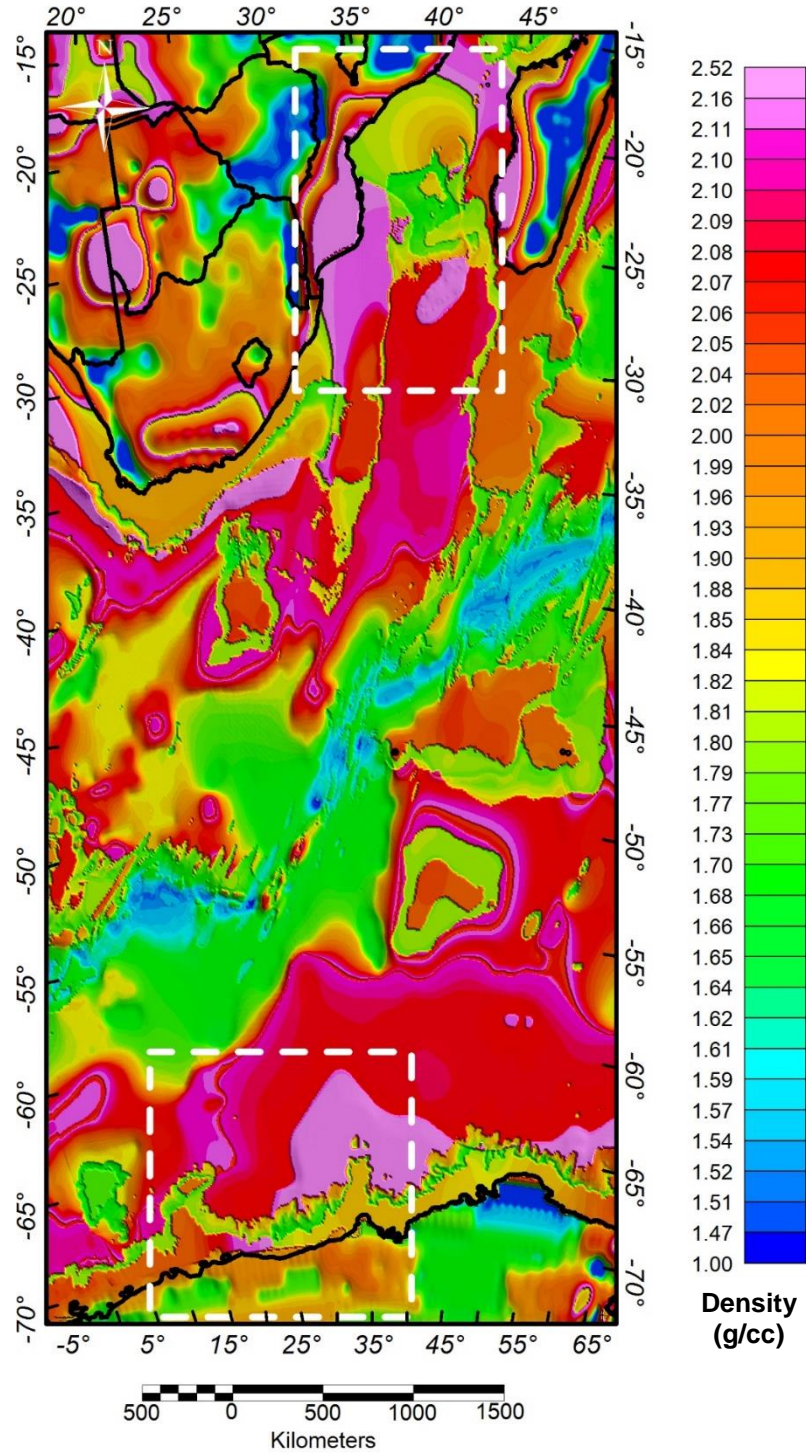
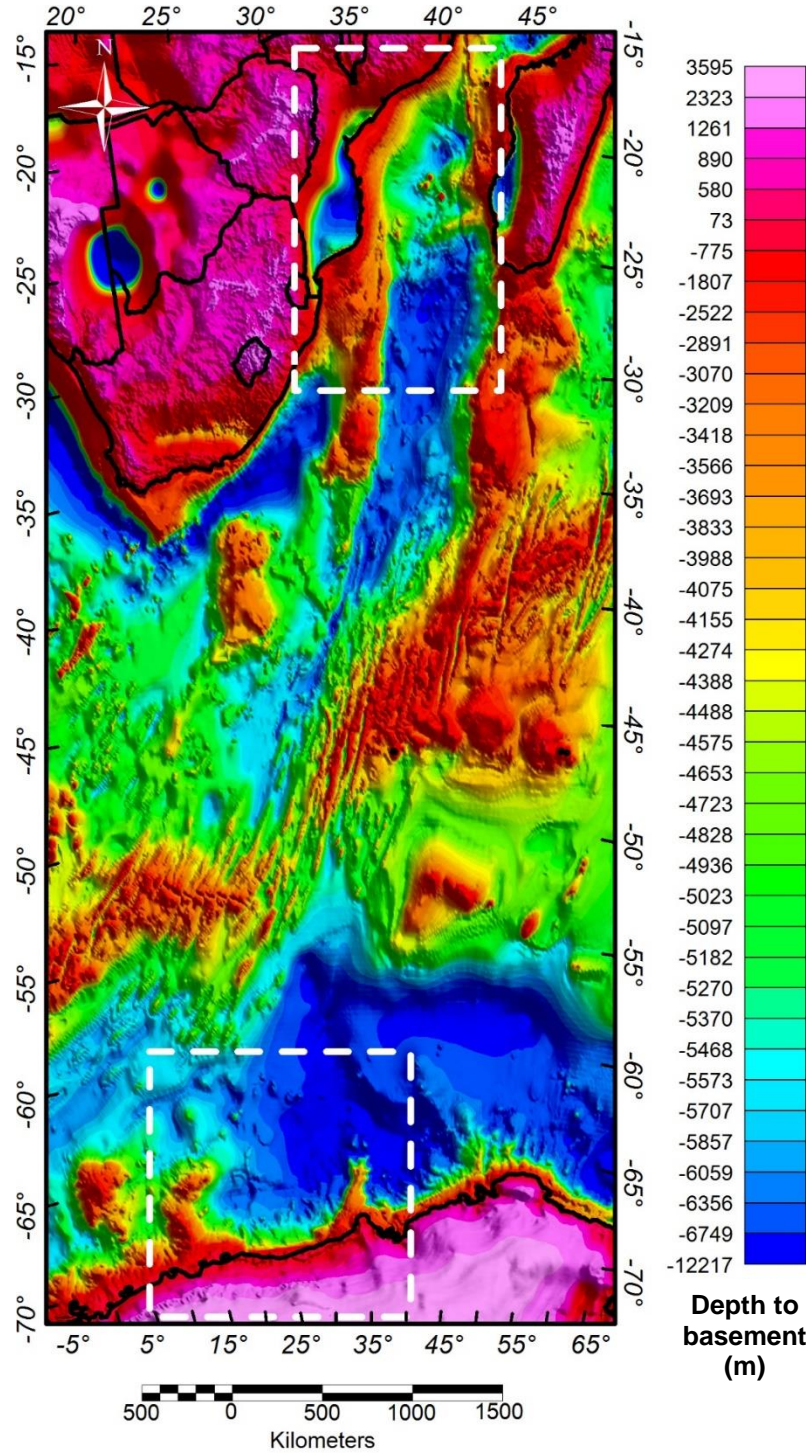


Figure 3.5: Depth to crystalline basement grid results from subtracting the sediment-thickness grid from the merged topography grid. Dashed white boxes indicate location of the Mozambique Basin in the north and the Riiser Larsen Sea in the south with their adjacent onshore areas.



3.2.2 Calculating isostatic Moho

Initial values for Moho depth are computed based on the assumption of isostatic equilibrium condition. That is in the area where the inversion is carried out there exists at depth an isobaric surface above which the total mass in a vertical column is everywhere constant. Following this idea, areas of topographic highs such as inland continent would show a deep Moho and offshore areas would have a shallower Moho. An illustration of this condition is shown in Figure 3.10. From this, at each node in the gridded area, an isostatic Moho that satisfies the condition of equal mass above the isobaric surface can be calculated using the equations in Figure 3.10. Values of the isobaric depth can be adjusted within a reasonable range (35-45 km) to generate a Moho that would yield a crustal thickness of about 6.5 km (+/- 2) in areas of normal oceanic crust.

Nevertheless, at dynamic locations such as the mid-ocean ridges where new crust is actively being formed, isostatic equilibrium conditions are not satisfied and thus isostatic calculation would not provide a true depth to Moho as it would show a very thick crust at the mid-ocean ridge. As a result, it is crucial to have a method that takes into account this complication in the calculation of isostatic Moho. Recent conductive cooling models that formulate the relationship between seafloor heat flow and ocean age are from Sclater et al. (1980) and Stein and Stein (1992). Both models show similar results that have small difference (maximum of 10 mW/m²) due to different sample size. This study adopts the model of Sclater et al. (1980) to create a proxy to

scale the isostatic calculation. Table 3.3 shows the Slater scale with the respective ocean age. In short, young oceanic crust at the mid-ocean ridge has a Slater scale of zero, meaning no isostatic calculation is applied. Closer to the continents where there is old oceanic crust, the Slater scale is close to one, suggesting a full application of isostatic calculation. Oceanic crust between these two end members would have a corresponding intermediate Slater scale.

Values from available seismic refraction data will be used to calibrate the isostatic Moho grid. New grid for Moho depth is generated with values from refraction data replacing those of the isostatic Moho grid. Figures 3.11 and 3.12 show the calculated isostatic Moho grid before and after the calibration of seismic refraction data. Crustal thickness between the basement and Moho grids is shown Figure 3.13.

3.2.3 Three-dimensional gravity inversion

Three-dimensional inverse model algorithms used are those developed by Parker (1972) and Blakely (1996). Inversion process is computed using Oasis Montaj software package which incorporates these algorithms. Base of the crust is adjusted while all other layers' parameters are held unchanged. The program function modifies the depth of the Moho horizon to achieve a minimum misfit between the model's gravity response and the observed gravity data. The minimum misfit is set to be 0.1 mGal. That is the program iteration would stop as either the mean error or the standard deviation of the error reaches 0.1 mGal. After each iteration, the inversion updates the calculated response and error. The iteration is repeated until the error is minimized. Within the Moho horizon, locations where values had previously been

Figure 3.6: Depth to basement map corrected with seismic reflection and refraction data in the northern Mozambique Basin. Triangles represent control points from seismic data. Dashed outline is area with depth to basement mapped by Buyl and Flores (1996).

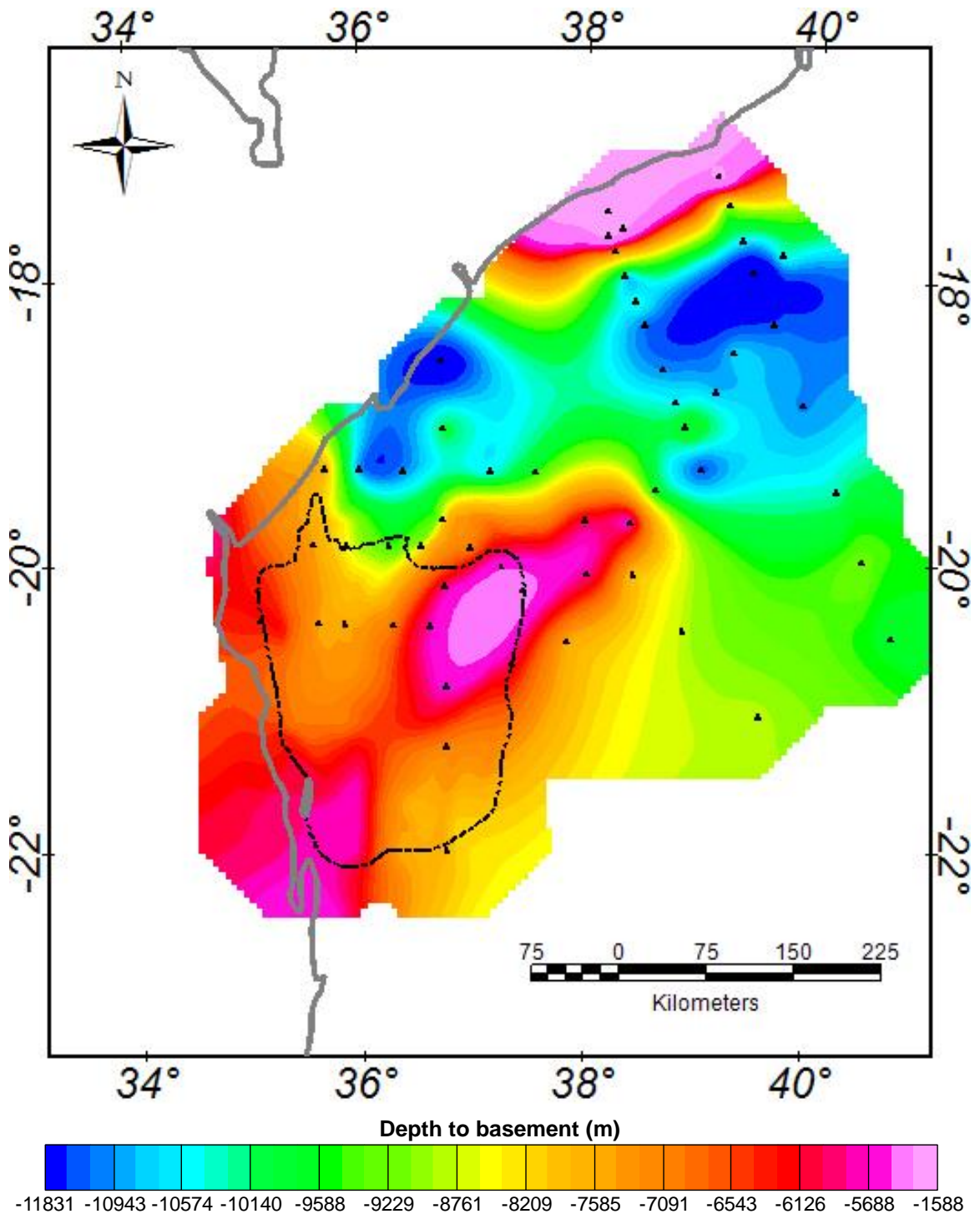


Figure 3.7: Depth to crystalline basement grid after calibration with local seismic reflection and refraction and well data. Calibrated basement is deeper in the Mozambique Basin and the Riiser Larsen Sea. Dashed white boxes indicate locations of the Mozambique Basin in the north and the Riiser Larsen Sea in the south with their adjacent onshore areas.

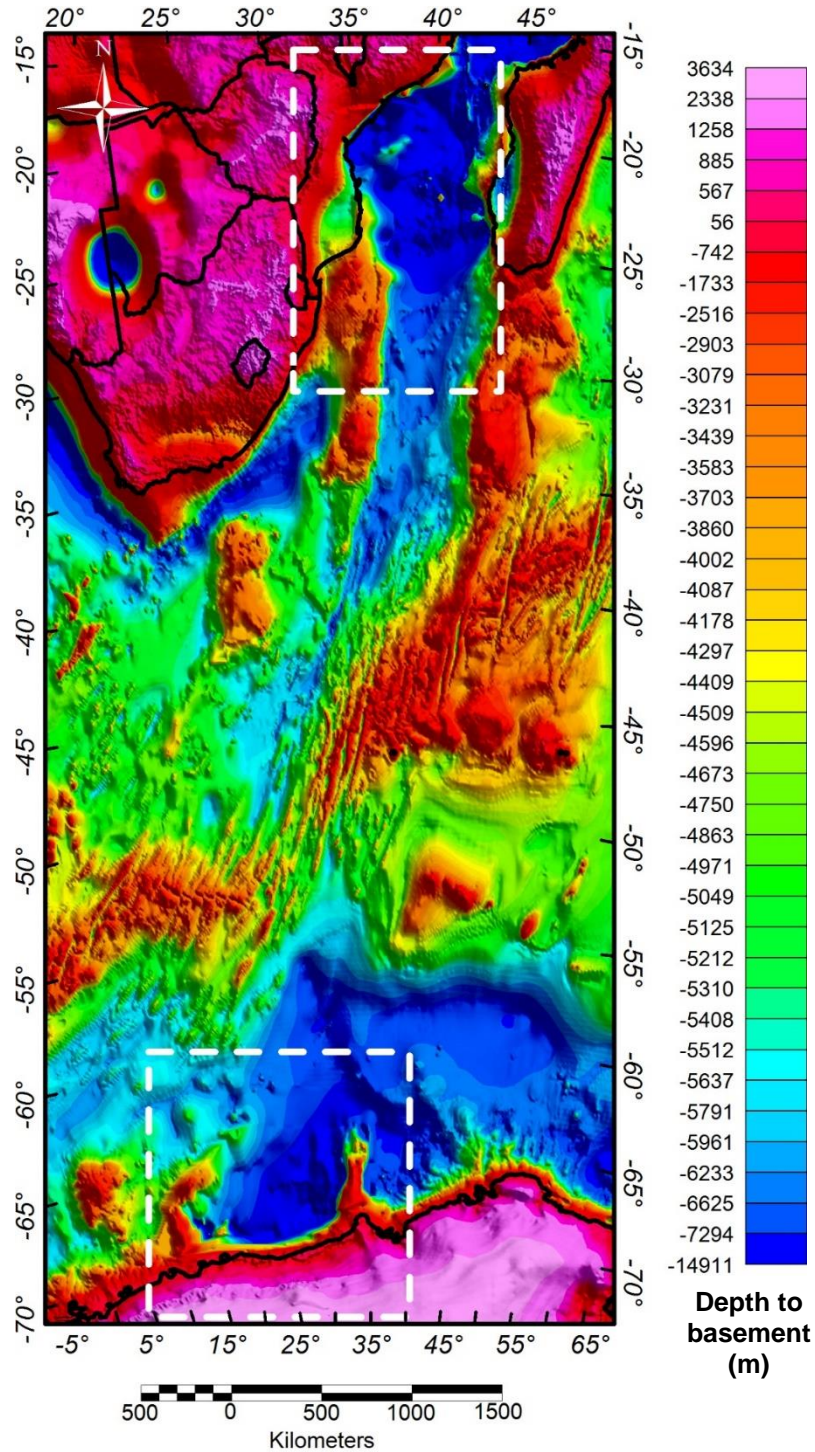


Figure 3.8: Sediment density updated after calibrating the basement grid. Sediment density is increased in areas of the Mozambique Basin and the Riiser Larsen Sea.

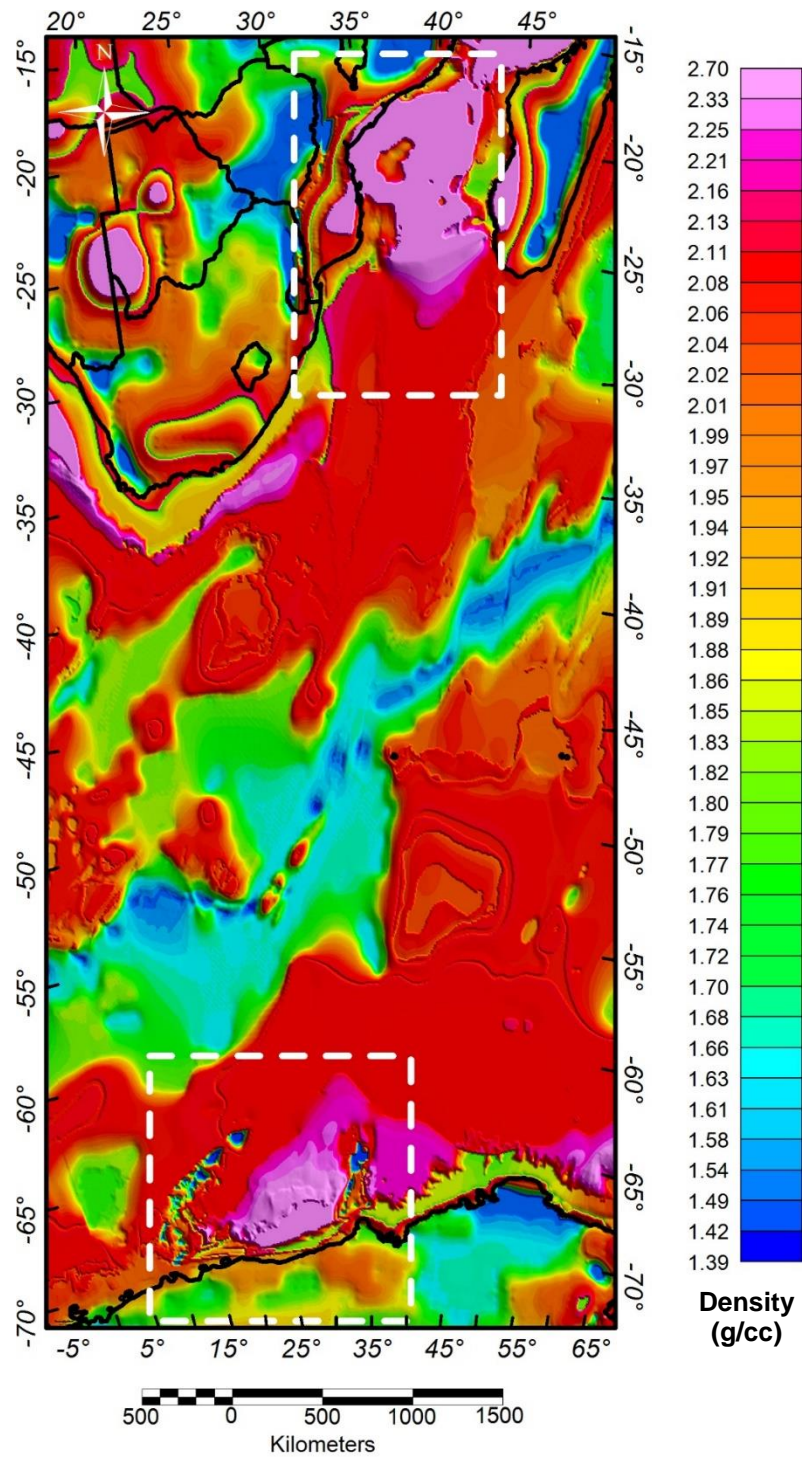


Figure 3.9: Difference between calibrated and un-calibrated basement grids

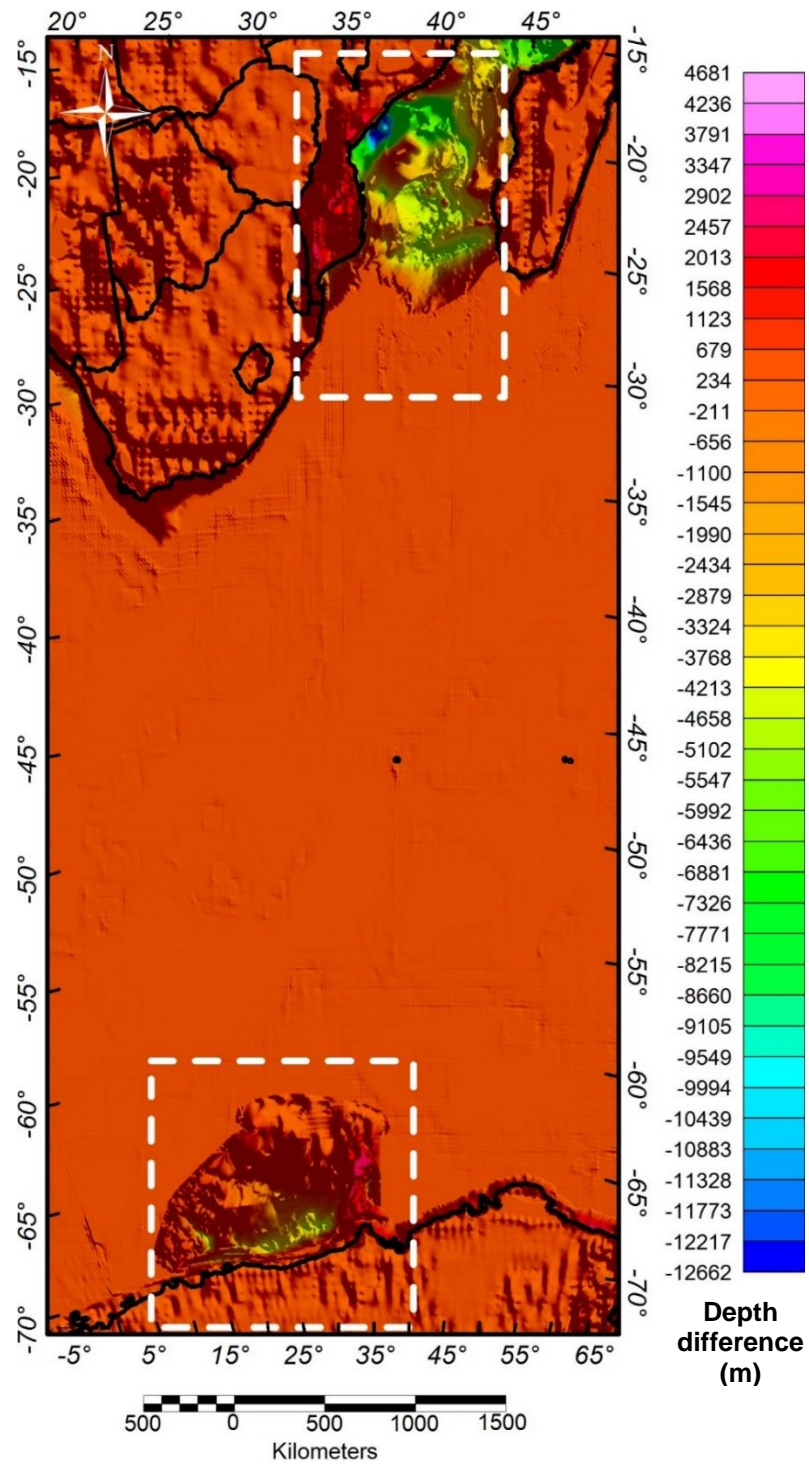
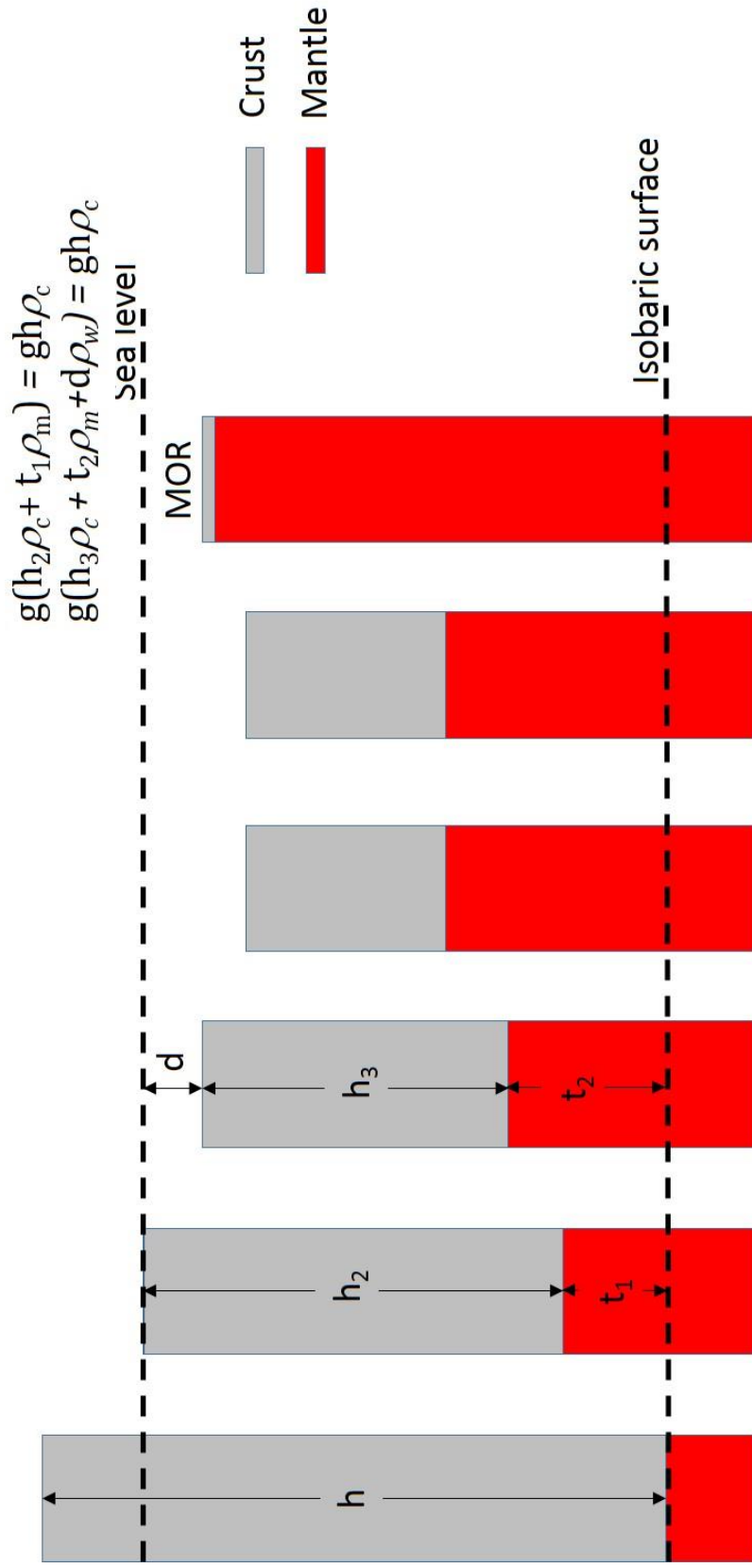


Figure 3.10: Schematic diagram illustrates the isostatic equilibrium conditions that are used to calculate for the isostatic Moho. Each bar represents a column of the Earth. Equations describe the condition of isostasy under which every column has the same weight above the isobaric surface. \mathbf{h} , \mathbf{h}_2 , \mathbf{h}_3 are the thicknesses of the crust. \mathbf{d} is water depth. \mathbf{g} is the gravitational acceleration. ρ_m , ρ_c and ρ_w are densities of the mantle, crust and water respectively. \mathbf{t} is the Moho distance above the isobaric surface. By choosing a depth to the isobaric surface and applying these equations, \mathbf{t}_1 and \mathbf{t}_2 can be calculated if other parameters are known. In a real calculation, it is necessary to include sediment layer and its density within the crust. Note that at the mid-ocean ridge (MOR), isostatic equilibrium condition does not apply.



calibrated with refraction data are held constant during the inversion. Though most available seismic refraction controls are incorporated into the isostatic Moho grid prior to the inversion, refraction controls from Leinweber and Jokat (2013) and Leitchenkov et al. (2008) are reserved to use as a quality control that can evaluate the reliability of the inversion's result. This is critical since these controls are located within the continental margins and are closed to the continent-ocean boundary.

3.3 Non-rigid reconstruction

Rigid plate reconstruction effectively places the continents at their respective locations prior to the initiation of sea floor spreading. Non-rigid reconstruction removes the extensional deformations caused by continental rifting. This is accomplished by a method of areal balancing that has been utilized by Sutra et al. (2013) and Williams et al. (2011) to restore the conjugate margins between Siberia and Newfoundland, Australia and Antarctica respectively. An illustration of areal balancing-method is shown in Figure 3.14.

In non-rigid reconstruction, multiple cross sections are extracted from the gravity inversion model. These two-dimensional cross sections are chosen so as to extend from the landward limit of undeformed crust, which is defined by typical thickness of continental cratons (40-45 km) (Mooney, 1998), seaward to the continent-ocean boundary. In the initial model, it is assumed that the direction of extension is parallel to that of the oldest total reconstruction pole used for the rigid reconstruction. Therefore, the cross sections will have this orientation which can be modified if a different pole of rotation for the non-rigid closing is required for a better closure

Figure 3.11: Calculated Moho based on the principle of isostasy. Dashed white boxes indicate locations of the Mozambique Basin in the north and the Riiser Larsen Sea in the south with their adjacent onshore areas.

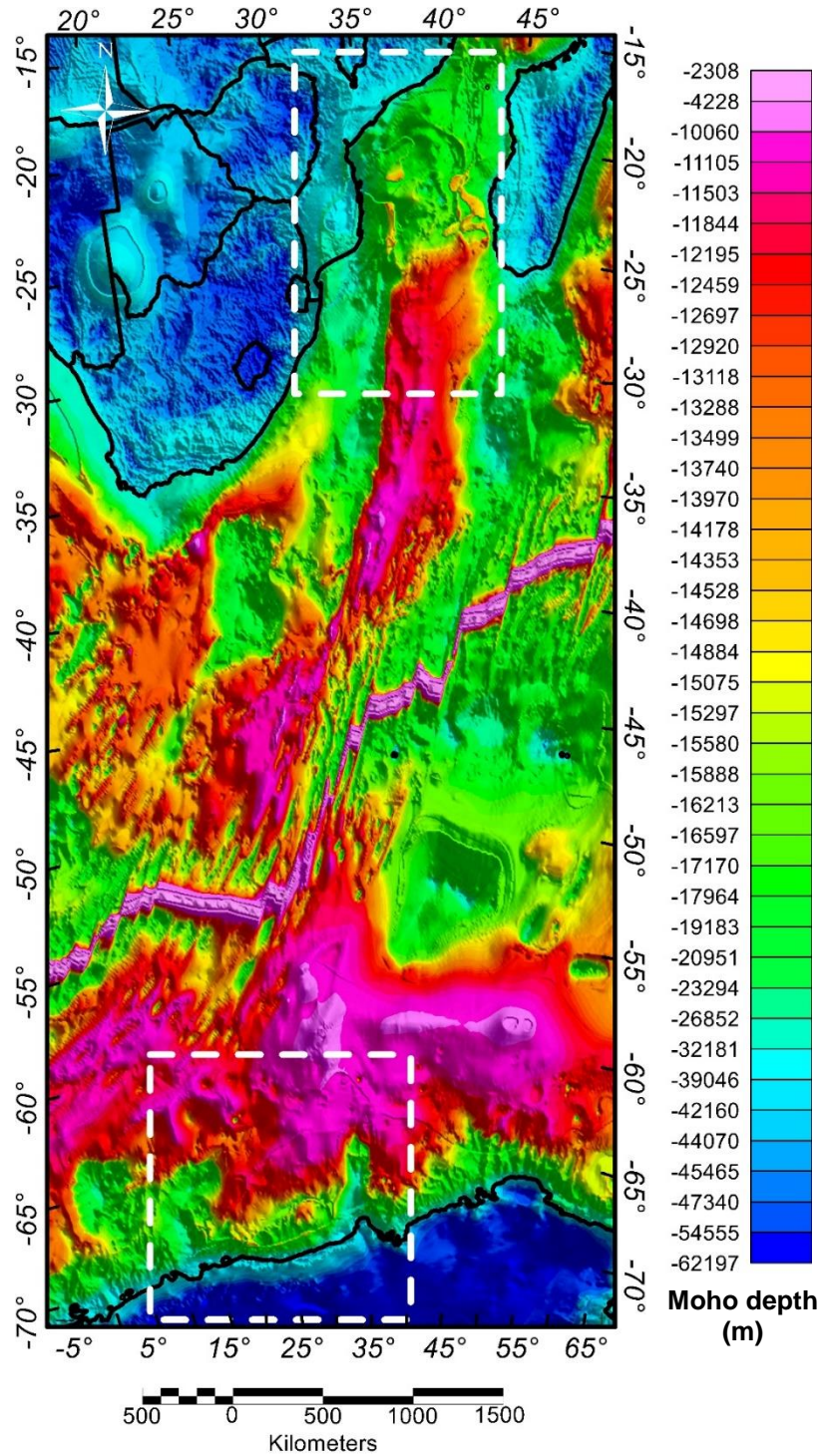


Figure 3.12: Isostatic Moho constrained by seismic refraction data. Black triangles are locations of refraction stations. Difference between calculated values based on isostasy and refraction measurements is about 5 km with only one anomalous point that the difference exceeds 10 km. Dashed white boxes indicate locations of the Mozambique Basin in the north and the Riiser Larsen Sea in the south with their adjacent onshore areas.

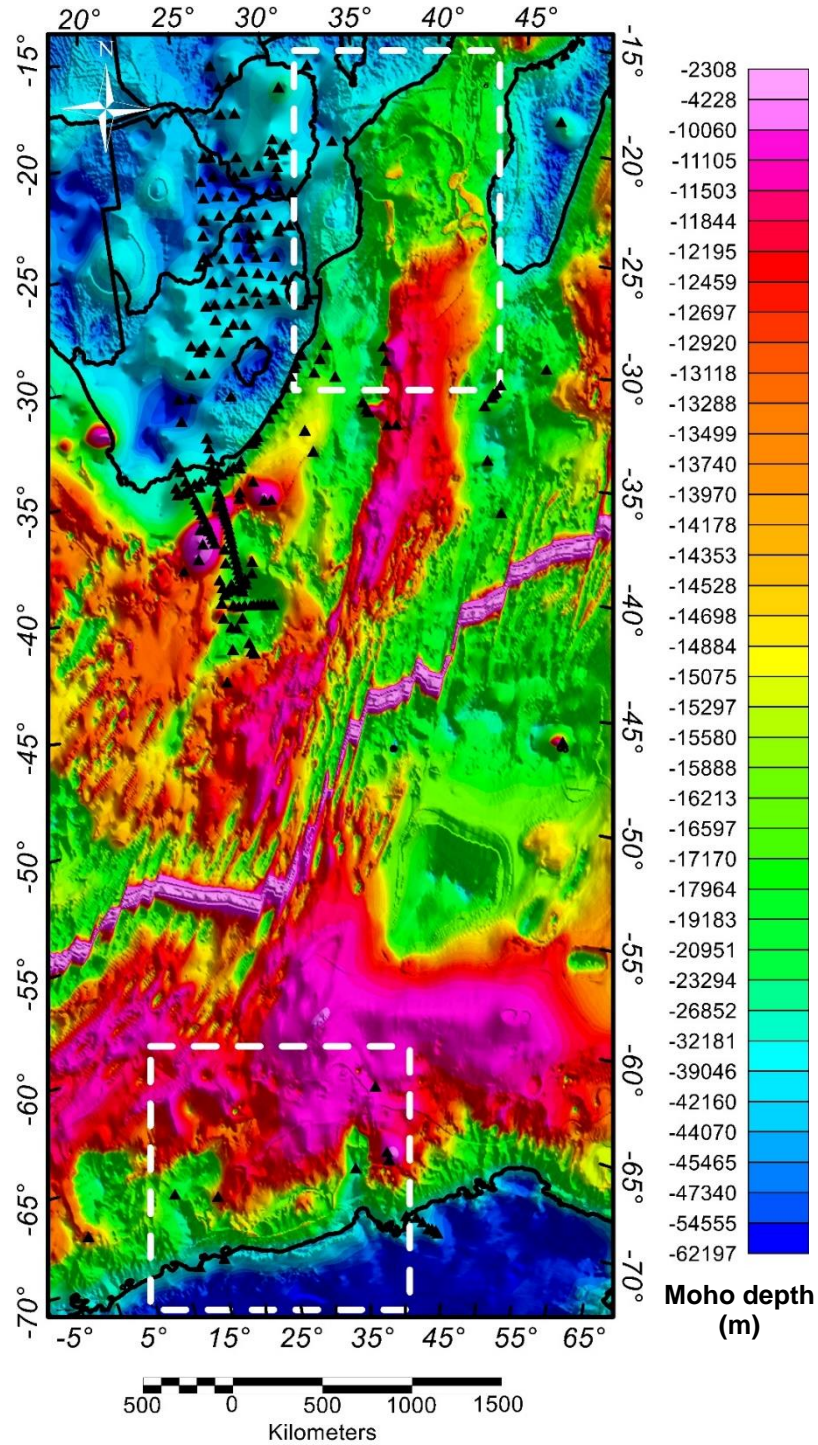


Figure 3.13: Crustal thickness calculated from the difference between basement grid and Moho grid. In the normal ocean areas, thickness ranges from 4.5 to 7 km which is consistent with the global average. Dashed white boxes indicate locations of the Mozambique Basin in the north and the Riser Larsen Sea in the south with their adjacent onshore areas

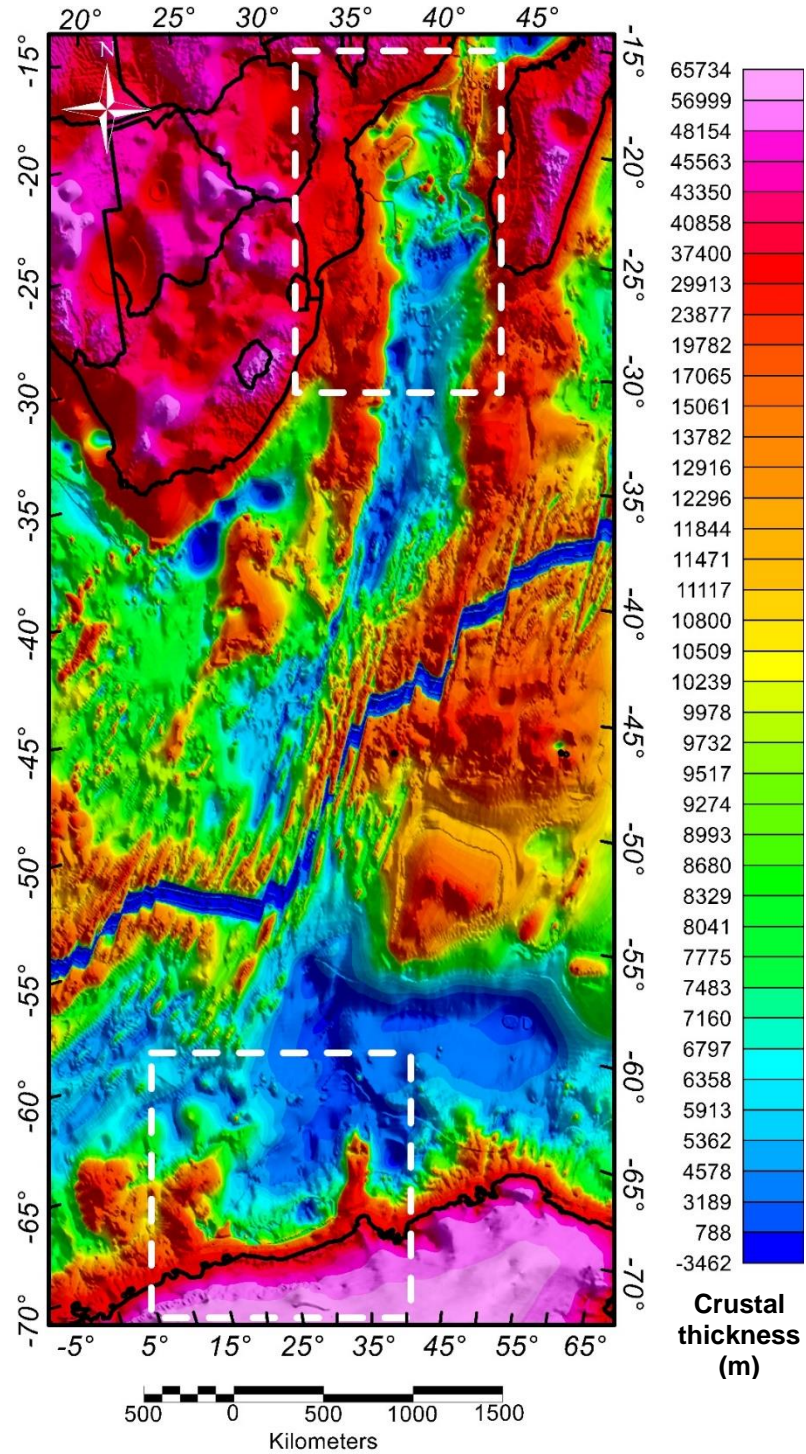


Table 3.3: Sclater’s factor to scale the isostatic Moho calculation based on age of the crust (Sclater, 1980). Isostasy calculation can be applied to crust from 50 Ma and older almost to the full extent. At age of 5 million years, scale factor decreases to less than 0.5 and approaches zero at about 2 million years.

Crust Age (Myr)	Scale Factor	Crust Age (Myr)	Scale Factor
0.0	0.00	26.4	0.82
2.4	0.00	29.8	0.84
2.7	0.05	29.8	0.84
2.9	0.09	34.3	0.86
3.1	0.13	38.4	0.88
3.2	0.18	43.6	0.89
3.3	0.22	48.1	0.91
3.7	0.27	54.4	0.92
4.0	0.31	61.1	0.93
4.5	0.35	66.8	0.93
5.0	0.38	70.9	0.94
5.8	0.42	76.6	0.94
6.2	0.45	83.7	0.95
6.7	0.49	90.5	0.96
7.5	0.53	96.6	0.96
8.1	0.55	101.1	0.97
8.6	0.57	105.5	0.97
9.3	0.60	110.7	0.97
10.1	0.62	115.0	0.98
10.8	0.64	119.8	0.98
11.7	0.66	125.3	0.98
12.5	0.68	130.0	0.99
13.8	0.70	135.4	0.99
14.9	0.72	143.3	0.99
16.6	0.74	148.4	1.00
18.5	0.76	153.5	1.00
20.5	0.78	160.4	1.00
23.4	0.80	168.2	1.00
		180.0	1.00

geometry. The area of the crystalline crust within each cross section is computed by Oasis Montaj. This area is maintained as each cross section is collapsed by progressively moving the continent-ocean boundary landward until the crustal thickness is everywhere uniform and equal to the original, undeformed thickness within the profile. Several different values of the initial thickness of the undeformed crust can be tested to compute the width of the pre-rift continental crust. The fit of the reconstructed margins is used to determine which initial thickness works best.

The method of areal balancing has been used to reconstruct conjugate margins in other parts of the world. However, one aspect of the conjugate African and Antarctic margins is their volcanic origin. In principle, areal balancing is difficult to achieve in the case of volcanic margins because the addition of magmatic material in form of seaward-dipping reflector and underplating are usually challenging to quantify. Volcanic materials were added during the rifting period and thus were not part of the original pre-rift crust. To properly reconstruct volcanic margins, appropriate amount of volcanic material must be excluded from the crustal thickness derived from gravity inversion model prior to collapsing the continent-ocean boundary.

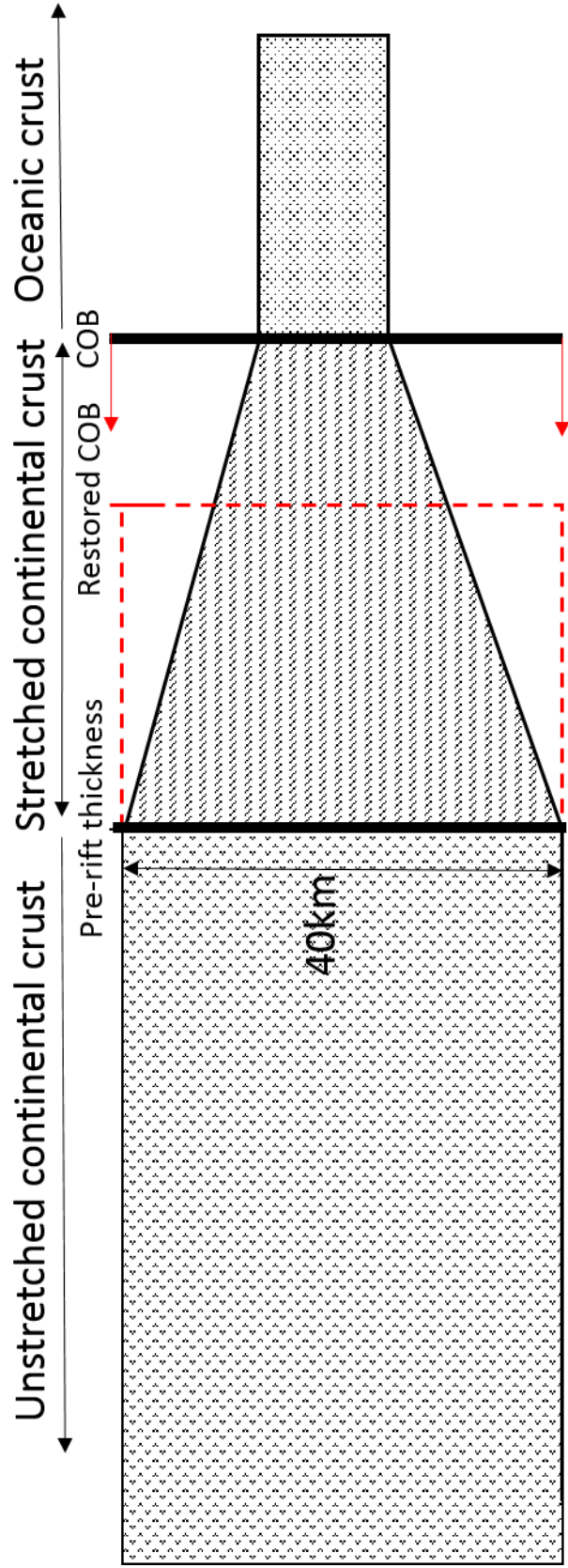
Proprietary seismic reflection data over parts of offshore East Africa that show imaging of seaward-dipping reflectors are used to estimate the amount of this kind of volcanic addition. The amount of underplating, however, remains unknown. In order to overcome this challenge, it is necessary to look at other volcanic margins around the world where both seaward-dipping reflectors and underplating have been encountered and documented (Namibia, Greenland, Argentina). From there, an

empirical relationship between the quantities of these two kind of volcanic matters is formulated. Such relationship helps to approximate the amount of underplating based on the extent of seaward-dipping reflectors. Table 3.4 shows the amount of seaward-dipping reflector and the corresponding amount of underplating in different margins around the world.

Table 3.4: Cross sectional areas of seaward-dipping reflectors (SDR) and their corresponding underplating in different margins around the world.

Margins	SDR (km²)	Underplating (km²)	SDR/Underplating (%)	Source
Namibia	580	953	60	Bauer et al. (2000)
Namibia	356	690	51	Bauer et al. (2000)
Greenland	544	1840	29.5	Voss and Jokat, (2007)
Greenland	500	1880	27	Schnabel et al. (2008)
Argentina	102	395	26	Schnabel et al. (2008)
Norway	232	517	45	Mjelde et al. (2005)
		Average	40	

Figure 3.14: Illustration of the areal-balancing method used in non-rigid reconstruction. Two dimensional cross sections are extracted from the inversion model showing thickness of the crystalline crust. The continent-ocean boundary (COB) is closed toward the boundary of pre-determined un-stretched crustal thickness while maintaining the sectional area of the stretched crust. The restored COB is determined at the location where crustal thickness is uniform and equal to thickness of undeformed crust.



CHAPTER 4

RESULTS AND ANALYSES

4.1 Fracture zones tracing

As mentioned previously, detecting fracture-zone traces greatly enhances the reliability of magnetic isochron identification. Crucial to this study is the new version (V23.1) of satellite-derived free-air gravity anomaly data published in Sandwell et al. (2014). With its improved resolution, fracture-zone traces become more visually detectable. From inspecting the gravity data, four and five fracture zones are identified in the Mozambique Basin and Riiser Larsen Sea, respectively. Figures 4.1 to 4.6 show the tilt derivative (Verduzco et al., 2004) of different residual gravity anomaly maps which result from subtracting the upward continued Bouguer gravity anomaly to various datums from the observed data. Multiple levels of upward continuation help delineate the anomaly caused by density contrast from within the upper crust. Distinctly recognized in these maps are the fracture zones extending from the mid-ocean ridge to the continental margins of Africa and Antarctica. Of the four fracture zones identified over the Mozambique Basin, three have been partly recognized as the Mozambique Fracture Zone and fracture zones E and F through previous gravity and magnetic anomaly interpretation (Segoufin, 1978; Simpson et al., 1979; Konig and Jokat, 2010, Leinweber and Jokat, 2012). A new fracture zone identified from this study is fracture zone G which is about 140 km east of fracture zone F. All four identified fracture zones have subparallel N-S trends. The northern end of fracture zones F and G can be confidently traced northwards to about 16°N

latitude, 70 km off the coast of Mozambique. Fracture zone E may extend as far north as the southern edge of the Beira High even though the gravity signature becomes noisy as it approaches the structure. To the south, the fracture zones terminate at latitudes 25-26°S where they join with another set of fracture zones that have a different orientation connecting the Mozambique Basin and the mid-ocean ridge in a NE-SW direction. These could be the continuations of the same fracture zones after a time of plate reorganization. Similarly, the Riiser Larsen Sea is separated into a number of sea floor spreading corridors by five recognized fracture zones. In the western end is the Astrid Fracture Zone (Konig and Jokat, 2010; Leinweber and Jokat, 2012) that trends NE-SW from the mid-ocean ridge to the Riiser Larsen Sea and bifurcates the Astrid Ridge into northern and southern parts. The other four fracture zones have also been partially distinguished by previous gravity and magnetic studies (Bergh, 1977; Konig and Jokat, 2010; Leinweber and Jokat, 2012). Nevertheless, the new gravity data enable this study to extend these fracture zones much farther south into the continental margin of Antarctica. In this study, these fracture zones are termed E1, F1, G1 and H1 from west to east. They are subparallel in a more NE-SW direction and can be traced as far south as 67°S latitude, approximately 75 km offshore Antarctica. The gravity data show continuous traces of the fracture zones to the mid-ocean ridge, though there is a noticeable bend in all traces at latitude 62°S where the fracture zones continue in a more NNE-SSW direction.

Figure 4.1: Tilt-derivative filter applied to 5 km residual gravity anomaly data over the Mozambique Basin. Note the roughly N-S linear trends that are subparallel to the Davie Fracture Zone (dashed outline). The sparsely dotted lines are interpreted fracture zones referred to as Mozambique Fracture Zone (MFZ), fracture zones E, F and G. Between latitude 25°S-27°S, the fracture zones change their trends from N-S to NNE-SSW direction.

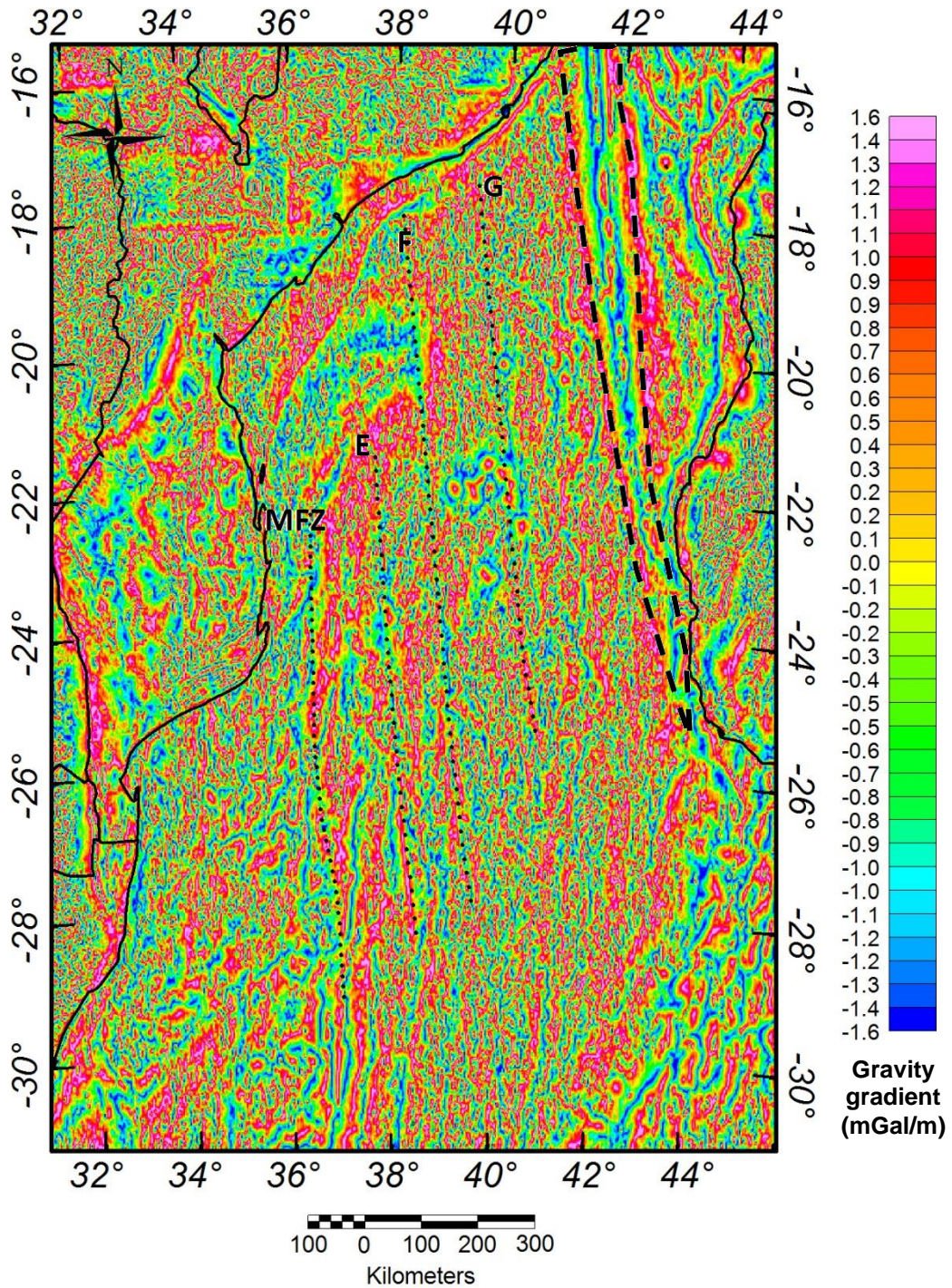


Figure 4.2: Tilt-derivative filter applied to 30 km residual gravity anomaly data over the Mozambique Basin. Note the NNW-SSE linear trends are now more visible than Figure 4.1. Map details are the same as in Figure 4.1

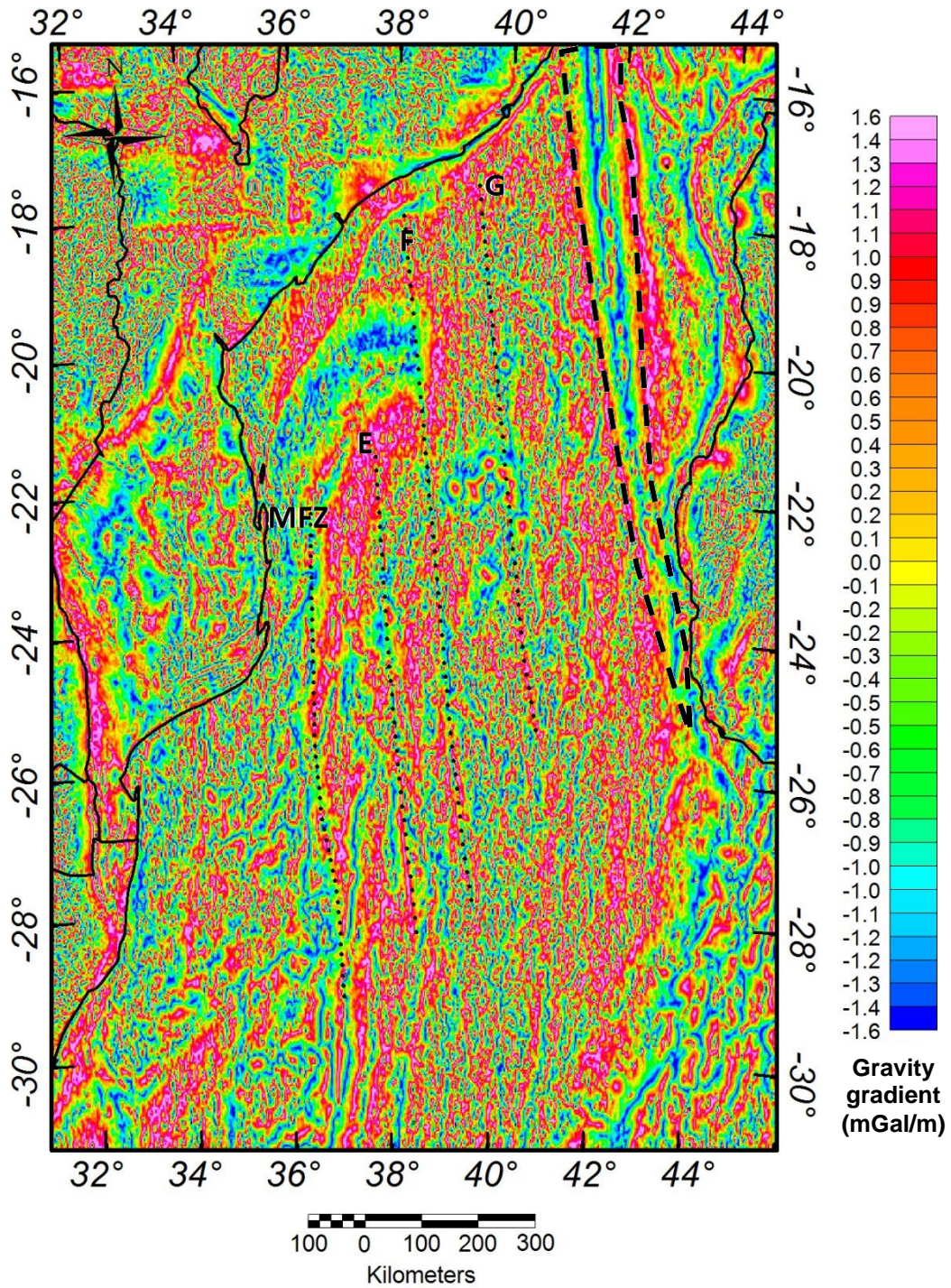


Figure 4.3: Tilt-derivative filter applied to 90 km residual gravity anomaly data over the Mozambique Basin. Most of the long wavelength gravity field from deep mantle are likely to be removed in this map. The present anomaly are mostly from structures within the crust. The same linear features remain visible as in Figures 4.1 and 4.2.

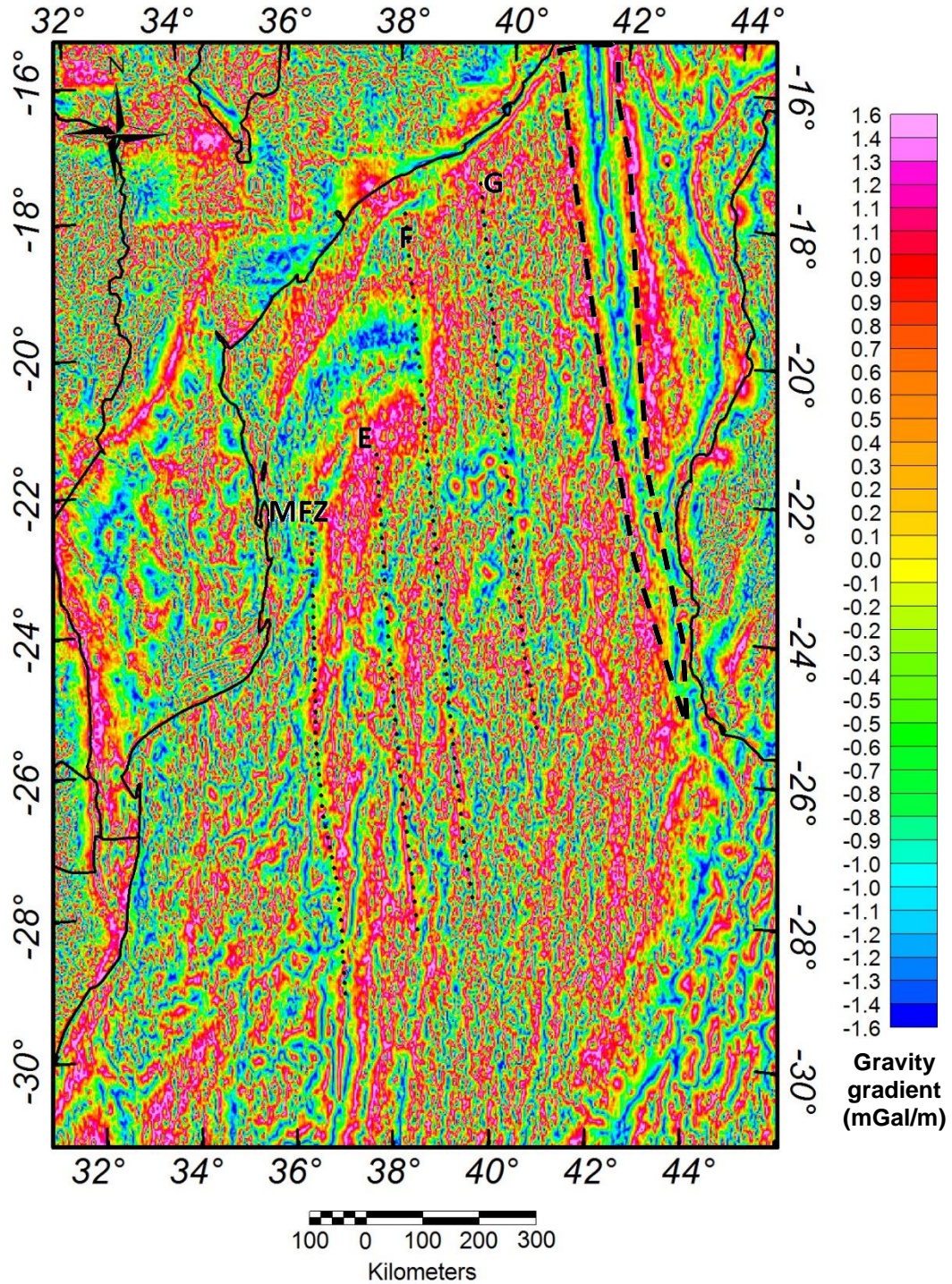


Figure 4.4: Tilt-derivative filter applied to 5 km residual gravity anomaly data over the Riiser Larsen Sea. NE-SW linear trends are visible at latitude 65°S and areas further north but faint toward the coast line. The dotted lines are interpreted fracture zones. Beside the most clearly defined Astrid Fracture Zone (AFZ), from left to right are fracture zone E1, F1, G1 and H.

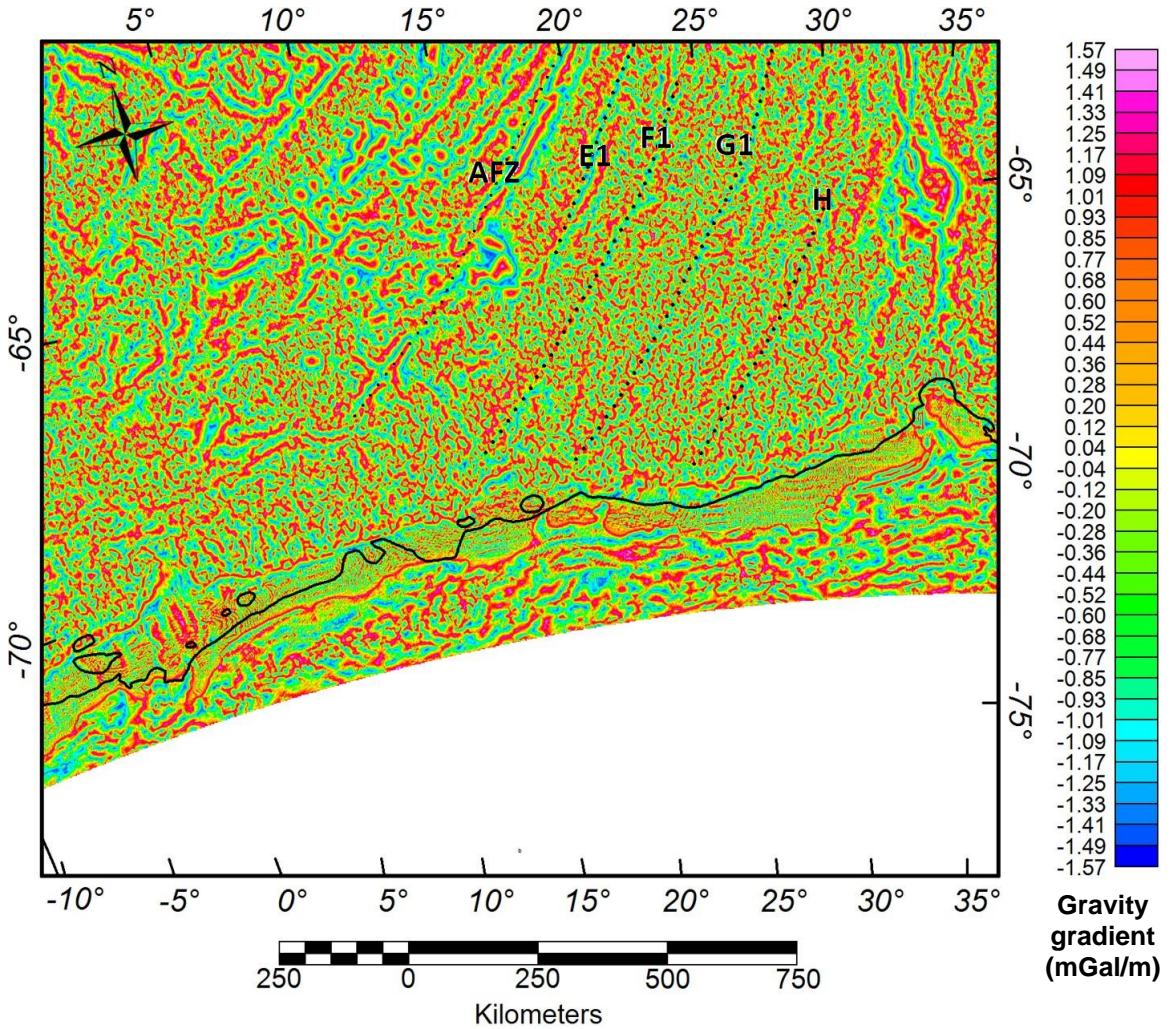


Figure 4.5: Tilt-derivative filter applied to 30 km residual gravity anomaly data over the Riiser Larsen Sea. Here the fracture zones are more visible especially in the southern part of the margin. Note a subtle bend at latitude 65°S where all fracture zone change to a more northward direction.

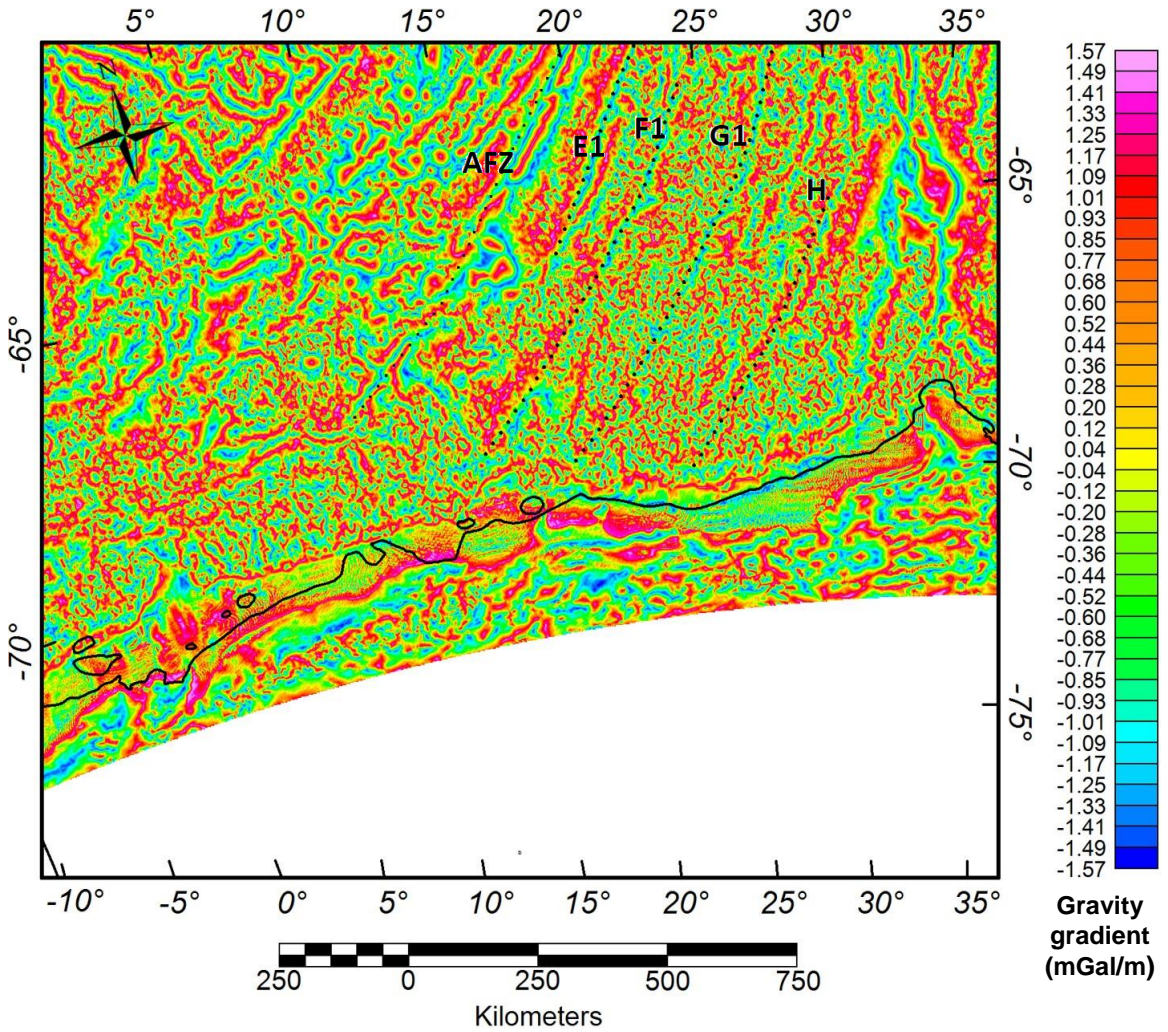
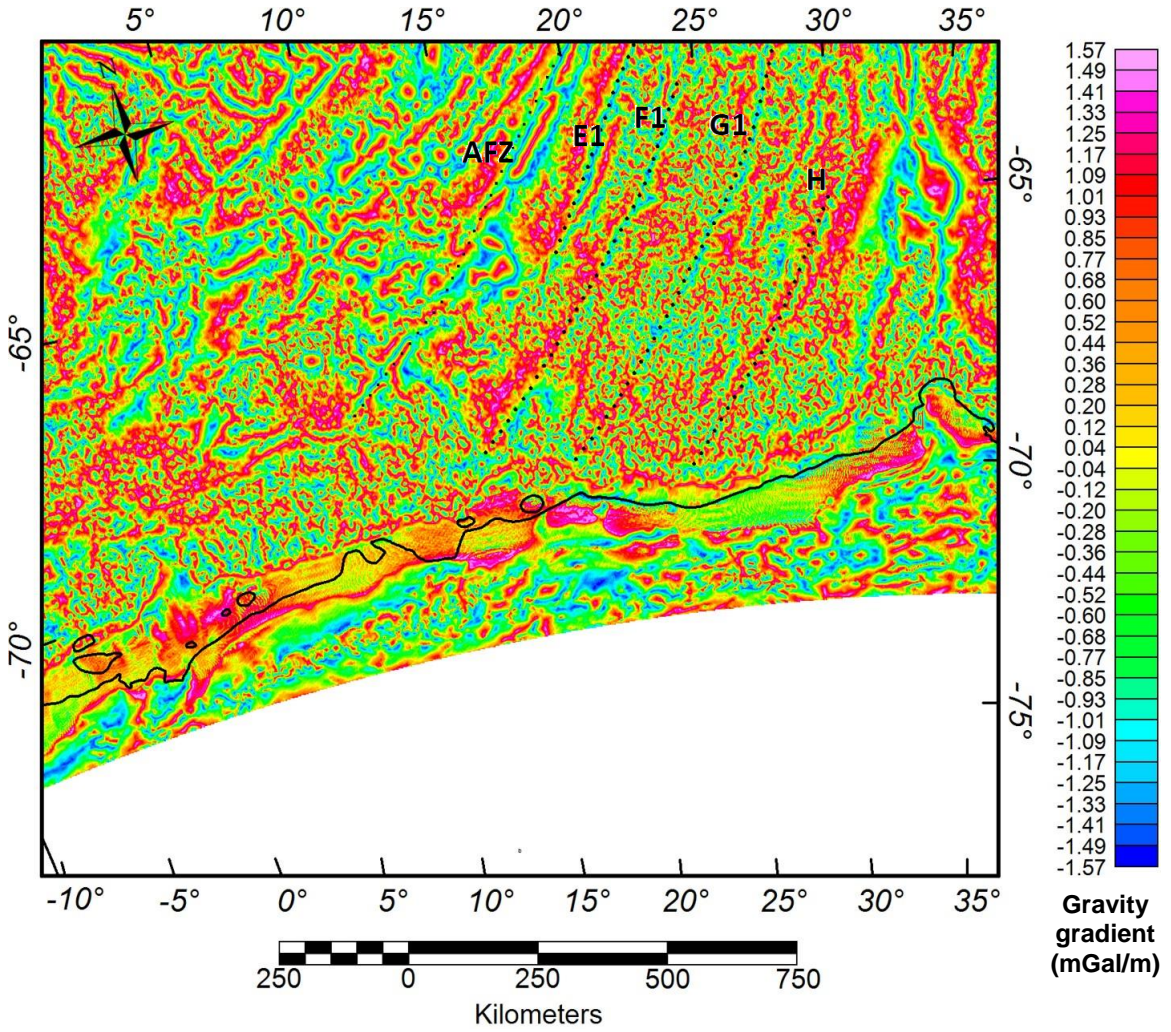


Figure 4.6: Tilt-derivative filter applied to 90 km residual gravity anomaly data over the Riiser Larsen Sea. Most long wavelength signals have been removed. Pronounced gravity anomalies reveal the traces of fracture zones.



4.2 Magnetic isochron identification

Since fracture zones over the Mozambique Basin dominantly strike in the N-S direction, the corresponding spreading magnetic anomalies should be in a roughly E-W direction. From the NGDC database, several ship tracks that trend at low angle to the N-S direction are chosen for magnetic anomaly interpretation. In the Riiser Larsen Sea, all interpreted magnetic profiles are from various publications and also orientated in favorable directions for interpretation purpose. Locations of interpreted profiles are shown together with the identified isochrons in Figures 4.7 and 4.8. After testing different seafloor spreading models, the model from the König and Jokat (2010), which used the geomagnetic polarity timescale of Gradstein et al. (2004), was determined to give the best correlation with the observed magnetic profiles. Hence, that model is adopted in this study to identify magnetic isochrons. The detailed correlation of all observed magnetic profiles and the synthetic model are shown in Figures 4.9 to 4.14. The youngest isochrons, M0r (124.8 Ma), over the Mozambique Basin are identified in the corridors between fracture zones E and F, and F and G. From the total thirteen interpreted profiles, M0r are identified in eight different profiles that show consistency in their pattern with respect to fracture zones orientations. Though M33n (159 Ma) are the oldest identified isochrons in the Mozambique Basin, identification for these chron is somewhat tentative. The more consistently identified isochrons are M22n1n (149.5 Ma) which can be determined in five different profiles across two fracture zones. In general, observed magnetic profiles show good correlation with the modeled seafloor spreading anomaly. The

Figure 4.7: Locations of interpreted magnetic profiles and identified isochrons in the Mozambique Basin. Blue lines are ship tracks from the NGDC. Profiles from König and Jokat (2010) are shown in green. Grey lines are from Segoufin (1978). Two black profiles are from Leinweber and Jokat (2013). Fracture zones are shown as dashed lines. Question marks denote tentative identifications.

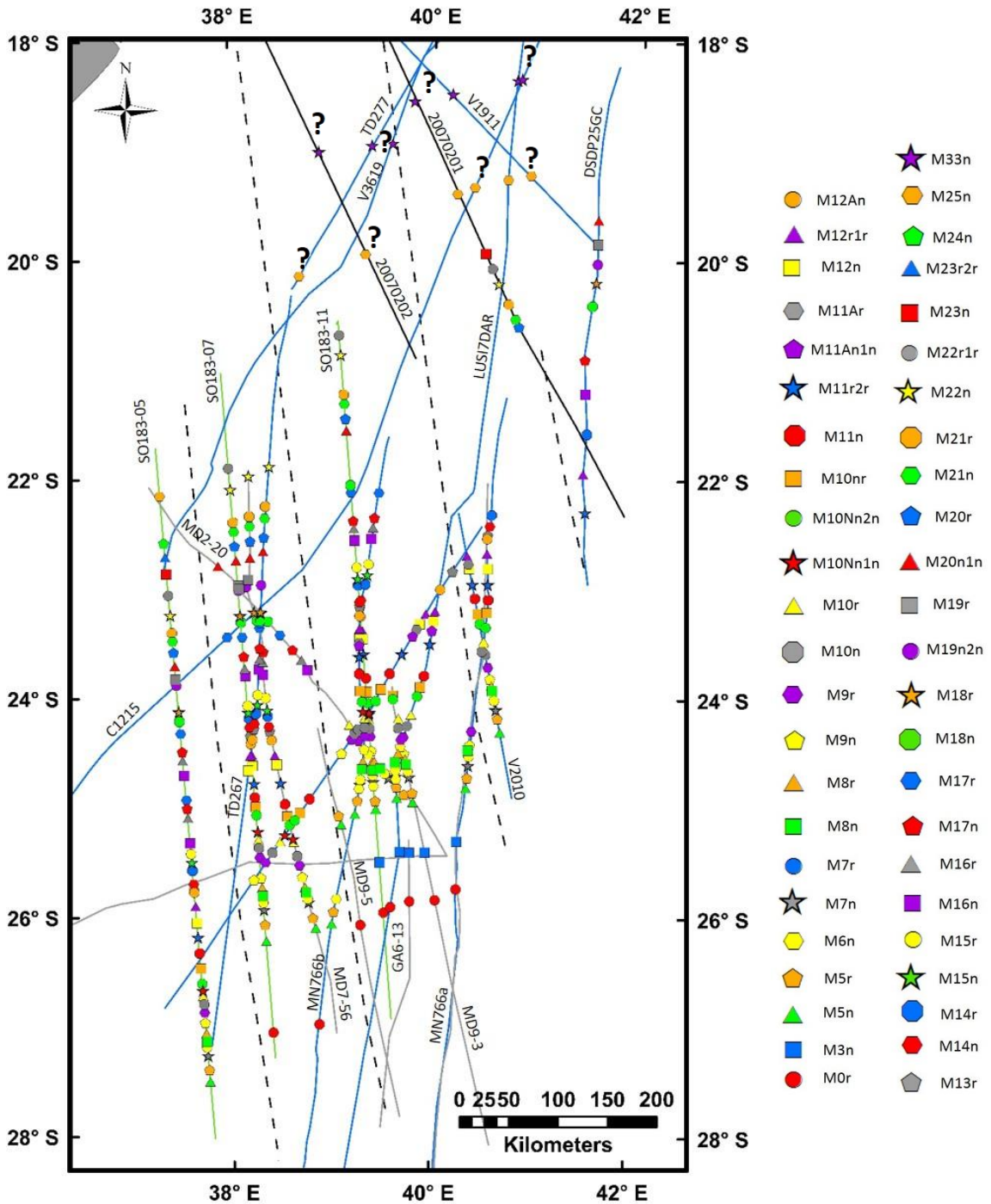
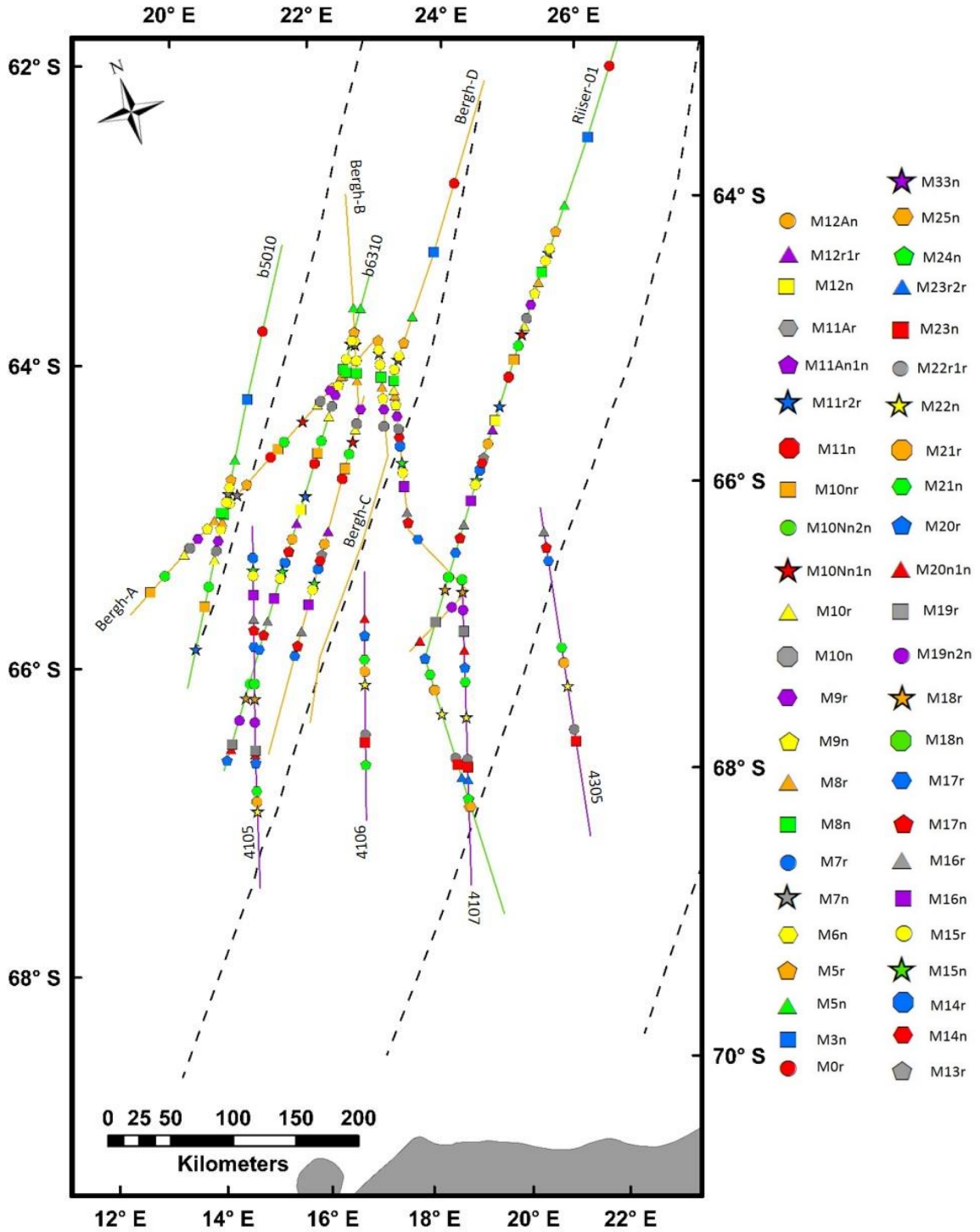


Figure 4.8: Locations of interpreted magnetic profiles and identified isochrons in the Riiser Larsen Sea. Profiles from König and Jokat (2010) are shown in green. Orange lines are from Bergh (1977). Purple are profiles from Leitchenkov et al. (2008). Fracture zones are shown as dashed lines.



identified isochrons express displacement patterns that are consistent with locations of fracture zones. Fracture zones E and F are associated with offset distances of about 90 km and 105 km respectively. There is, however, a significant change in magnetic signal in profiles east of fracture zone G. Across this fracture zone, the average magnetic amplitude is subdued from 200 nT on its western side to less than 100 nT on the eastern side. This is consistent with the study from Konig and Jokat (2010) who reported a zone of subdued magnetic anomaly amplitudes east of longitude 41°E, though fracture zone G was not recognized in that study. Even though low signal amplitude presents a challenge in interpreting the magnetic data in that region, magnetic isochrons are identified in three NGDC profiles. The existence of fracture zones G is supported by approximately 50 km displacement of identified isochrons. Offsets of magnetic isochrons also suggest the presence of another fracture zone about 80 km east of fracture zone G that could have a maximum displacement of 55 km. In the northern Mozambique Basin close to the coast line, two magnetic profiles in Leinweber and Jokat (2013) and four NGDC profiles reveal magnetic data with dominantly long wavelength at very low amplitude (<50 nT). As a result, isochrons from M25n (154.7 Ma) to M33n (159.1 Ma) as identified in these profiles (Figure 4.12) are rather tentative and hence not incorporated in the reconstruction model. Questionable isochrons are denoted with question marks in Figure 4.7.

Picks of magnetic isochrons in the Riiser Larsen Sea are similar to those seen in the Mozambique Basin. The observed data correlate well with the synthetic model. The youngest isochrons are M0r identified in three profiles among the total eleven

Figure 4.9: Correlations of magnetic profiles in the Mozambique Basin and seafloor spreading model of Konig and Jokat (2010). Blue color indicates ship tracks from the NGDC. Black and grey lines are profiles from published papers. Profiles locations and reference sources can be found in Figure 4.7.

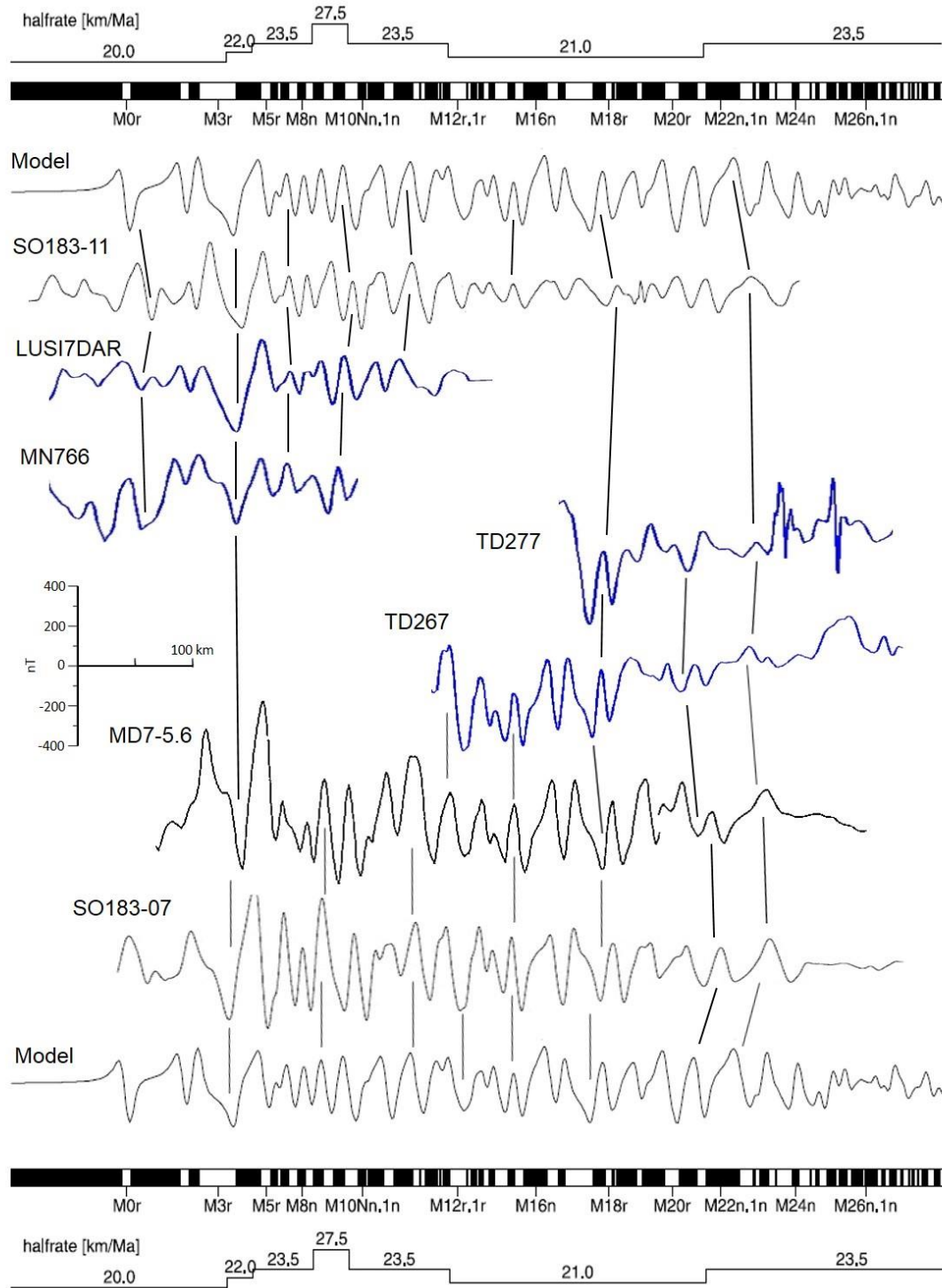


Figure 4.10: Correlations of magnetic profiles in the Mozambique Basin (continued). Red boxes indicate repeated section along the same profile.

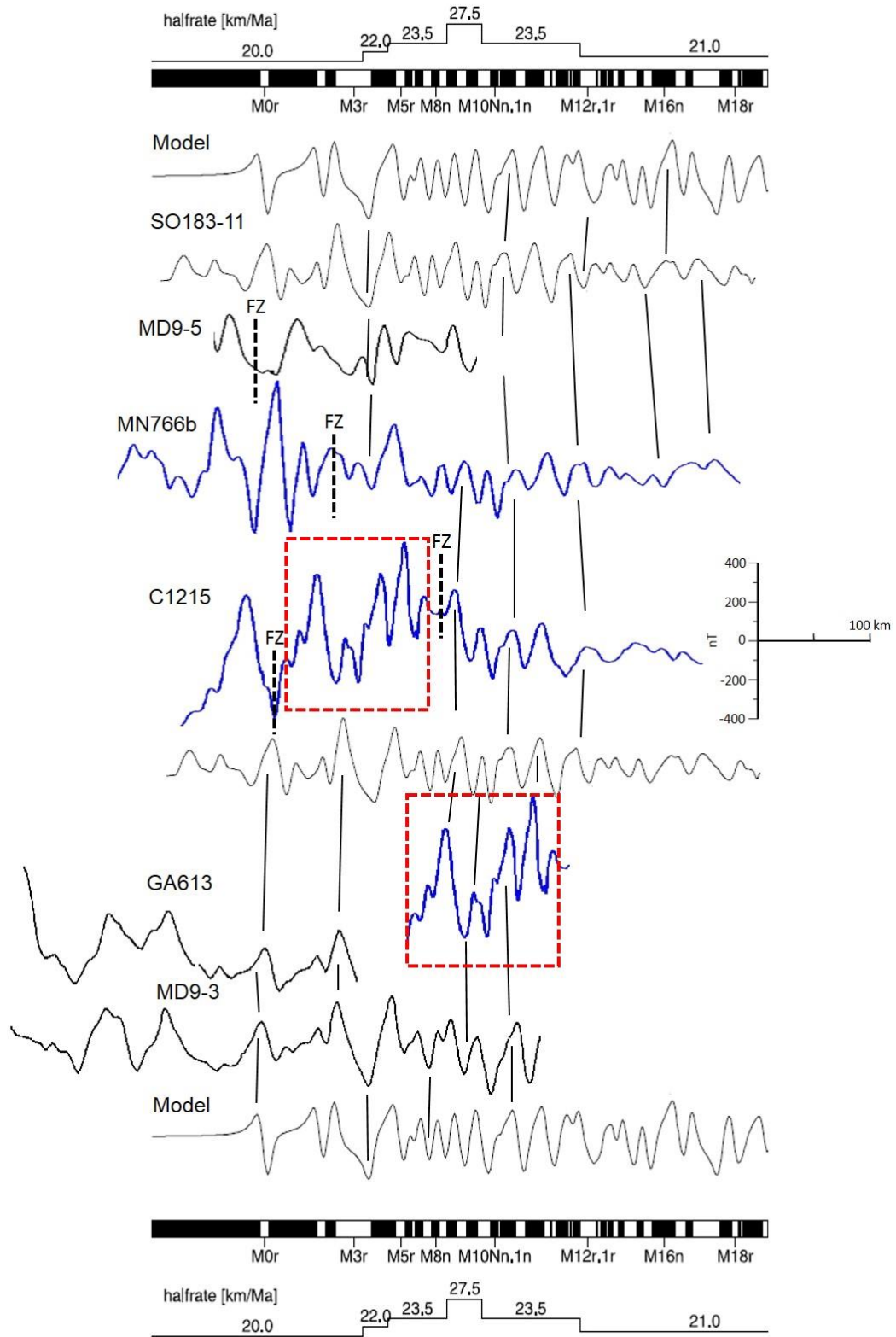


Figure 4.11: Correlations of magnetic profiles in the Mozambique Basin (continued).

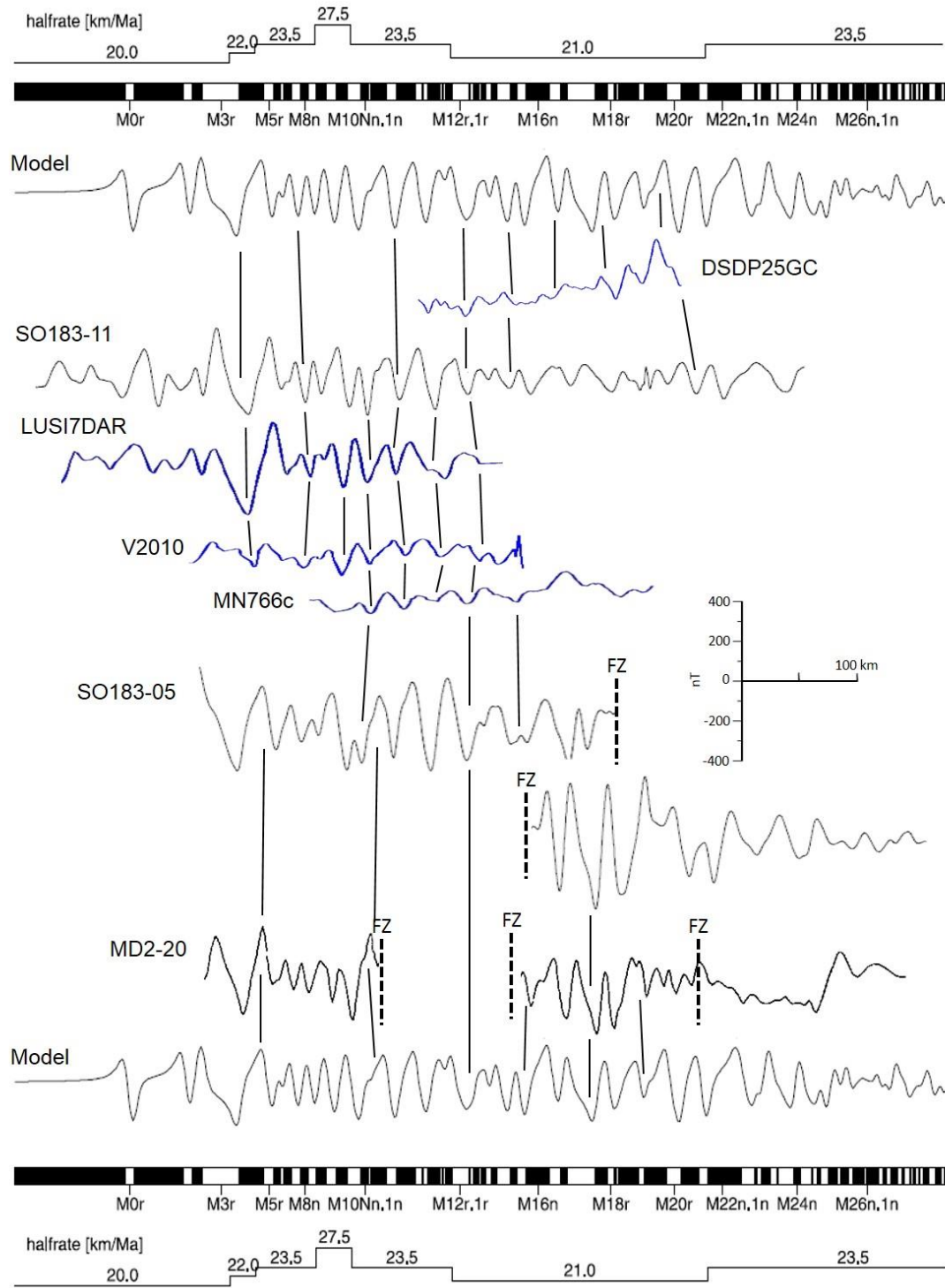


Figure 4.12: Correlation of magnetic data collected in the northern region of the Mozambique Basin. Note the subdued amplitude across all profiles. The synthetic model is from Leinweber and Jokat (2013). Blue color indicates ship tracks from the NGDC. Black and grey lines are profiles from published papers. Profiles locations and reference sources can be found in Figure 4.7.

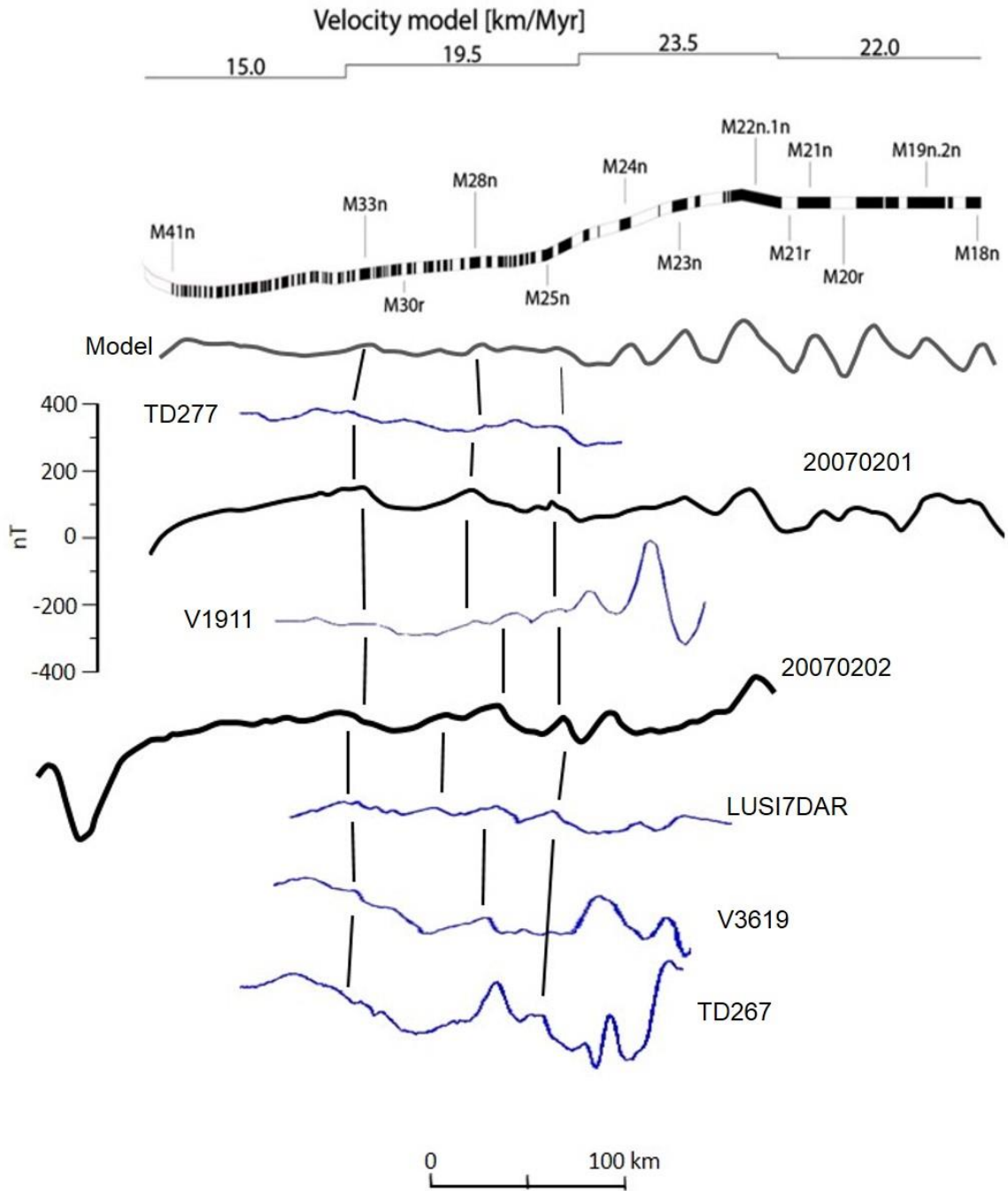


Figure 4.13: Correlations of magnetic profiles in the Riiser Larsen and seafloor spreading model of König and Jokat (2010). Profiles locations and reference sources are shown in Figure 4.8. Red boxes indicate repeated section along the same profile.

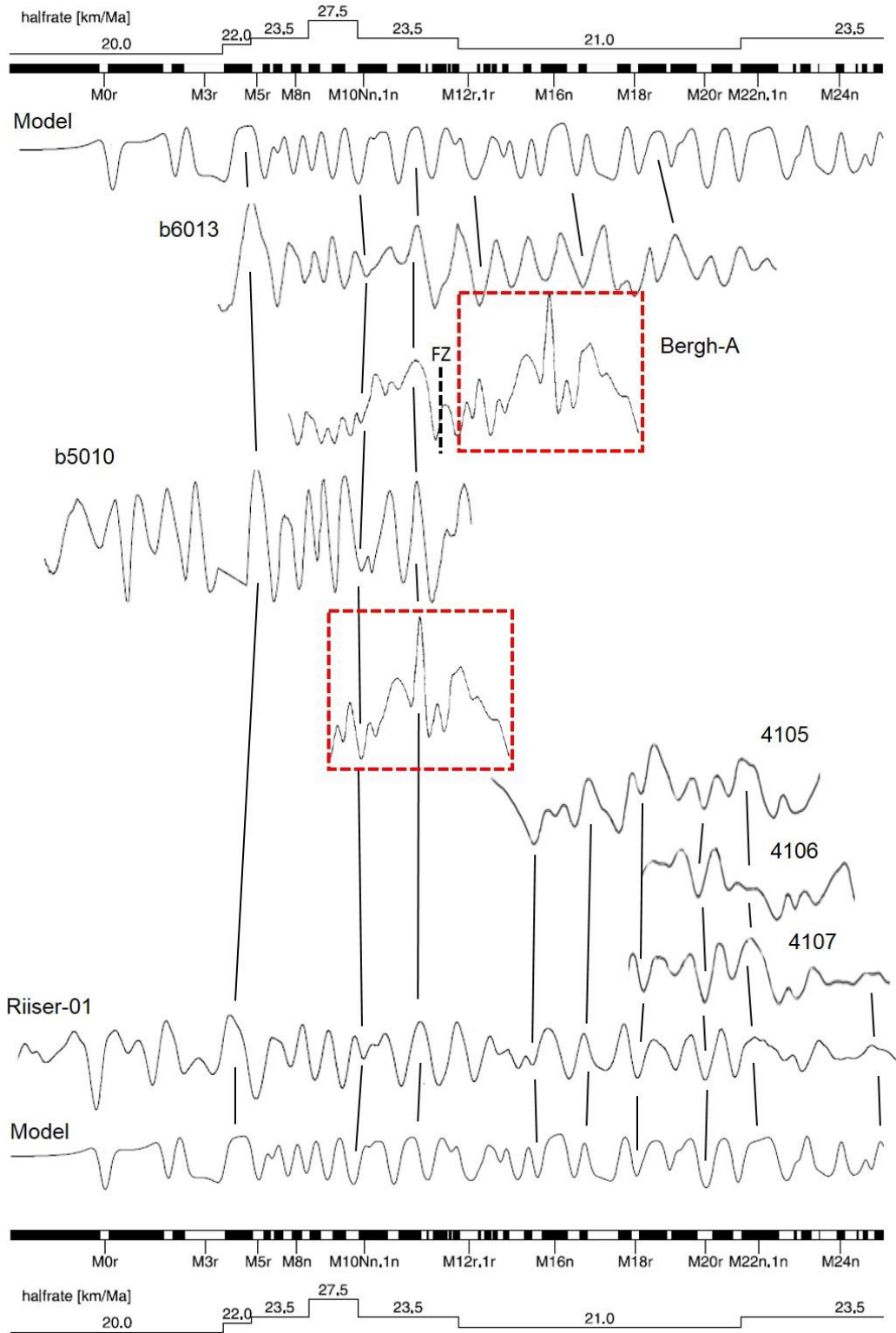
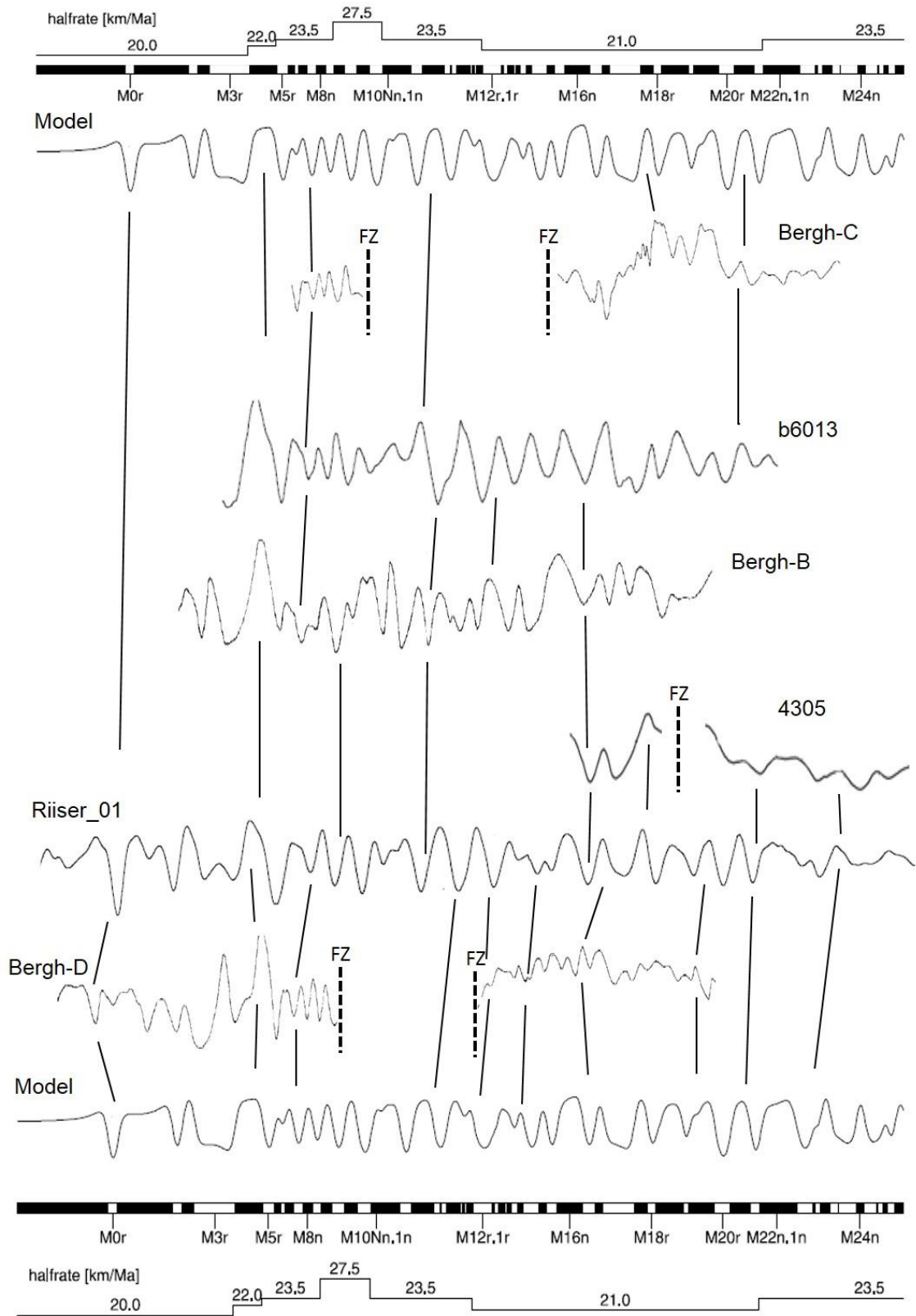


Figure 4.14: Correlations of magnetic profiles in the Riiser Larsen (continued).



interpreted profiles. All three isochrons are in different spreading corridor separated by fracture zones E1 and F1. M25n are the oldest isochrons identified in profile Riiser-01 and 4107. Isochrons displacements along fracture zone E1, F1 are 130 km and 110 km respectively. These findings are also similar to those reported in Leinweber and Jokat (2012), König and Jokat (2010). In addition, this study re-interprets profile 4305 which was published by Leitchenkov et al. (2008). The newly identified isochrons confirm the presence of fracture zone G1 that is revealed in the filtered gravity anomaly map. This fracture zone has an average offset of about 35 km.

4.3 Three-dimensional gravity inversion

Shown in Figure 4.15 is the free-air gravity anomaly at datum 3805m above sea level generated by a five-layer structural model (Chapter 3). The error grid which is the difference between the observed data (Figure 4.16) and the calculated gravity anomaly, is shown in Figure 4.17. The mean error is about 1.5 mGal with a standard deviation of about 15.2 mGal. The maximum and minimum errors are 275.2 mGal and -132.0 mGal respectively. High errors are observed in areas close to the mid-ocean ridge whereas the continents and their margins have maximum difference of about 40 mGal. The anomalously high error at the mid-ocean ridge could be due to underestimated mantle density (3.0 g/cc). Nevertheless, these errors can be tolerated as the crustal thickness at the mid ocean ridge is not involved in the rigid and non-rigid reconstructions. More importantly, over the Mozambique Basin and Mozambique continental margin, the average error is less than 10 mGal with the maximum error of about 40 mGal close to the shelf break along latitude 15°S-17°S.

Figure 4.15: Free-air gravity anomaly generated by the three-dimensional gravity inversion model. White boxes mark areas of the Mozambique Basin and the Riiser Larsen Sea.

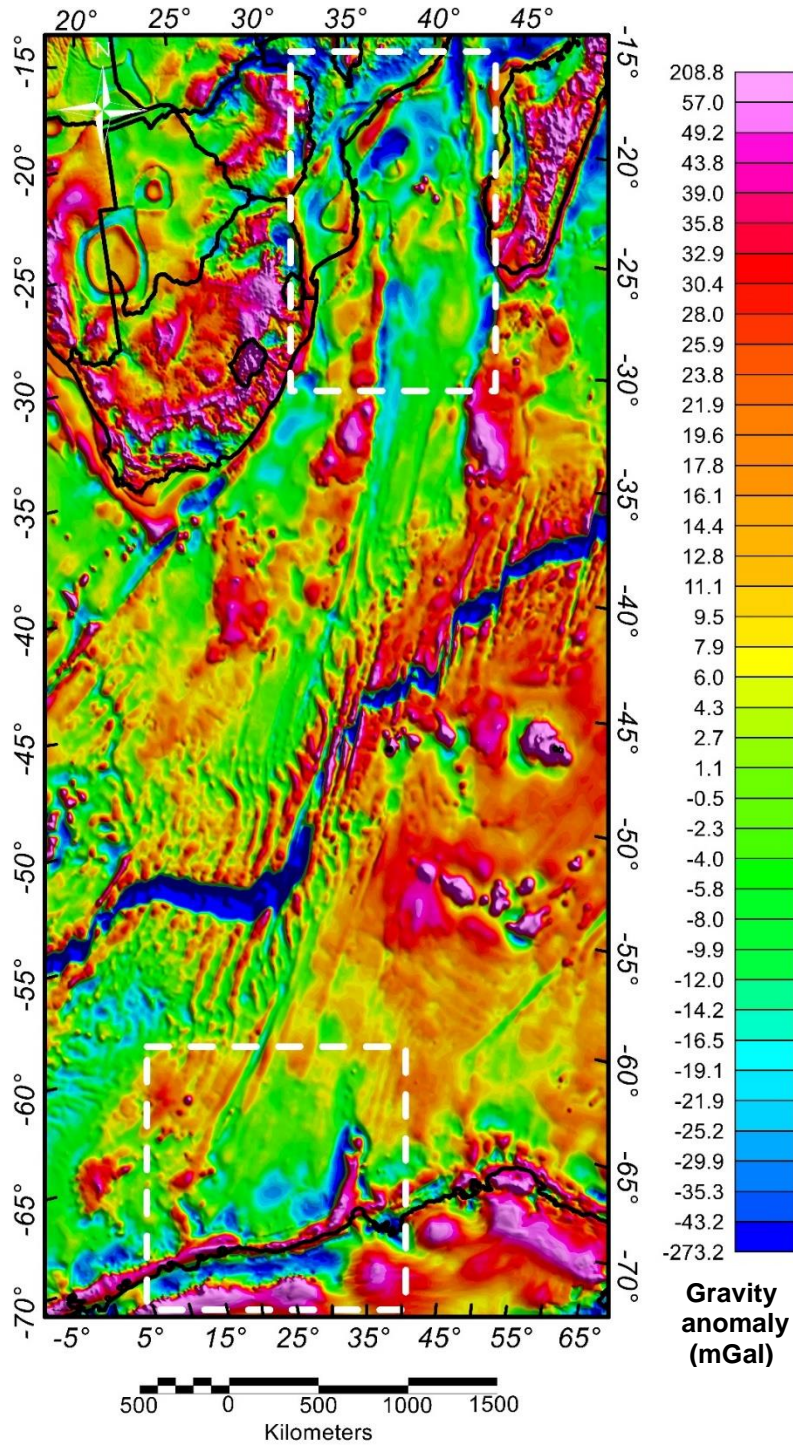


Figure 4.16: Free-air gravity anomaly derived from upward continuing the satellite-derived gravity data to datum 3808 m above sea-level. White boxes mark areas of the Mozambique Basin and the Riiser Larsen Sea.

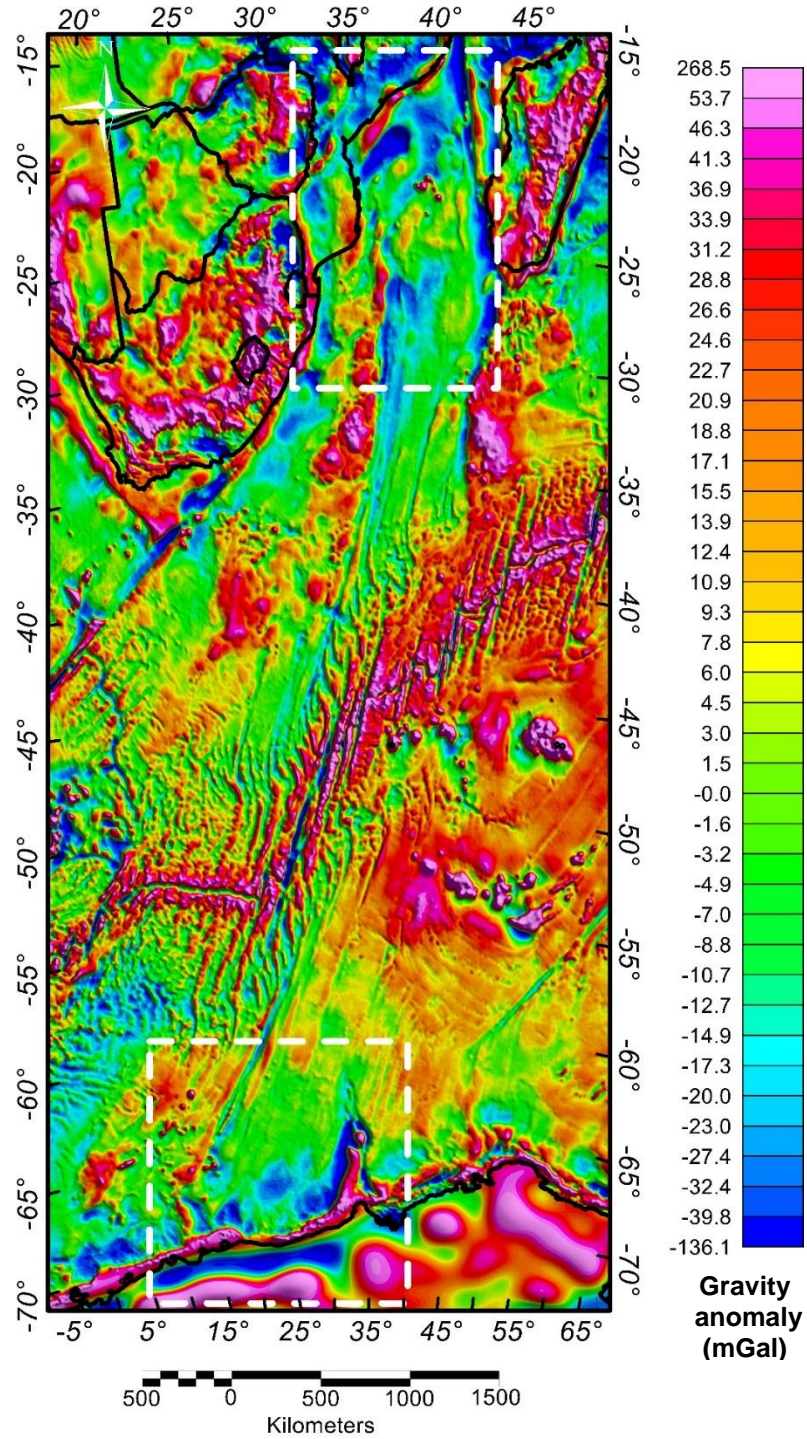
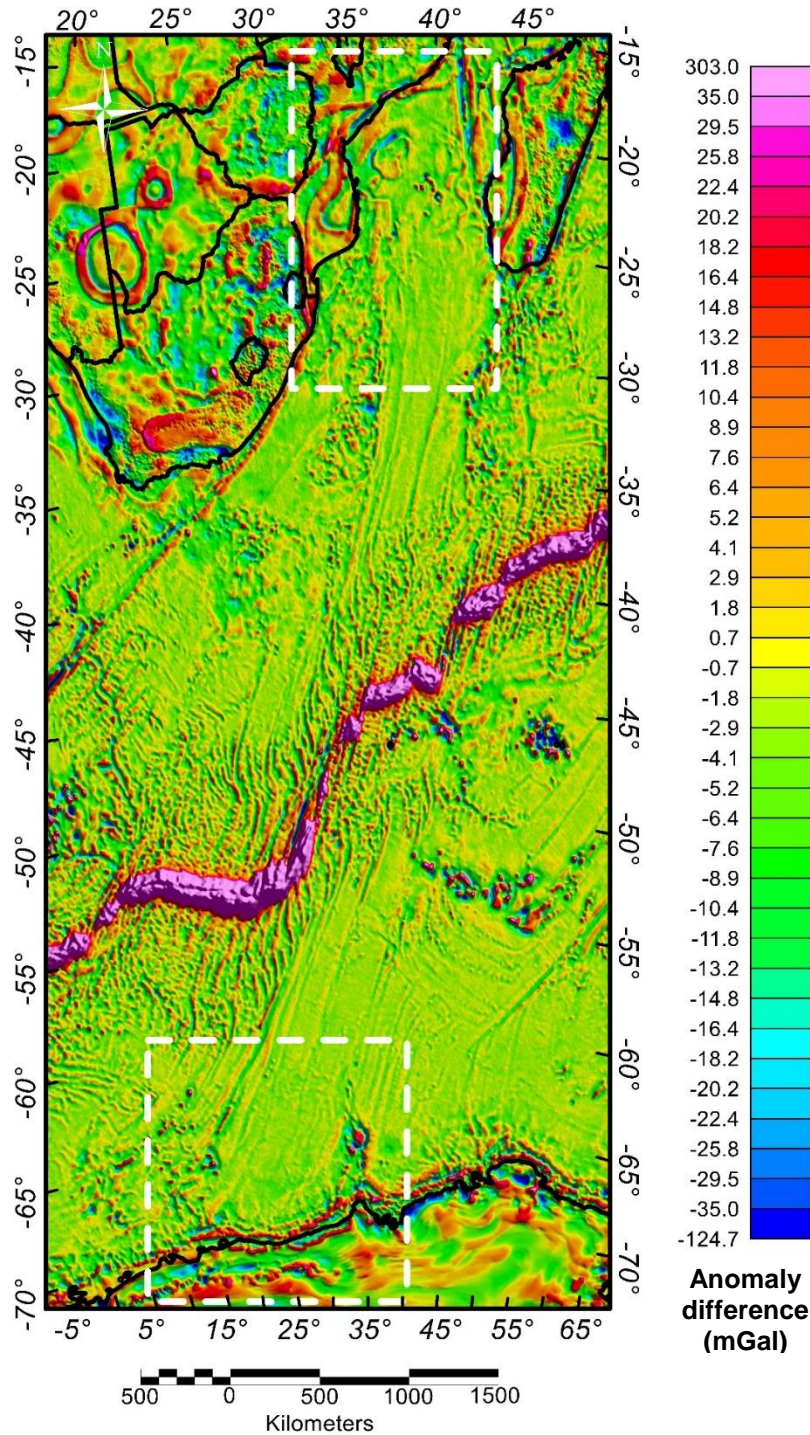


Figure 4.17: Error grid comparing the observed gravity data and values calculated from the model response. Highest error is at the mid-ocean ridge. Over the Mozambique Basin, highest error is about 40 mGal close to the coast line. Error is only a few mGal over the Riiser Larsen Sea. White boxes mark areas of the Mozambique Basin and the Riiser Larsen Sea.



Here, the lower-than-observed gravity anomaly calculated from the model might suggest a higher density should be used for the sediment package. Presence of magmatic material which is not incorporated in the model might also cause such error. This error would affect depth of the inverted Moho and thus the crustal thickness. Favorably, in this area across the error anomaly, there are seismic refraction profiles that can be used to test for the inversion results and account for inaccurate crustal thickness. On the other hand, the calculated gravity anomaly from the model's response is in very good agreement with the observed data over the Riiser Larsen Sea and Antarctic margin where error values are in range of only few mGal. Figure 4.18 displays the depth to Moho grid after gravity inversion process. The difference between the inverted Moho grid and the initial calculated isostatic Moho grid is shown in Figure 4.19. This difference grid shows that most parts of the study areas are close to isostatic equilibrium as the difference values range from a few hundred meters to about several kilometers. To produce a more geologically plausible Moho, the inverted Moho was run through a low-pass filter to eliminate spiky and abrupt changes in Moho depth that have wavelength less than 50 km. Crustal thickness calculated by subtracting the inverted Moho from the basement grid is shown in Figure 4.20. Onshore African and Antarctic continents, the average crustal thicknesses are about 40 km and 55 km respectively. In the central Mozambique Basin and Riiser Larsen Sea, the crust is about 7 to 11 km thick. In the deep ocean basins beyond the continental margins, crustal thickness ranges from 4.5 to 7 km. Submarine plateaus (Maud Rise, Madagascar Plateau, Astrid Ridge, etc.,) are

20 km thick on average. In general, the resulting values are closed to that of the global average for crustal thickness of various structures (Mooney et al., 1998). Quality control of the inversion results is carried out using two seismic refraction profiles in the Mozambique margin (Figure 4.21) and another pair of refraction-constrained gravity models in the Antarctic margin (Figure 4.22). Over the Mozambique Basin, the crustal thickness model from gravity inversion is very close to that of the P-wave model. Along both profiles, the average difference in thickness of the crystalline crust is less than 2 km. More importantly, the area landward of where fracture zones terminate has crustal thickness difference of less than 1 km. It is also noted that even though high density underplating body was not incorporated into the gravity inversion model, the inverted depth to Moho is very consistent with P-wave model. This might occur if high density lower crust is offset by low density sedimentary layers resulting in unchanged Moho depth. This observation is critical in non-rigid reconstruction where calculations are carried out to account for the effect of magmatic underplating on crustal thickness. Over the Riiser Larsen Sea, comparisons between crustal thicknesses also yield similar results. In profile A of Figure 4.22, which trends N-S across the margin, crustal thickness from gravity inversion is generally in agreement with the ray tracing model to several hundred meters. The only noticeable differences are seen at a few narrow zones along this profile where the inverted Moho is about 2 km deeper than that of the P-wave model. These zones are likely oceanic in nature.

Figure 4.18: Grid of Moho depth computed from gravity inversion. White boxes mark areas of the Mozambique Basin and the Riiser Larsen Sea.

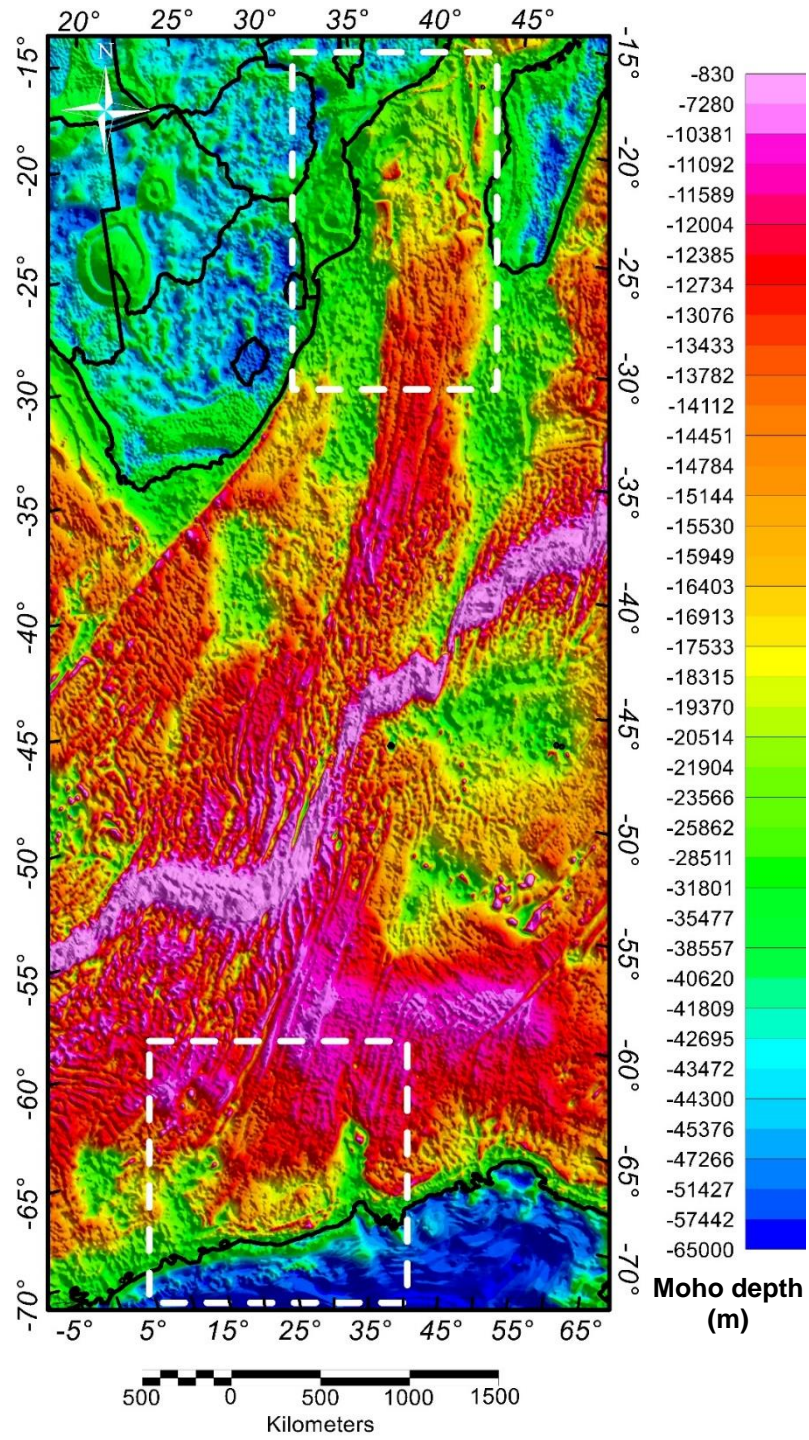


Figure 4.19: Difference between the inverted Moho and input isostatic Moho. Over areas of continental margins, average difference is about 3-4 km with maximum of 8-9 km. White boxes highlight areas of the Mozambique Basin and the Riiser Larsen Sea.

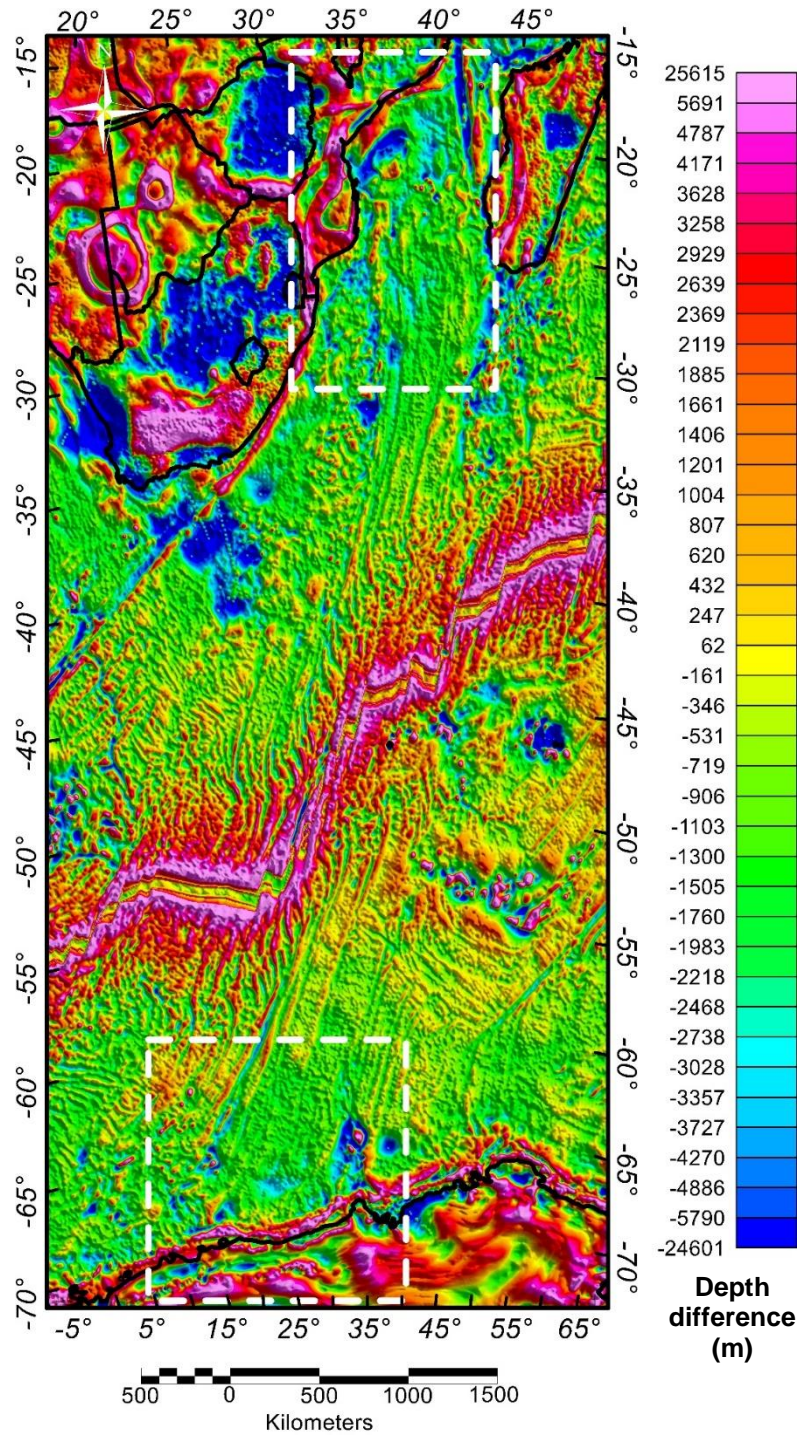


Figure 4.20: Thickness map of the crystalline crust calculated by subtracting the inverted Moho from the basement depth. The result is consistent with global means for thickness of continental and oceanic crusts. Continental crust is about 50 km in average. Thickness of ocean crust is in the range of 4.5-10 km. Lines A, B, C and D in the Mozambique Basin and the Riiser Larsen Sea are location of profiles used evaluate the inversion results.

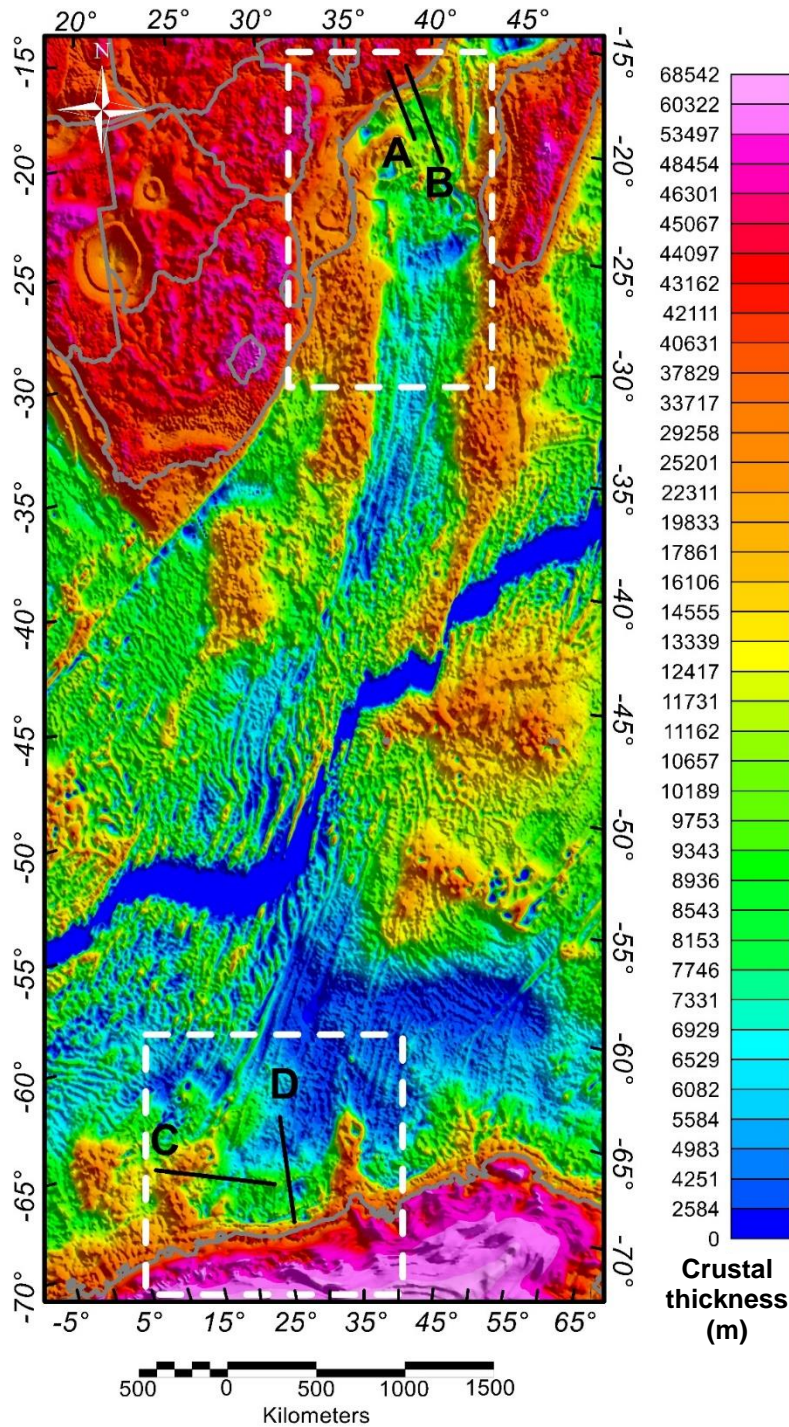


Figure 4.21: Comparing crustal thickness derived from gravity inversion and seismic-constrained P-wave model in the Mozambique Basin. The results are very comparable along Profile A. At about 200 km from the coast in Profile B, the inversion may overestimate the crustal thickness by 3-5 km.

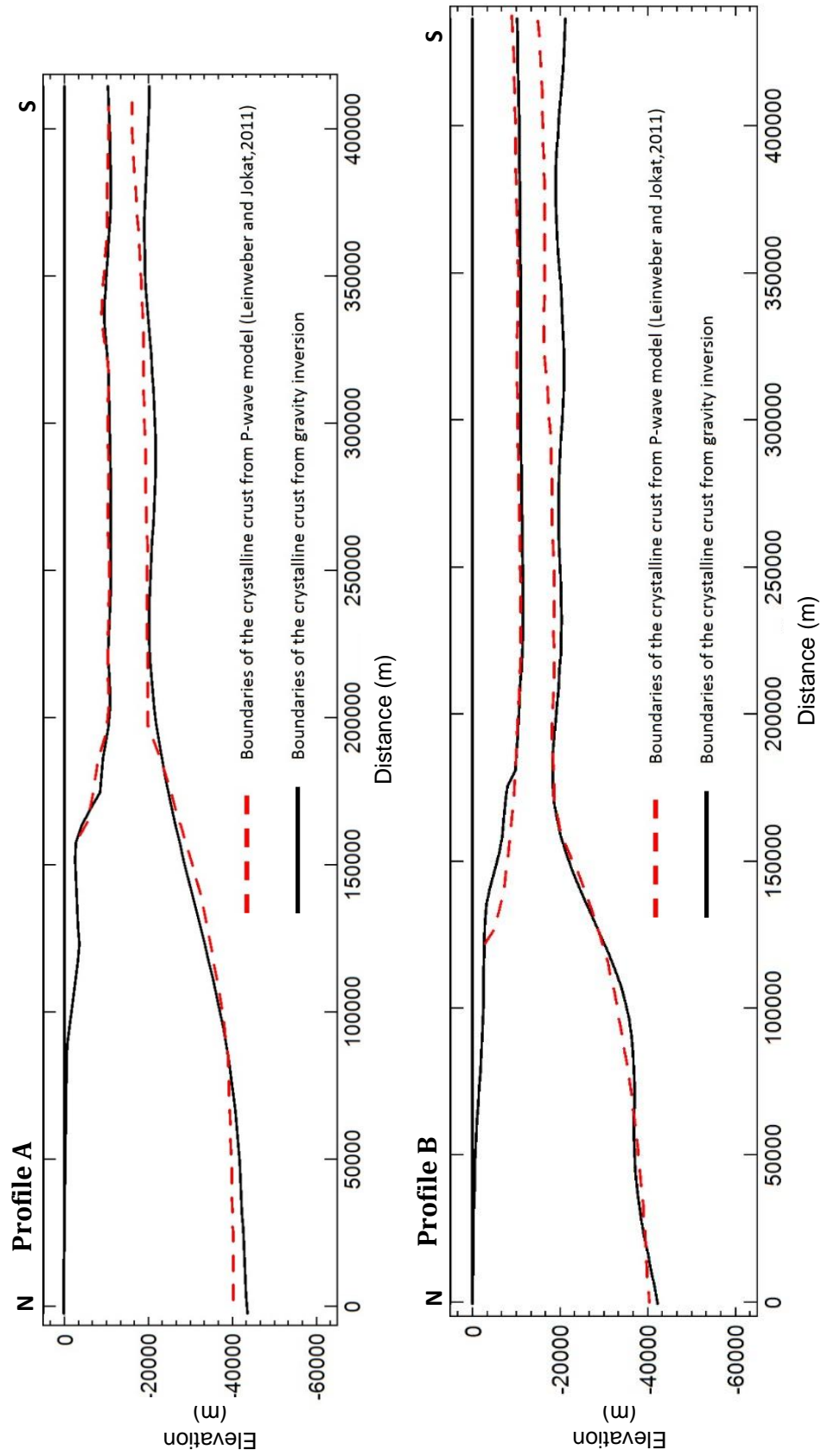
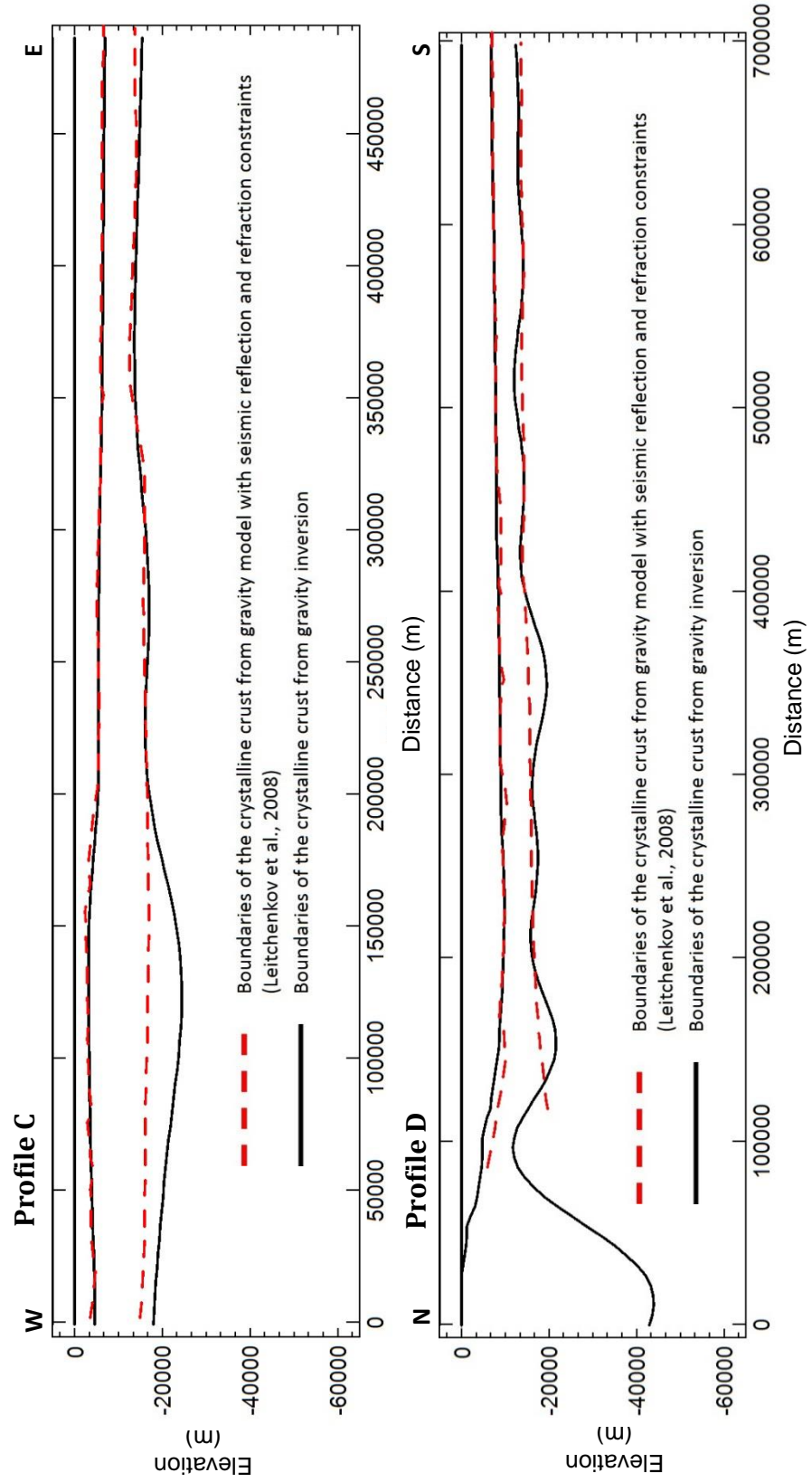


Figure 4.22: Comparing crustal thickness derived from gravity inversion and seismic-constrained gravity model in the Riiser Larsen Sea. Similar crustal thickness are estimated along most of Profile C except for area of the Astrid Ridge where inverted crustal thickness is greater from 1-6 km. Along Profile D, the results agree to a few hundred meters with only one or two locations where the difference reach maximum of 5 km.



Profile B of Figure 4.22 is in the E-W direction extending across the Astrid Ridge into the western half of the Riiser Larsen Sea. Along this profile, crustal thickness derived from the two model types are in very good agreement with the only exception at the Astrid Ridge where ray-tracing model shows Moho depth at more than 6 km shallower than the inverted Moho. One possible explanation of this discrepancy is the volcanic nature of the Astrid Ridge. Crustal density of the ridge might be much higher than the uniform 2.85 g/cc used in the gravity model. In addition, unlike the situation in the Mozambique Basin, a very thin sediment layer covers the Astrid Ridge and thus does not compensate for the increased crustal density. In such area, the effect of crustal thinning from high density volcanic body will be accounted for during the non-rigid reconstruction stage. Nevertheless, the overall results from the gravity inversion is considered good as the calculated values are in close range with the observed measurements throughout most of the areas of interest.

4.4 Locations of the continent-ocean boundaries (COBs)

COBs in the conjugate margins of Africa and Antarctica are important parameters for both rigid and non-rigid reconstructions. Positive magnetic anomalies have been proposed as indicators of the continent-ocean boundaries in other rifted margins such as the eastern US (Hutchinson et al., 1983; Austin et al., 1990), southern Brazil (Rabinowitz and Labreque, 1977), northwestern Australia (Veevers et al., 1985). Edge effect due to magnetization contrast between adjacent oceanic and continental crust (Rabinowitz and Labreque, 1977; Hutchinson et al., 1983) or rift-related volcanic (Austin et al., 1990) are among the speculations for the source of such

magnetic anomaly. Furthermore, since the difference between the thickness of oceanic and continental or transitional crusts are quite considerable, inspecting for an abrupt change in crustal thickness along a continental margin might also be a good indicator for the COB. Lastly, fracture zones are oceanic structures directly associated with the spreading center, thus their presence is strong evidence for oceanic crust. Utilizing the preceding observations on the nature of COBs, this study interprets magnetic anomaly, changes in crustal thickness, and fracture-zone traces to determine locations of the COBs in the study areas.

Gridded magnetic anomaly dataset (WDMAM) is enhanced with reduction to the pole, a phase transformation process that essentially places the anomalies directly over the source body (Blakey, 1995) that is computed by Geosoft software package. Magnetic anomaly map for Antarctica region (Maus et al., 2007) is shown in Figure 4.23. In the eastern Lazarev Sea around latitude 67.5°S and longitude 7°E, a NE-SW elongated positive magnetic anomaly with an average amplitude of 300 nT has been postulated as mark of the COB along its northern edge (Jokat et al., 2004). Their proposed COB was supported by seismic refraction data which indicate an abrupt change in crustal thickness from 7 km to 15 km over a distance of 30 km. It was also recognized that the magnetic anomaly marks the seaward extension of the seaward-dipping reflector sequences (SDRs) in this area. That interpretation of the COB in the Lazarev Sea is incorporated in this study. A similarly prominent positive magnetic anomaly is present along the Antarctica coast line over the Riiser Larsen Sea spanning between latitudes 20°E-32°E and longitude 67.5°S-71°S. This anomaly is in a zone

where the crust thins from 42 km to 7 km over a distance of 80 km. Other pieces of evidence that suggest the magnetic anomaly might be associated with the COB are the fracture zones traced from satellite-derived gravity anomaly. Figure 4.24 shows the fracture zones terminate against the proposed COB picked from the magnetic anomaly and crustal thickness boundary. The white dashed portion of the COB indicates area of the Astrid Ridge where the magnetic anomaly is disrupted and the trend of crustal boundary is discontinuous due to the thick volcanic emplacement that makes up the ridge. Carrying the same analysis to the conjugate margin over the Mozambique Basin, another magnetic anomaly with similar characteristics in wavelength, amplitude and shape is located along the Mozambique coastline in the area between latitudes 16°S-18°S and longitudes 36°E-40°E (Figure 4.24). Correlation between this anomaly and the boundary of high crustal thickness gradient also yields a good match (Figure 4.25). As with the COB over the Riiser Larsen Sea, fracture zones F and G can be traced back landward until they reach the magnetic anomaly. The trend of crustal thickness and magnetic anomaly continue eastward to the Davie Fracture Zone which marks the boundary between continental Africa and oceanic crust of the Somali Basin. In contrast, the westward extension of the COB in Mozambique is not well defined. The E-W magnetic anomaly is terminated by a N-S magnetic anomaly which also marks the westward extent of the crustal thickness boundary. There is a possibility that the COB might continue southward following the crustal thickness boundary (dashed line in Figure 4.25). It is also possible that the COB continues westward to another N-S oriented magnetic anomaly

Figure 4.23: A) Reduction to the pole of the total intensity magnetic anomaly map (Maus et al., 2007) over the Antarctica region shows a positive anomaly lineament along latitude 68°S. This anomaly is proposed as a strong candidate for the COB along this margin. **B)** Crustal thickness map overlain with the COB picked along the magnetic anomaly. There is a good correlation between the COB, crustal thickness boundary and termination of fracture zones. Dashed portion marks area of disruption of magnetic anomaly and crustal thickness trend due to the Astrid Ridge. AR: Astrid Ridge. GR: Gunnerus Ridge.

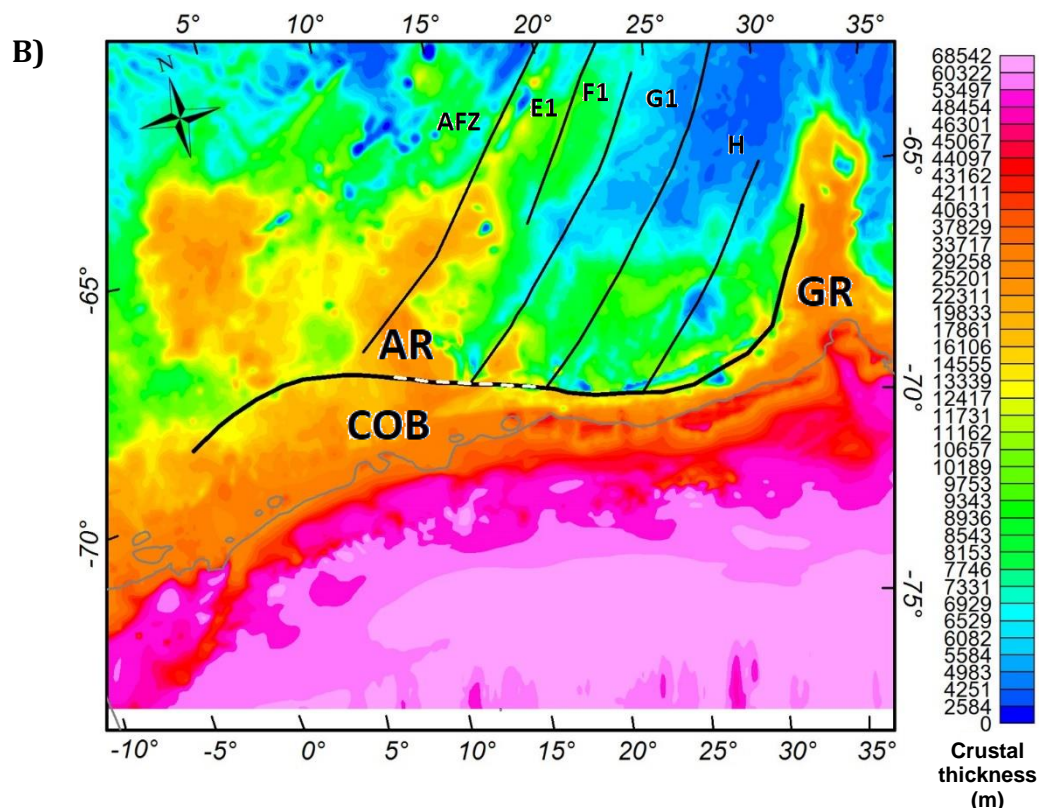
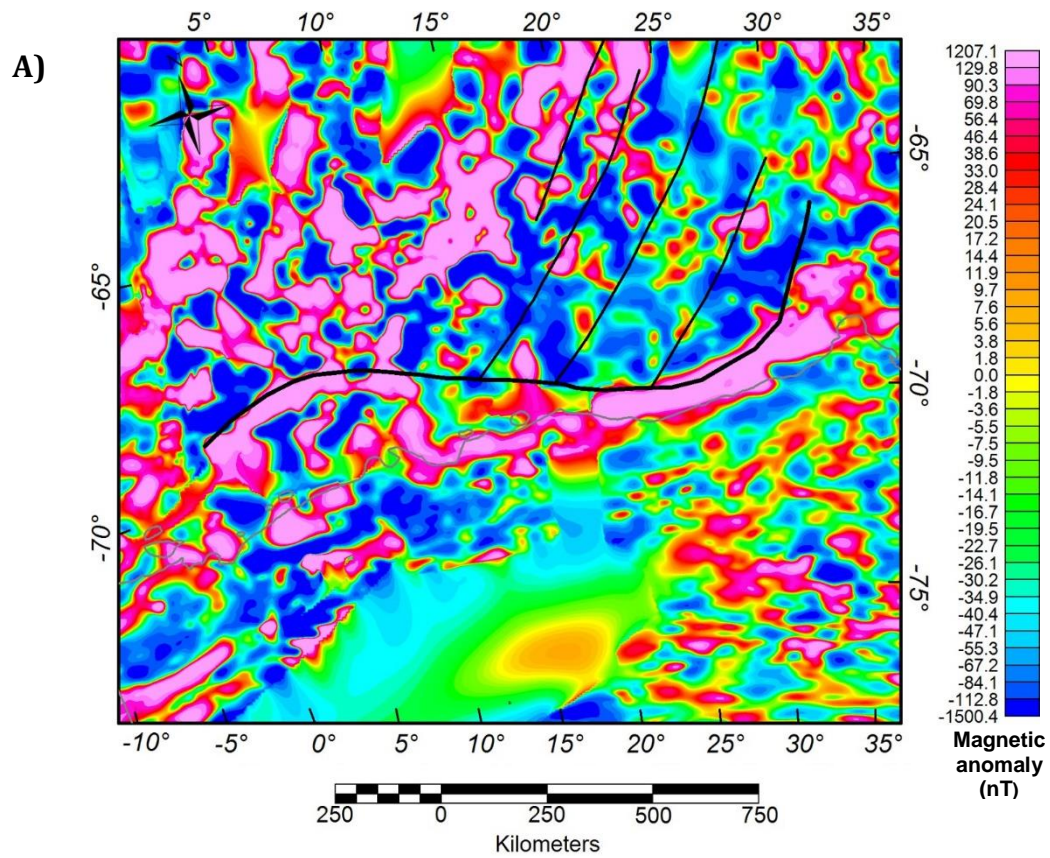


Figure 4.24: Reduction to the pole of the total intensity magnetic anomaly map over the Mozambique Basin (Maus et al., 2007). A strong positive anomaly is present along the northeastern coast of Mozambique where fracture zones terminate. COB is sketched along this anomaly. Dashed lines indicate possible trace of the COB following different magnetic anomaly trends.

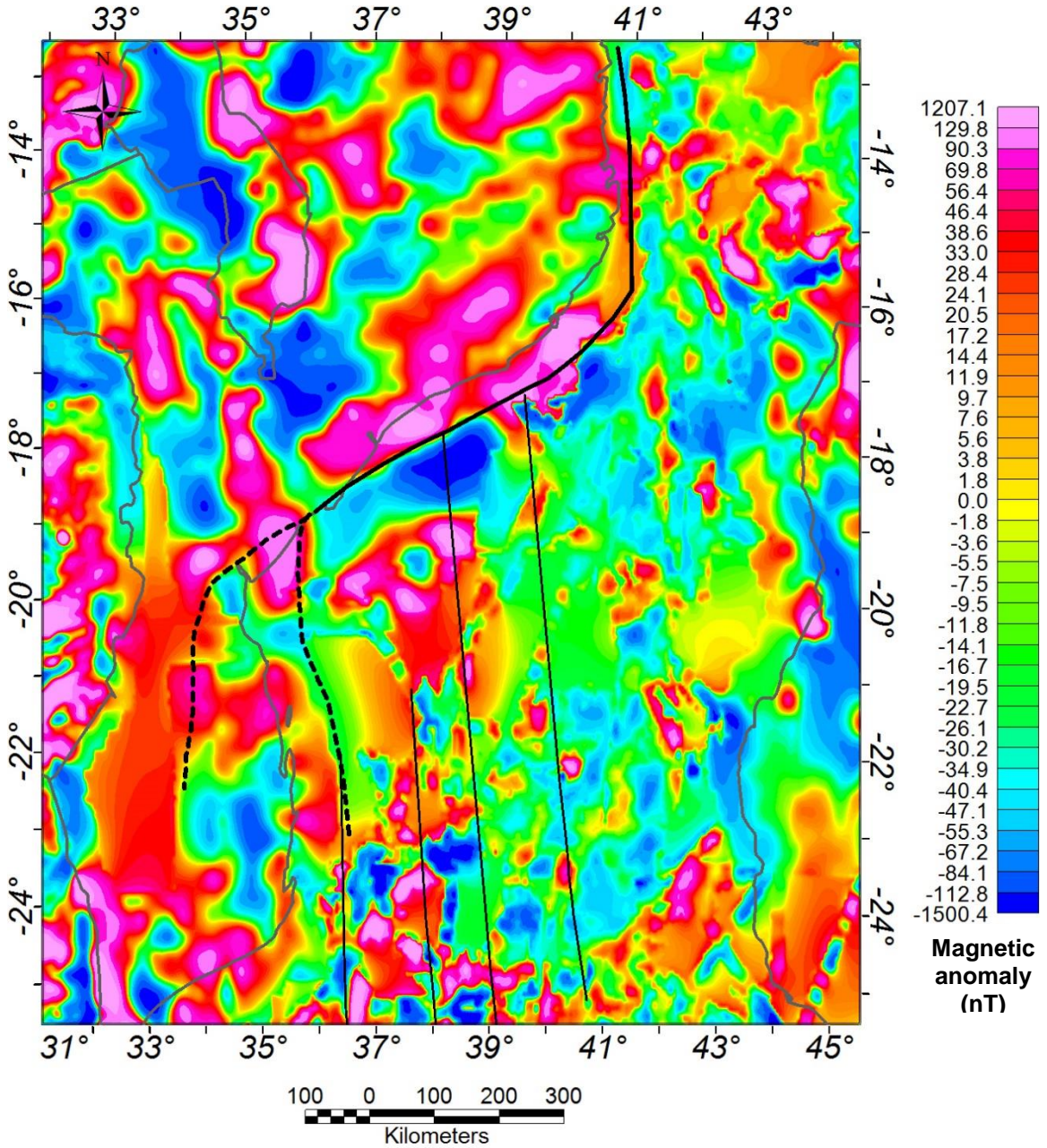
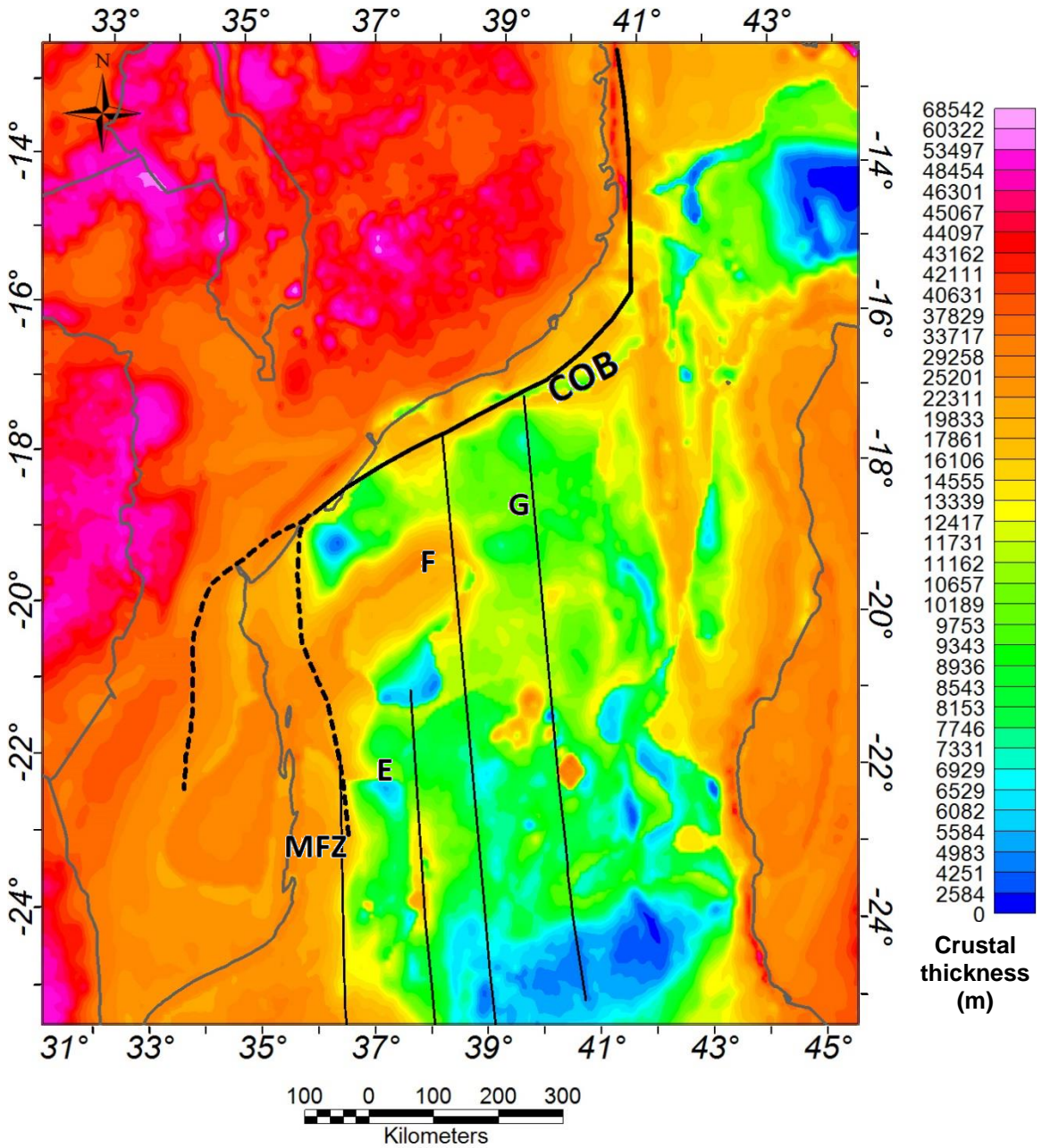


Figure 4.25: The COB trace determined from magnetic anomaly is overlaid on crustal thickness map of the Mozambique Basin. The COB follows the trend of crustal thickness boundary closely.



along longitude 34°S even though the crustal thickness is relatively uniform over the Mozambique Coastal Plain. Nevertheless, a more complete COB over the Mozambique Basin can be determined by rigidly restoring the COB over the Riiser Larsen Sea back to the African side.

4.5 Rigid reconstruction

Rigid reconstruction is performed by matching both magnetic isochrons and fracture zones (Chapter 3). Plates are restored incrementally with each set of isochrons from M0r (124.81 Ma) to M22n1n (149.49 Ma). Figures 4.26-4.28 illustrate the matches of isochrons M0r, M10n and M22n1n as well as the corresponding fracture zones. Offsets of isochrons from the African and Antarctic margins show high consistency. The fracture zones from the conjugate margins, as determined from satellite-derived free-air gravity anomaly, are remarkably well correlated. Indeed, the matching reveals that fracture zones over the Mozambique Basin are conjugate to those identified over the Riiser Larsen Sea. The pairs of conjugate fracture zones are Astrid Fracture Zone and Mozambique Fracture Zone, fracture zones E1 and E, fracture zones F1 and F, fracture zones G1 and G.

As previously noted, M22n1n is the oldest chron that is used for rigid reconstruction since older chrons can only be identified tentatively due to subdued magnetic amplitude. To fully close the ocean basin to time older than M22n1n (149.5 Ma), Antarctica is progressively moved northward following the traces of fracture zones F-F1, G-G1 until the COBs in both margins come into contact. This final stage of rigid reconstruction is illustrated in Figure 4.29. Though parts of the two

Figure 4.26: Rigid reconstruction showing the continents at M0r (124.8 Ma). Blue dots are M0r identified in the Riiser Larsen Sea. Orange dots are the conjugate M0r over the Mozambique Basin. Conjugate fracture zones in both margins are also shown in color code. Blue indicates Antarctica feature and orange is for Africa features. Reconstruction is achieved by matching both isochrons and conjugate fracture zones. Overlap of fracture zones where isochrons are present suggests good consistency of the model

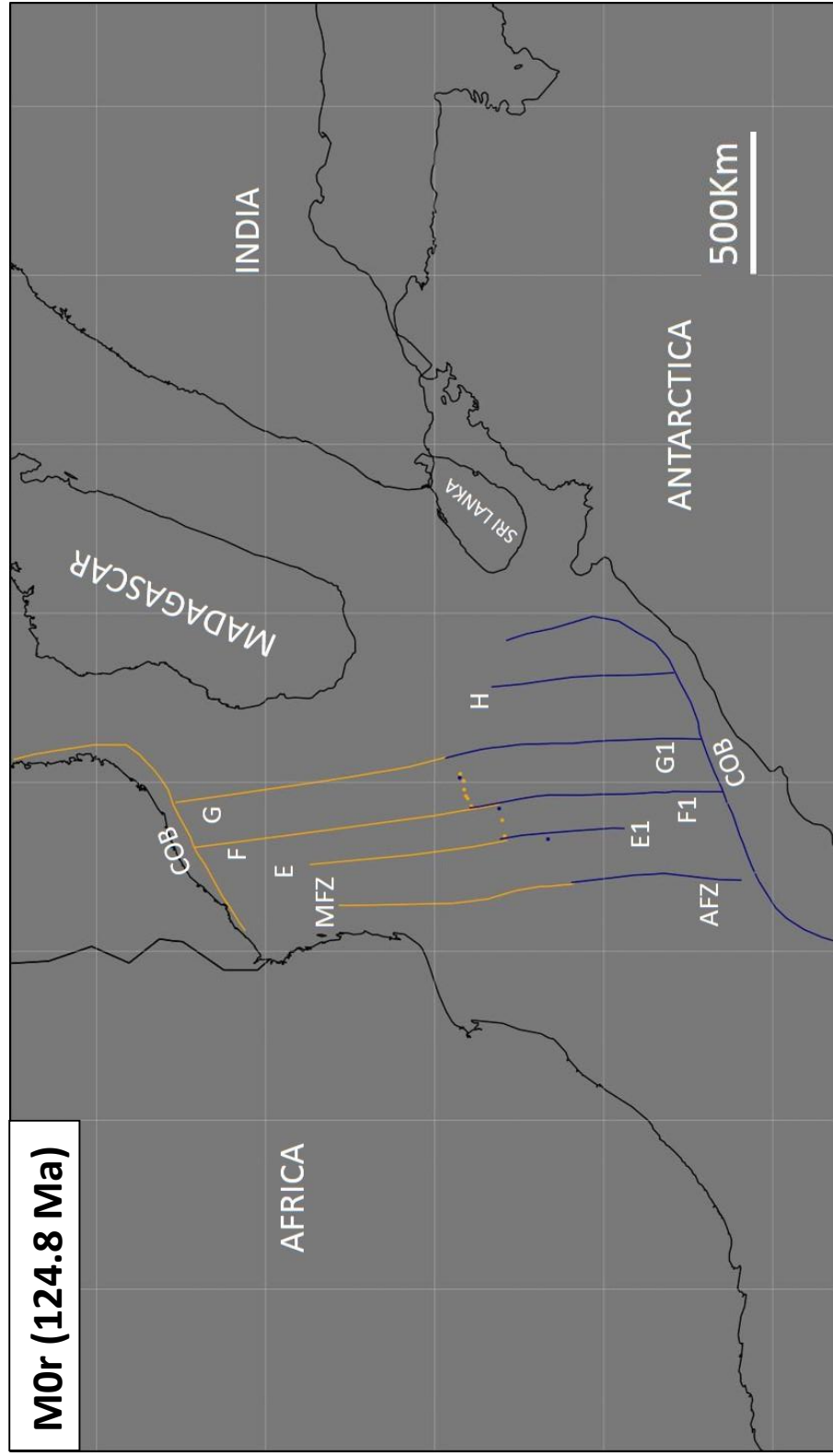


Figure 4.27: Rigid reconstruction showing the continent at M10n (133.7 Ma). Blue dots are M10n identified in the Riiser Larsen Sea. Orange dots are the conjugate M0r over the Mozambique Basin. Other map descriptions are as in Figure 4.26

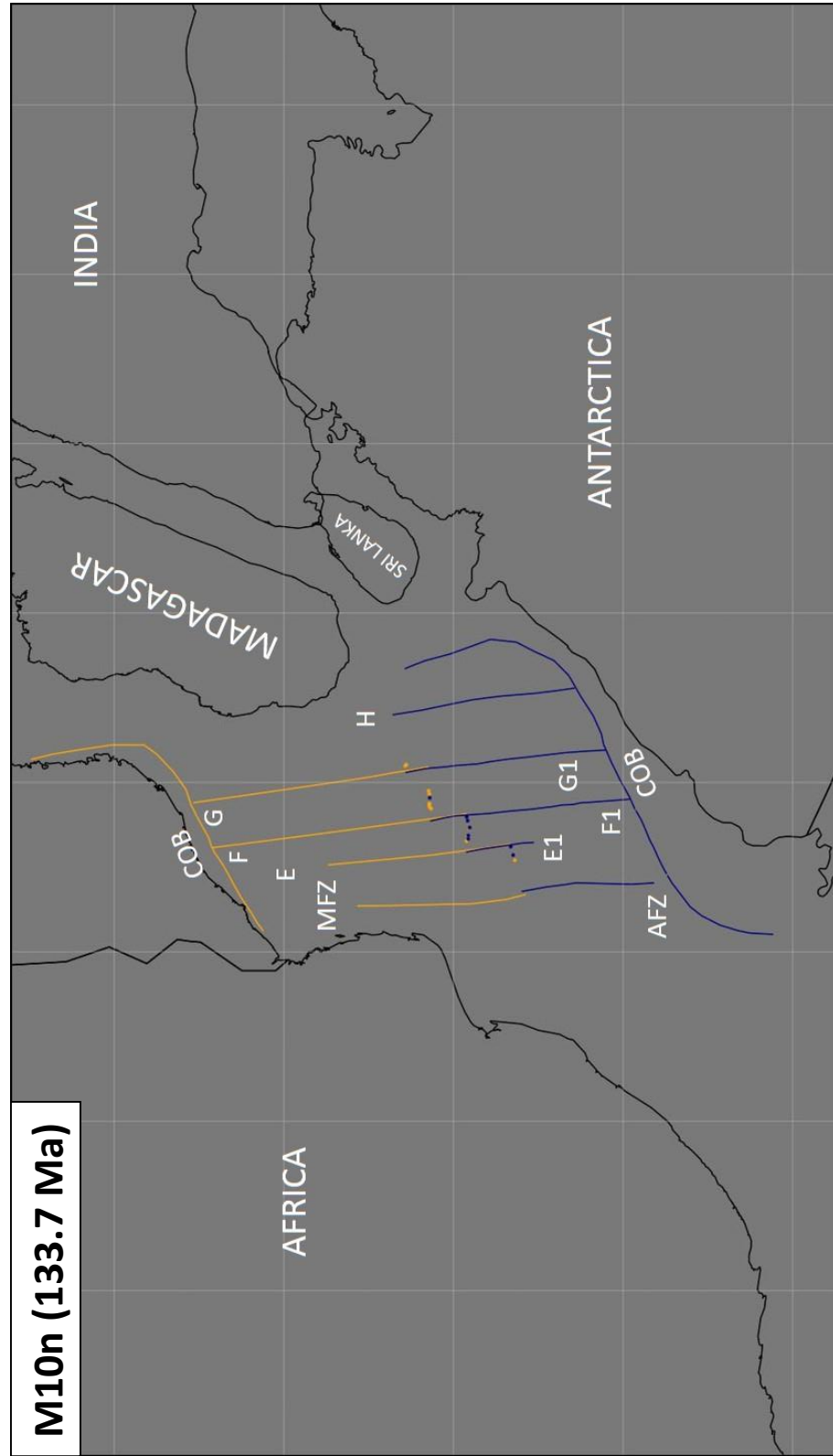


Figure 4.28: Rigid reconstruction showing the continent at M22n1n (146.5 Ma). Blue dots are M22n1n identified in the Riiser Larsen Sea. Orange dots are the conjugate M22n1n over the Mozambique Basin. Other map descriptions are as in Figure 4.26

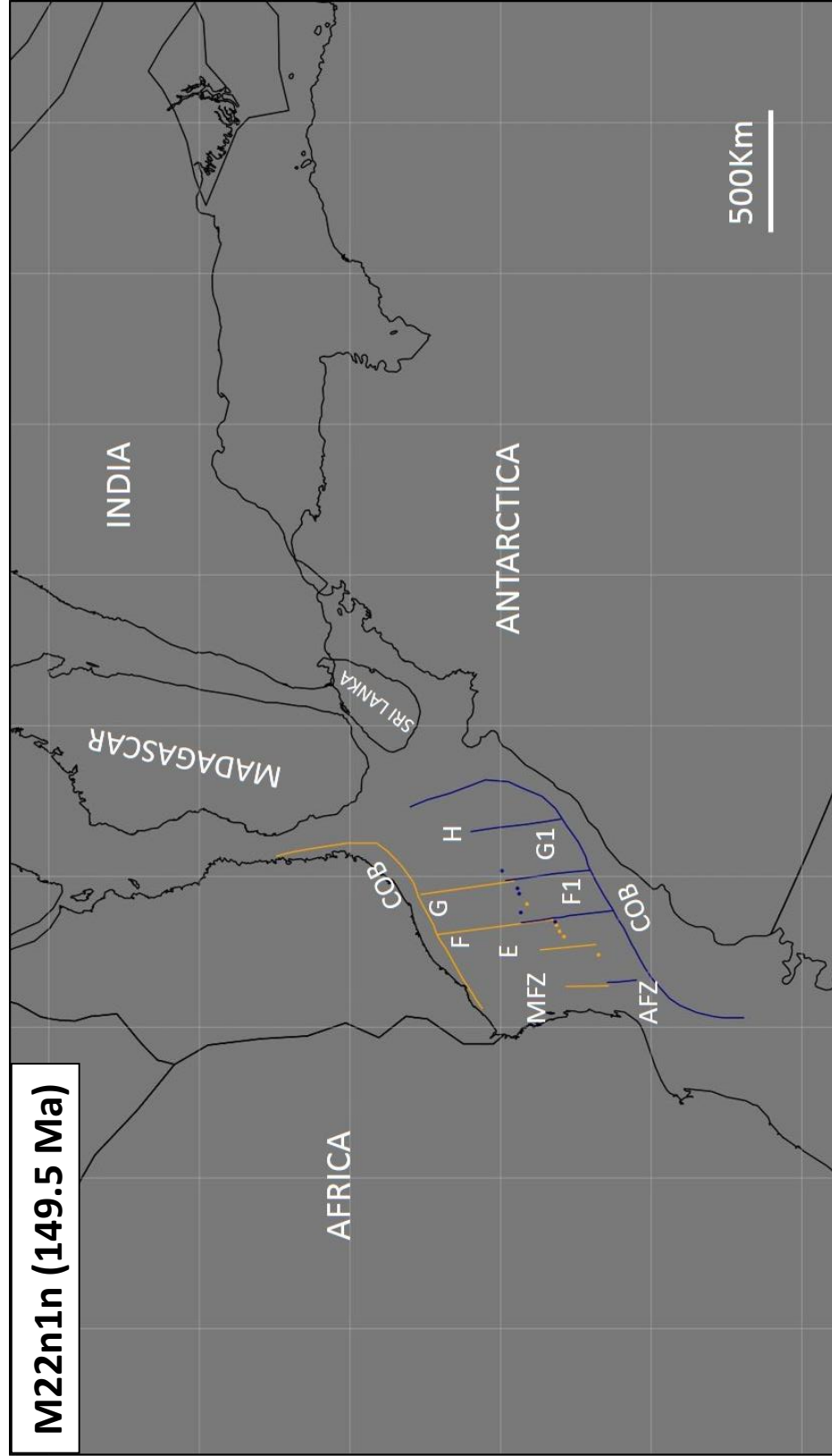
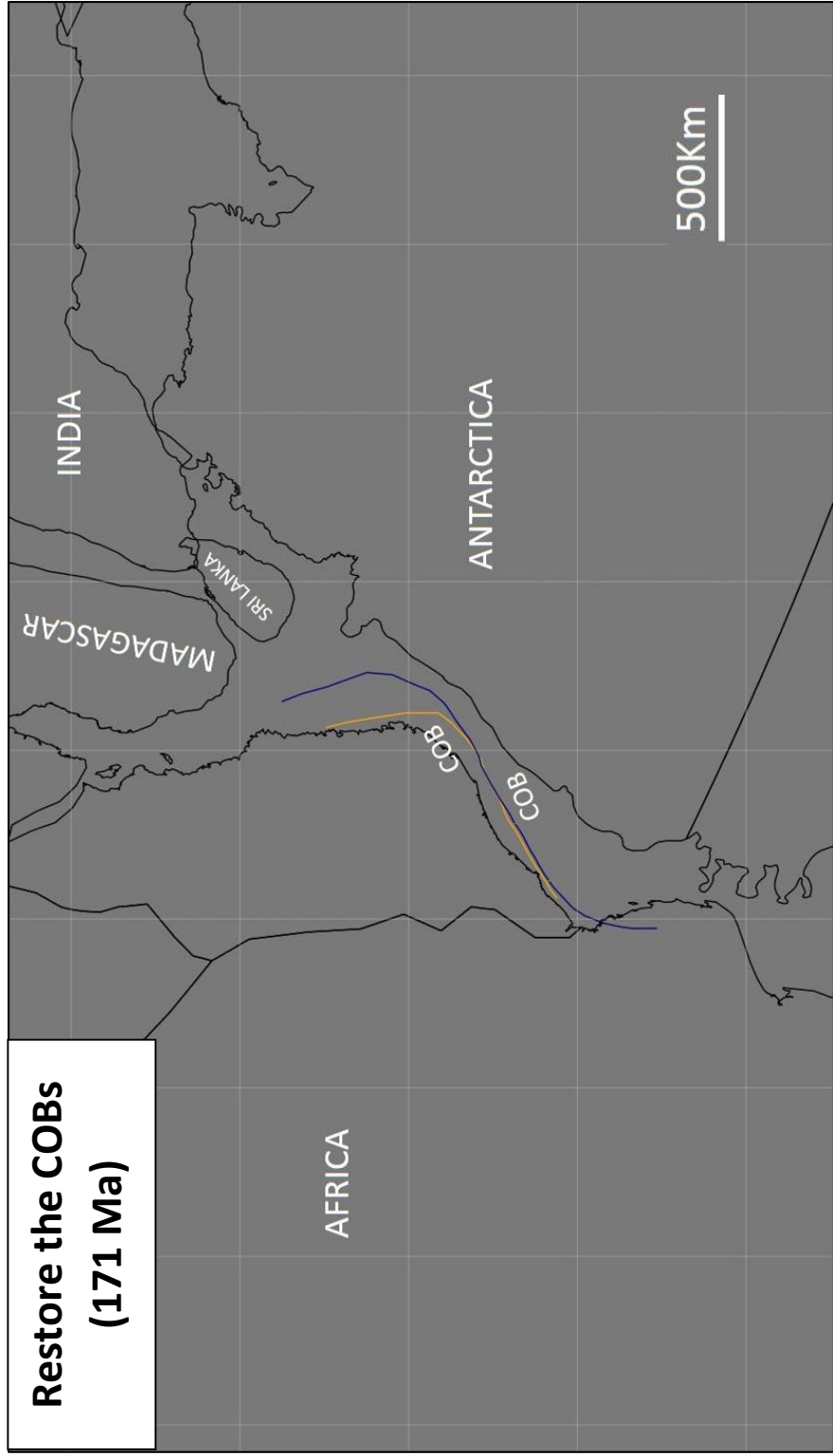


Figure 4.29 Rigid reconstruction to time at onset of seafloor spreading by moving Antarctica from its position at 149.5 Ma along the fractures F and G to where the two COBs meet. Note that, the predicted COB from Antarctica overlaps the present day location of the Davie Fracture Zone while fracture H lines up neatly with the Davie Ridge. This is an indication of a transform boundary along fracture zone H over the Riiser Larsen Sea. The two COBs show good overlap in their central sections. The eastern end of the Antarctica COB is determined from its Africa counterpart. Likewise, the Antarctica COB is used to define the westward extension of the Mozambique COB.



COBs show good correlation, the eastern end of the Antarctica COB overlaps the Davie Fracture Zone. In addition, fracture zone H from Antarctica is almost coincident with the Davie Fracture Zone and the Africa COB. From this revelation, fracture zone H is interpreted as the conjugate of the Davie Fracture Zone and marks a transform boundary over the Riiser Larsen Sea. The Mozambique COB is extended westward by adopting that part of the Antarctica COB. This is the COB used for the non-rigid reconstruction of both margins. Implications of other choices for the COBs such as the dashed lines in Figure 4.25 will be discussed later.

Since the last stage of rigid reconstruction was not based on magnetic isochrons, the timing of final closure is not well constrained. Tentative identification of isochrons M25n and older (Figure 4.13) suggest a slow average spreading rate of 17 km/Myr. Using this spreading rate and the distance between M22n1n isochrons and the COB in Mozambique, the time at which the continents are restored is estimated at 171 Ma.

4.6 Non-rigid reconstruction

Different models are tested to account for the amount of continental stretching during rifting period. The first scenario assumes the direction of stretching is similar to that of earliest stage of rigid plate motion. Ten N-S and NE-SW oriented cross sectional profiles are extracted from the gravity model across both margins of Africa and Antarctica, respectively (Figures 4.30 and 4.31). The extent of stretched continental crust is defined by the COB on the seaward end and the boundary of 42-km-thick crust on the landward end of these profiles. The total area of this extended crust is calculated in each profile.

Figure 4.30: Construction of N-S oriented two dimensional cross sections across the continental margin of Mozambique. Each profile extends from the COB landward to 42 km crustal thickness boundary. Restored locations are shown in colored squares. Red are restoration with account for magmatic underplating whereas simple reconstruction without accounting for addition magmatic volume results in black squares. The line connecting the red points represent original pre-rift boundary.

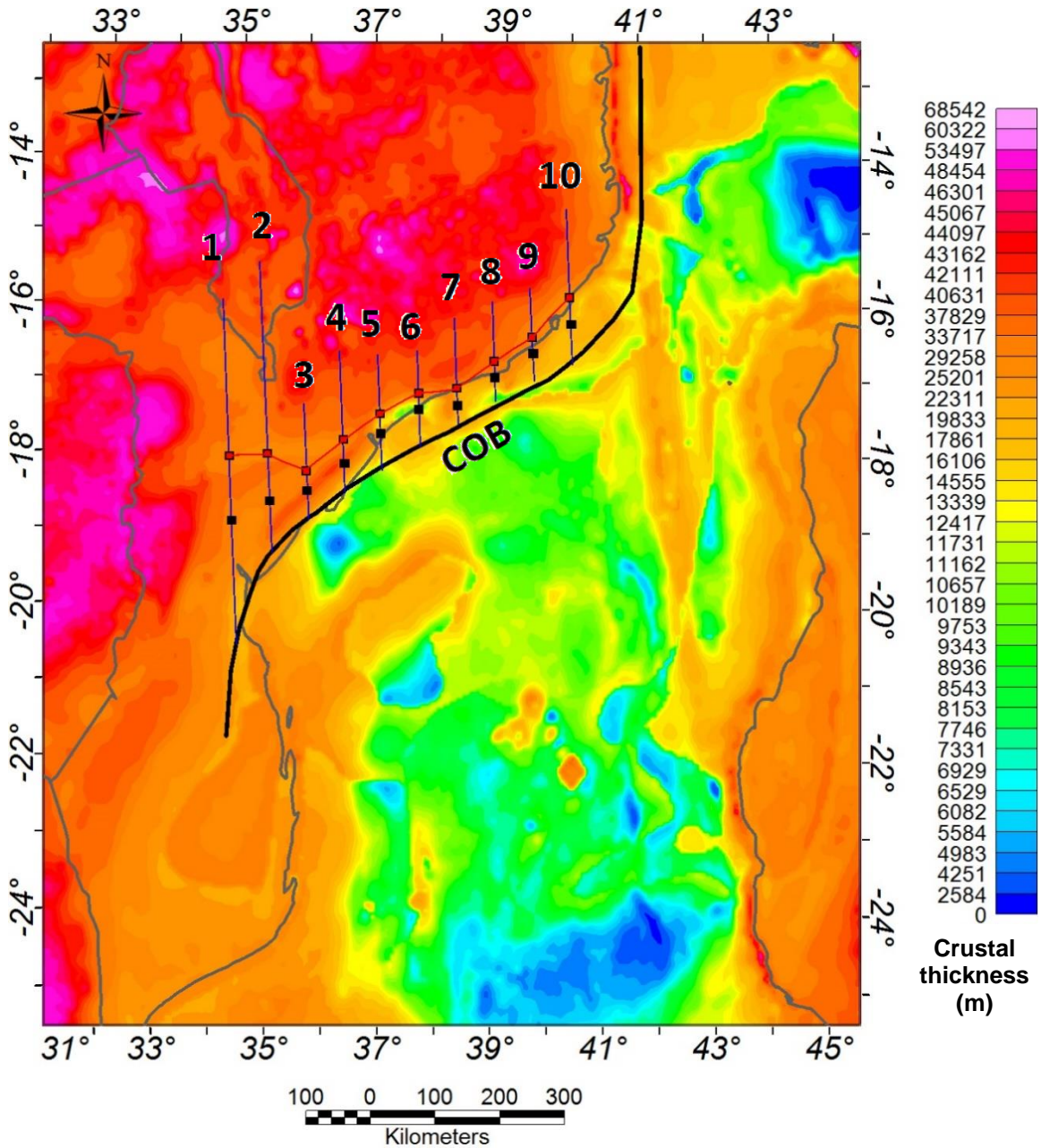
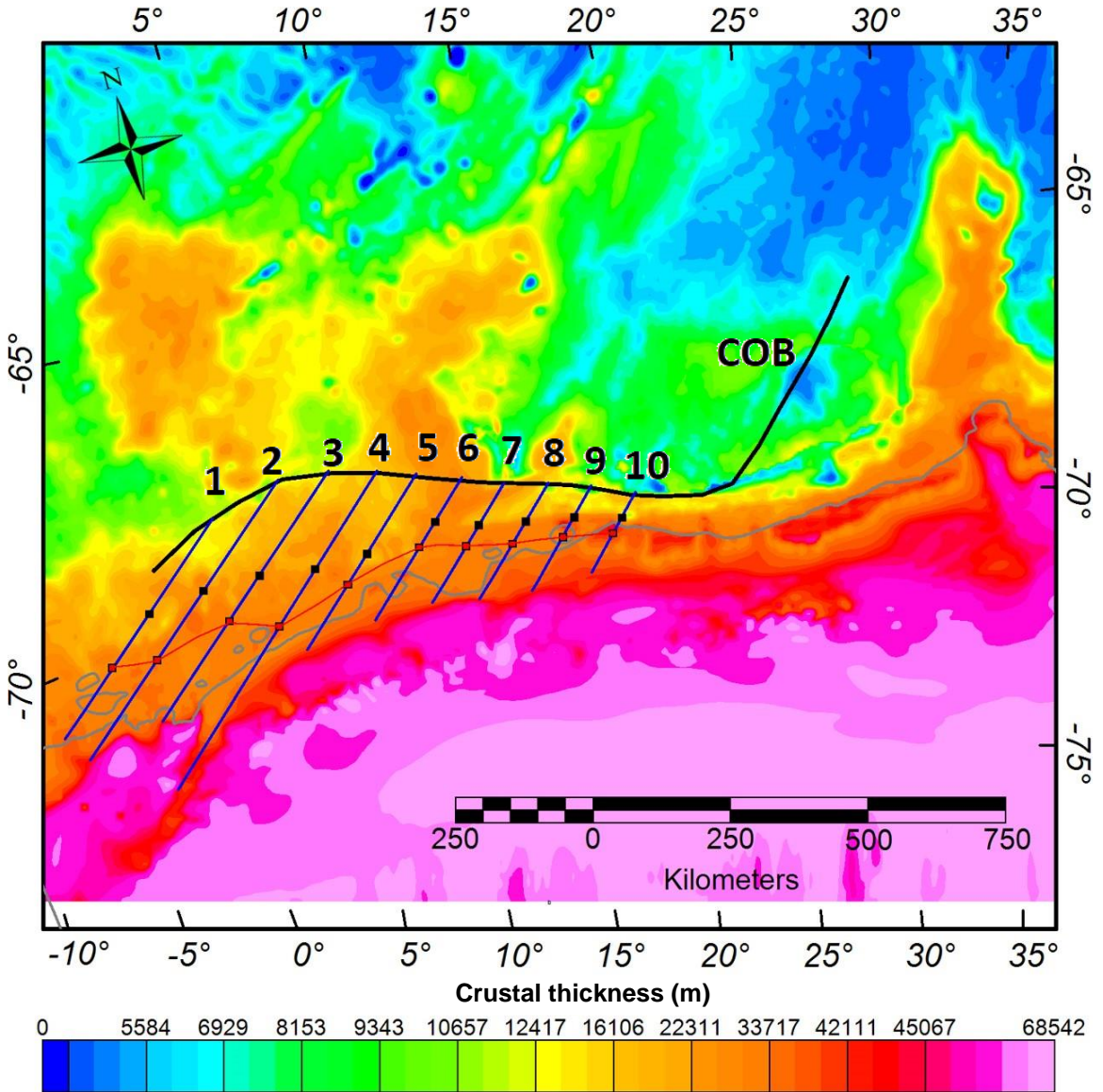


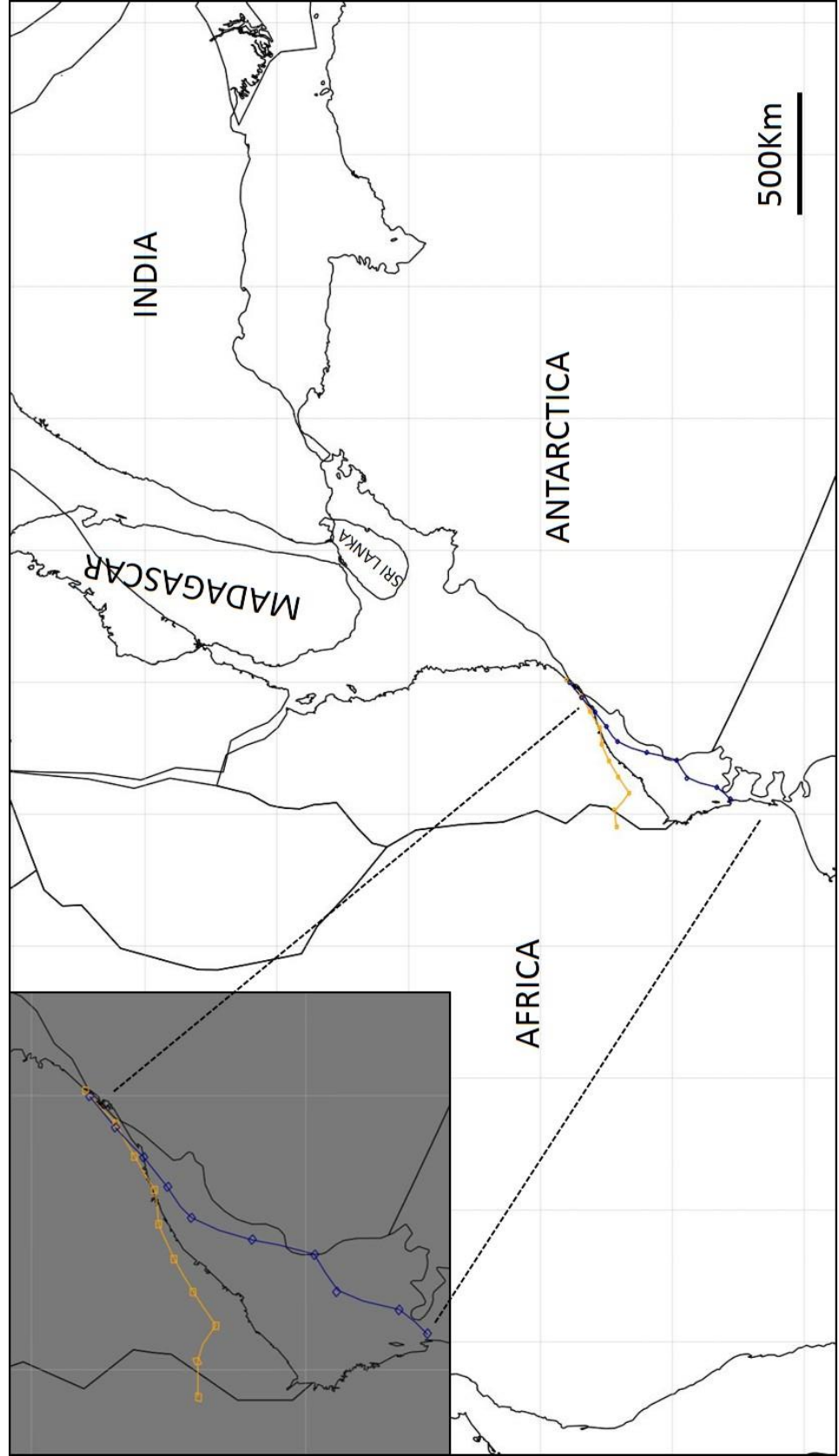
Figure 4.31: Construction of cross sections in direction equivalent to the N-S oriented profiles in Mozambique. Red squares are restored points with account for magmatic under plating. Black squares are restoration without removing magmatic volume. Red line is pre-rift boundary.



As discussed earlier, since high-density magmatic bodies were not incorporated in the gravity inversion model, the true Moho depth is likely to be different than calculated. However, comparison in Figure 4.21 also suggests that along the northern Mozambique margin, little correction is needed for Moho depth. In each profile crossing the northern Mozambique margin, the area of additional magma is estimated and subtracted from the total crustal area. On the other hand, for profiles located along the southwest margin, where the amount of magmatic underplating is estimated to be significantly greater (P. Ball, personal communication, March 28, 2015), inverted Moho must be corrected. Such correction is calculated based on isostasy and the density contrast between the crystalline crust (2.85 g/cc), magmatic underplating (3.05 g/cc) and upper mantle (3.3 g/cc). Using the formula $x*(3.05-2.85) = (1-x)*(3.3-3.05)$ where x is the amount (in km) the crust thins for each thickness (in km) of added underplating, x is estimated to be 0.55 km. Note that this calculation effectively removes the magmatic body from the crust and no further correction is needed.

Table 4.1 lists the total crustal area, underplating area, original crustal area for each profiles across both margins. Shown in Figures 4.30 and 4.31 are the restored points along each profiles. Black squares are results of restoration without removing the magmatic underplating. Red squares are restored points after magmatic volumes had been accounted for. The line connecting restoration points represent the boundary of original crustal thickness prior to rifting. Non-rigid reconstruction is

Figure 4.32: Reconstruction model where the same N-S direction of rigid motion is used for non-rigid stretching. Antarctica is moved progressively northward until the restored boundaries overlap. The final geometry shows poor correlation between the conjugate boundaries. This model also produces large overlap between Madagascar and Africa.



carried out as described in Chapter 3. Figure 4.32 illustrates the relative position of Antarctica with respect to Africa after Antarctica moved northward until the pre-rift boundaries in two continents come into contact. The significant mismatch between the two boundaries suggests continental extension was not in the N-S direction. Restoring Antarctica in this direction also produces an overlap of Madagascar onto Africa. Geological evidences suggest the Grunehogna Craton was originally connected to the Kaapvaal Province (Groenewald et al., 1991; Grantham et al., 2008) and part of the Explora Wedge is a conjugate feature of the Lebombo Monocline (Cox, 1992; Konig and Jokat 2010). To bring these features into proximity with each other and simultaneously reduce the overlap of Africa and Madagascar, Antarctica is restored in a NW-SE direction. Figures 4.33 and 4.34 show parallel NW-SE cross sections constructed across the Mozambique and Antarctic margins along with their corresponding restoration points. Information about crustal areas of the profiles are listed in Table 4.2. The fit of the continents is tested as Antarctica is moved in the direction of the profile until the restored boundaries overlap (Figure 4.35). Though the overall shape of the boundaries are similar in both continents, the closing geometry does not yield a good correlation. In addition, the issue of overlapping Africa and Madagascar remains. This study recognizes that the overall trend of the non-rigid boundaries can be better correlated if a component of clockwise rotation is added to the motion of Antarctica. This would also rotate Madagascar away from and thus helps to resolve the issue of overlap. To model the rotation of Antarctica, cross sections are constructed in slightly different orientations (Figures 4.36 and 4.37).

Figure 4.33: Construction of the profiles in uniform NW-SE direction in the Mozambique Basin. Red squares are reconstruction points along each profiles after removal of magmatic volume. Black squares are reconstruction points in a simple model assuming no magmatic addition. Red line is the pre-rift boundary.

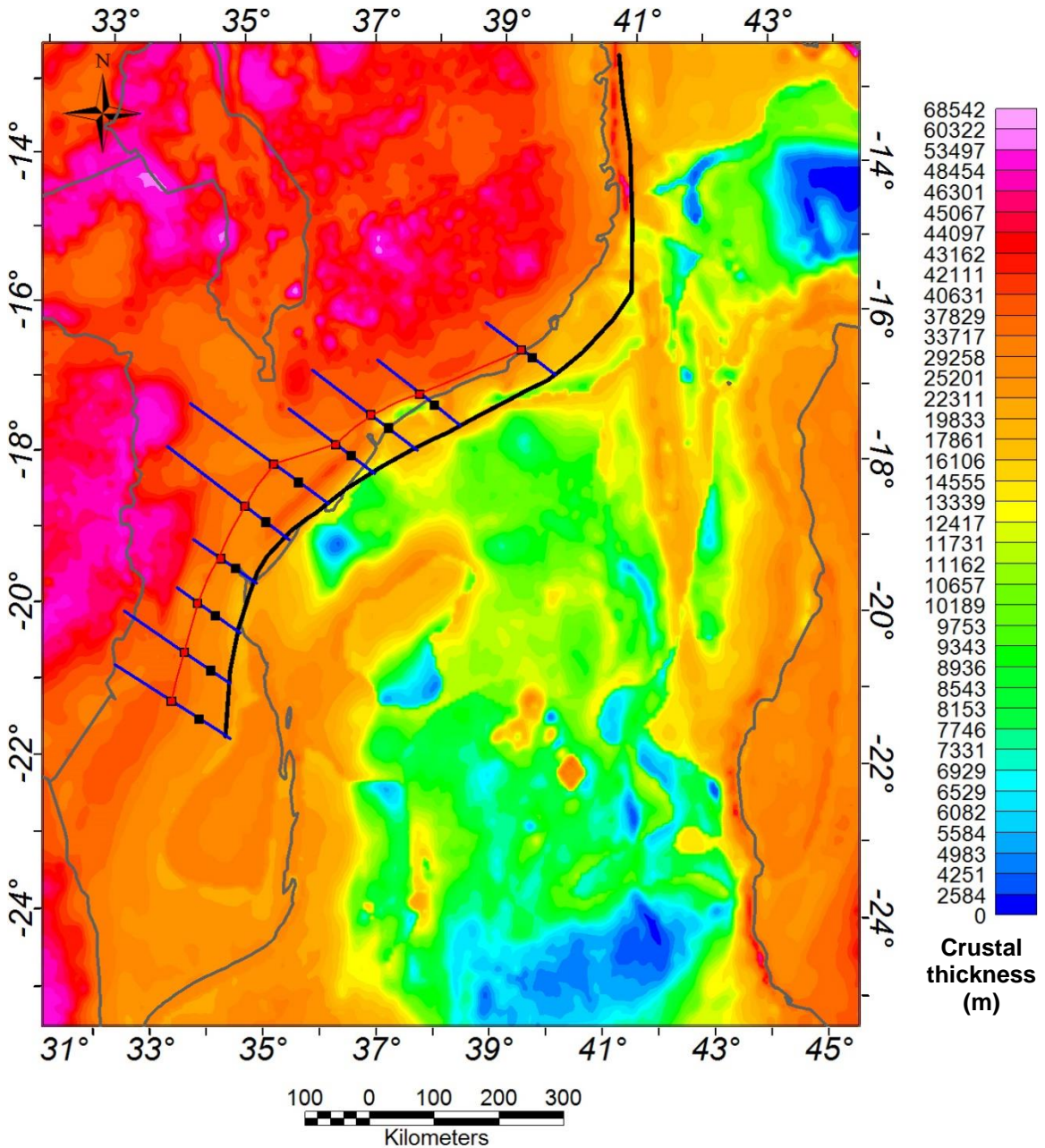


Figure 4.34: Construction of the profiles in uniform NW-SE direction in the Riiser Larsen Sea. Red squares are reconstruction points along each profiles after removal of magmatic volume. Black squares are reconstruction points in a simple model assuming no magmatic addition. Red line is the pre-rift boundary.

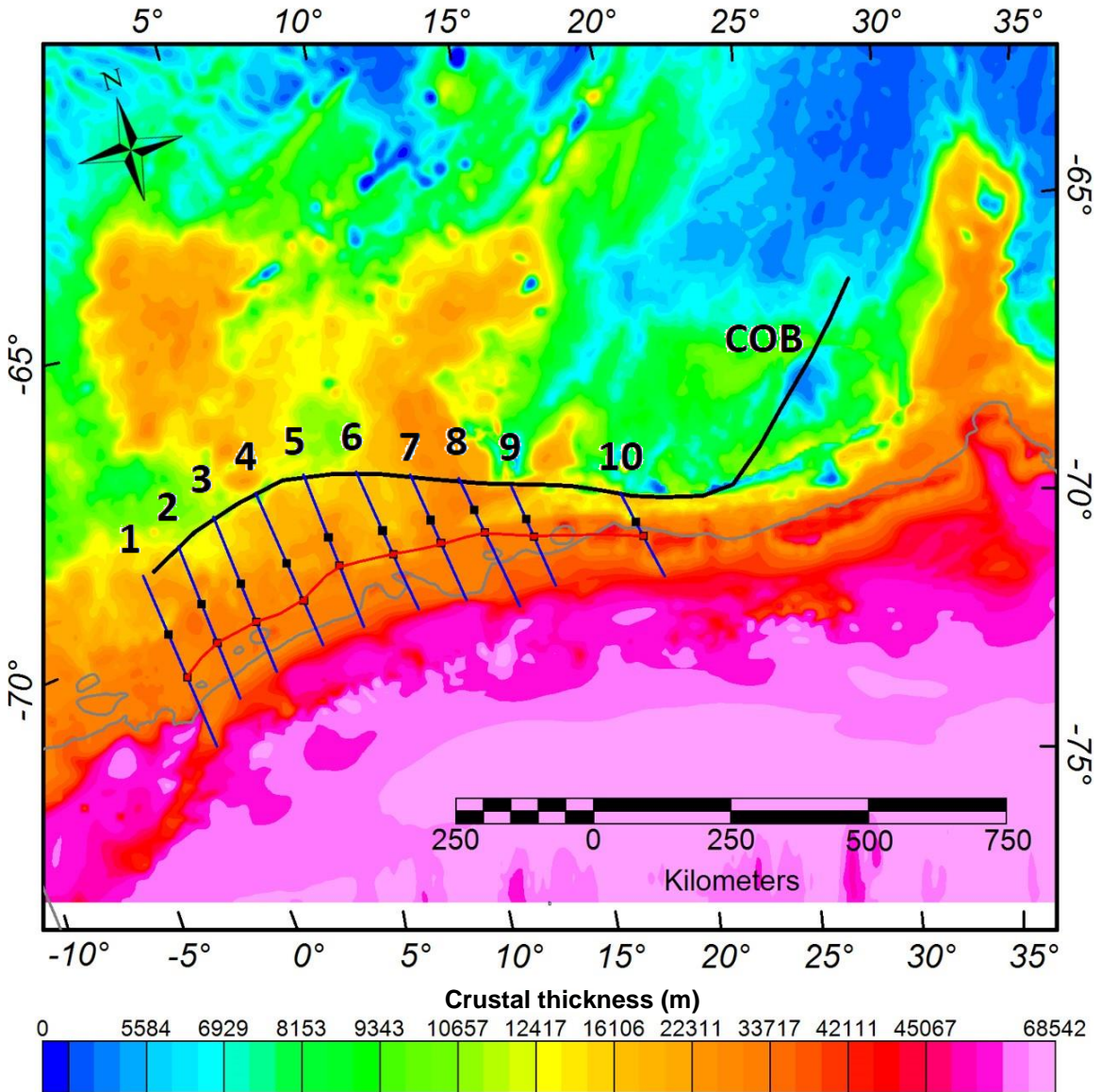
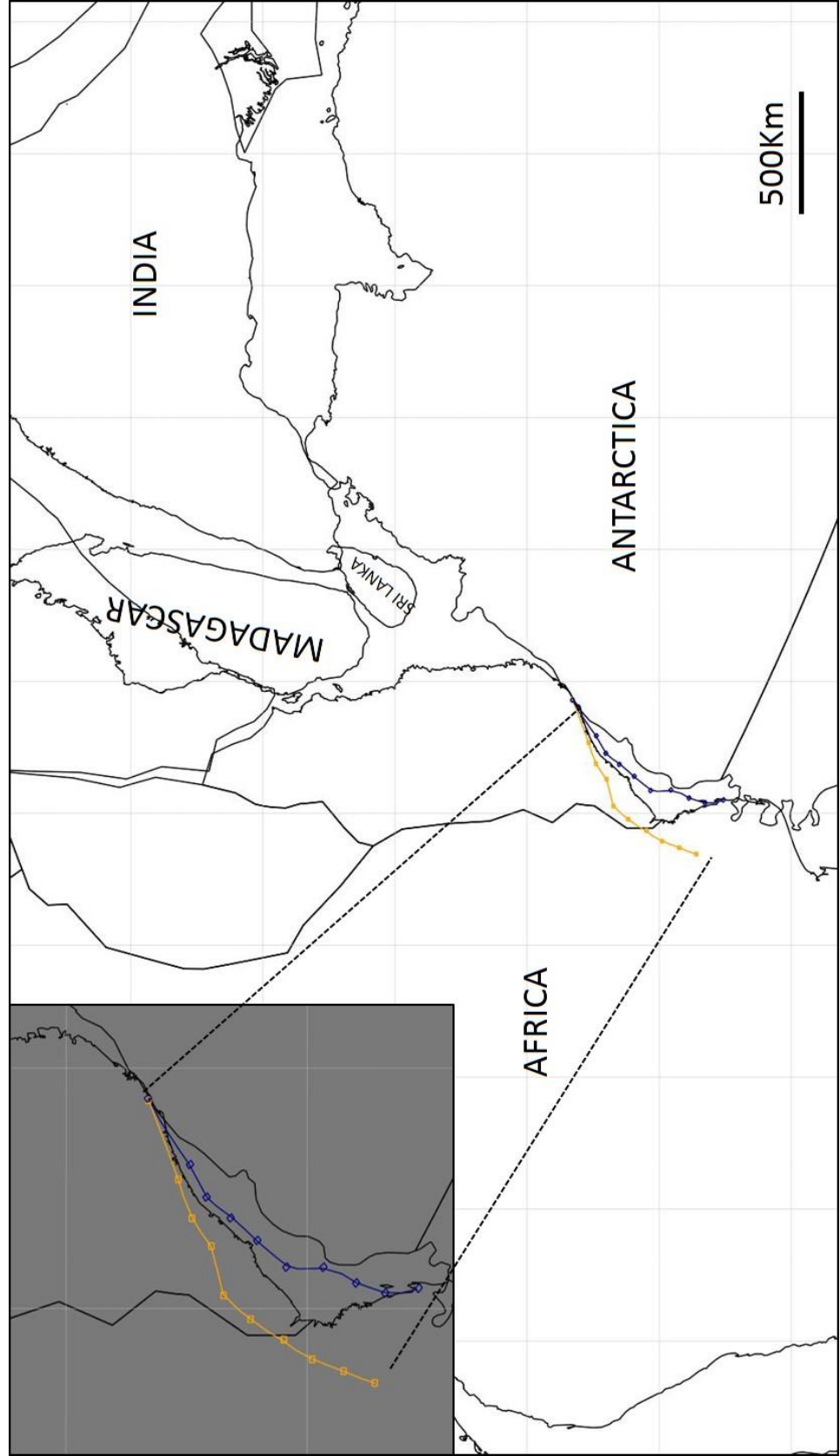


Figure 4.35: Non-rigid reconstruction modeling a NW-SE closing of Antarctica against Africa. The correlation between the pre-rift boundaries is still poor and the issue of overlapping Madagascar onto Africa still persists. The geometry of the two boundaries suggests a counter clockwise rotation of Antarctica with relative to Africa is needed in order to achieve a better fit.



Again, red squares along the profiles are underplating-corrected restored points as compared to the uncorrected ones (black squares). Sequentially, Antarctica is rotated clockwise from its position at 171 Ma to bring the restored boundaries together. Figure 3.38 shows a good correlation between the conjugate boundaries. Note that India is now separated from Madagascar. The juxtapositions between the Explora Wedge and the Lebombo Monocline, Grunehogna Craton and the Kaapvaal Province also adds confidence to this particular closing geometry. Timing of the non-rigid closure is taken to be 186 Ma coeval with the eruption of Karoo flood basalt (Duncan et al., 1997).

Figure 4.39 shows the correlation of magnetic anomaly from Africa and Antarctica in the full fit reconstruction. Similar magnetic characters (wavelengths and amplitudes) are observed between the Kaapvaal Province and the Grunehogna Craton. Likewise, magnetic anomalies over the Mozambique Province and the Central Dronning Maud Land also express similar patterns.

Since the final model, which describes the initial motion of Antarctica as a counter-clockwise rotation from Africa, generates a consistent match of the restored boundaries without any major overlap or gap in the reconstruction and effectively brings back geological features that are conjugate, it is considered to be the preferred model of this study. Adopting this final closure and the relative plate positions at the onset of seafloor spreading implies area of the Mozambique Coastal Plain underwent the highest rate of continental extension and it is underlain by both continental (western half) and oceanic crust (eastern half). Table 4.3 summarizes the poles of

rotation of Antarctica with respect to Africa for different ages corresponding to magnetic isochrons, rigid closure (171 Ma) and non-rigid closure. Poles of rotations for other plates (Madagascar, Australia, etc.) are adopted from Seton et al. (2012).

Figure 4.36: Construction of profiles in the Mozambique Basin. To account for the clockwise rotation of Antarctica, each profile is placed at slightly different angles. Red squares are results of collapsing each profile after removing area of magmatic underplating. Black squares are restored points without removing magmatic underplating.

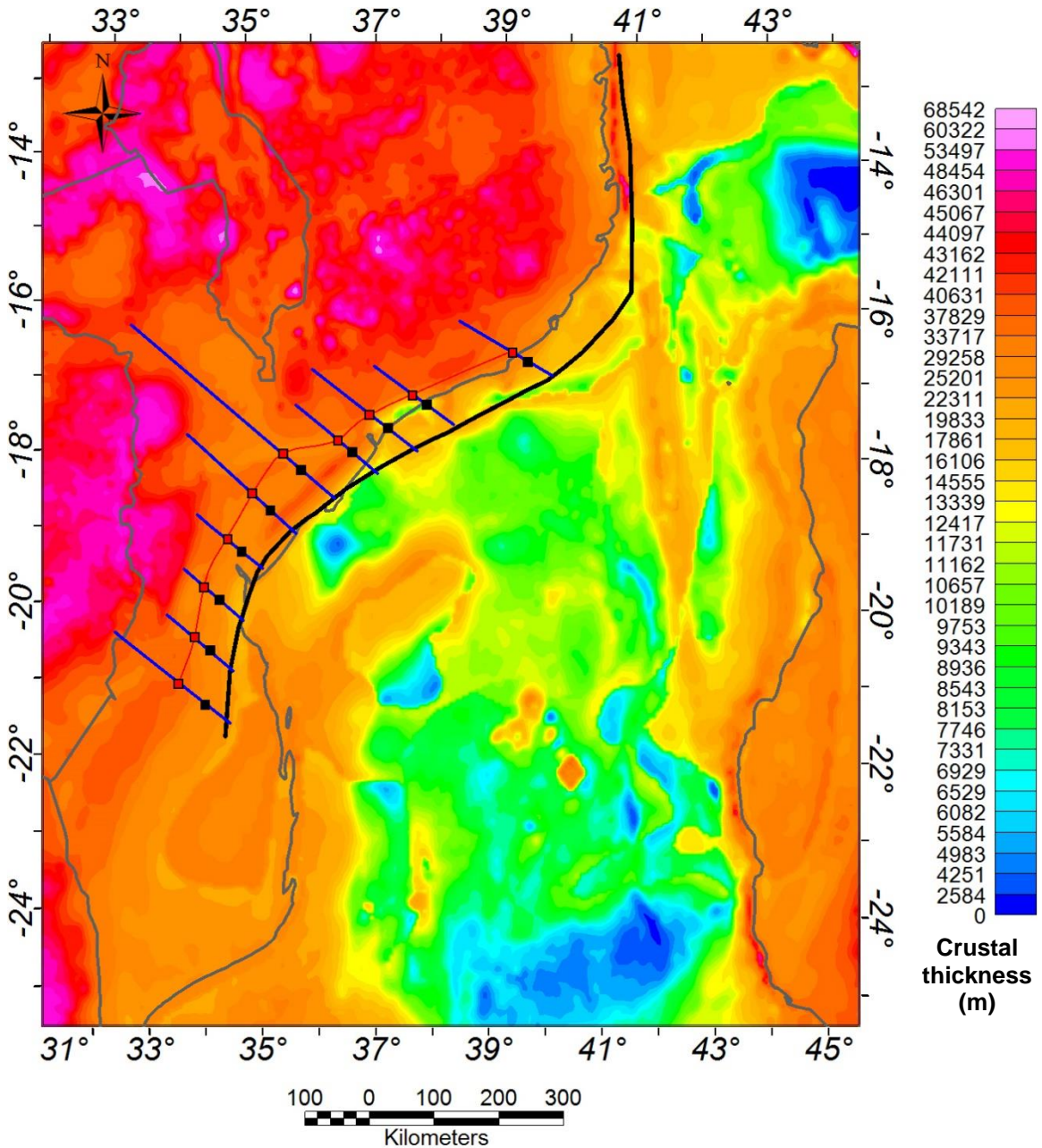


Figure 4.37: Construction of profiles in the Riiser Larsen Sea. To account for the clockwise rotation of Antarctica, each profile is placed at slightly different angles. Red squares are results of collapsing each profile after removing area of magmatic underplating. Black squares are restored points without removing magmatic underplating.

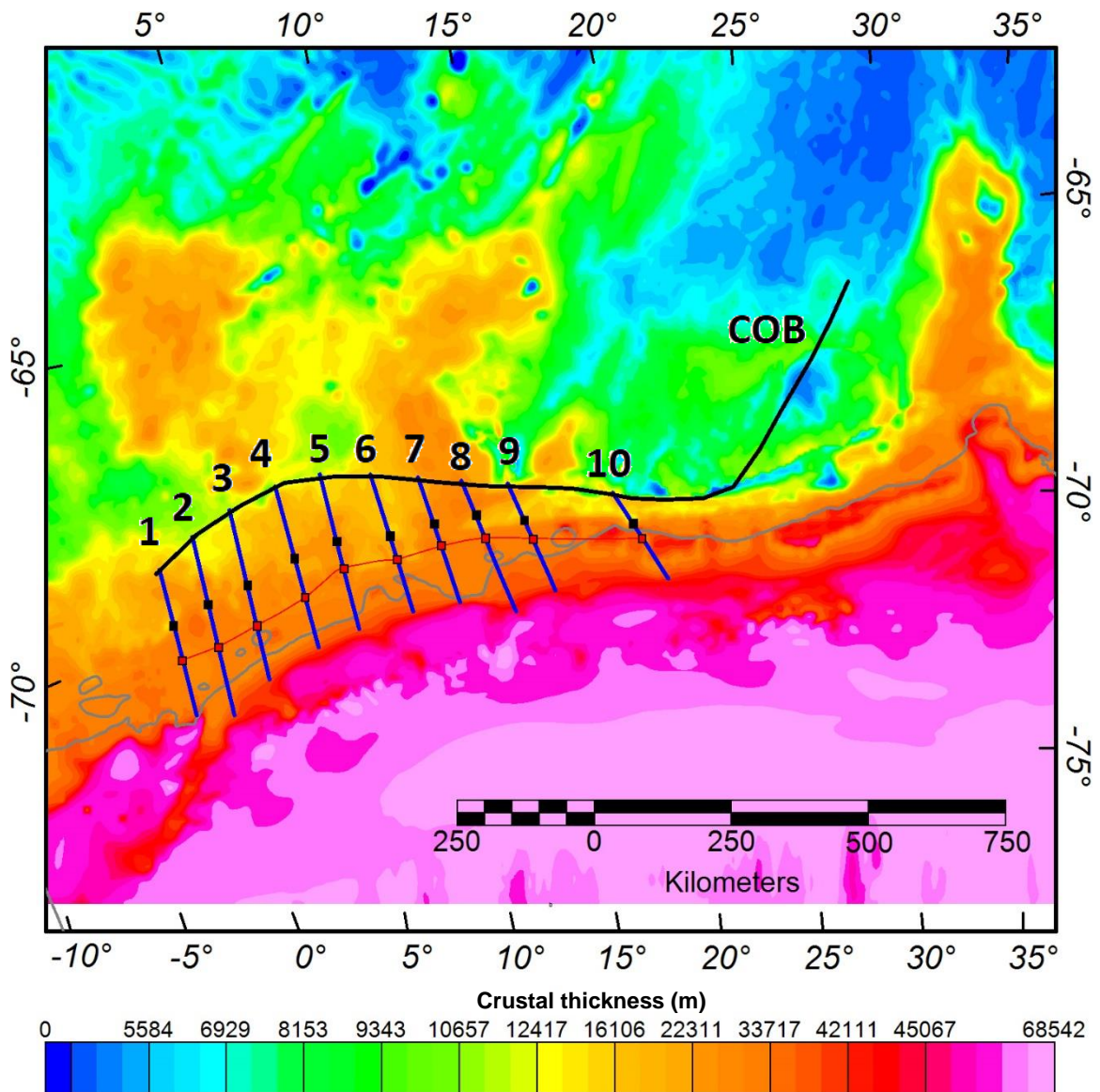


Figure 4.38: Non-rigid closing geometry as Antarctica is rotated clockwise with respect to Africa. The correlation between the pre-rift boundaries are greatly improved. This geometry also resolves the overlap between Madagascar and Africa. This model show good correlation between conjugate geological structure of Africa and Antarctica. EW: Explora Wedge, GC: Grunehogna Craton, KP: Kaapvaal Province, ZP: Zimpabwe Province.

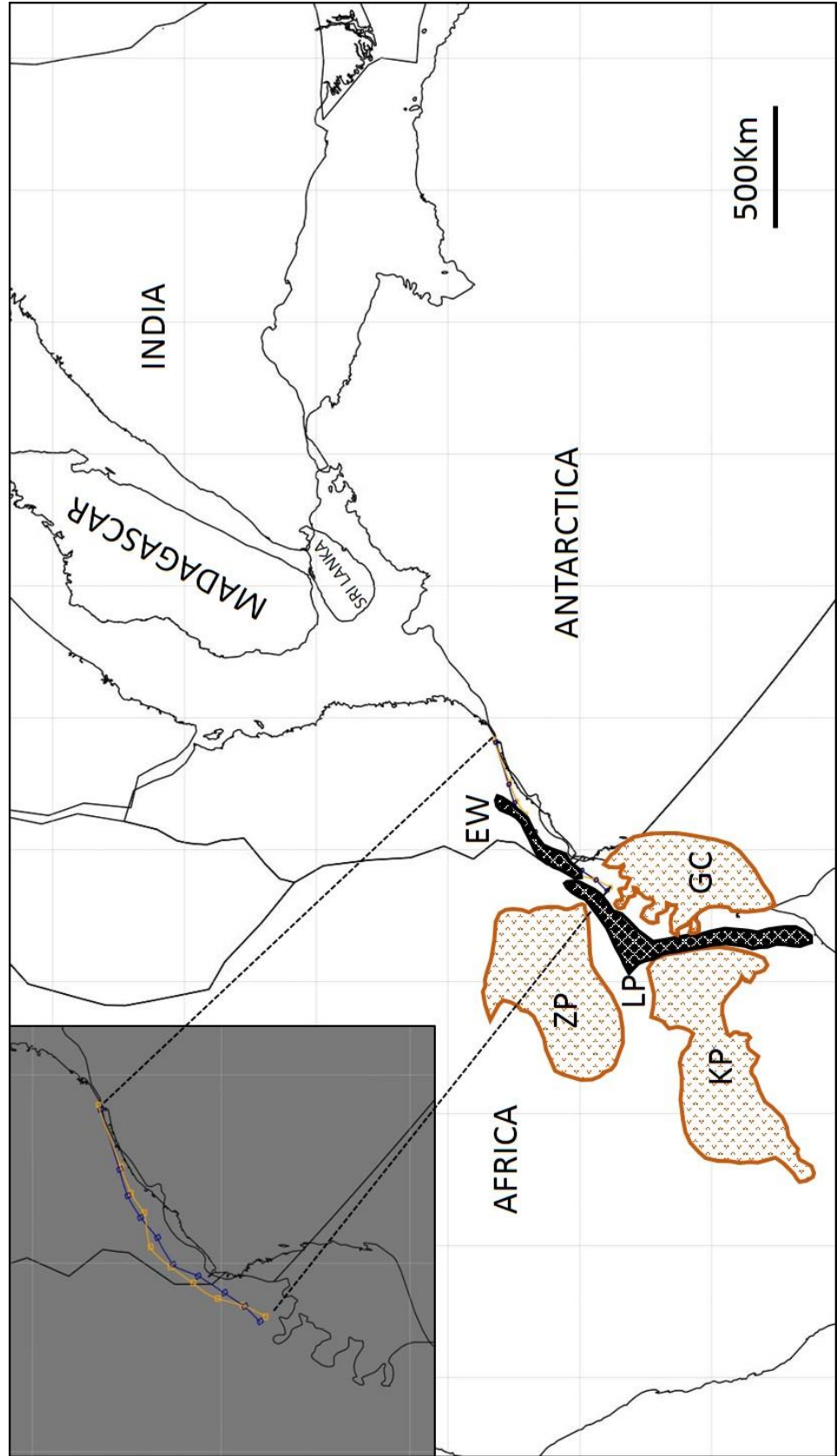


Figure 4.39: Correlation of the magnetic anomalies over Africa and Antarctica in their original position as restored by rigid and non-rigid reconstruction. Dashed outlines are regions that express magnetic anomalies of similar wavelengths and amplitudes. KP: Kaapvaal Province, GC: Grunehogna Craton, MZP: Mozambique Province, CDMiL: Central Dronning Maud Land. Map overlay is reduction to the pole of the total intensity magnetic anomaly (Maus et al., 2007).

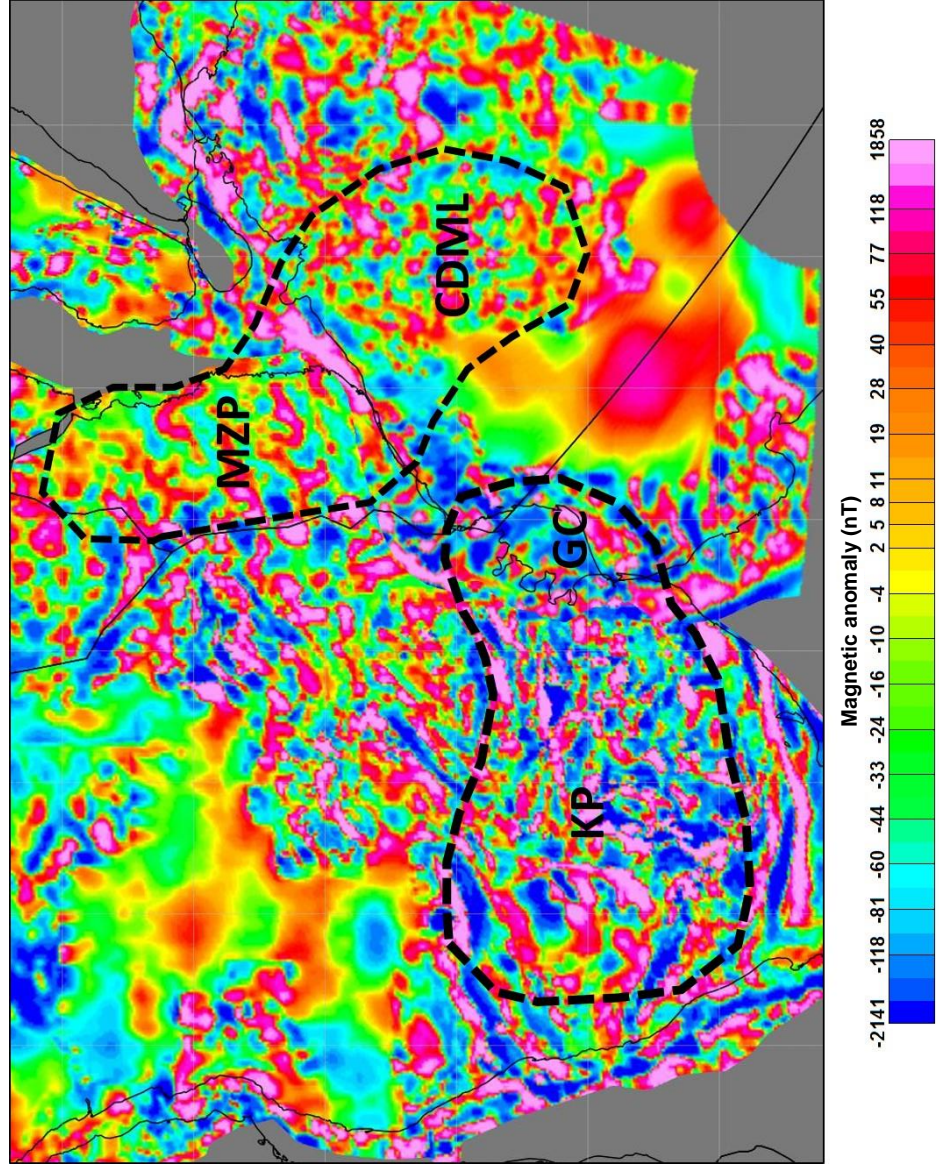


Table 4.1: Information for profiles constructed in the N-S direction in the Mozambique Basin and the Riiser Larsen Sea

Profiles	Total crustal area (Km ²)	Simple restoration Length from pre-rift thickness (Km)	Volcanic restoration Length from pre-rift thickness (Km)	Thickness of SDRs (Km)	Thickness of Underplating (Km)	Volcanic area (Km ²)	Profile length (Km)
MZB-1	16561.5	394.3	258.0	5.0	12.5	5719.0	558.0
MZB-2	17298.2	412.0	290.0	5.0	12.5	5084.0	496.0
MZB-3	5894.0	140.3	107.3	3.0	7.5	1387.5	185.0
MZB-4	7575.5	180.4	140.6	3.0	7.5	1672.5	223.0
MZB-5	5419.8	129.0	96.0	3.0	7.5	1387.5	185.0
MZB-6	3763.4	89.6	62.2	3.0	7.5	1147.5	153.0
MZB-7	5746.8	137.0	107.7	3.0	7.5	1230.0	164.0
MZB-8	5064.4	120.6	92.9	3.0	7.5	1162.5	155.0
MZB-9	4293.7	102.2	75.0	3.0	7.5	1140.0	152.0
MZB-10	7430.0	177.0	133.2	3.0	7.5	1837.5	245.0
RLS-1	11292.9	268.9	152.5	5.0	12.5	3577.5	477.0
RLS-2	15248.8	363.1	181.8	5.0	12.5	4567.5	609.0
RLS-3	13086.8	311.6	215.7	3.0	7.5	4027.5	537.0
RLS-4	19182.3	456.7	255.2	3.0	7.5	5077.5	677.0
RLS-5	8478.8	201.9	136.3	3.0	7.5	2752.5	367.0
RLS-6	8628.1	205.4	150.6	3.0	7.5	2302.5	307.0
RLS-7	6809.3	162.1	116.4	3.0	7.5	1920.0	256.0
RLS-8	6672.6	158.9	115.7	3.0	7.5	1815.0	242.0
RLS-9	6262.8	149.1	109.8	3.0	7.5	1650.0	220.0
RLS-10	4599.6	109.5	77.5	3.0	7.5	1342.5	179.0

Table 4.2: Information for profiles constructed in the uniform NW-SE direction in the Mozambique Basin and the Riiser Larsen Sea

Profiles	Total crustal area (Km ²)	Simple restoration Length from pre-rift thickness (Km)	Volcanic restoration Length from pre-rift thickness (Km)	Thickness of SDRs (Km)	Thickness of Underplating (Km)	Volcanic area (Km ²)	Profile length (Km)
MZB-1	6881.5	163.8	109.4	5.0	12.5	2285.8	223.0
MZB-2	6983.5	166.3	115.8	5.0	12.5	2121.8	207.0
MZB-3	3053.1	72.7	39.0	5.0	12.5	1414.5	138.0
MZB-4	3440.8	81.9	52.4	5.0	12.5	1240.3	121.0
MZB-5	8141.8	193.9	151.4	3.0	7.5	1785.0	238.0
MZB-6	8889.9	211.7	162.4	3.0	7.5	2070.0	276.0
MZB-7	5051.5	120.3	90.1	3.0	7.5	1267.5	169.0
MZB-8	6391.6	152.2	114.5	3.0	7.5	1582.5	211.0
MZB-9	4616.5	109.9	81.7	3.0	7.5	1185.0	158.0
MZB-10	3757.2	89.5	65.5	3.0	7.5	1005.0	134.0
RLS-1	9191.7	218.8	135.1	5.0	12.5	3515.8	343.0
RLS-2	7709.0	183.5	111.1	5.0	12.5	3044.3	297.0
RLS-3	6951.9	165.5	92.8	5.0	12.5	3054.5	298.0
RLS-4	6592.9	157.0	83.0	5.0	12.5	3105.8	303.0
RLS-5	7139.2	170.0	117.7	3.0	7.5	2197.5	293.0
RLS-6	6336.6	150.9	102.7	3.0	7.5	2025.0	270.0
RLS-7	6507.3	154.9	110.5	3.0	7.5	1867.5	249.0
RLS-8	8055.8	191.8	147.3	3.0	7.5	1867.5	249.0
RLS-9	5529.6	131.7	97.6	3.0	7.5	1432.5	191.0
RLS-10	4639.6	110.5	80.6	3.0	7.5	1252.5	167.0

Table 4.3: Information for profiles constructed at various angles to account for the rotation of Antarctica

Profiles	Total crustal area (Km ²)	Simple restoration Length from pre-rift thickness (Km)	Volcanic restoration Length from pre-rift thickness (Km)	Thickness of SDRs (Km)	Thickness of Underplating (Km)	Volcanic area (Km ²)	Profile length (Km)
MZB-1	7664.7	182.5	126.8	5.0	12.5	2337.0	228.0
MZB-2	3483.7	82.9	51.0	5.0	12.5	1342.8	131.0
MZB-3	3114.5	74.2	41.7	5.0	12.5	1363.3	133.0
MZB-4	3804.7	90.6	59.1	5.0	12.5	1321.2	128.9
MZB-5	7492.9	178.4	137.7	3.0	7.5	1710.0	228.0
MZB-6	14462.2	344.3	268.3	3.0	7.5	3195.0	426.0
MZB-7	4922.0	117.2	87.5	3.0	7.5	1245.0	166.0
MZB-8	6401.1	152.4	114.7	3.0	7.5	1582.5	211.0
MZB-9	4280.0	101.9	73.7	3.0	7.5	1185.0	158.0
MZB-10	5183.8	123.4	93.8	3.0	7.5	1245.0	166.0
RLS-1	6848.9	163.1	98.4	5.0	12.5	2716.3	265.0
RLS-2	8594.2	204.6	124.1	5.0	12.5	3382.5	330.0
RLS-3	7265.4	173.0	97.3	5.0	12.5	3177.5	310.0
RLS-4	7097.4	169.0	94.3	5.0	12.5	3136.5	306.0
RLS-5	6983.5	166.3	116.1	3.0	7.5	2107.5	281.0
RLS-6	5889.1	140.2	94.5	3.0	7.5	1920.0	256.0
RLS-7	6333.0	150.8	108.3	3.0	7.5	1785.0	238.0
RLS-8	7926.2	188.7	142.8	3.0	7.5	1927.5	257.0
RLS-9	5740.5	136.7	99.4	3.0	7.5	1567.5	209.0
RLS-10	4868.2	115.9	81.1	3.0	7.5	1462.5	195.0

Table 4.4: Total reconstruction poles of Antarctica with respect to Africa from present time, generated in this study.

Isochrons	Time (Ma)	Latitude	Longitude	Angle
M0r	124.81	-12.75	-24.05	43.89
M3n	127.86	-12.71	-24.46	44.78
M5n	130.28	-12.55	-24.84	45.67
M5r	131.00	-13.04	-24.40	46.28
M6n	131.30	-13.10	-24.44	46.57
M7r	132.03	-12.97	-24.62	46.67
M8n	132.36	-13.10	-24.53	46.92
M8r	132.68	-12.90	-24.75	46.88
M9n	132.99	-13.43	-24.26	47.41
M9r	133.32	-14.31	-23.38	48.19
M10n	133.69	-14.91	-22.81	48.82
M10r	134.09	-15.61	-22.09	49.54
M10Nn2n	134.83	-16.39	-21.24	50.51
M10Nr	135.49	-16.47	-21.26	50.83
M11r2r	136.81	-16.45	-21.32	51.58
M12n	137.71	-16.17	-21.63	51.67
M15n	140.51	-15.25	-22.66	52.11
M15r	140.86	-15.18	-22.75	52.16
M18r	144.73	-14.14	-23.97	53.23
M19n2n	145.51	-14.51	-23.61	53.97
M19r	146.06	-14.78	-23.32	54.39
M20n1n	146.32	-14.47	-23.70	54.41
M20r	147.47	-14.26	-23.96	54.58
M21n	148.16	-14.46	-23.74	54.91
M21r	148.73	-14.57	-23.65	55.32
M22n1n	149.49	-14.11	-24.16	55.60
Rigid Fit	171.00	-12.52	-26.20	60.85
Full Fit	186.00	-2.28	-38.46	56.31

CHAPTER 5

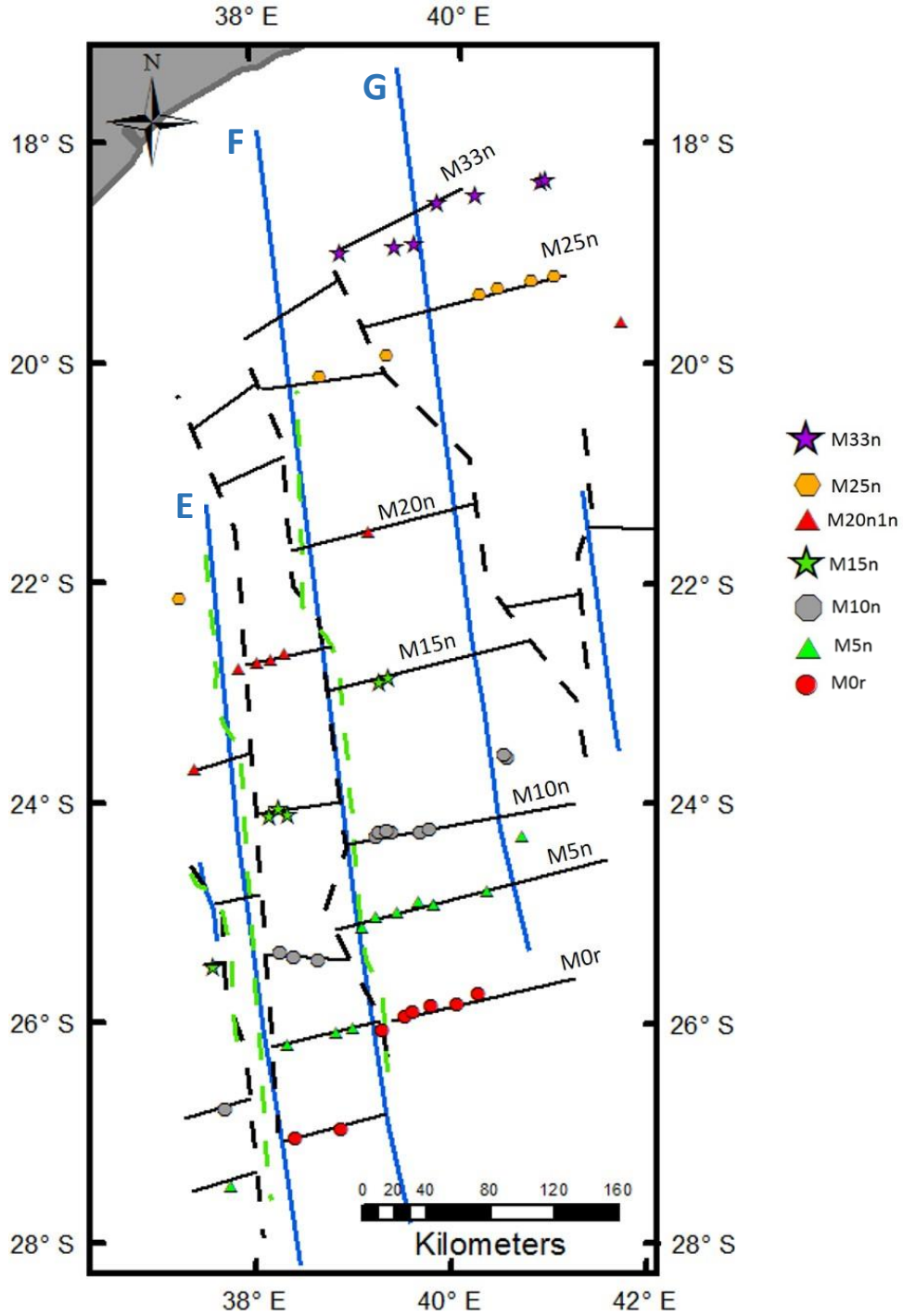
DISCUSSION

In this chapter, the study's results are discussed in more detail with regards to their implications, assumptions and limitations. Furthermore, alternative models to the preferred model of this study are also discussed.

5.1 Magnetic isochron identification

Magnetic isochrons picked over the Mozambique Basin and the Riiser Larsen Sea in this study conform well to identifications from recent studies of Leinweber and Jokat (2012), and Konig and Jokat (2010). This is especially true for the Antarctic margin where both chron and fracture zone identifications are very similar. Over the conjugate African margin, the overall correlations are comparable with other studies. Figure 5.1 illustrates the comparison between magnetic isochrons and fracture zones identified in this study and those from Leinweber and Jokat (2012), and Konig and Jokat (2010). The central difference from this study is the recognition of fracture zone G and its associated isochrons offset. As previously shown in Chapter 4, fracture zone G was initially identified from filtered satellite-derived gravity anomaly maps. In addition, interpretation of magnetic profiles across this fracture zone show isochrons offset of ~50 km. The presence of fracture zone G is also consistent with the identification of fracture G1 with comparable offset over the Riiser Larsen Sea which is most likely to be the conjugate of G1 according to the current reconstruction model. The northern part of fracture zone G1 had been recognized in previously studies and

Figure 5.1: Comparison of magnetic isochrons and fracture zones identified in this study and those of Leinweber and Jokat (2012) and König and Jokat (2010). Colored symbols are isochrons from this study. Black solid lines with labels are isochrons identified by Leinweber and Jokat (2012). Blue lines are fracture zones from this study. Dashed black lines are fracture zones from Leinweber and Jokat (2012). Green dash lines are fracture zones from König and Jokat (2010).



is extended farther south in this study as revealed in the filtered gravity anomaly maps. Identified magnetic isochrons indicate an average offset of 35 km across fracture zone G1.

Fracture zone E and F were originally identified by magnetic interpretation of Segoufin (1978), and Simpson et al. (1979) and recently confirmed by König and Jokat (2010). Independent identifications of fracture E and F using satellite-derived gravity anomaly data show strong consistency with those previous findings (Figure 5.1). New gravity data enable this study to extend fracture F farther north. The resulting extension shows a parallel trend with fracture zone G. Leinweber and Jokat (2012) show fracture zones that bend westward to a NW-SE direction between latitude 20°S-21°S. This change in fracture zone orientation is not evident in this study. Rather, the fracture zones are interpreted as extending in a continuous N-S direction.

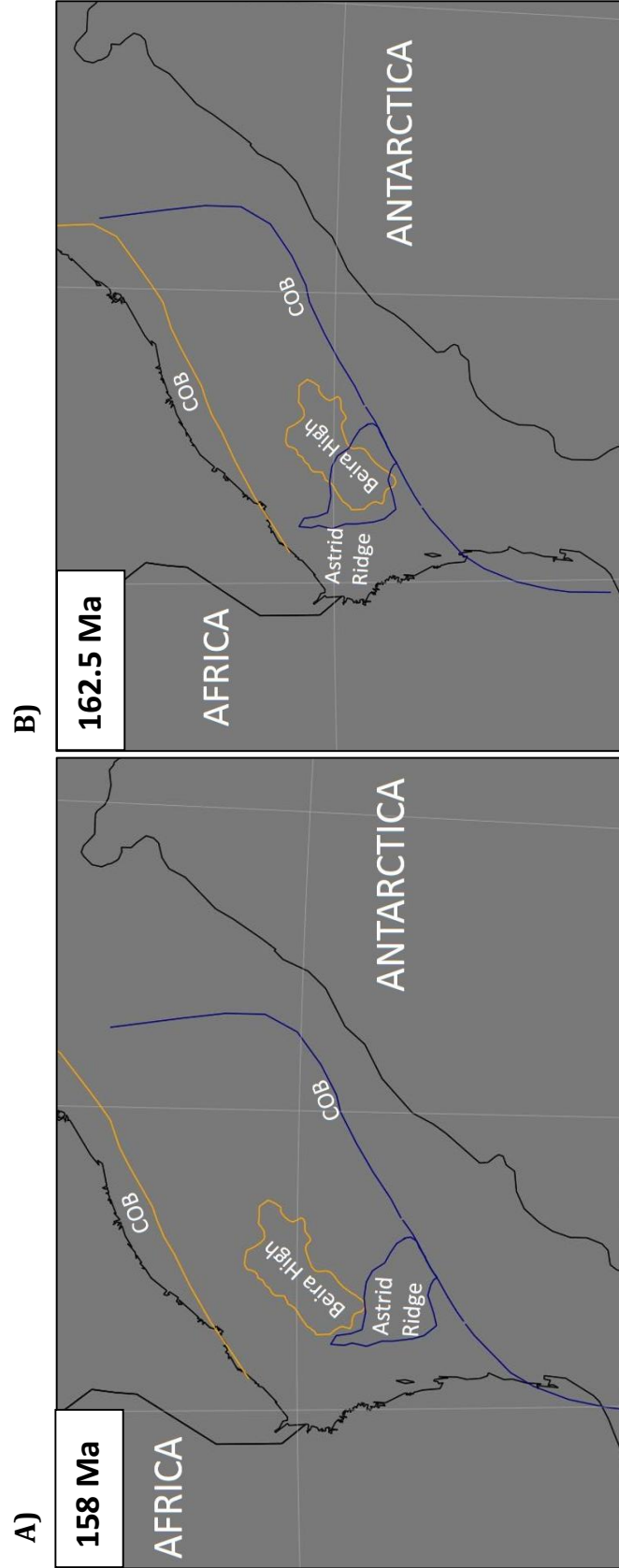
5.2 Rigid reconstruction

The northward extension of fracture F along with identification of fracture G play an important role in the rigid plate reconstruction. In Leinweber and Jokat (2012), change in fracture zones orientation leads to a model of early counter-clockwise rotation of Antarctica with respect to Africa during seafloor spreading. A similar motion of Antarctica is also proposed in Eagles and König (2008). Data interpreted in this study do not agree with such a model because of the lack of fracture zone bends. In fact, fracture zones traces and magnetic isochrons identified in the northern Mozambique Basin both support a continuous south ward drift of Antarctica until

M0r (124.8 Ma). This is in agreement with the reconstruction model of König and Jokat (2010) in which Antarctica is restored steadily northward.

The current preferred model presented in Chapter 4 has two important implications. First, the Beira High and the ocean from its northern edge landward are floored by oceanic crust. From the reconstruction sequence, it is postulated that the Beira High could be the conjugate feature of southern Astrid Ridge. The southern Astrid Ridge is interpreted as oceanic structure based on its similar magnetic character with the adjacent Riiser Larsen Sea (Leinweber and Jokat, 2012). Seismic refraction over this ridge shows upper crust velocity of 4.2-5.0 km/s and lower crust velocity of 6.9-7.0 km/s also similar to the velocities of oceanic crust in the Riiser Larsen Sea. Figure 5.2 shows the relative positions of the Beira High and southern Astrid Ridge at 158 Ma and their overlap at 162 Ma. The similar shapes of the two structures and their juxtaposition in the reconstruction model make the argument for their conjugate highly favorable. In a simple, symmetric spreading model, conjugate features would likely to form at the spreading ridge symmetrically centered between the conjugate COBs. It is, however, observed that Beira High is situated more than 100 km from the interpreted COB of Africa whereas the Astrid Ridge is attached to Antarctica. One possible explanation for this discrepancy is an asymmetric spreading model. The oceanic crust over the Mozambique Basin might have experienced faster spreading rate than its Antarctica counterpart. Such asymmetry is evident in this particular reconstruction model as the distances between isochrons and the COB on the Africa side are greater than those of the Antarctica side (Figures 4.27-4.29). Since

Figure 5.2: A) Reconstruction at 158 Ma showing the juxtapositions of the Beira High and the southern Astrid Ridge. Beira High is outlined as in Mahanjane (2012). Boundary of the Astrid Ridge is estimated using gravity data and crustal thickness model. **B)** Reconstruction at 162.5 Ma showing the overlap of the Beira High and the Astrid Ridge. Yellow and Blue lines are the interpreted COBs for the African and Antarctic margins, respectively.



the amount of asymmetry in each spreading corridor remains relatively unchanged from 150 Ma to 124 Ma, it is likely that most of the asymmetric spreading took place in the older period of the basin history. Another scenario that could have placed the Beira High farther offshore than the Astrid Ridge is a ridge jump in the early spreading history of the margins where a younger ridge jumped southward from the former ridge. To investigate both the existence of early ridge jump and the progressive increase in asymmetry across the spreading corridor from east to west, more detailed magnetic data are needed in the northern part of Mozambique basin.

Another implication from this model is that the eastern part of the Mozambique Coastal Plain was formed by seafloor spreading and thus is thickened oceanic crust whereas its western half is occupied with stretched continental crust. This results strictly from the location of the COB picked for the African margin which in turn was inferred by the COB picked in the Antarctic margin. As mentioned in Chapter 4, the COB in the Mozambique Basin is only well constrained in its eastern part. Its western half was adopted from that of the Antarctica COB based on their closing geometry at 171 Ma in the reconstruction model. Another candidate for the COB is shown in Figures 5.3a and 5.4a as it follows the trend of crustal thickness southward and join with the Mozambique Fracture Zone. If this is truly the COB then the entire Mozambique Coastal Plain is continental. Considering this as the COB for the Mozambique Basin would also change the geometry of the conjugate COB in the Riiser Larsen Sea (Figures 5.3b and 5.4b). Final non-rigid restoration based on this alternative COB yields an equivalently good correlation of the pre-rift boundaries as

Figure 5.3: Display of alternative COBs (heavy dashed lines) in the Mozambique Basin and the Riiser Larsen Sea on the regional magnetic anomaly maps with reduction to the pole. Solid lines are the current COBs in the preferred model.

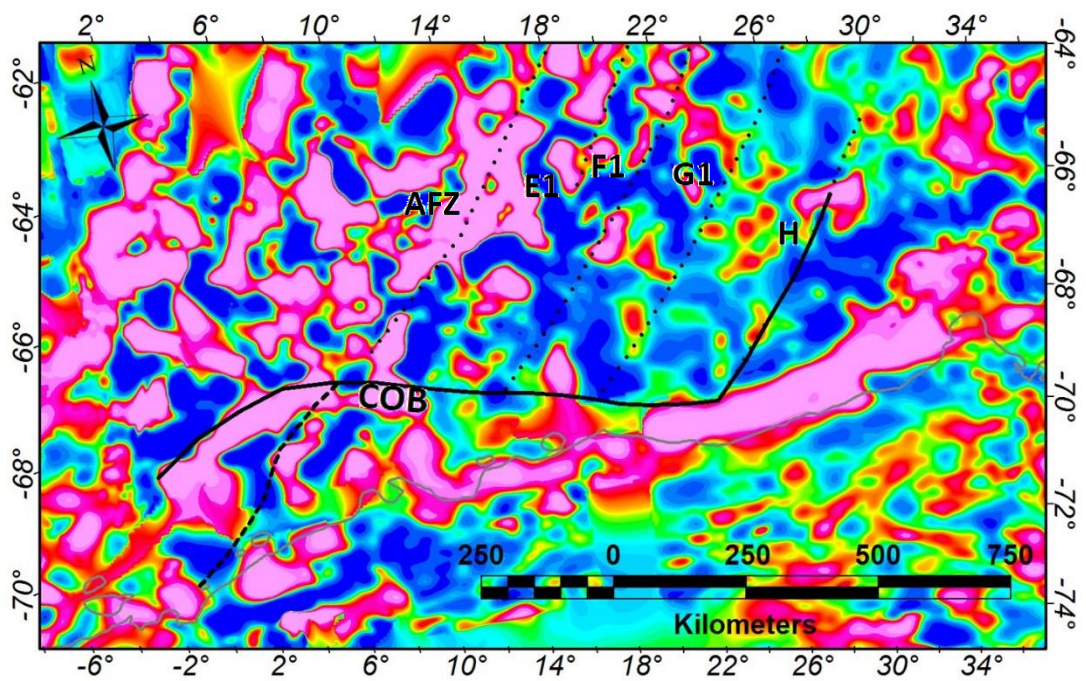
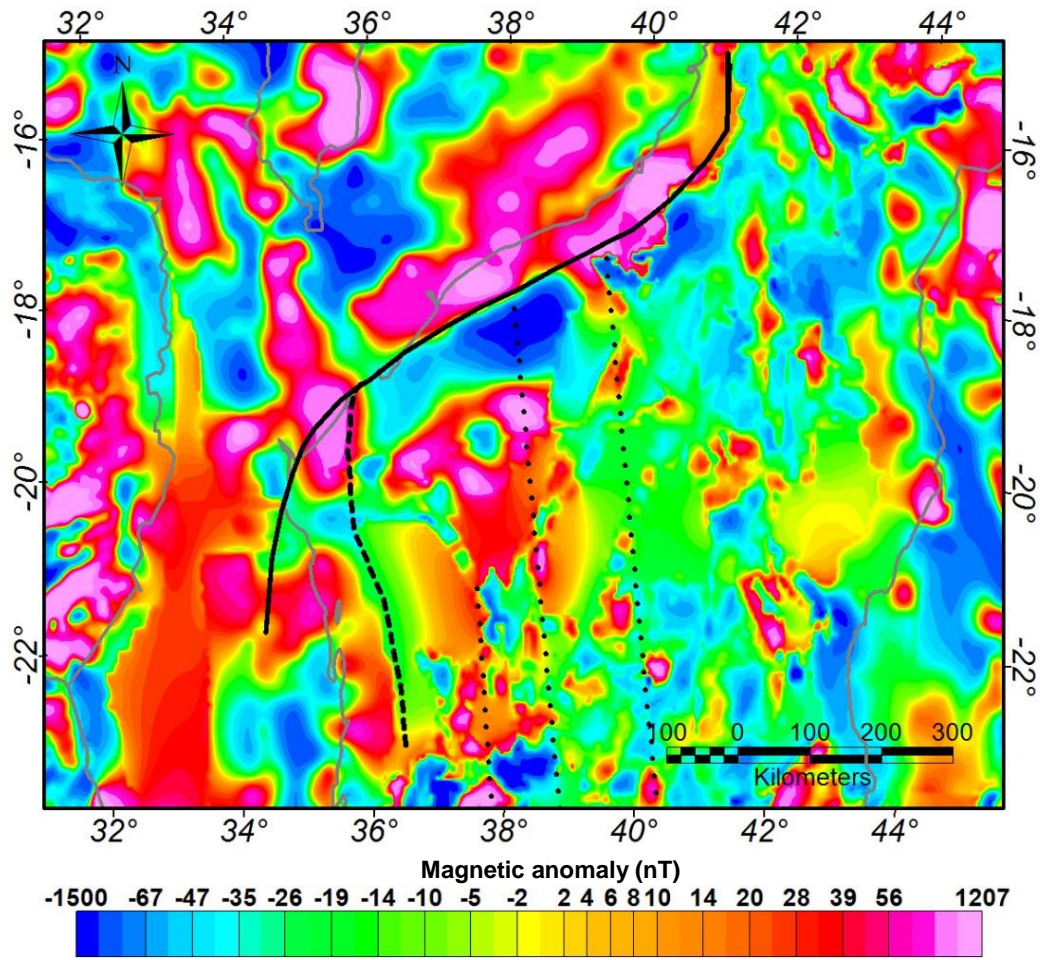


Figure 5.4: Display of alternative COBs (heavy dashed lines) in the Mozambique Basin and the Riiser Larsen Sea on the crustal thickness maps. Solid lines are the current COBs in the preferred model.

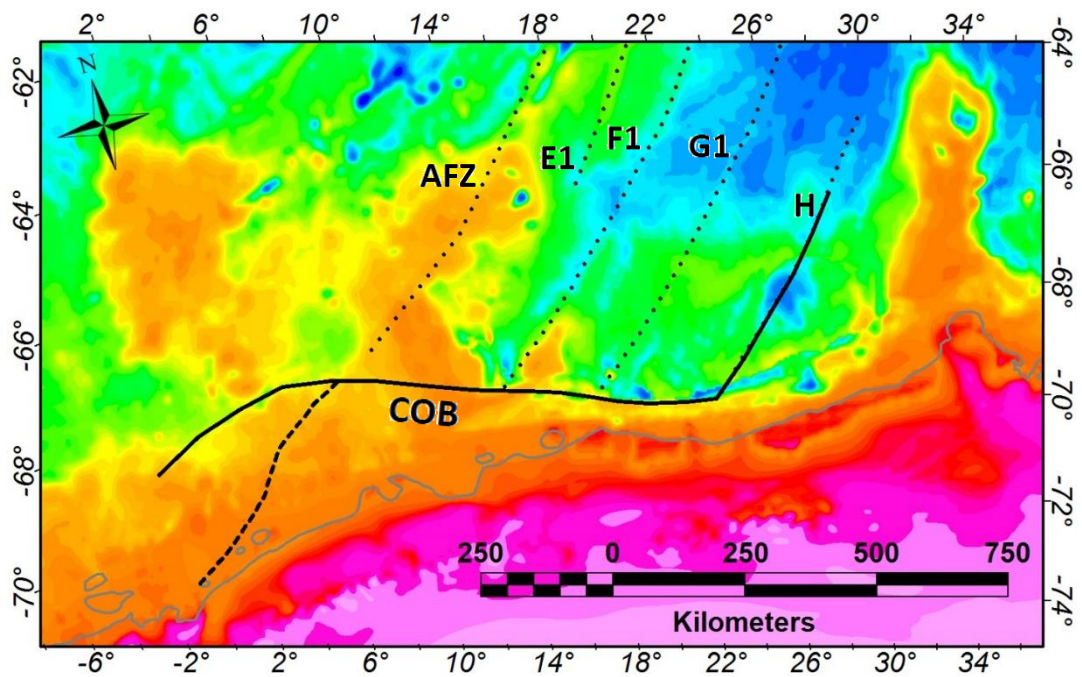
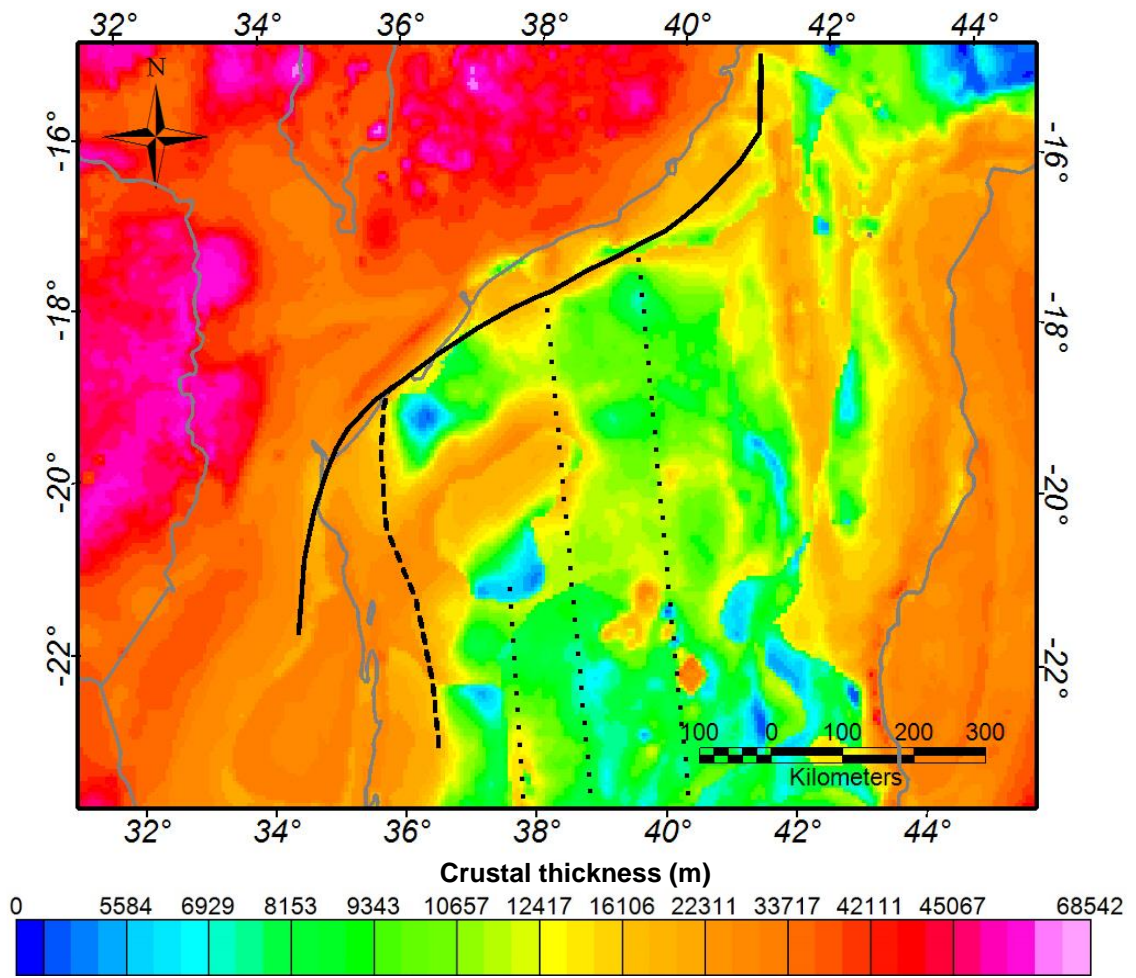
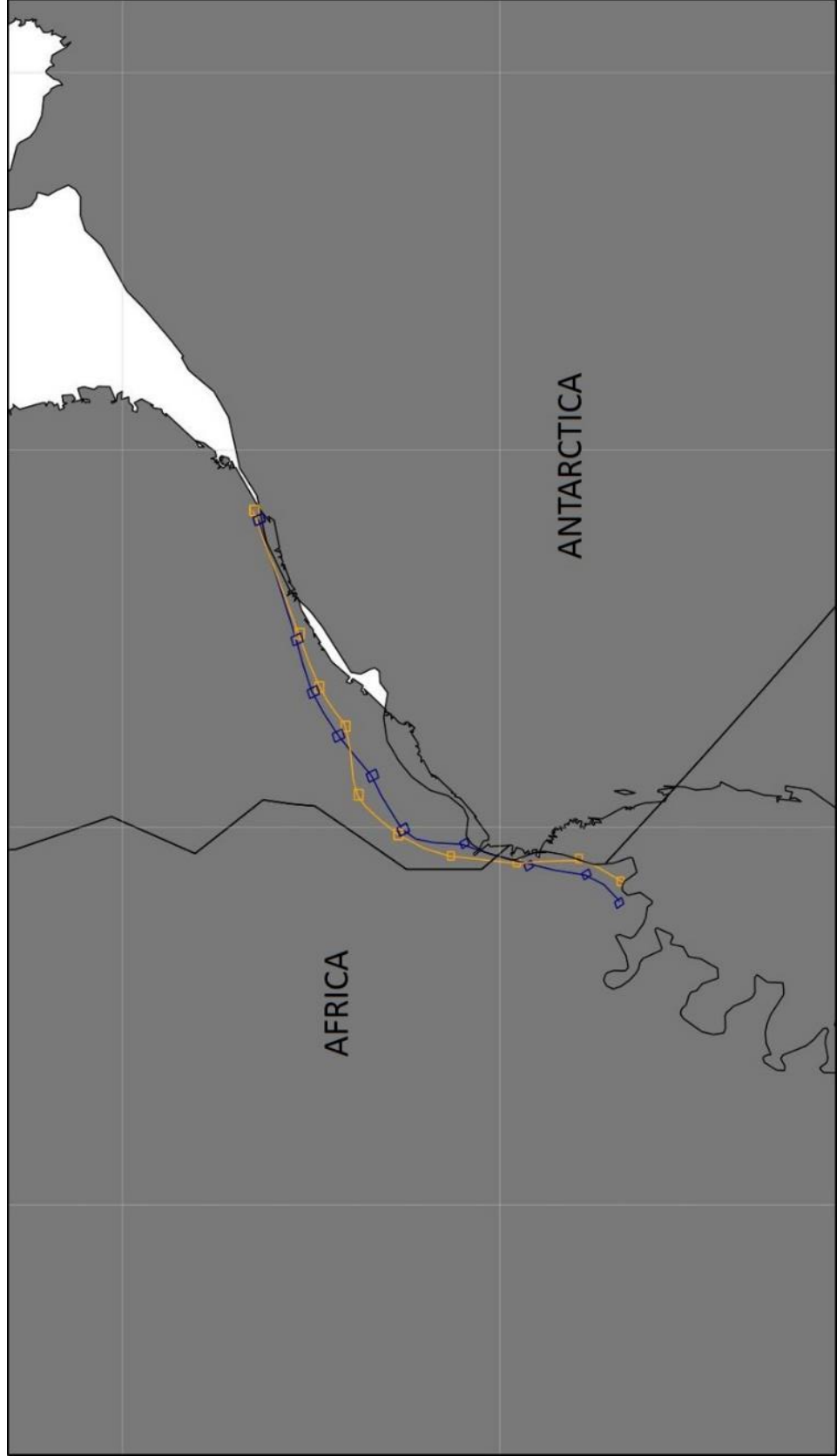
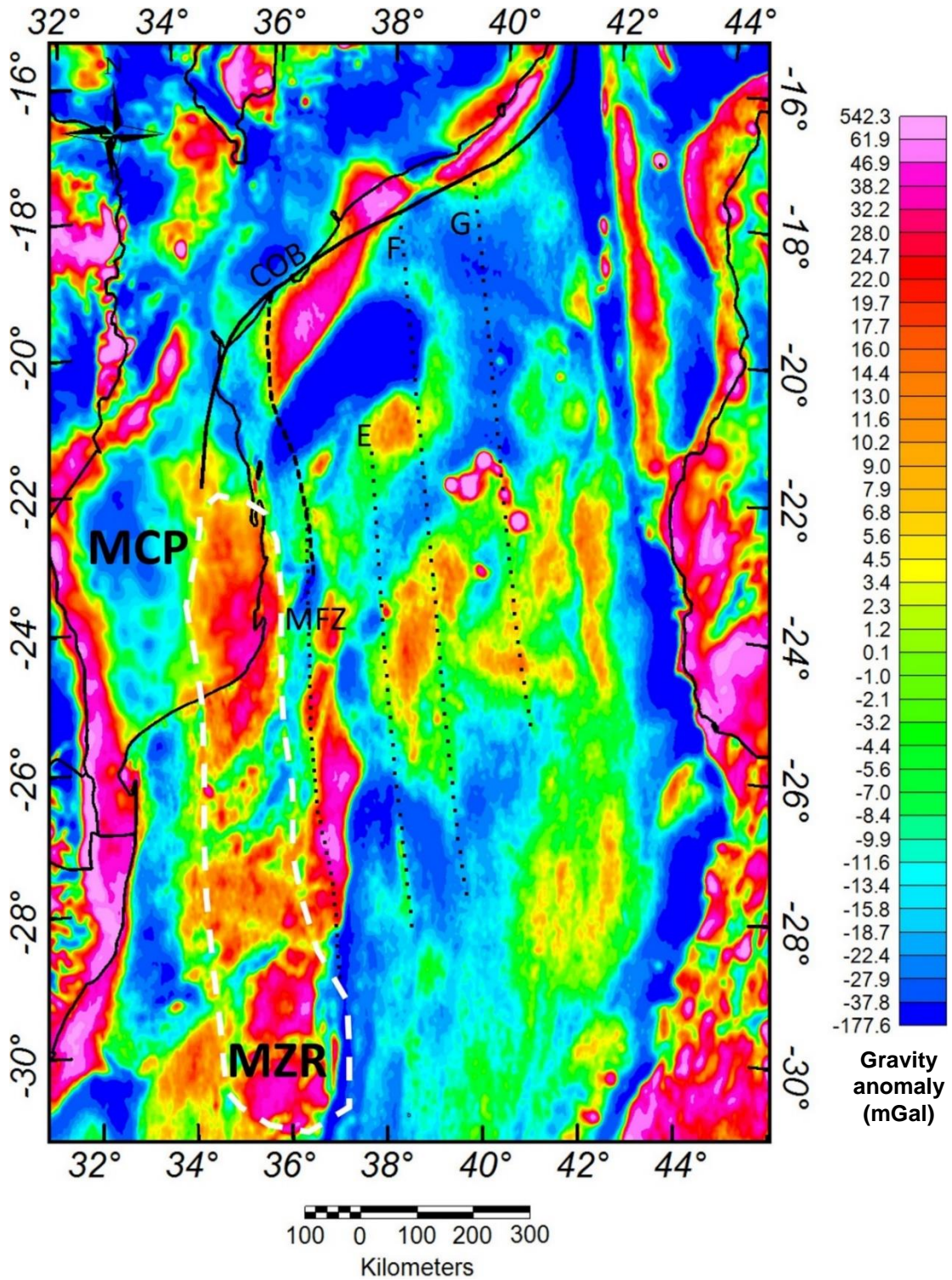


Figure 5.5: Non-rigid fit results from using the alternative COBs as shown in Figure 5.4. The restored boundaries (Africa: orange, Antarctica: blue) show an equivalently good correlation as compared to the preferred model.



compared to the preferred model's COB (Figure 5.5). Thus, the COB cannot be delineated based on the non-rigid fit of the continents. It is also noted that the nature of the crust situated between the two COB candidates is still a subject of speculation. Gravity and flexural model of Watts (2001) supports an oceanic origin for this area. Leinweber and Jokat (2011) recognize a gravity anomaly in the eastern coastal plain that is joined with an elongated positive anomaly of the Mozambique Ridge suggesting a common origin for both structures (Figure 5.6). Interpretation of the most recent magnetic data over the Mozambique Ridge describes it as an oceanic feature. Wells drilled onshore of the Mozambique Coastal Plain terminate in a basalt layer that is likely to be 127-147 Ma in age (Flores, 1983). Though its age range excludes it from being identified as a Karoo feature, its composition was interpreted as similar to a younger volcanic layer overlying the Lebombo Range (Flores, 1983). However, a basalt layer underlying Neocomian (145 Ma) sediment is also encountered in DSDP well 2539 (Vallier, 2007) above the Mozambique Ridge. In short, available geophysical and geological data do not provide an unequivocal determination for the crustal nature of the Mozambique Coastal Plain. It is, however, preferable to use the currently picked COB since it is supported by pronounced magnetic anomaly, seismic refraction data and crustal thickness boundary while the alternative COB does not correlate well with any one of those observations in the Antarctic margin.

Figure 5.6: Free-air gravity anomaly map showing the positive anomaly in the eastern Mozambique Coastal Plain (MCP), white dashed outline, forms a continuous trend with the elongated anomaly of the Mozambique Ridge (MZR). Solid line is the current COB in the preferred model. Heavy dashed line is the alternative COB.



5.3 Alternative models

Mahanjane (2012) interpreted seismic reflection data over the Beira High and concluded it is a continental fragment. This finding was incorporated in the reconstruction model of Leinweber and Jokat (2012) wherein the Beira was attached to Africa for time before 167 Ma and then started to drift southward together with Antarctica until 159 Ma at which time it reached its present day location. It is inferred from their model that a narrow zone of oceanic crust occupied the area between the Beira High and Africa and hence a ridge jump must have taken place at around 159 Ma that separate the Beira High from Antarctica.

This study finds that the above scenario entails complications that are currently not explainable. Figure 5.7a displays the plate reconstruction at 162.5 Ma where the Antarctica COB roughly comes into contact with the Beira High whose boundary is defined seismically by Mahanjane (2012). At this stage, the width of the ocean basin along fracture zones east of the Beira High is close to double that of the basin immediately north of the structure. Assuming the Beira High now moves northward together with Antarctica, Figure 5.7b shows the reconstruction at a time when the high makes contact with the Africa COB (~166 Ma). As the ocean basin separating the Beira High from Africa is now closed, 115 km of oceanic crust still remains on its eastern side. Under a few unlikely circumstances, two basins to the north and east of the Beira High can be closed simultaneously. From 166 Ma to 162.5 Ma, Antarctica must have rotated clockwise and the pole of rotation must be very close to produce such extreme variation in amount of spreading over relatively short distance.

Figure 5.7: A) Reconstruction at 162 Ma showing the Antarctica COB contacts the Beira High and there are unequal amount of oceanic crust to the north and east of the Beira High. **B)** Reconstruction at 166 Ma, assuming the ocean is closed between the Beira High and Africa, extra oceanic crust still remains in the adjacent area.

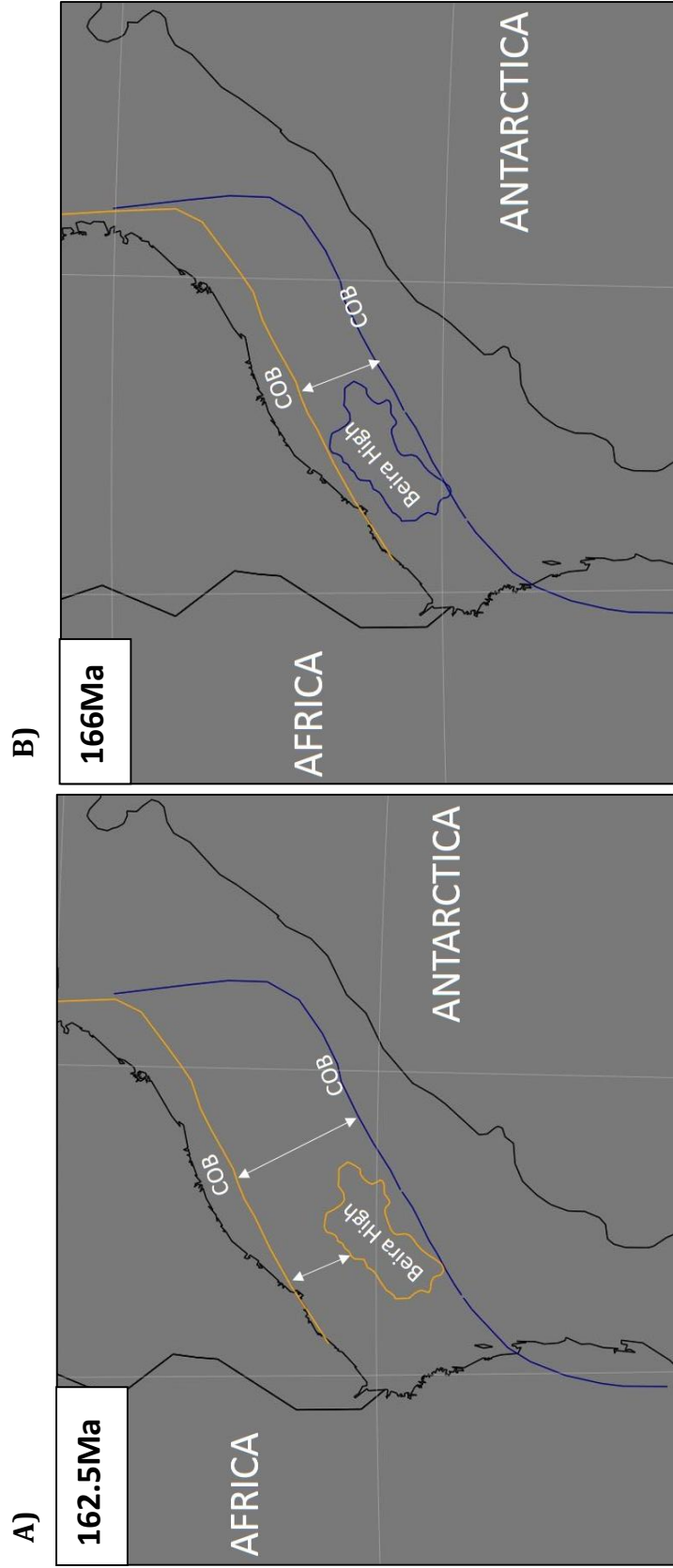
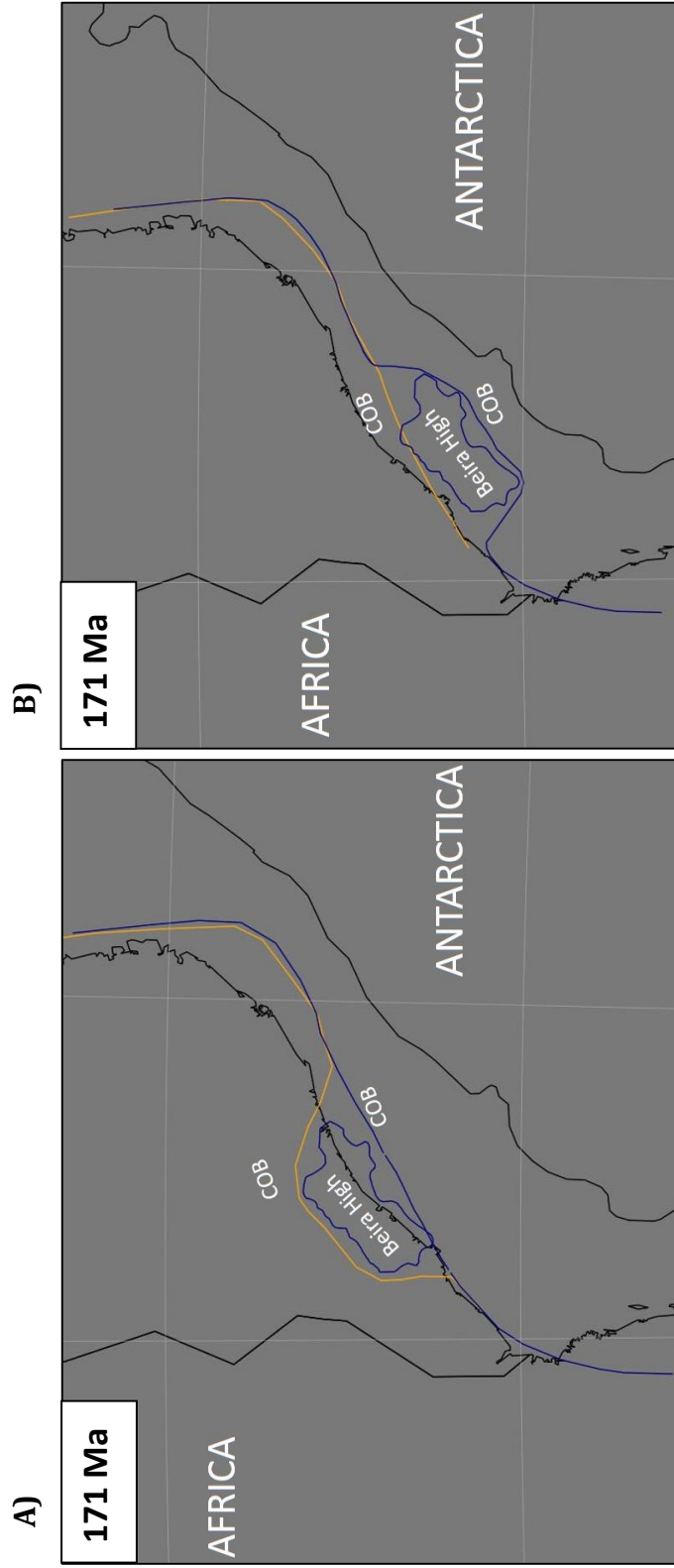


Figure 5.8: Reconstruction map at 171Ma showing **A)** modified Africa COB to accommodate the continental Beira High without issue of gap and **B)** alternative model where the Antarctica COB is modified to accommodate the Beira High.



However, that rotation would violate fracture zones traces which show continuous N-S trends. Alternatively, the requirement for rotated motion can be eliminated if a modified COB is adopted on either side of the conjugate margins (Figure 5.8). Since the Beira High is about 120 km wide, if the section between longitude 36°E and 38°E of the current Africa COB is moved 120 km northward (farther inland), the issue with gap can be resolved. Alternatively, modification can be made to the Antarctica COB so that between longitude 9°E and 15°E it is pushed back 120 km landward (Figure 5.8b). Figures 5.9 and 5.10 show the location of modified COBs in both margins in correlation with the magnetic anomaly map as well as the crustal thickness grid. Though these scenarios are possible they are rather improbable as very little correlation can be made between the modified COBs and geophysical controls. The presence of oceanic crust directly north of the Beira High is supported by the crustal thickness model which shows a 115-120 km wide area between the Beira High and the Africa COB that has crustal thickness ranges from 4.5 to 10 km. This is similar to that of the crustal thickness in ocean basin east of the Beira High.

It has been proposed in Cox (1992) that the initial motion of Antarctica during the rifting period was along an ENE-WSW strike slip fault. The combination of this direction of rifting and the obvious N-S direction of seafloor spreading requires a radical change in direction of the stress field. More importantly, there is no analog for this model where the directions of rifting and drifting are almost perpendicular. In addition, while an E-W extension would account for the stretched crust in the coastal plain area, it suggests that no extension occurred along the northeast margin of.

Figure 5.9: Correlation of the modified Africa COB from Figure 5.8 to **A)** crustal thickness model and **B)** regional magnetic anomaly. The modified COB does not correlate well with any trend in either map.

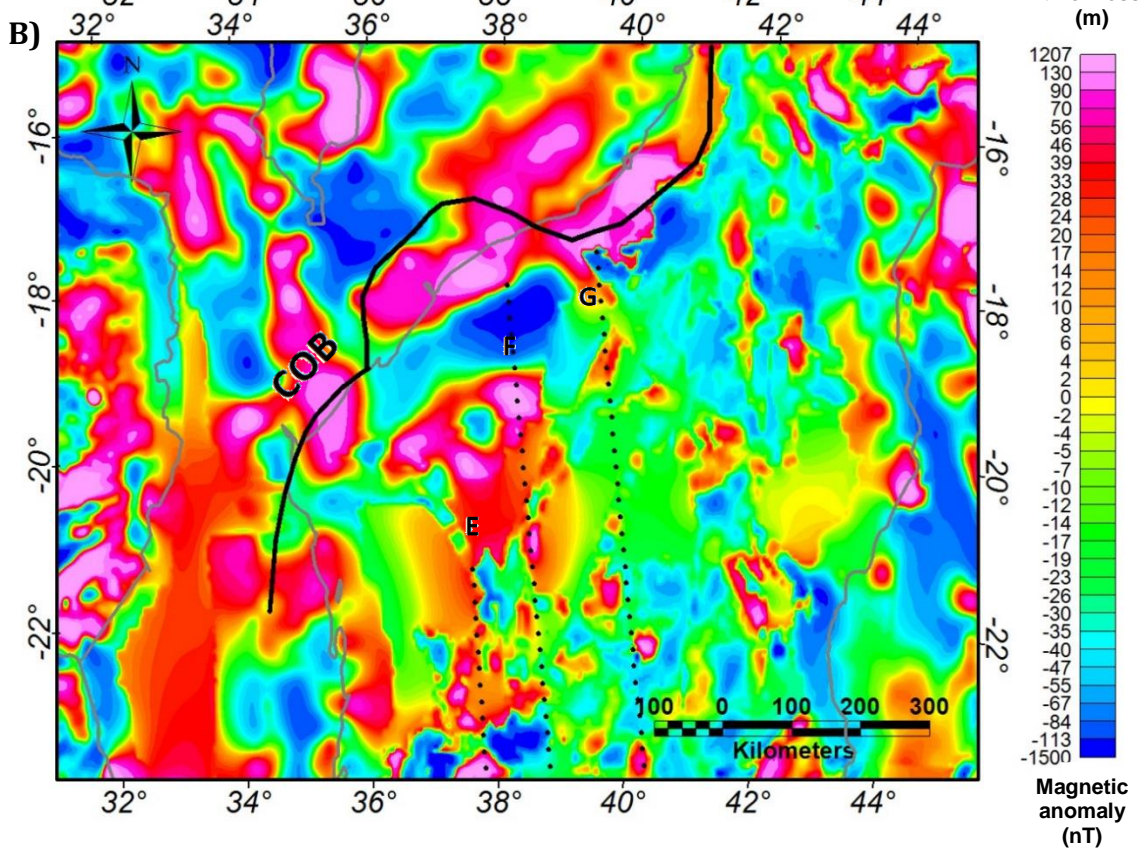
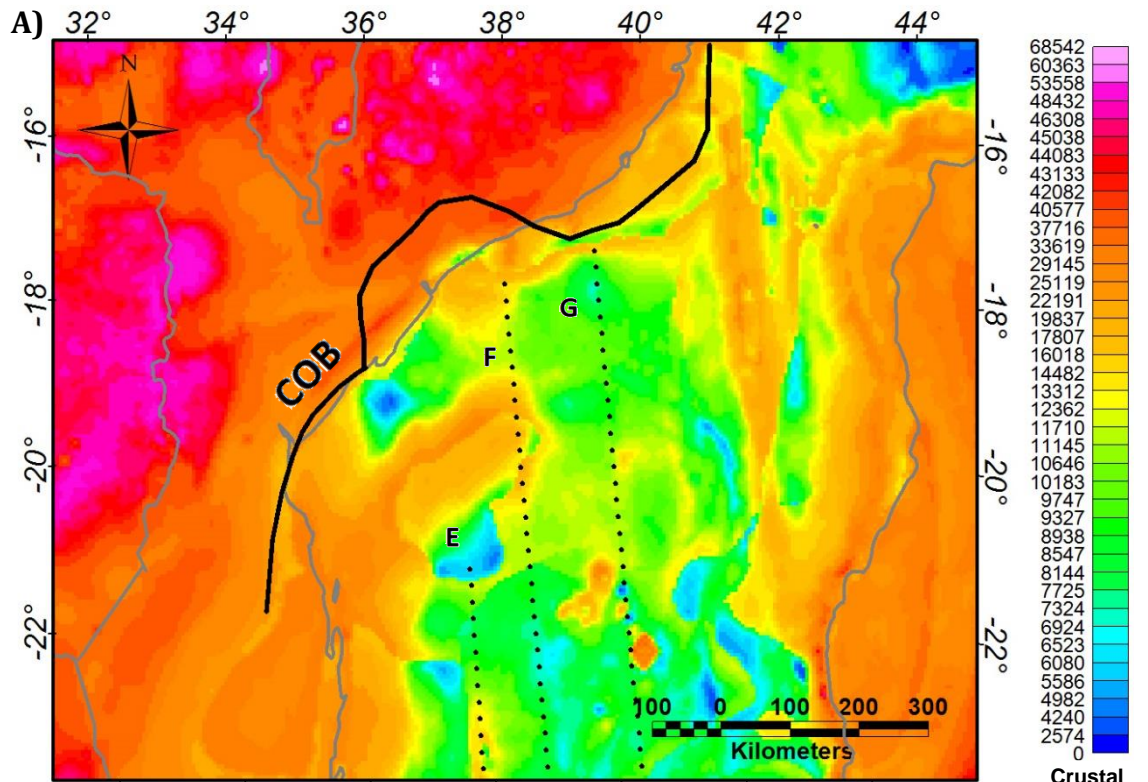
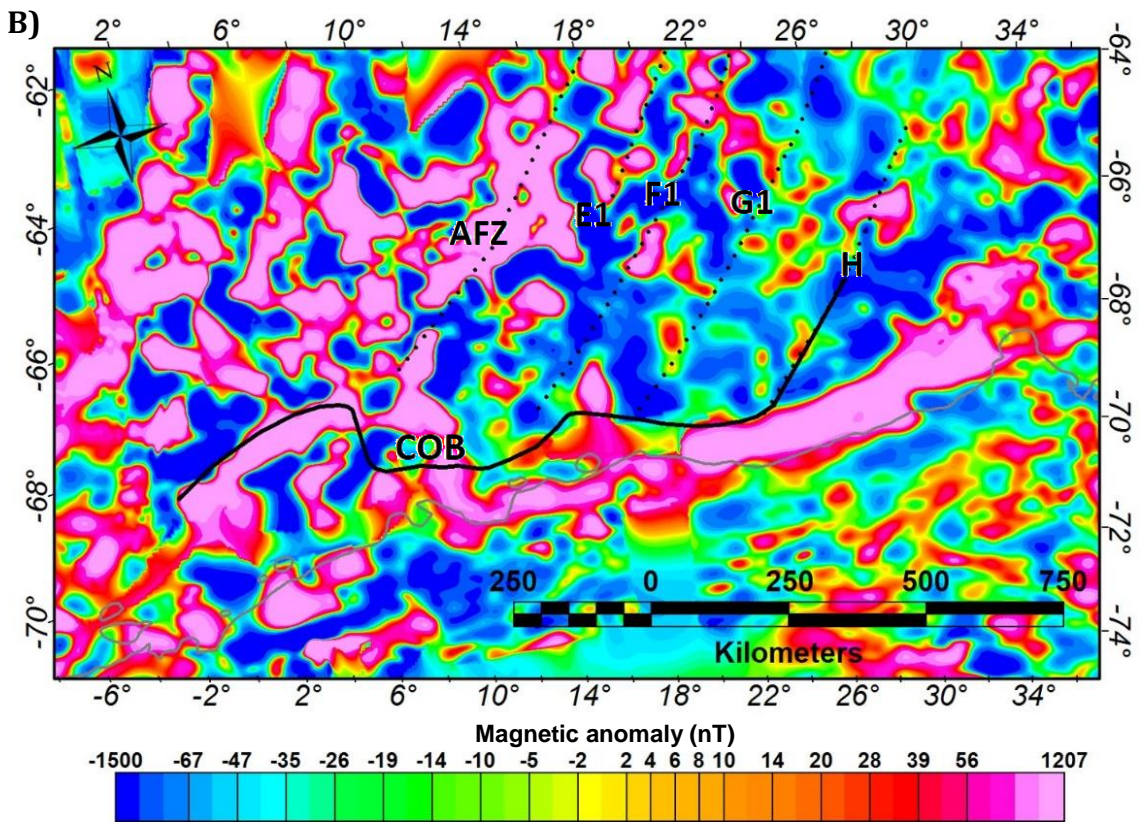
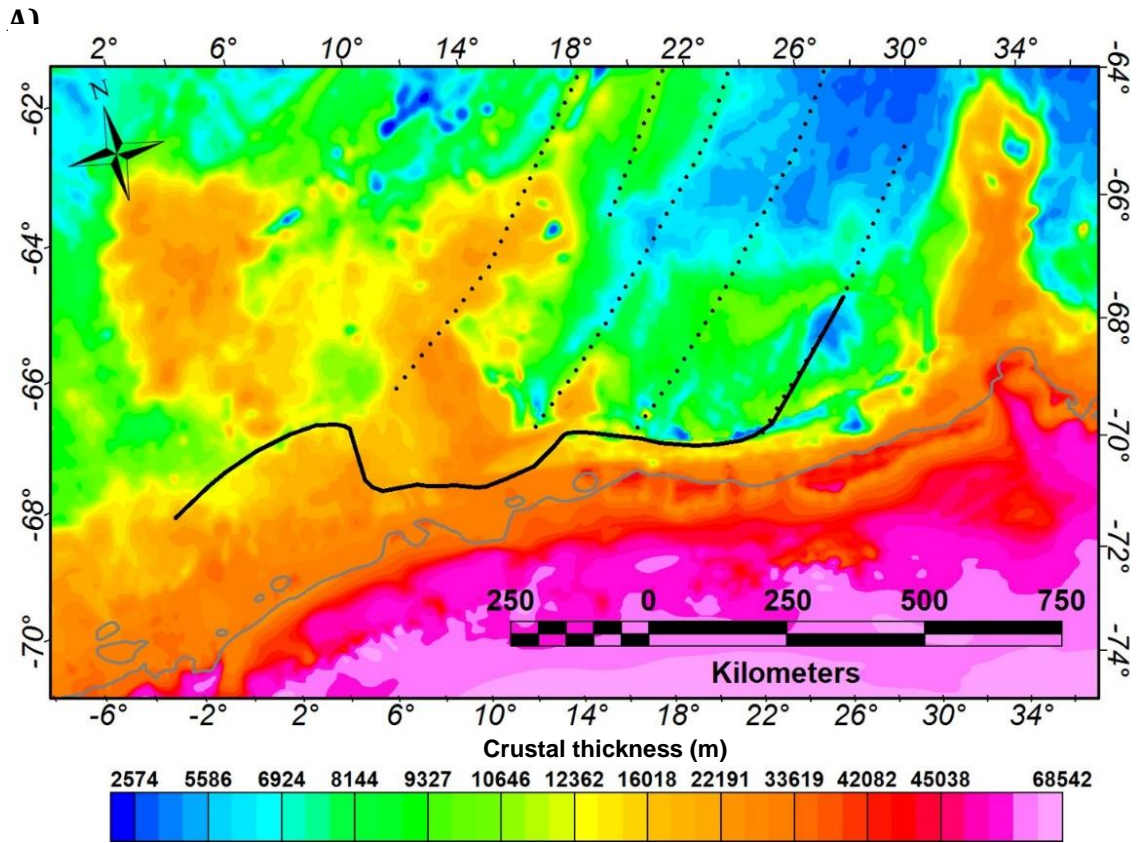


Figure 5.10: Correlation of the modified Antarctica COB from Figure 5.8 to **A)** crustal thickness and **B)** regional magnetic anomaly. Similar to the Africa side, not much correlation can be made between this COB and the anomaly or crustal thickness trend.



Mozambique. This is not consistent with the derived crustal thickness model. Instead, a counter-clockwise rotation is the better model to account for progressive increase in extension from northeast to southwest along the African margin

5.4 Model assumptions and limitations

The main assumptions that might have important influences on the outcome of this study include those made for the gravity-inversion process and calculation for non-rigid reconstruction. The crustal thickness model is an important part of this study and is derived by fitting a calculated gravity response to the observed data. However, land-based, gravity anomaly data are not available for onshore areas. Instead, data based on a geoid model was employed in the calculation. This might affect the accuracy of inversion product. The result can only be tested at limited locations where constraints are available. To put it in perspective, if crustal thickness is consistently under or overestimated by 5 km for a distance of 100 km, the error in estimated pre-rift boundary is about 10-12 km. Nevertheless, the close comparison of the model's calculation to the global average is a favorable sign.

Accounting for total volcanic volume is also an influential step. Current model assumes the plate underwent pure shear rifting (McKenzie, 1978) thereby equivalent amounts of magmatic underplating are expected in both margins. This may or may not be correct since most evidence for volcanic activity is found on the Africa side and very little data suggest volcanic presence in the Riiser Larsen Sea (Leitchenkov et al., 2008; Hinz et al., 2004). Favorably, the non-rigid calculation in Antarctica shows an average difference of 30 km between magmatic and non-magmatic pre-rift

boundaries. In addition, the difference is relatively uniform among all reconstructed profiles as the overall shapes of the two boundaries are very similar. If the Riiser Larsen Sea is in fact not affected with volcanic activity then Antarctica would simply move back 30 km away from Africa along the same direction as currently used in the reconstruction model resulting in a less tight fit (Figure 5.11).

In non-rigid reconstruction, it is assumed that the Karoo rift between ~184-174 Ma is the only period of rifting affecting the Africa continent. Contrarily, younger extensional events in different directions are known to have taken place since Antarctica drifted away. Hence, accounting for continental stretching all at once might be an over simplification. Consistency between the shapes of the two restored margins, however, might suggest that younger extensions are not significant and the Karoo rift was the dominant factor contributing to continental stretching.

Finally, even though the crustal thickness models show Antarctica is about 10 km thicker than the Africa craton, the model restores both margins to an equal pre-rift thickness. This can be justified by assuming a gradual change in thickness over Gondwana supercontinent. Thereby, at location of initial rifting, the crust is uniform in thickness. Although this study uses 42 km for the initial, pre-rift thickness. The impact of using other thicknesses on the non-rigid reconstruction is also examined. The crust of Antarctica, in general, is thicker than that of Africa. Hence the initial, pre-rift thickness used in non-rigid reconstruction is constrained by crustal thickness of Africa. Figure 5.12a-d show various contours of crustal thicknesses for areas with at least 40 km thick crust in Africa. To be consistent with global average of continental

craton thickness (Mooney, 1998) 40 km is considered as the lower limit of initial crustal thickness. Figure 5.12a-d show that contours of 40, 42 and 44 km cover a relative large region of onshore Africa. Only a few local areas have crustal thickness above 46 km. These observations suggest initial crustal thicknesses to be tested are in the range between 40 km and 46 km. These thicknesses are tested along three profiles in both margins. The comparisons are shown in Table 4.5. Over the African margin, the current pre-rift boundary would be moved about 4.5 km seaward from its current location if 40 km is used as the initial crustal thickness. On the other hand, the present boundary is shifted 11 km and 21 km landward for initial crustal thicknesses of 44 km and 46 km, respectively. The comparisons are similar in Antarctica. Changing the initial crustal thickness from 42 km to 40 km would shift the pre-rift boundary 7 km seaward. Using crustal thicknesses of 44 km and 46 km would move the boundary landward 7 km and 14 km, respectively. Overall, if 46 km is excluded from the range of initial thickness, since the region of 46 km thick crust is relatively more local than that of 40-44 km thick crust, the African and Antarctic pre-rift boundaries can be defined with uncertainty of about 15 km and 14 km, respectively.

Figure 5.11: Full fit geometry after non-rigid reconstruction of non-volcanic margins.

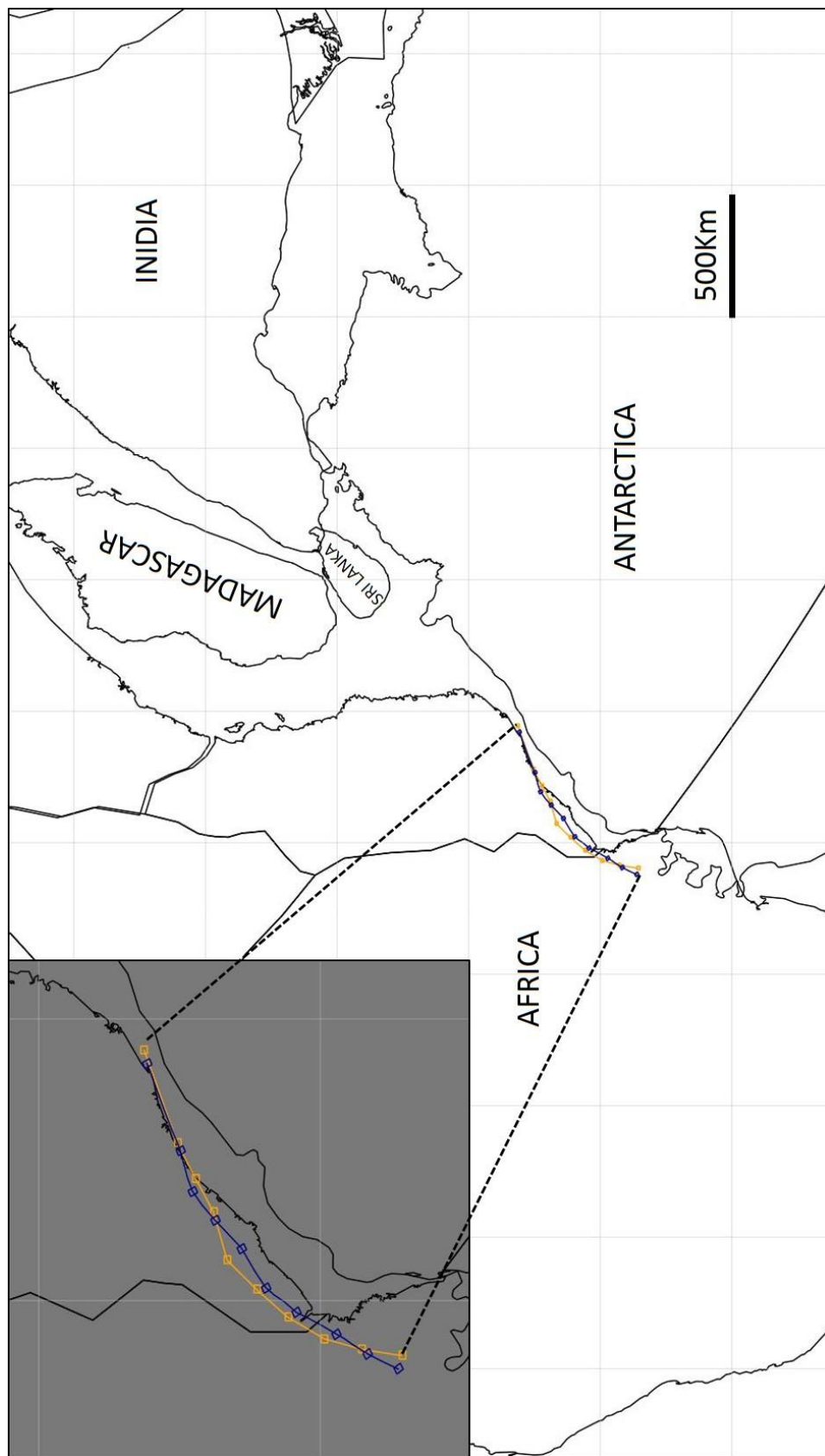


Figure 5.12: Crustal thickness map of Africa with contour of **A)** 40 km thickness, **B)** 42 km thickness, **C)** 44 km thickness, **D)** 46 km thickness. Crustal thickness above 46 km is only found in very local areas and thus not considered as the initial pre-rift thickness for non-rigid reconstruction.

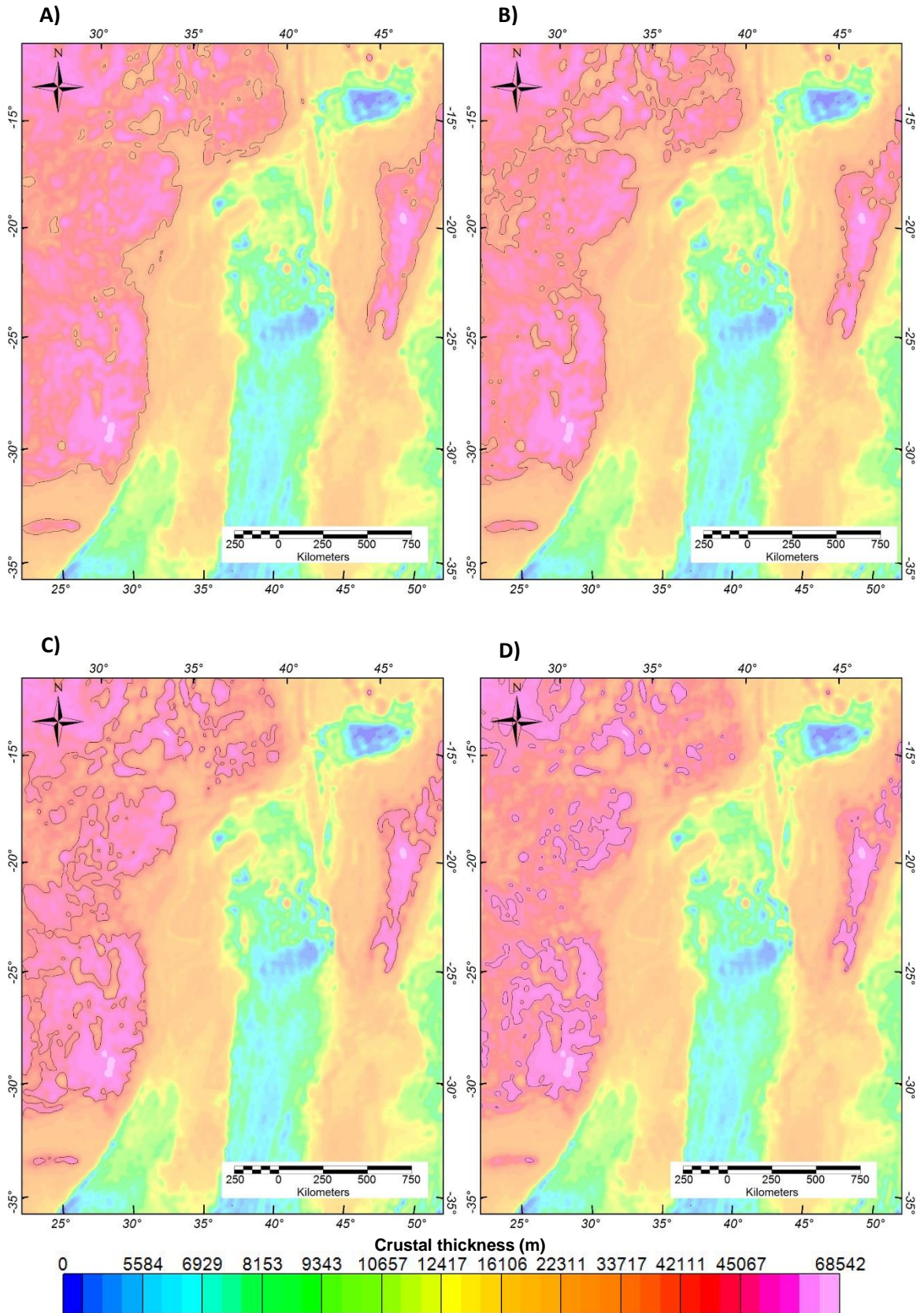


Table 5.1: Shifts the pre-rift boundary (PRB) using different initial thicknesses in the non-rigid reconstruction as compared to the current boundary using 42 km pre-rift thickness in **A) Africa, B) Antarctica.**

A)

Initial crustal thickness	40 km	44 km	46 km
PRB shift along MZB-1	5.1 km seaward	12.1 km landward	20.5 km landward
PRB shift along MZB-5	5.0 km seaward	11.7 km landward	18.9 km landward
PRB shift along MZB-10	3.4 km seaward	10.1 km landward	23.1 km landward
Average	4.5 km seaward	11.3 km landward	20.8 km landward

B)

Initial crustal thickness	40 km	44 km	46 km
PRB shift along ANT-1	6.1 km seaward	8.7 km landward	16.2 km landward
PRB shift along ANT-5	9.4 km seaward	5.4 km landward	14.1 km landward
PRB shift along ANT-10	5.3 km seaward	6.2 km landward	11.7 km landward
Average	6.9 km seaward	6.8 km landward	14.0 km landward

CHAPTER 6

CONCLUSION

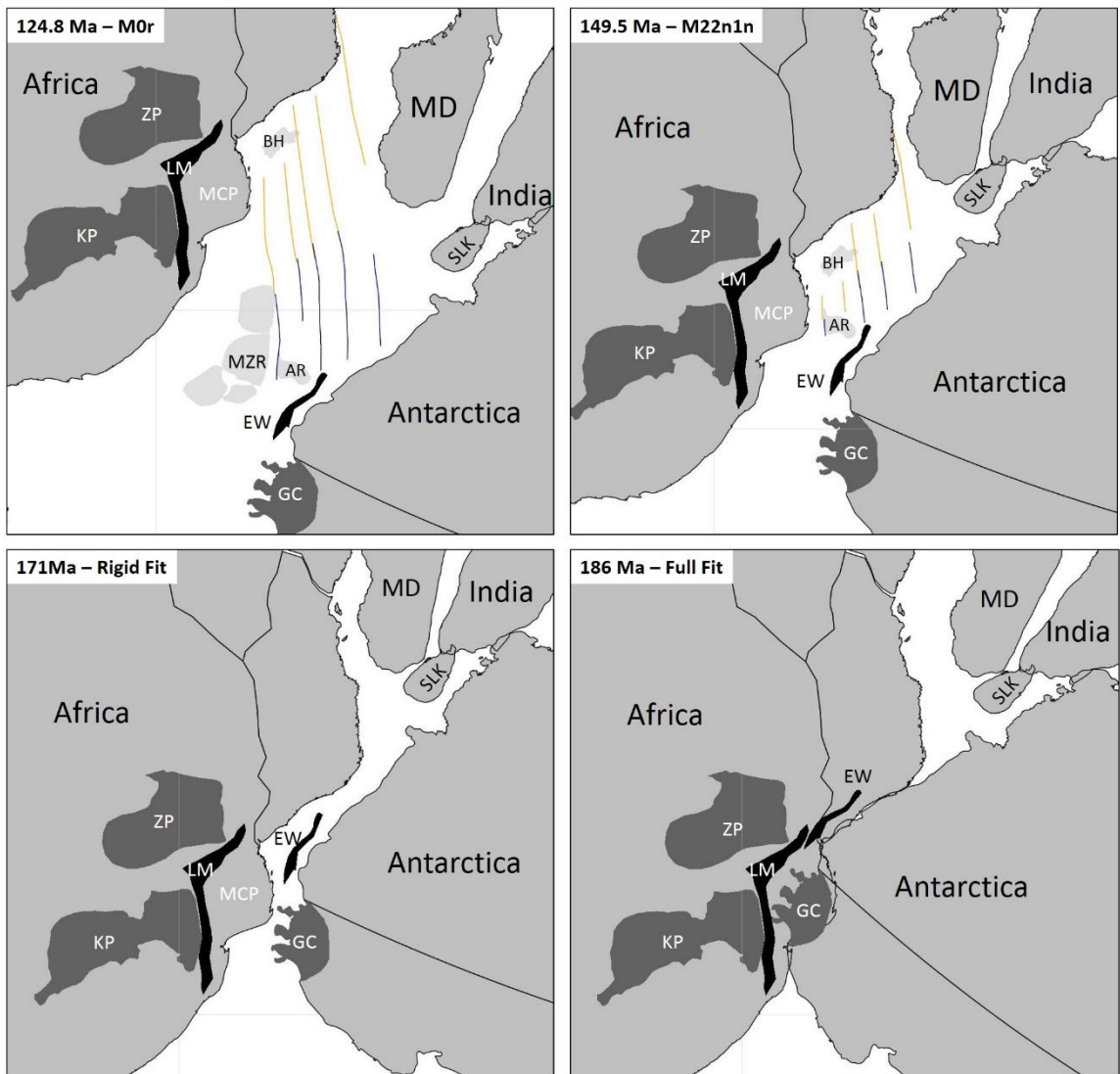
By interpreting marine magnetic anomaly data, satellite-derived gravity data, published seismic reflection and refraction data together with constructing a crustal-thickness model based on inversion of gravity, a complete break-up model of Africa and Antarctica involving both seafloor spreading and continental rifting has been achieved. Analysis of gravity anomaly data reveals fracture zones that can be traced as far landward as 70 km off of African and Antarctic coastlines. Identified magnetic isochrons have ages ranging from 124.8Ma (M0r) to 159.1Ma (M33n) over the Mozambique Basin. M0r and M25n are the youngest and oldest identified isochrons over the Riiser Larsen Sea, respectively. The Mozambique Basin is separated into at least four spreading corridors. Likewise, the five fracture zones are identified over the Riiser Larsen Sea which are determined to be conjugates of the fracture zones over the Mozambique Basin.

3-D gravity inversion has produced a crustal thickness model that shows onshore Africa and Antarctica have average crustal thickness of 40 km and 55 km respectively. The oceanic crust over the Mozambique Basin and the Riiser Larsen Sea has thickness ranging from 4 to 10 km. Analyses of magnetic anomalies and crustal thickness along with identified fracture zones reveal the COBs that are located significantly closer to the coasts of Africa and Antarctica than previously recognized.

The conjugate margins of Africa and Antarctica are reconstructed by correlating magnetic isochrons and fracture zones azimuths together with the identified COBs. The results show early plate motion was in a N-S direction when Antarctica started drifting southwardly with respect to Africa at 171 Ma. Of several scenarios examined to determine the crustal character of the Beira High, the preferred model assigns it an oceanic origin and suggests that it may be a conjugate feature of the southern Astrid Ridge emplaced between 162 Ma and 158 Ma.

An areal-balancing method that involves restoring the crust to a uniform pre-rift thickness has been used to perform the non-rigid reconstruction. This restoration has been carried out for both a non-volcanic and volcanic margin with magmatic underplating. Based upon the results, Africa underwent extension of 65-105 km while Antarctic crust was stretched by 90-190 km. Both margins reveal a trend of increasing extension from east to west. Various models tested to determine the direction of extension during rifting suggest that Antarctica underwent a counter-clockwise rotation with respect to Africa during the period between 186-171 Ma. In the final fit of the continents, the Grunehogna Craton occupies the present area of the Mozambique Coastal Plain and part of the Explora Wedge is placed adjacent to the Lebombo and Mateke-Sabi Monoclines. Figure 6.1 recaps the plate reconstruction at different times from 124.8 Ma to 186 Ma.

Figure 6.1: Plate reconstructions showing the evolution of the continental margin of Africa along the Mozambique Basin and its conjugate Antarctic margin over the Riiser Larsen Sea. Reconstruction poles for plates other than Antarctica are from Seton et al. (2012). AR: Astrid Ridge, BH: Beira High, EW: Explora Wedge, GC: Grunehogna Craton, KP: Kaapvaal Province, LM: Lebombo Monocline, MCP: Mozambique Coastal Plain, MD: Madagascar, MZR: Mozambique Ridge, SLK: Sri Lanka, ZP: Zimbabwe Province. Yellow and blue lines are fracture zone on the African and Antarctic sides, correspondingly.



BIBLIOGRAPHY

- Allan, C., & Brian, H. (2009). *Plate Tectonics: How it works*. Hoboken: Wiley-Blackwell.
- Austin, J. A. (1990). Crustal structure of the Southeast Georgia Embayment-Carolina Trough: preliminary results of a composite seismic image of a continental suture (?) and a volcanic passive margin. *Geology*, 18(10), 1023–1027. [http://doi.org/10.1130/0091-7613\(1990\)018<1023:CSOTSG>2.3.CO;2](http://doi.org/10.1130/0091-7613(1990)018<1023:CSOTSG>2.3.CO;2)
- Baier, B., Beckhemer, H., Gajewski, D., Green, R. W., Grimsel, C., & Prodehl, C. (1983). Deep seismic sounding in the area of the Damara Orogen, Namibia, Southwest Africa. In H. Marin & F. W. Eder (Eds.), *Intracontinental Fold Belts: case studies in the Variscan belt and in the Damara belt in Namibia* (pp. 885–900). Berlin: Springer-Verlag.
- Ball, P., Eagles, G., Ebinger, C., McClay, K., & Totterdell, J. (2013). The spatial and temporal evolution of strain during the separation of Australia and Antarctica. *Geochemistry, Geophysics, Geosystems*, 14(8), 2771–2799. <http://doi.org/10.1002/ggge.20160>
- Barret, D. M. (1977). Agulhas Plateau off southern Africa: A geophysical study. *The Geological Society of America Bulletin*, 88(6), 749–763.
- Bauer, K., Neben, S., Schreckenberger, B., Emmermann, R., Hinz, K., Fechner, N., Weber, K. (2000). Deep structure of the Namibia continental margin as derived from integrated geophysical studies. *Journal of Geophysical Research*, 105(B11), 25829–25853. <http://doi.org/10.1029/2000JB900227>
- Bentley, C. R. (1991). Configuration and structure of the subglacial crust. In R. J. Tingey (Ed.), *The Geology of Antarctica* (pp. 335–364). Oxford: Oxford University Press.
- Bergh, H. W. (1977). Mesozoic sea floor off Dronning Maud land, Antarctica. *Nature*, 269, 686–687.
- Bergh, H. W. (1987). Underlying fracture zone nature of Astrid Ridge off Antarctica's Queen Maud Land. *Journal of Geophysical Research*, 92(B1), 475–484. <http://doi.org/10.1029/JB092iB01p00475>
- Bertill, D., & Regnault, J. M. (1998). Seismotectonics of Madagascar. *Tectonophysics*, 294(1-2), 57–74. [http://doi.org/doi:10.1016/S0040-1951\(98\)00088-2](http://doi.org/doi:10.1016/S0040-1951(98)00088-2)
- Blakely, R. J. (1995). *Potential Theory in Gravity and Magnetic Applications*. New York: Cambridge University Press.

- Block, S., Hales, A. L., & Landisman, M. (1969). Velocities in the crust and upper mantle of southern Africa from multi-mode surface wave dispersion. *Seismological Society of America Bulletin*, 59, 1599–1629.
- Buyl, M. D., & Flores, G. (1984). Southern Mozambique Basin: most promising hydrocarbon province offshore East Africa. *AAPG Bulletin*, 68, 399–425. <http://doi.org/10.1306/AD461719-16F7-11D7-8645000102C1865D>
- Chave. (1979). Lithospheric structure of the Walvis Ridge from Rayleigh wave dispersion. *Journal of Geophysical Research*, 87(B12), 6840–6848.
- Chetty, P., & Green, R. W. E. (1977). Seismic Refraction observations in the Transkei Basin and adjacent areas. *Marine Geophysical Researches*, 3, 197–208.
- Cox, K. (1992). Karoo igneous activity, and the early stages of the break-up of Gondwanaland. *Magmatism and the Causes of Continental Break-Up*, 137–148.
- De Wit, M., Jeffrey, M., Bergh, H., & Nocolaysen, L. (1988). *Geologic map of sectors of Gondwana reconstructed to their disposition at 150Ma (1:10000000)*. Tulsa: American Association of Petroleum Geology.
- Duncan, R. A., Hooper, P. R., Rehacek, J., Marsh, J. S., & Duncan, A. R. (1997). The timing and duration of the Karoo igneous event, southern Gondwana. *Journal of Geophysical Research*, 102(B8), 18127–18138. <http://doi.org/10.1029/97JB00972>
- Durrheim, R. J., Barker, W. H., & Green, R. W. E. (1992). Seismic studies in the Limpopo Belt. *Precambrian Research*, 55, 187–200.
- Eagles, G., & König, M. (2008). A model of plate kinematics in gondwana breakup. *Geophysical Journal International*, 173(2), 703–717. <http://doi.org/10.1111/j.1365-246X.2008.03753.x>
- Encarnación, J., Fleming, T. H., Elliot, D. H., & Eales, H. V. (1996). Synchronous emplacement of Ferrar and Karoo dolerites and the early breakup of Gondwana. *Geology*, 24(6), 535–538. [http://doi.org/10.1130/0091-7613\(1996\)024<0535:SEOFAK>2.3.CO;2](http://doi.org/10.1130/0091-7613(1996)024<0535:SEOFAK>2.3.CO;2)
- Flores, G. (1973). The Cretaceous and Tertiary sedimentary basins of Mozambique and Zululand. *Assoc. Serv. Geol. Afr.*, 81–111.
- Fournou, J. P. (1987). Contribution a l'étude de la discontinuite de Mohorovicic d'apres les ondes sismiques observees a Madagascar *Annales. Geophysicae*, 2, 175–186.

- Gaina, C., Müller, R. D., Brown, B., Ishihara, T., & Ivanov, S. (2007). Breakup and early seafloor spreading between India and Antarctica. *Geophysical Journal International*, *170*(1), 151–169. <http://doi.org/10.1111/j.1365-246X.2007.03450.x>
- Gibbons, A. D., Barckhausen, U., Van Den Bogaard, P., Hoernle, K., Werner, R., Whittaker, J. M., & Müller, R. D. (2012). Constraining the Jurassic extent of Greater India: Tectonic evolution of the West Australian margin. *Geochemistry, Geophysics, Geosystems*, *13*(5), 1–25. <http://doi.org/10.1029/2011GC003919>
- Gohl, K., & Uenzelmann, N. (2001). The crustal role of the Agulhas Plateau, southwest Indian Ocean: evidence from seismic profiling. *Geophysical Journal International*, *144*(3), 632–646. <http://doi.org/10.1046/j.1365-246x.2001.01368.x>
- Golynsky, A. V., Morris, P., Kovacs, L. C., & Ferris, J. K. (2002). A new magnetic map of the Weddell Sea and the Antarctic Peninsula. *Tectonophysics*, *347*(1-3), 3–11. [http://doi.org/10.1016/S0040-1951\(01\)00234-7](http://doi.org/10.1016/S0040-1951(01)00234-7)
- Gore, J., James, D. E., Zengeni, T. G., & Gwavana, O. (2009). Crustal structure of the Zimbabwe Craton and the Limpopo Belt of Southern Africa; a new constraints from seismic data and implications for its evolution. *South African Journal of Geology*, *112*(3-4), 213–228. <http://doi.org/10.2113/gssajg.112.3-4.213>
- Goslin, J., Recq, M., & Schilch, R. (1981). Structure profonde du plateau de Madagascar- Relations avec le plateau de Crozet. *Tectonophysics*, *76*, 75–97.
- Grantham, G. H., Macey, P. H., Ingram, B. A., Roberts, M. P., Armstrong, R. A., Hokada, T., Manhica, V. (2008). Terrane correlation between Antarctica, Mozambique and Sri Lanka; comparisons of geochronology, lithology, structure and metamorphism and possible implications for the geology of southern Africa and Antarctica. *Geological Society, London, Special Publications*, *308*(1), 91–119. <http://doi.org/10.1144/SP308.4>
- Green, R. W. E., & Durrheim, R. J. (1990). Seismic refraction investigation of the Namaqualand metamorphic complex, South Africa. *Journal of Geophysical Research*, *95*(B12), 19927–19932.
- Green, R. W. E., & Hales, A. L. (1966). Seismic refraction measurements in the southwestern Indian Ocean. *Journal of Geophysical Research*, *71*, 1637–1647. <http://doi.org/10.1029/JZ071i006p01637>
- Groenewald, P. B., Grantham, G. H., & Watkeys, M. K. (1991). Geological evidence for a Proterozoic to Mesozoic link between southeastern Africa and Dronning Maud

- Land, Antarctica. *Journal of the Geological Society*, 148(6), 1115–1123.
<http://doi.org/10.1144/gsjgs.148.6.1115>
- Hales, A. L., & Nation, J. B. (1972). A crustal structure profile on the Agulhas Bank. *Bulletin of the Seismological Society of America*, 62(4), 1029–1051.
- Hales, A. L., & Sacks, E. S. (1959). Evidence for an intermediate layer from crustal structure studies in the eastern Transvaal. *Geophysical Journal International*, 2, 15–33.
- Hayes, D. F., Manley, P. L., Malin, J. W., & Houtz, R. E. (1991). Crustal structure: Circum Antarctic to 30°S. In D. E. Hayes (Ed.), *Marine Geological and Geophysical Atlas of the Circum-Antarctic to 30°S* (pp. 21–24). Washington: American Geophysical Union.
- Hinz, K., Neben, S., Gouseva, Y. B., & Kudryavtsev, G. A. (2004). A compilation of geophysical data from the Lazarev Sea and the Riiser Larsen Sea, Antarctica. *Marine Geophysical Researches*, 25(3-4), 233–245.
<http://doi.org/10.1007/s11001-005-1319-y>
- Hinze, W. J., Frese, R. R. B., & Saad, A. H. (2013). *Gravity and magnetic exploration: principles, practices, and applications*. New York: Cambridge University Press.
- Hirsch, K. K., Bauer, K., & Scheck-Wenderoth, M. (2009). Deep structure of the western South African passive margin — Results of a combined approach of seismic, gravity and isostatic investigations. *Tectonophysics*, 470(1-2), 57–70.
<http://doi.org/10.1016/j.tecto.2008.04.028>
- Huebscher, C., Jokat, W., & Miller, H. (1996). Crustal structure of the Antarctic continental margin in the eastern Weddell Sea. In B. C. Storey, E. C. King, & R. A. Livermore (Eds.), *Weddel Sea Tectonics and Gondwana breakup* (108th ed., pp. 165–174). London: Geological Society Special Publication.
- Hutchinson, D. R., Grow, J. A., Klitgord, K. . D., & Swift, B. A. (1983). Deep Structure and Evolution of the Carolina Trough. In J. S. Watkins & C. L. Drake (Eds.), *Studies in Continental Margin Geology* (34th ed., pp. 129–152). Mem. geol. Soc. Am.
- Ikami, A., Ito, K., & Kaninuma, K. (1983). Deep crustal structure along the profile between Syowa and Mizuho Stations, East Antarctica. *Memoirs of National Institute of Polar Research*, 28(43), 19–28.
- Ikami, A., Ito, K., Shibuya, K., & Kaninuma, K. (1983). Crustal structure of the Mizuho Plateau, Antarctica, revealed by explosion seismic experiments. In R. L. Oliver, P.

- R. James, & J. B. Jago (Eds.), *Antarctic Earth Science* (pp. 509–513). Cambridge: Cambridge University Press.
- Jacobsen, B. H. (1987). A case for upward continuation as a standard separation filter for potential field maps. *Geophysics*, *52*(8), 1138–1148. <http://doi.org/10.1190/1.1442378>
- Jokat, W. (2003). Timing and geometry of early Gondwana breakup. *Journal of Geophysical Research*, *108*(B9), 1–15. <http://doi.org/10.1029/2002JB001802>
- Jokat, W., Ritzmann, O., Reichert, C., & Hinz, K. (2004). Deep crustal structure of the continental margin off the Explora Escarpment and in the Lazarev Sea, East Antarctica. *Marine Geophysical Researches*, *25*(3-4), 283–304. <http://doi.org/10.1007/s11001-005-1337-9>
- Jones, E. J. W. (1999). *Marine Geophysics*. Chichester: Wiley.
- Jourdan, F., Féraud, G., Bertrand, H., & Watkeys, M. K. (2007). From flood basalts to the inception of oceanization: Example from the ⁴⁰Ar/³⁹Ar high-resolution picture of the Karoo large igneous province. *Geochemistry, Geophysics, Geosystems*, *8*(2), 1–20. <http://doi.org/10.1029/2006GC001392>
- Kamen-Kaye, M. (1983). Mozambique-Damagascar geosyncline, II: petroleum geology. *Journal of Petroleum Geology*, *5*(3), 287–308.
- Kogan, A. L. (1972). Results of deep seismic sounding of the Earth's crust in east Antarctica. In R. J. Adie (Ed.), *Antarctic Geology and geophysics* (pp. 485–489). Oslo: Universitets Forlaget.
- König, M., & Jokat, W. (2010). Advanced insights into magmatism and volcanism of the Mozambique Ridge and Mozambique Basin in the view of new potential field data. *Geophysical Journal International*, *180*(1), 158–180. <http://doi.org/10.1111/j.1365-246X.2009.04433.x>
- Kurinin, R. G., & Grikurov, G. E. (1982). Crustal structure of part of East Antarctica from geophysical data. In C. Craddock (Ed.), *Symposium on Antarctic Geology and Geophysics-International Union of Geological Sciences* (4th ed., pp. 895–901). Madison: University of Wisconsin Press.
- Kydryavtzev, G. A., Butzenko, V. V., & Kadmina, I. N. (1991). Crustal section across the Western Queen Maud Land continental margin from geophysical data. In Y. Yoshida, K. Kaminuma, & K. Shiraishi (Eds.), *International Symposium on Antarctic Earth Sciences* (pp. 330–335). Tokyo: National Institute of Polar Research.

- Laske, G., & Masters, G. (1997). A global digital map of sediment thickness. *EOS Trans*, 78(F483).
- Leinweber, V. T., & Jokat, W. (2011). Is there continental crust underneath the northern Natal Valley and the Mozambique Coastal Plains? *Geophysical Research Letters*, 38(14), 1–7. <http://doi.org/10.1029/2011GL047659>
- Leinweber, V. T., & Jokat, W. (2012). The Jurassic history of the Africa-Antarctica corridor - new constraints from magnetic data on the conjugate continental margins. *Tectonophysics*, 530-531, 87–101. <http://doi.org/10.1016/j.tecto.2011.11.008>
- Leinweber, V. T., Klingelhoefer, F., Neben, S., Reichert, C., Aslanian, D., Matias, L., Jokat, W. (2013). The crustal structure of the Central Mozambique continental margin - Wide-angle seismic, gravity and magnetic study in the Mozambique Channel, Eastern Africa. *Tectonophysics*, 599, 170–196. <http://doi.org/10.1016/j.tecto.2013.04.015>
- Leitchenkov, G., Guseva, J., Gandyukhin, V., Grikurov, G., Kristoffersen, Y., Sand, M., Aleshkova, N. (2008). Crustal structure and tectonic provinces of the Riiser Larsen Sea area (East Antarctica): Results of geophysical studies. *Marine Geophysical Researches*, 29(2), 135–158. <http://doi.org/10.1007/s11001-008-9051-z>
- Li, X., Kind, R., & Yuan, X. (2003). Seismic study of upper mantle and transition zone beneath hotspots. *Physics of the Earth and Planetary Interiors*, 136(1-2), 79–92. [http://doi.org/doi:10.1016/S0031-9201\(03\)00021-9](http://doi.org/doi:10.1016/S0031-9201(03)00021-9)
- Livermore, R. A., & Hunter, J. (1996). Mesozoic seafloor spreading in the southern Weddell Sea. In C. C. Storey, E. C. King, & R. A. Livermore (Eds.), *Weddell Sea tectonics and Gondwana break-up* (108th ed., pp. 227–241). London: Geological Society Special Publication.
- Ludwig, W. J., Nafe, J. E., Simpson, E. S. W., & Sacks, S. (1968). Seismic refraction measurements on the southeast Africa continental margin. *Journal of Geophysical Research*, 73(12), 3707.
- Mahanjane, E. S. (2012). A geotectonic history of the northern Mozambique Basin including the Beira High - A contribution for the understanding of its development. *Marine and Petroleum Geology*, 36(1), 1–12. <http://doi.org/10.1016/j.marpetgeo.2012.05.007>
- Malinverno, A., Hildebrandt, J., Tominaga, M., & Channell, J. E. T. (2012). M-sequence geomagnetic polarity time scale (MHTC12) that steadies global spreading rates

- and incorporates astrochronology constraints. *Journal of Geophysical Research*, 117(6), 1–17. <http://doi.org/10.1029/2012JB009260>
- Marks, K. M., & Tikku, A. A. (2001). Cretaceous reconstructions of East Antarctica, Africa and Madagascar. *Earth and Planetary Science Letters*, 186(3-4), 479–495. [http://doi.org/10.1016/S0012-821X\(01\)00262-X](http://doi.org/10.1016/S0012-821X(01)00262-X)
- Marschall, H. R., Hawkesworth, C. J., Storey, C. D., Dhuime, B., Leat, P. T., Meyer, H. P., & Tamm-Buckle, S. (2010). The Annandagstoppane Granite, East Antarctica: Evidence for Archaean Intracrustal recycling in the Kaapvaal-Grunehogna Craton from zircon O and Hf isotopes. *Journal of Petrology*, 51(11), 2277–2301. <http://doi.org/10.1093/petrology/egq057>
- Martin, A. K., & Hartnady, C. J. H. (1986). Cretaceous reconstructions of East Antarctica, Africa and Madagascar. *Earth and Planetary Science Letters*, 91(B5), 479–495.
- Maus, S., Sazonova, T., Hemant, K., Fairhead, J. D., & Ravat, D. (2007). National geophysical data center candidate for the world digital magnetic anomaly map. *Geochemistry, Geophysics, Geosystems*, 8(6), 1–10. <http://doi.org/10.1029/2007GC001643>
- Mjelde, R., Raum, T., Myhren, B., Shimamura, H., Murai, Y., Takanami, T., Naess, U. (2005). Continent-ocean transition on the Vøring Plateau, NE Atlantic, derived from densely sampled ocean bottom seismometer data. *Journal of Geophysical Research*, 110(5), 1–19. <http://doi.org/10.1029/2004JB003026>
- Mooney, W. D., Laske, G., & Masters, T. G. (1998). CRUST 5.1: A global crustal model at 5° × 5°. *Journal of Geophysical Research*, 103(B1), 727–747. <http://doi.org/10.1029/97JB02122>
- Müller, R. D., & Roest, W. R. (1992). Fracture zones in the North Atlantic from combined Geosat and Seasat data. *Journal of Geophysical Research*, 97(B3), 3337–3350. <http://doi.org/10.1029/91JB02605>
- Müller, R. D., Sdrolias, M., Gaina, C., & Roest, W. R. (2008). Age, spreading rates, and spreading asymmetry of the world's ocean crust. *Geochemistry, Geophysics, Geosystems*, 9(4), 1–19. <http://doi.org/10.1029/2007GC001743>
- Nain, S. K., Gao, S. S., Liu, K. H., & Silver, P. G. (2006). Southern African crustal evolution and composition: Constraints from receiver function studies. *Journal of Geophysical Research*, 111(B2), 2156–2202. <http://doi.org/10.1029/2005JB003802>

- Neprochnov, Y. P., Levchenko, O. V., Merklin, L. R., & Sedov, V. V. (1988). *New data on crustal structure and seismicity of Atlantic and India ocean basins. SRIPTA Technica Inc.*
- Nguuri, T. K., James, D. E., Webb, S. J., Wright, C., Zengeni, T. G., Gwavava, O., & Snoke, J. A. (2001). Crustal structure beneath southern Africa and its implications for the formation and evolution of the Kaapvaal and Zimbabwe cratons. *Geophysical Research Letters*, 28(13), 2501–2504. <http://doi.org/10.1029/2000GL012587>
- Norton, I. O., & Sclater, J. G. (1986). A model for the evolution of the Indian Ocean and the breakup of Gondwanaland. *Journal of Geophysical Research*, 84(B12), 6803–6830.
- Parker, R. L. (1973). The Rapid Calculation of Potential Anomalies. *Geophysical Journal International*. <http://doi.org/10.1111/j.1365-246X.1973.tb06513.x>
- Parsiegla, N., Stankiewicz, J., Gohl, K., Ryberg, T., & Uenzelmann, G. (2009). Southern African continental margin: Dynamic processes of a transform margin. *Geochemistry, Geophysics, Geosystems*, 10(3), 1–20. <http://doi.org/10.1029/2008GC002196>
- Pavlis, N. K., Holmes, S. A., Kenyon, S. C., & Factor, J. K. (2013). Erratum: Correction to the development and evaluation of the earth gravitational model 2008 (EGM2008). *Journal of Geophysical Research: Solid Earth*, 118(5), 1–38. <http://doi.org/10.1002/jgrb.50167,2013>
- Qiu, X., Priestley, K., & McKenzie, D. (1996). Average lithospheric structure of southern Africa. *Geophysical Journal International*, 127(3), 563–581.
- Rabinowitz, P. D., Coffin, M. F., & Falvey, D. (1983). The separation of Madagascar and Africa. *Science*, 220(4592), 67–69. <http://doi.org/10.1126/science.220.4592.67>
- Rabinowitz, P. D., & Labrecque, J. L. (1977). Ocean-Continent Boundary At Passive Continental Margins I. *Earth and Planetary Science Letters*, 35, 145–150.
- Rao, D. G., Ramana, M. V., & Sarma, K. V. L. N. S. (1992). Tectonic development of graben over the Astrid Ridge off Dronning Maud Land, Antarctica. In A. Yoshida, K. Kaminuma, & K. Shiraishi (Eds.), *Recent Progress in Antarctic Earth Sciences* (pp. 639–647). Tokyo: Terra Scientific Publishing Company.
- Raum, T., Mjelde, R., Digranes, P., Shimamura, H., Shiobara, H., Kodaira, S., Thorbjørnsen, T. (2002). Crustal structure of the southern part of the Vøring Basin, mid-Norway margin, from wide-angle seismic and gravity data.

Tectonophysics, 355(1-4), 99–126. [http://doi.org/10.1016/S0040-1951\(02\)00136-1](http://doi.org/10.1016/S0040-1951(02)00136-1)

- Reccq, M., Goslin, J., Charvis, P., & Operto, S. (1998). Small-scale crustal variability within an intraplate structure, the Crozet Bank (southern Indian Ocean). *Geophysical Journal International*, 134, 145–156.
- Reeves, C. (2000). The geophysical mapping of Mesozoic dyke swarms in southern Africa and their origin in the disruption of Gondwana. *Journal of African Earth Sciences*, 30(3), 499–513. [http://doi.org/10.1016/S0899-5362\(00\)00035-X](http://doi.org/10.1016/S0899-5362(00)00035-X)
- Roeser, A. (1996). The development of the crust off Dronning Maud Land, East Antarctica. *Weddell Sea Tectonics and Gondwana Break-Up*, 108, 243–264.
- Saki, T., Tamura, Y., Tokuhashi, S., Kodata, T., Mizukoshi, I., & Amano, H. (1987). Preliminary report of geological and geophysical surveys off Dronning Maud Land, East Antarctica. In *National Institute of Polar Research Symposium: Antarctica Geoscience* (pp. 23–40). Tokyo.
- Sandwell, D. T., Müller, R. D., Smith, W. H. F., Garcia, E., & Francis, R. (2014). New global marine gravity model from CryoSat-2 and Jason-1 reveals buried tectonic structure. *Science*, 346(65), 65–67. <http://doi.org/DOI:10.1126/science.1258213>
- Schettino, A., & Scotese, C. R. (2005). Apparent polar wander paths for the major continents (200 Ma to the present day): A palaeomagnetic reference frame for global plate tectonic reconstructions. *Geophysical Journal International*, 163(2), 727–759. <http://doi.org/10.1111/j.1365-246X.2005.02638.x>
- Schnabel, M., Franke, D., Engels, M., Hinz, K., Neben, S., Damm, V., Dos Santos, P. R. (2008). The structure of the lower crust at the Argentine continental margin, South Atlantic at 44°S. *Tectonophysics*, 454(1-4), 14–22. <http://doi.org/10.1016/j.tecto.2008.01.019>
- Sclater, J. G., Jaupart, C., & Galson, D. (1980). The heat flow through oceanic and continental crust and the heat loss of the Earth. *Reviews of Geophysics*, 18(1), 269–311. <http://doi.org/10.1029/RG018i001p00269>
- Segoufin, J. (1978). Anomalies magn'étiques m'esozi''iques dans le bassin de Mozambique. *Comptes Rendus Hebdomadaires Des Seances de l'Academie Des Sciences. Serie D: Sciences Naturelles*, 287, 109–112.
- Seton, M., Müller, R. D., Zahirovic, S., Gaina, C., Torsvik, T., Shephard, G., Chandler, M. (2012). Global continental and ocean basin reconstructions since 200Ma. *Earth-*

- Simpson, E. S. W., Sclater, J. G., Parsons, B., Norton, I., & Meinke, L. (1979). Mesozoic magnetic lineations in the Mozambique Basin. *Earth and Planetary Science Letters*, 43(2), 260–264. [http://doi.org/10.1016/0012-821X\(79\)90209-7](http://doi.org/10.1016/0012-821X(79)90209-7)
- Simpson, R. W., Blakely, R. J., & Saltus, R. W. (1986). A new isostatic residual gravity map of the conterminous United States with a discussion on the significance of isostatic residual anomalies. *Journal of Geophysical Research*, 91, 8348–8372.
- Simpson, R. W., Jachens, R. C., & Blakely, R. J. (1986). A new isostatic residual gravity map of the conterminous United States with a discussion on the significance of isostatic residual anomalies. *Journal of Geophysical Research*, 91, 8348–8372.
- Sinha, M. C., Louden, K. E., & Parsons, B. (1981). The crustal structure of the Madagascar Ridge. *Geophysical Journal International*, 66(2), 351–377.
- Stampfli, G. M., Hochard, C., Vérard, C., Wilhem, C., & vonRaumer, J. (2013). The formation of Pangea. *Tectonophysics*, 593, 1–19. <http://doi.org/10.1016/j.tecto.2013.02.037>
- Stein, C. A., & Stein, S. (1992). A model for the global variation in oceanic depth and heat flow with lithospheric age. *Nature*, 359, 123–129. <http://doi.org/10.1038/359123a0>
- Steinhar, J. S., & Meyer, R. P. (1961). Explosion studies of continental structure. *Carnegie Inst. Wash. Publ.*, (622), 226–383.
- Stuart, G. W., & Zengeni, T. G. (1987). Seismic crustal structure of the Limpopo mobile belt, Zimbabwe. *Tectonophysics*, 144, 323–335.
- Sutra, E., Manatschal, G., Mohn, G., & Unternehr, P. (2013). Quantification and restoration of extensional deformation along the Western Iberia and Newfoundland rifted margins. *Geochemistry, Geophysics, Geosystems*, 14(8), 2575–2597. <http://doi.org/10.1002/ggge.20135>
- Sykes, T. J. S. (1996). A correction for sediment load upon the ocean floor: Uniform versus varying sediment density estimations - Implications for isostatic correction. *Marine Geology*, 133(1-2), 35–49. [http://doi.org/10.1016/0025-3227\(96\)00016-3](http://doi.org/10.1016/0025-3227(96)00016-3)

- Tikku, A. A., Marks, K. M., & Kovacs, L. C. (2002). An Early Cretaceous extinct spreading center in the northern Natal valley. *Tectonophysics*, 347(1-3), 87–108. [http://doi.org/10.1016/S0040-1951\(01\)00239-6](http://doi.org/10.1016/S0040-1951(01)00239-6)
- Tominaga, M., & Sager, W. W. (2010). Revised Pacific M-anomaly geomagnetic polarity timescale. *Geophysical Journal International*, 182(1), 203–232. <http://doi.org/10.1111/j.1365-246X.2010.04619.x>
- Totterdell, J. M., Blevin, J. E., Struckmeyer, H. I. M., Bradshaw, B. E., Colwell, J. B., & Kennard, J. M. (2000). A new sequence framework for the Great Australian Bight: Starting with a clean slate. *AAPEA J.*, 40, 95–117.
- Vallier, T. L. (1974). *Valcanogenic sediments and their relation to landmass volcanism and sea floor-continent movements, western Indian Ocea, Leg 25, Deep Sea Drilling Project. Initial Reports Of The Deep Sea Drilling Project* (25th ed.). Washington D.C.
- Veevers, J. J., Tayton, J. W., & Johnson, B. D. (1985). Prominent magnetic anomaly along the continent-ocean boundary between the northwestern margin of Australia (Exmouth and Scott Plateaus) and the Argo Abyssal Plain. *Earth and Planetary Science Letters*, 72(4), 415–426. [http://doi.org/10.1016/0012-821X\(85\)90062-7](http://doi.org/10.1016/0012-821X(85)90062-7)
- Verduzco, B., Fairhead, J. D., Green, C. M., & MacKenzie, C. M. (2004). New insights into magnetic derivatives for structural mapping. *The Leading Edge*, 23(2), 116–119. <http://doi.org/10.1190/1.1651454>
- Vine, B. F. J., & Matthews, D. H. (1963). Magnetic Anomalies Over Oceanic Ridges. *Nature*, 199(4897), 947–949.
- Voss, M., & Jokat, W. (2007). Continent-ocean transition and voluminous magmatic underplating derived from P-wave velocity modelling of the East Greenland continental margin. *Geophysical Journal International*, 170(2), 580–604. <http://doi.org/10.1111/j.1365-246X.2007.03438.x>
- Watts, A. B. (2001). Gravity anomalies, flexure and crustal structure at the Mozambique rifted margin. *Marine and Petroleum Geology*, 18, 445–455.
- Webb, S. J., & Cawthorn, R. G. (2003). Gravity modeling of Bushveld Complex connectivity supported by Southern African Seismic Experiment results. *South African Journal of Geology*, 107(1-2), 207–218. <http://doi.org/doi:10.2113/107.1-2.207>

- Whittaker, J., Goncharov, A., Williams, S., Muller, R. D., & Leitchenkov, G. (2013). Global sediment thickness dataset updated for the Australian-Antarctic Southern Ocean. *Geochemistry, Geophysics, Geosystems*, *14*(8), 3297–3305.
- Williams, S. E., Whittaker, J. M., & Müller, R. D. (2011). Full-fit, palinspastic reconstruction of the conjugate Australian-Antarctic margins. *Tectonics*, *30*(6), 1–21. <http://doi.org/10.1029/2011TC002912>
- Zhao, M., Langston, C. A., Nyblade, A. A., & Owens, T. J. (1999). Upper mantle velocity structure beneath southern Africa from modeling regional seismic data. *Journal of Geophysical Research*, *104*, 4783–4794. <http://doi.org/10.1029/1998JB900058>

APPENDIX 1

Identified magnetic isochrons in the Mozambique Basin and the Riiser Larsen Sea

Latitude	Longitude	Latitude	Longitude	Latitude	Longitude	Latitude	Longitude
M0r-125.82 Ma		-65.197	19.029	-25.833	39.049	-65.274	18.606
-64.201	20.050	-65.131	18.804	-24.839	39.275	-26.971	51.467
-63.550	23.662	-64.555	22.223	M5r-131.00 Ma		-24.761	39.289
-62.972	26.460	-64.390	21.480	-64.491	21.822	-24.675	39.638
-28.188	51.604	-64.045	25.078	-64.388	21.485	-24.543	40.368
-27.071	38.408	-63.879	25.309	M7n-131.71 Ma		-24.030	40.616
-26.996	38.879	-27.822	51.558	-65.248	18.819	M8n-132.36 Ma	
-26.088	39.292	-27.612	51.533	-65.219	18.683	-65.347	18.503
-25.974	39.524	-27.407	37.753	-64.663	22.056	-65.332	18.467
-25.923	39.593	-26.084	38.329	-64.582	21.782	-64.799	21.900
-25.871	39.785	-26.077	39.000	-64.476	21.437	-64.749	21.708
-25.858	40.041	-26.024	38.812	-64.463	21.376	-64.675	21.334
-25.757	40.251	-25.966	39.018	-64.184	24.886	-64.649	21.170
M3n-127.86 Ma		-25.089	39.071	-27.278	37.740	-64.623	21.139
-64.629	19.473	-25.074	39.234	-27.169	51.483	-64.309	24.708
-63.989	23.078	-24.953	39.437	-25.946	38.317	-27.150	37.731
-63.439	25.899	-24.951	39.257	-25.880	38.768	-26.743	51.442
-28.020	51.588	-24.892	39.723	-24.802	39.281	-25.821	38.307
-25.514	39.485	-24.878	39.806	-24.778	39.415	-25.790	38.744
-25.426	39.778	-24.825	39.647	-24.743	39.569	-24.672	39.413
-25.422	39.936	-24.738	40.353	-24.734	39.772	-24.665	39.302
-25.417	39.683	-24.195	40.651	-24.726	39.641	-24.658	39.487
-25.321	40.253	M6n-131.30 Ma		-24.625	40.362	-24.616	39.744
M5n-130.28 Ma		-65.181	18.735	-24.114	40.634	-24.600	39.633
-65.007	18.971	-64.641	22.088	M7r-132.03 Ma		-24.488	40.359
-64.392	22.473	-64.558	21.793	-65.287	18.656	-23.940	40.597
-64.238	21.689	-64.453	21.448	-64.724	21.954	M8r-132.68 Ma	
-64.222	21.578	-64.443	21.405	-64.662	21.747	-65.396	18.433
-27.516	37.760	-64.158	24.922	-64.591	21.378	-64.902	21.846
-26.234	38.341	-27.402	51.516	-64.590	21.389	-64.817	21.678
-26.117	38.840	-25.852	39.047	-64.560	21.235	-64.728	21.306
-25.169	39.095	-24.844	39.275	-64.236	24.811	-64.666	21.108
-25.029	39.443	-24.819	39.419	-27.202	37.730	-64.371	24.618
-24.963	39.812	-24.756	39.643	-25.884	38.312	-27.074	37.725
-24.963	39.812	M6r-131.48 Ma		-25.849	38.760	-25.746	38.301
-24.927	39.653	-64.425	22.019	-24.721	39.410	-25.742	38.731
-24.834	40.342	-24.814	39.418	-24.704	39.531	-24.595	39.406
-24.322	40.678	-24.752	39.643	-24.682	39.760	-24.591	39.425

Identified magnetic isochrons in the Mozambique Basin and the Riiser Larsen Sea (continued)

Latitude	Longitude	Latitude	Longitude	Latitude	Longitude	Latitude	Longitude
M8r-132.68 Ma		-64.929	21.232	-65.631	18.097	-65.212	20.834
-65.369	18.312	-25.997	51.354	-65.054	21.052	-25.175	38.579
-64.665	21.074	-25.545	38.678	-64.863	21.855	-25.132	38.631
-26.498	51.415	-25.517	38.335	-64.810	20.562	-24.987	51.256
-24.593	39.312	-25.471	38.279	-64.653	24.228	-24.059	39.361
-24.568	39.733	-24.405	39.269	-26.733	37.696	-24.048	39.302
-24.517	39.663	-24.395	39.691	-25.489	51.307	-24.040	39.440
-23.895	40.587	-24.393	39.200	-25.330	38.620	-24.022	39.611
M9n-132.99 Ma		-24.371	39.716	-25.324	38.483	-23.996	39.851
-65.439	18.373	-24.366	39.387	-25.308	38.265	-23.363	40.526
-65.404	18.160	-24.361	39.332	-24.257	39.176	-23.330	40.466
-64.965	21.821	-24.314	40.393	-24.212	39.374	M10Nr-135.49 Ma	
-64.895	21.642	-23.729	40.552	-24.197	39.665	-65.922	17.668
-64.725	20.887	M10n-133.69 Ma		-24.196	39.328	-65.695	16.875
-64.718	20.991	-65.577	18.175	-24.193	39.341	-65.302	20.697
-64.441	24.519	-65.496	17.766	-24.163	39.791	-65.139	20.330
-26.975	37.714	-65.136	21.753	-23.510	40.505	-65.028	19.713
-26.253	51.395	-65.092	21.527	-23.489	40.507	-64.870	23.926
				M10Nn1n-134.46 Ma			
-25.671	38.217	-65.020	21.101			-26.481	37.675
-25.654	38.289	-64.852	20.783	-65.134	20.951	-25.095	38.558
-25.648	38.706	-64.794	20.626	-64.892	20.246	-25.063	38.683
-24.526	39.368	-64.605	24.294	-64.707	24.153	-25.007	38.241
-24.521	39.722	-26.809	37.702	-26.683	37.692	-24.759	51.233
-24.518	39.100	-25.752	51.328	-25.301	38.613	-23.989	39.609
-24.493	39.398	-25.458	38.655	-25.263	38.530	-23.957	39.352
-24.478	39.325	-25.426	38.405	-25.233	38.259	-23.948	39.286
-24.454	39.686	-25.383	38.272	-25.232	51.281	-23.932	39.493
-24.436	40.378	-24.338	39.229	-24.161	39.369	-23.913	39.881
-23.832	40.573	-24.299	39.266	-24.146	39.374	-23.239	40.447
M9r-133.32 Ma		-24.289	39.380	-24.135	39.312	-23.228	40.536
				M10Nn2n-134.83 Ma		M11n-136.07 Ma	
-65.516	18.263	-24.287	39.665				
-65.454	17.946	-24.285	39.330	-65.798	17.852	-65.204	20.227
-65.049	21.787	-24.267	39.753	-65.622	17.205	-65.068	19.554
-64.976	21.605	-23.609	40.526	-65.064	20.448	-64.980	23.769
-64.782	20.892	-23.582	40.491	-64.995	19.846	-26.342	37.663
-64.739	20.831	M10r-134.09 Ma		-64.780	24.051	-24.984	38.533
-64.518	24.413	-65.525	17.639	-26.620	37.687	-24.920	38.234
-26.885	37.709	-64.912	20.689	-25.083	38.247	-23.829	39.341

Identified magnetic isochrons in the Mozambique Basin and the Riiser Larsen Sea (continued)

Latitude	Longitude	Latitude	Longitude	Latitude	Longitude	Latitude	Longitude
M11n-136.07 Ma		-28.174	51.892	M13r-139.41 Ma		-65.707	18.733
-65.365	20.602	-24.676	38.167	-65.836	19.881	-65.258	21.701
-24.936	38.781	-24.621	38.452	-65.742	19.358	-27.137	51.775
-24.520	51.216	-23.472	39.311	-65.491	23.026	M15n-140.51 Ma	
-23.808	39.918	-23.469	39.277	-27.580	51.820	-66.012	19.607
-23.790	39.273	-23.335	39.874	-25.761	37.615	-65.862	19.142
-23.789	39.578	-23.306	40.008	-24.356	38.188	-65.790	18.668
-23.110	40.549	-22.826	40.541	-24.315	38.384	-65.634	22.811
-23.098	40.417	-22.825	40.358	-24.294	38.225	-65.374	21.653
M11r2r-136.81 Ma		M12r1-138.19 Ma		-23.184	39.279	-26.939	51.746
-66.184	17.273	-65.690	20.107	-23.170	39.278	-25.509	37.593
-65.405	19.913	-65.570	19.633	-22.850	40.194	-24.144	38.171
-65.166	23.503	-65.312	23.291	-22.517	40.539	-24.124	38.358
-26.195	37.647	-27.986	51.882	M14n-139.65 Ma		-24.072	38.261
-24.795	38.224	-25.913	37.627	-65.874	19.821	-22.922	39.258
-24.789	38.489	-24.539	38.188	-65.745	19.349	-22.886	39.352
-24.234	51.182	-24.538	38.434	-65.527	22.973	M15r-140.86 Ma	
-23.635	39.273	-24.532	38.202	-65.195	21.727	-66.053	19.541
-23.611	39.315	-23.395	39.304	-27.370	51.802	-65.905	19.068
-23.609	39.695	-23.378	39.276	-25.711	37.610	-65.827	18.639
-23.517	39.973	-23.241	39.932	-24.281	38.182	-65.664	22.767
-22.970	40.542	-23.218	40.024	-24.275	38.376	-65.445	21.624
-22.969	40.389	-22.707	40.333	-24.247	38.232	-26.723	51.734
-22.301	41.490	-22.688	40.531	-23.136	39.275	-25.433	37.587
M11An1n-137.15 Ma		-21.952	41.465	-23.120	39.292	-24.081	38.166
-24.024	51.162	M12An-138.91 Ma		-22.438	40.558	-24.011	38.345
-23.808	51.141	-65.770	19.984	M14r-140.07 Ma		-23.983	38.265
-23.532	39.273	-65.669	19.479	-65.925	19.742	-22.819	39.249
-23.507	39.274	-65.407	23.156	-65.811	19.229	-22.789	39.365
-23.444	39.803	-27.791	51.853	-65.572	22.904	M16n-141.56 Ma	
-23.392	39.993	-25.788	37.619	-25.585	37.600	-66.028	18.857
-23.384	39.841	-24.433	38.197	-24.194	38.175	-65.959	18.534
-22.786	40.350	-24.400	38.405	-24.180	38.365	-65.765	22.620
M12n-137.71 Ma		-24.394	38.212	-24.155	38.247	-25.335	37.580
-65.487	19.769	-23.269	39.289	-22.982	39.262	-24.716	37.528
-65.257	23.372	-23.263	39.278	-22.971	39.334	-23.808	38.144
-26.064	37.640	-23.020	40.075	-22.335	40.575	-23.758	38.758
-24.632	38.210	-22.554	40.536	-21.586	41.496	-22.571	39.228

Identified magnetic isochrons in the Mozambique Basin and the Riiser Larsen Sea (continued)

Latitude	Longitude	Latitude	Longitude	Latitude	Longitude	Latitude	Longitude
M16n-141.56 Ma		-65.793	21.475	-66.324	21.772	-24.479	51.489
-66.147	19.395	-25.971	51.651	-25.207	51.576	-22.803	37.880
-65.543	21.582	-20.906	41.467	-24.133	37.478	-22.730	38.195
-26.478	51.707	M17r-143.44 Ma		-23.258	38.094	-22.671	38.325
-23.800	38.321	-66.461	18.880	-23.233	38.298	-21.566	39.145
-23.751	38.280	-66.306	18.251	-23.226	38.233	-19.629	41.581
-22.556	39.393	-66.095	22.124	-23.225	38.296	M20r-147.47 Ma	
-21.219	41.478	-24.941	37.546	-20.199	41.566	-67.084	17.588
M16r-142.31 Ma		-24.335	37.495	M19n2n-145.51 Ma		-66.998	17.116
-66.309	19.130	-23.455	38.115	-66.814	17.821	-66.896	21.731
-66.165	18.623	-23.437	38.488	-66.763	17.570	-66.753	21.089
-66.117	18.406	-23.372	38.286	-66.501	21.981	-66.473	20.175
-66.106	23.722	-22.133	39.191	-66.459	21.802	-24.216	51.469
-65.915	22.397	M17r-143.44 Ma		-24.969	51.545	-23.590	37.432
-65.723	21.505	-66.336	18.324	-23.893	37.458	-22.621	38.043
-26.229	51.666	-66.319	23.673	-23.029	38.080	-22.576	38.198
-25.105	37.559	-65.929	21.555	-22.997	38.158	-22.540	38.332
-24.580	37.511	-25.716	51.610	-22.979	38.306	-21.455	39.135
-23.743	38.138	-23.456	37.966	-20.030	41.578	-20.610	40.821
-23.685	38.318	-23.328	38.295	M19r-146.06 Ma		M21n-148.16 Ma	
-23.665	38.701	-22.137	39.466	-67.001	17.657	-67.276	17.430
-23.654	38.285	M18n-144.31 Ma		-66.903	17.298	-66.996	21.666
-22.463	39.219	-66.555	18.043	-66.646	21.890	-66.939	23.523
-22.452	39.408	-66.544	17.969	-66.528	21.451	-66.876	21.090
M17n-142.70 Ma		-66.290	22.110	-24.741	51.528	-66.638	20.043
-66.396	18.987	-66.247	21.892	-23.838	37.449	-23.995	51.447
-66.247	18.480	-25.470	51.591	-23.010	38.087	-23.489	37.424
-66.219	23.696	-24.221	37.485	-22.979	38.076	-22.491	38.036
-66.192	18.345	-23.317	38.104	-22.927	38.178	-22.441	38.193
-65.998	22.272	-23.311	38.370	-19.848	41.580	-22.369	38.342
-25.016	37.552	-23.302	38.262	M20n1n-146.32 Ma		-21.323	39.125
-24.499	37.509	-23.301	38.297	-67.028	17.634	-20.543	40.788
-23.630	38.129	-22.066	39.186	-66.935	17.252	M21r-148.73 Ma	
-23.588	38.322	-20.414	41.532	-66.776	21.808	-67.348	17.369
-23.572	38.613	M18r-144.73 Ma		-66.625	21.089	-66.992	21.092
-23.554	38.288	-66.655	17.957	-66.359	20.262	-66.718	19.985
-22.390	39.213	-66.629	17.815	-23.716	37.443	-23.413	37.418
-22.363	39.421	-66.374	22.060	-22.754	38.058	-22.403	38.029

Identified magnetic isochrons in the Mozambique Basin and the Riiser Larsen Sea (continued)

Latitude	Longitude	Latitude	Longitude	Latitude	Longitude
M21r-148.73 Ma		M23r2r-151.95 Ma		-26.914	51.963
-67.049	23.496	-67.609	23.351	-18.550	39.801
-23.779	51.426	-67.582	21.275	-18.345	40.832
-22.350	38.190	-67.545	21.107		
-22.258	38.349	-67.199	19.593		
-21.235	39.118	-27.772	52.065		
-20.405	40.721	-22.872	37.370		
M22n1n-149.49 Ma		-19.942	40.496		
-67.412	17.314	M23r2r-151.95 Ma			
-67.239	21.507	-67.668	21.215		
-67.214	23.454	-67.640	21.111		
-67.168	21.094	-27.557	52.039		
-66.807	19.915	-22.719	37.359		
-28.147	52.111	M24Ar-153.45 Ma			
-23.249	37.404	-22.466	37.338		
-22.103	38.005	M24n-152.38 Ma			
-21.981	38.183	-67.800	21.123		
-21.894	38.386	-67.796	21.117		
-20.873	39.088	-67.349	19.482		
-20.218	40.623	-27.350	52.014		
M22r-150.47 Ma		-22.588	37.346		
-67.528	21.311	M25n-154.23 Ma			
-67.526	23.373	-67.859	21.119		
-67.496	21.105	-67.854	21.085		
-67.147	19.646	-27.123	51.991		
-27.969	52.096	-22.161	37.312		
-23.069	37.386	-20.155	38.685		
-21.910	37.987	-19.954	39.330		
-20.693	39.073	-19.398	40.218		
-20.081	40.563	-19.337	40.386		
M23n-151.18 Ma		-19.267	40.706		
-67.609	23.351	-19.226	40.925		
-67.582	21.275	M33n-159.08 Ma			
-67.545	21.107	-19.015	38.877		
-67.199	19.593	-18.956	39.391		
-27.772	52.065	-18.935	39.590		
-22.872	37.370	-18.485	40.168		
-19.942	40.496	-18.355	40.790		

APPENDIX 2

FORTRAN PROGRAM

MIDPT.FOR

C This program reads ASCII file describing the azimuth of a straight line and determines the line's midpoint. Inputs file include line ID, latitude and longitude of points along the line and magnetic anomaly at each point.

```
integer line(2),kt
doubleprecision x(3),y(3)
doubleprecision xmid,ymid
character*12 hdr,filin,filout
C
write(*,*)' i/p ?'
read (*,'(a12)')filin
write(*,*)' o/p ?'
read (*,'(a12)')filout
open (1,file=filin,status='old')
open (2,file=filout,status='new')
C
read (1,'(a80)')hdr
read (1,*)line(1),x(1),y(1)
kt = 1
10 read (1,*,end=20)line(2),x(2),y(2)
C
if (line(2).eq.line(1)) then
    kt = kt + 1
    x(3) = x(2)
    y(3) = y(2)
else
    xmid = ((x(3) - x(1))/2) + x(1)
    ymid = ((y(3) - y(1))/2) + y(1)
    write(2,200)line(1),kt,xmid,ymid
C
    line(1) = line (2)
    x(1) = x(2)
    y(1) = y(2)
    kt = 1
endif
goto 10
C
200 format(i6,i10,2f13.1)
20 xmid = ((x(3) - x(1))/2) + x(1)
ymid = ((y(3) - y(1))/2) + y(1)
write(2,200)line(1),kt,xmid,ymid
stop
end
```

LINPRJ.FOR

This program reads ASCII file describing the azimuths of profiles and their calculated midpoints. The program computes the slope of the profiles and projects them into a user defined slope by rotating the profiles about their midpoints. Inputs include profiles' IDs, latitude and longitude of profiles' points and magnetic anomalies collected at each point. Location of the midpoint as computed by MIDPT.FOR is also required.

```
integer line,kt(21),nline
doubleprecision x,y,mag,xp,yp
doubleprecision xmid(21),ymid(21),plsn,plb,plbn
character*12 hdr,filxyz,filmid,filout
c
write(*,*)' i/p xyz ?'
read (*,'(a12)')filxyz
write(*,*)' i/p mid ?'
read (*,'(a12)')filmid
write(*,*)' no of lines ?'
read (*,*)nline
write(*,*)' o/p ?'
read (*,'(a12)')filout
open (1,file=filxyz,status='old')
open (2,file=filmid,status='old')
open (3,file=filout,status='new')
c
plsn = -18.68424982          ! slope of projection line
plbn = 0.0535210142        ! projection onto pl
c
do i=1,nline
  read (2,150)line,kt(i),xmid(i),ymid(i)
enddo
c
read (1,'(a80)')hdr
do j=1,nline
  plb = ymid(j) - plsn*xmid(j)    ! b intercept of proj line
  do k=1,kt(j)
    read (1,*,end=20)line,x,y,mag
    plbn = y - plsn*x             ! b int of perp to proj line
    xp = (plbn-plb)/(plsn-plsn)  ! x projected
    yp = plsn*xp + plbn         ! y projected
    write(3,100)line,xp,yp,mag
  enddo
enddo
c
100 format(i8,2f13.1,f11.2)
150 format(i6,i10,2f13.1)
20 stop
end
```